UNIVERSIDADE TÉCNICA DE LISBOA

INSTITUTO SUPERIOR TÉCNICO

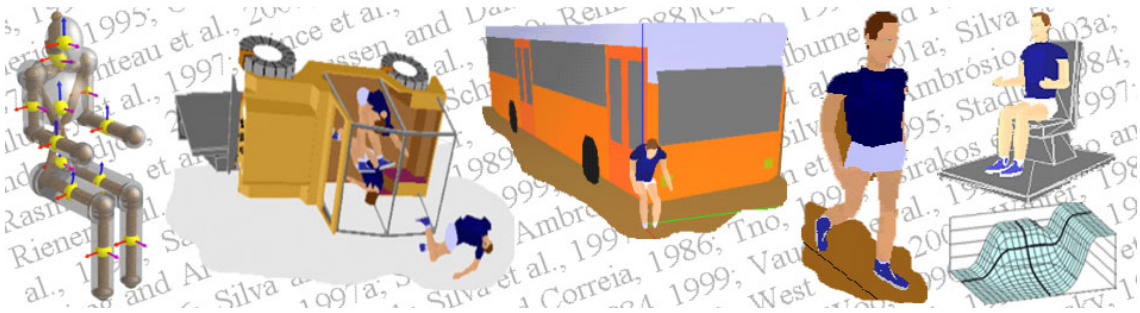

HUMAN MOTION ANALYSIS USING MULTIBODY DYNAMICS AND OPTIMIZATION TOOLS

MIGUEL PEDRO TAVARES DA SILVA
(MESTRE)

Dissertação para a obtenção do grau de Doutor em
Engenharia Mecânica

Orientador
Doutor Jorge Alberto Cadete Ambrósio

Júri

Presidente:	Reitor da Universidade Técnica de Lisboa
Vogais:	Doutor Gert-Peter Brüggemann
	Doutor João Manuel Cunha da Silva Abrantes
	Doutor Manuel Frederico Oom de Seabra Pereira
	Doutor João Arménio Correia Martins
	Doutor Jorge Alberto Cadete Ambrósio
	Doutor Rogério Augusto da Costa Pereira Leal

JULHO 2003

Resumo

Nesta dissertação são apresentadas metodologias que permitem realizar a análise dinâmica de movimentos humanos tridimensionais complexos. No âmbito da dinâmica de corpos múltiplos, são desenvolvidos dois modelos biomecânicos tridimensionais e de resposta total. Um modelo com 29 g.d.l. para aplicações em dinâmica directa, e um modelo com 44 g.d.l. para aplicações em dinâmica inversa. Em ambos os modelos, a estrutura cinemática de corpos rígidos e juntas articulares é descrita utilizando uma formulação de corpos múltiplos com coordenadas naturais. Em analise dinâmica directa, é feita a descrição da gama de movimento admissível de cada junta, sendo a prevenção de posturas humanas inviáveis feita através da aplicação de momentos de penalização articular. Com o objectivo de representar a interacção entre os vários segmentos anatómicos e o meio circundante é introduzido um modelo continuo de força de impacto-contacto. Em análises dinâmicas inversas, os momentos de força nas juntas, produzidos pelo aparelho muscular são calculados como sendo a solução dum problema determinado de dinâmica inversa. Quando é necessário o cálculo de forças musculares, o problema de dinâmica inversa torna-se indeterminado, sendo necessário introduzir modelos musculares do tipo Hill. Na sua resolução são utilizadas técnicas de optimização. Por forma a identificar quais as fontes de erro mais significativas nos dados de entrada para uma análise dinâmica inversa é também realizada uma completa análise de sensibilidades. Para cada tipo de análise dinâmica são apresentados diversos casos de aplicação, sendo os resultados obtidos discutidos no âmbito das metodologias propostas.

Abstract

In this thesis, a comprehensive methodology for the dynamic analysis of complex three-dimensional human motions is presented. In the framework of multibody dynamics two distinct whole-body response biomechanical models are developed: a 29 degree-of-freedom model for forward dynamic analysis and a 44 d.o.f. model for inverse dynamic analysis, respectively. The kinematic structure of rigid bodies and joints is described for both models, using a multibody formulation with fully Cartesian coordinates. In forward dynamic analysis, the admissible range of motion of each human joint is described and unfeasible human postures are prevented using joint penalty moments. A continuous contact-impact force model is used to describe the interaction between the anatomical segments and the surrounding environment. In inverse dynamic analysis, the joint moments produced by the muscle apparatus are calculated as the solution of a determinate inverse dynamics problem. To calculate muscle forces, the indeterminate inverse dynamics problem incorporates Hill-type muscle models and is solved with optimization techniques. The reaction forces at the joints are calculated independently of the type of dynamic analysis performed. A thorough sensitivity analysis is performed to identify the most significant sources of error in the input data of the inverse dynamic analysis. Several application cases are presented for both types of analyses and the results are discussed in the framework of the proposed methodologies.

Palavras-Chave

Biomecânica, Sistemas de corpos múltiplos, Dinâmica directa e inversa, Modelos biomecânicos, Forças musculares redundantes, Optimização.

Keywords

Biomechanics, Multibody systems, Forward and inverse dynamics, Biomechanical models, Redundant muscle forces, Optimization.

Agradecimentos

É com enorme prazer que aqui deixo, nas linhas que se seguem, um sincero voto de agradecimento a todo um conjunto de pessoas que, de várias formas, contribuíram para a realização desta dissertação.

Ao Professor Jorge Ambrósio, Pró-Reitor da Universidade Técnica de Lisboa e meu orientador científico, quero agradecer todo o apoio, coordenação e motivação que sempre me deu e transmitiu ao longo de todo o doutoramento. Para trás fica uma longa e árdua caminhada que sinto ter sido feita muitas vezes, lado a lado, em conjunto. Para o futuro, ficará sempre a admiração, o respeito e uma enorme amizade.

Ao Professor Manuel Seabra Pereira, Vice-Reitor da Universidade Técnica de Lisboa, quero também agradecer o apoio e motivação que sempre me transmitiu, assim como toda a simpatia e amizade que sempre senti receber.

Ao Doutor Mathew Kaplan da Universidade de Stanford, USA, quero agradecer a positiva troca de ideias que tivemos ao longo de um ano, o trabalho desenvolvido em conjunto e acima de tudo, a amizade, forte, que ficará para sempre.

Ao Professor Adam Czaplicki do Instituto do Desporto e Educação Física de Biala Podlaska, Polónia, quero agradecer as importantes e proveitosas discussões que tivemos relativamente à partilha das forças musculares e redundância biomecânica, i.e., to Professor Adam Czaplicki from the Faculty of Physical Education in Biala Podlaska, Poland, I would like to thank the important and fruitful discussions regarding the redundant problem in biomechanics and the muscle-force sharing problem.

Ao Professor João Abrantes, Pró-Reitor da Universidade Técnica de Lisboa, ao Professor António Veloso e ao Dr. Orlando Fernandes da Faculdade de Motricidade Humana e também ao Dr. Luís Jacinto do Laboratório de Marcha do Centro de Medicina e Reabilitação do Alcoitão, quero agradecer a ajuda prestada na recolha dos dados experimentais e a disponibilização dos meios necessários para a recolha dos mesmos.

To Professors Michael Richardson, Carol Teitz and Daniel Graney from the University of Washington, USA, I would like to thank the courtesy of letting me use in my PhD dissertation the excellent images from their online atlas of the lower extremity muscle apparatus.

To Professor Krister Svanberg from the Royal Institute of Technology in Stockholm, Sweden, I would like to thank the courtesy of letting me use the FORTRAN code with the globally convergent version of the Method of Moving Asymptotes.

Aos meus colegas e amigos João Pombo, Paula Jorge, João Folgado, João Dias, João Gonçalves, Inês Barbosa, João Milho, Luís Sousa, Virgínia Infante, Paulo Fernandes e José Aguilar, quero agradecer a salutar camaradagem e aquela palavra amiga.

À Fundação para a Ciência e Tecnologia quero agradecer a Bolsa de Doutoramento PRAXIS/4/4.1/BD/2851.

Quero também agradecer o apoio e incentivo dado por toda a minha família e amigos. Em particular quero agradecer ao meu pai Fernando por ter estado sempre a meu lado e ao meu irmão Nuno pelo seu apoio e preocupação.

Estes agradecimentos não estariam completos sem dedicar uma palavra de carinho muito especial à minha esposa Maria Helena e às minhas filhas Beatriz Maria e Inês Maria. A Elas agradeço a alegria, o carinho e o aconchego, que foram o garante da minha força de vontade e incentivo maior para aqui chegar. Por tudo isso, a Elas dedico este trabalho.

À Maria Helena, Beatriz Maria e Inês Maria

Contents

List of Tables

List of Figures

List of Symbols

Convention

a, A, α	Scalar
$\mathbf{a}$	Vector
$\mathbf{A}$	Matrix

Over script

$\dot{\mathbf{a}}$	First time derivative
$\ddot{\mathbf{a}}$	Second time derivative
$\tilde{\mathbf{a}}$	Skew-symmetric matrix

Superscript

$\mathbf{a}^T$, $\mathbf{A}^T$	Transpose of a vector or matrix
$\mathbf{A}^{-1}$	Inverse matrix
$\mathbf{a}'$	Quantity expressed in the local reference frame

Latin Symbols

a, b, c	Semi-axes describing an (hyper)ellipsoid during contact
a^m	Activation of muscle m
a	Vector with information regarding the first area moment of a body
b	Vector of the unit lever-arm associated with moment **m**
c_1, c_2, c_3	Coordinates of segment $\mathbf{r}_{ip}$ in a generic three-dimensional vector base
c	Vector containing previous coefficients c_1, c_2 and c_3
C	Coordinate transformation matrix
$\mathcal{C}_\lambda^m$	Scalar factor for muscle actuator m
d, $\overline{d}$	Center-of-mass location with respect to the proximal joint
D	Hysteretic damping coefficient between contacting surfaces
e	Restitution coefficient describing the type of impact
f_c, f_s	Filter's cut-off frequency and sampling frequency of capture device
f_i	Static optimization constraint equations
f	Vector with the Cartesian components of a generic force
F^m, F_0^m	Force and maximum isometric force produced by muscle m
F_L^m, $F_{\dot{L}}^m$	Force-length and Force-velocity relationship for muscle m
$\mathcal{F}_0$	Physiological criterion or objective (cost) function
g	Vector of generalized forces
$\mathbf{h}_G$	Angular momentum vector with respect to body's center-of-mass
HIC	Head Injury Criteria
i, j, k, p	Generic points
$I_{\xi\xi}$, $I_{\eta\eta}$, $I_{\zeta\zeta}$	Moments of inertia with respect to the principal axes of a rigid body
I, …, XVI	Anatomical segment number
$\mathbf{I}_3$	Identity matrix (3x3)
j	Joint damping coefficient
J	Matrix with information regarding the inertia tensor of a rigid body

Latin Symbols (cont.)

K	Relative stiffness coefficient between contacting surfaces
L_{ij}, $L_{\mathbf{u}}$	Lengths of segment $\mathbf{r}_{ij}$ and unit vector $\mathbf{u}$
L^m , L_0^m	Length and resting length of muscle m
$\dot{L}^m$, $\dot{L}_0^m$	Contractile velocity and maximum contractile velocity of muscle m
m	Rigid body mass
m_p	Joint penalty moment
$\partial m/\partial a$	Sensitivity of moment m to parameter a
$\mathbf{m}$	Cartesian components of a generic moment-of-force
$\mathbf{M}$, $\mathbf{M}_e$	System's (global) mass matrix and rigid body's (local) mass matrix
n_c	Number of generalized coordinates
n_h	Number of holonomic kinematic constraints
n_{ma}	Number of muscle actuators
n_{sv}	Number of state variables in optimization problems
n_{tc}	Number of total constraints in optimization problems
N	Number of recorded frames
$\mathcal{P}^*$	Virtual power
$\mathbf{q}$, $\dot{\mathbf{q}}$, $\ddot{\mathbf{q}}$	Vectors of generalized coordinates, velocities and accelerations
$\mathbf{r}_i$, $\mathbf{r}_j$, $\mathbf{r}_k$, $\mathbf{r}_p$	Vectors with the Cartesian coordinates of generic points i, j, k and p
R	Residual associated with the filtered/non-filtered signal
SI	Severity Index
t	Time variable or current time step of analysis
$\mathbf{u}$, $\mathbf{v}$	Generic unit vectors
$\mathbf{V}$	Coordinate transformation matrix
ω, $\dot{\omega}$	Angular velocity and angular acceleration of a rigid body
W, δW	Work and virtual work
x, x^F	Raw signal and filtered signal

Latin Symbols (cont.)

xyz	Global reference frame
$\mathbf{x}$	Vector containing the state variables for optimization problems
$\mathbf{X}$, $\mathbf{X'}$	Matrices representing a generic three-dimensional base of vectors
$\mathcal{X}_L$, $\mathcal{X}_m$, $\mathcal{X}_I$	Anthropometric scaling factors for length, mass and inertia
$\mathbf{y}$, $\dot{\mathbf{y}}$	Auxiliary vectors used in the direct integration process
$\mathbf{Z}$	Matrix obtained from a transformation (rotation) of matrix $\mathbf{J}$

Greek Symbols

α, β, ω, μ	Parameters used in the Augmented Lagrange Formulation
β, $\dot{\beta}$	Joint limiting angle and relative angular velocity
δ, $\dot{\delta}$	Pseudo penetration and pseudo penetration velocity during contact
$\mathbf{\Phi}$	Vector of kinematic constraints
$\mathbf{\Phi_q}$	Jacobian matrix of kinematic constraints
$\boldsymbol{\lambda}$	Vector of Lagrange multipliers
μ	Friction coefficient between contacting surfaces
$\boldsymbol{\nu}$	Right-hand-side vector of velocity equations
$\boldsymbol{\gamma}$	Right-hand-side vector of acceleration equations
$\mathbf{\Gamma}$	Matrix with geometric information regarding driving constraints
ρ	Rigid body density
Ω	Rigid body volume
$\xi\eta\zeta$	Local reference frame

Chapter 1

Introduction

1.1 Motivation

The study of the human body as an articulated system and in particular the analysis of its movement and the estimation of muscle forces, joint reactions and external forces acting on its skeletal structure is a challenging research field that has undergone enormous developments over the last fifty years. Computer simulation of several human capabilities has shown to be useful in many research and development activities, such as: analysis of top athletic actions (Alvarez *et al.*, 1993a; Alvarez *et al.*, 1993b), to improve different sporting performances (Raasch *et al.*, 1997); optimization of the design of sportive equipment (Zappa *et al.*, 1995); ergonomic studies, to assess operating conditions for comfort and efficiency in different aspects of human body interactions with the environment (Rasmussen *et al.*, 2002a); orthopedics, to improve the design and analysis of prosthesis (Andriacchi and Hurwitz, 1997); movement control, to define strategies for human body control (Ambrósio *et al.*, 1999b; Flashner *et al.*, 1987, 1988; Lo *et al.*, 2002) and humanoid design (Adolfsson *et al.*, 2001; Gruber and Schiehlen, 2002); gait analysis, for generation of normal gait patterns (Chau, 2001; Eng *et al.*, 1994; Gerritsen *et al.*, 1995; Olney and Winter, 1985; Sadeghi *et al.*, 2000;

Winter, 1995; Winter and Yack, 1987) and consequent diagnosis of pathologies and disabilities (Horak, 1997; Ounpuu *et al.*, 1995; Prince *et al.*, 1997; Winter, 1984); and occupant dynamic analysis for crashworthiness and vehicle safety related research and design (Ambrósio *et al.*, 1997; Ambrósio *et al.*, 1996; Pereira and Ambrósio, 1994, 1995; Silva and Ambrósio, 2002c; Silva *et al.*, 1997).

Computational simulation of human motion requires the implementation of mathematical models that correctly describe the behavior of the human body and its interaction with the surrounding environment. From this perspective, the use of multibody dynamics and optimization techniques has proved to be a successful option to describe these mathematical models, producing quality results with affordable computational costs. Another important feature of multibody methodologies is that the information obtained is the result of the application of mechanical laws of physics to living structures and, therefore, it is not obtained using invasive measuring techniques. In other words, the calculation of the reaction forces at the joints or the determination of the muscle forces developed in a particular muscle apparatus are obtained from the solution of a set of equations of motion, assembled in a systematic way for the biomechanical system under analysis, instead of being obtained using specific force measuring devices, such as buckle or implantable transducers, that need to be implanted *in vivo* in the joint or muscle of the subject. It is the purpose of this work to provide a fully integrated multibody methodology that can be used to describe the human body in detail and to simulate its dynamic response during general three-dimensional activities.

The proposed methodology uses a general multibody formulation with fully Cartesian coordinates to describe the anatomical segments and the topological structure of the human body. As a result, it provides quantitative information on the external forces acting on the skeletal structure, as well as on the forces developed at the joints and by the muscles of the subject as a consequence of the task being performed.

Two whole-body response biomechanical models are described using this multibody formulation. These models are used to describe mathematically the human body in terms of its anthropometry and topology. The models share a common structure of anatomical

segments and use the same anthropometric data to describe the physical characteristics of each one of these segments.

Depending on the purpose of the analysis, the solution of the equations of motion of the system can be obtained using either forward or inverse dynamics methodologies. The forward dynamics procedure is aimed at predicting the dynamic response of the human body when subjected to external forces, while the inverse dynamics procedure is intended to predict the internal and external forces that are required to produce an observed dynamic response. When using the latter type of analysis, the calculation of the redundant muscle forces developed in a particular muscle apparatus of the human body during the execution of a prescribed task is also considered to be a strong motivation of the present work.

1.2 Literature Review

The development of accurate mathematical models of the human body has been a major challenge for the biomechanics community over the past decades (Nigg and Herzog, 1995). Interest in the simulation of different human actions stems from the need to predict with sufficient accuracy the mechanical behavior of the human body in various conditions of its activity. However, it is well known that human body representations can be very sensitive to the type of mathematical formalisms used and their capability to support the efficient description of the biomechanical aspects of the human activities under analysis.

1.2.1 Multibody Formulations and Generalized Coordinates

In many biomechanical applications, the use of "gross-motion" simulators (Prasad, 1984; Schiehlen, 1990) is preferred to more computational expensive finite element based approaches (Haug, 1996; Kan *et al.*, 2001; Saha *et al.*, 1991). During the last three decades, the techniques and methods used in the former type of approach have evolved from a manual graphics art to a highly specialized research field where the kinematics and dynamics of complex mechanical systems are analyzed (Haug, 1989; Huston, 1990; Jalón and Bayo, 1994; Nikravesh, 1988; Roberson and Schwertassek, 1988; Shabana, 1994). With the growing development of computers, many elegant methods of analytical dynamics (Greenwood, 1965;

Meirovitch, 1970), which were especially tailored to analyze specific mechanisms, are being gradually substituted by efficient computer codes that, using multibody approaches, allow for the systematic formulation and solution of the equations of motion of general mechanical systems with high levels of complexity (Pereira and Ambrósio, 1995; Schiehlen, 1993).

Although some authors consider that all the fundamental equations of dynamics can be viewed as projections of the force and moment balances onto directions affected by the velocity variables (Baruh, 2000), experience shows that, depending on the type of coordinates selected to describe a particular multibody system, significant differences can be found in the efficiency and simplicity of the underlying mathematical formulation. Therefore, the choice of the most appropriate set of coordinates is not indifferent. Often it is a compromise between the advantages and simplifications it brings to the construction of the supporting multibody formulation, and the type of mechanical system to describe, the situation to simulate or the type of dynamic analysis to perform. Hence, it is not strange that so many different types of coordinates and multibody formulations can be found in the literature for the description of the dynamics of the human body. Aiming for the numerical efficiency of the multibody formulation, several authors prefer to describe their mechanical systems using Hamiltonian (Bayo *et al.*, 1994) or Lagrangian approaches. Due to their numerical efficiency, these methods often bring the dynamic analysis closer to the real-time simulation and in some cases improvements are also reported in the stability of the integration process. However, for large multibody systems, the differentiation of the scalar energy functions is an extremely difficult and cumbersome process (Huston, 1990). For dynamic analyses involving open-loop systems, many authors prefer to formulate the equations of motion of the mechanical system using Kane's method – also called Lagrange's form of d'Alembert's principle – that describes the system with a minimal set of independent generalized joint coordinates (Lee and Nikravesh, 1994), or generalized speeds (Amirouche *et al.*, 1990; Komistek *et al.*, 1998). This formulation has very interesting features, being its numerical efficiency and simplicity two of the most important. However, several studies suggest that the use of independent coordinates is not a suitable solution for general-purpose analyses of three-dimensional mechanical systems, with topologies having closed loops and complex kinematic joints (Jalón

and Bayo, 1994). This important drawback drew the attention of many researchers to the use of alternative multibody formulations, in which the mechanical system is described with a set of dependent coordinates. Using this approach, the number of coordinates is usually higher than the number of degrees of freedom of the system, and therefore not minimal. However, these formulations serve general-purpose applications and perform well in the simulation of general three-dimensional mechanical systems. Among the multibody formulations using this type of coordinates, the ones in which the mechanical systems are described with Cartesian coordinates (Haug, 1989; Nikravesh, 1988) and with fully Cartesian coordinates (Jalón and Bayo, 1994; Nikravesh, 1994), are emphasized. The latter type, in particular, presents additional advantages in the simulation of biomechanical systems since many relevant body landmarks can be directly used, as generalized coordinates, in the description of the system (Celigüeta, 1996; Silva and Ambrósio, 2002a). This feature is particularly important in inverse dynamics applications, in which the motion is acquired experimentally using digitizing techniques (Silva *et al.*, 2001). A multibody formulation with fully Cartesian coordinates is presented in this work and used in the description of mechanical systems in general and biomechanical models in particular.

1.2.2 Equations of Motion of Multibody Systems

The equations of motion of multibody systems, described with dependent coordinates, are expressed by a system of Differential Algebraic Equations (DAE) of index 3 (Haug, 1989; Jalón and Bayo, 1994; Nikravesh, 1988). The solution of this type of equations and their integration in time, introduces several numerical problems, namely the existence and uniqueness of solutions and instability for higher index systems (Jalón and Bayo, 1994). Specific numerical algorithms that enforce the stability of the solution are often required (Petzold *et al.*, 1998). An alternative approach for the solution of the equations of motion, transforms the set of DAEs in its underlying set of Ordinary Differential Equations (ODEs), which are solved by integration in time (Gear, 1981; Marsden and West, 2001; West *et al.*, 2000). However, the substitution of the algebraic equations of the DAE system by their differential counterpart in the ODE system introduces mild instabilities and drift problems in

the integration process (Ascher *et al.*, 1995), which can be attenuated using stabilization techniques such as the Baumgarte method (BM) (Baumgarte, 1972) or the iterative Augmented Lagrangian Formulation (ALF) (Avello and Bayo, 1992). Other methods such as the K-U formulation, based in the application of the Moore-Penrose generalized inverse/pseudo-inverse matrix to multibody systems, are also applied with success, increasing the efficiency and robustness of the formulation in the presence of redundant, degenerate and intermittent constraints (Arabyan and Wu, 1998). The ALF, in particular, offers important additional advantages since it also improves the robustness of the multibody formulation, making it suitable for use in singular positions of the system and in the presence of redundant constraints. The ALF is used in this work for the stabilization of the equations of motion.

1.2.3 Biomechanical Models

In "gross-motion" simulators, the different segments of the human body are typically represented, within the framework of multibody systems, by a set of rigid bodies interconnected by different types of joints and actuators with a varying degree of complexity. In recent years and throughout the world, many biomechanical models have been developed, with different purposes and using different approaches, depending on the nature of the research, the objectives of the analysis, and the expected results. There are essentially two major groups of biomechanical models: the ones described using multibody formulations and the ones described using finite element methods (Prasad, 1984; Wismans *et al.*, 1994). Multibody models are usually applied in cases where gross-motions are involved and when complex interactions with the surrounding environment are expected (Alvarez *et al.*, 1993b; Amirouche *et al.*, 1990; Anderson and Pandy, 2001b; Celigüeta, 1996; Hatze, 1984; Huang, 1995; Laananen, 1991; Laananen *et al.*, 1983; Morecki *et al.*, 1984; Rasmussen *et al.*, 2002b; Reich *et al.*, 1999; Silva and Ambrósio, 2002a; Wismans, 1996), while finite element models are applied in cases where localized structural deformations or soft tissues need to be described and analyzed in detailed (Bandak *et al.*, 1996; Bedewi and Bedewi, 1996; Dinis *et al.*, 1999; Haug, 1996; Kan *et al.*, 2001; Miller and Chinzei, 1997; Saha *et al.*, 1991). The use of multibody and finite element hybrid models is another possible approach – and probably a

future trend – that is already been used by several research groups (Eberhard *et al.*, 1999; Maurel and Thalmann, 1999; T.N.O., 1997), in an attempt to join together the advantages of both mathematical formulations, to construct more detailed models. However, creating and simulating finite element models can be computationally very expensive, making these methods less attractive in dynamic analyses where "real-time" is an issue or in optimization schemes involving many function evaluations.

Biomechanical models can vary in detail, complexity and topology depending on the objectives of the analysis. When describing biomechanical models, there are essentially two categories that can be distinguished: detailed partial models (Abdel-Rahman and Hefzy, 1993; Brelin-Fornari *et al.*, 1998; Engel *et al.*, 1997; Gilchrist and Winter, 1996; Horst *et al.*, 1997; Leardini *et al.*, 1999; Maurel and Thalmann, 1999; Mommersteeg *et al.*, 1997; Sathasivam and Walker, 1997; Shelburne and Pandy, 1997; Tumer and Engin, 1993; Wismans, 1980; Wynarsky and Greenwald, 1983), and whole body response models (Aleshinsky and Zatsiorsky, 1978; Celigüeta, 1996; Hatze, 1984; Laananen *et al.*, 1983; Rasmussen *et al.*, 2002b; Reich *et al.*, 1999; Silva and Ambrósio, 2002b). The first ones usually correspond to partial representations of the human body in which a particular anatomical segment, joint, organ or physiological function is represented with a high level of detail, while the second ones represent the human body as a whole, with the objective of capturing general characteristics rather than obtaining highly detailed information on particular components. With increasing computer power and the continuous development of new and more efficient numerical methods and formulations, biomechanical models tend to be less partial and more detailed, i.e., biomechanical models tend to be whole body response models with detailed representations of particular components and functions.

In this work, two whole body response biomechanical models are defined. The models share a common structure of anatomical segments and use the same anthropometric model to describe the physical characteristics of each of their segments (Kroemer *et al.*, 1988; Laananen *et al.*, 1983). This anthropometric model has sixteen anatomical segments and is based on the anthropometric data provided in the computer code SOM-LA (Laananen, 1991; Laananen *et al.*, 1983), which refers to the uniform mass distribution and body size of the

50th percentile aircrew member (Chandler, 1981). Other types of anthropometric models use known geometrical shapes to approximate the human body and to calculate approximated values for the moments of inertia of several anatomical segments (Hanavan, 1964). This type of models has also proved to be in fairly close agreement with the experimental results obtained for living subjects. In both biomechanical models, the relative motion between anatomical segments is described using a set of nominal or geometrical ideal joints (Cole *et al.*, 1993; Zatsiorsky, 1998) instead of detailed joint representations (Kapandji, 1973, 1974a, b; Zatsiorsky, 1998). This type of joint description is adopted since it is considered to be the most suitable and efficient solution for the type of analyses foreseen, in which specific details of the joint motion are not an issue. Restrictions on the relative range of motion between different biomechanical segments are introduced using joint-limiting angles (Laananen *et al.*, 1983; Panero and Zelnik, 1987) and motion-limiting moments (Laananen, 1991; S.A.E., 1980). These moments are applied between adjacent anatomical segments anytime their relative position is detected to be outside the cone of feasible motion of the anatomical joint connecting them.

1.2.4 Forward Dynamic Analysis and Injury Biomechanics

The safety of occupants and their potential survival in crash events involving transportation systems include many different aspects, such as the structural crashworthiness of the vehicle, the efficacy of the restraint systems and the shape and material properties of the interior trim of the passenger compartment (King, 1996; Viano and King, 1996). The analysis of such aspects is currently undertaken in modern automobile, aircraft and passenger train design, particularly in the initial design stages. Some well-known simulation programs are now available for that purpose: PAM CRASH (Haug and Ulrich, 1988) and DYNA 3D (Halquist, 1982) for structural impact and MADYMO (T.N.O., 1997), SOMLA/TA (Laananen, 1991) and ADAMS (Mechanical Dynamics, 1998) for occupant dynamics. These programs are able to simulate with detail frontal, rear and side impact scenarios, although in most cases, the structural impact and occupant dynamics are treated separately. This sequence of analysis normally involves calculating the relevant acceleration pulses from the structural

crashworthiness analysis and subsequently applying these accelerations in the occupant analysis phase. In this latter phase, several important injury criteria, such as the Head Injury Criterion (HIC) (Hutchinson *et al.*, 1998; Wismans *et al.*, 1994) and the Severity Index (SI) (Lankarani, 1992; Wismans *et al.*, 1994) are evaluated. The results obtained are converted to equivalent injury scales (Parenteau *et al.*, 2001; Wismans *et al.*, 1994) and used to assess design performance.

This procedure may be valid for some impact scenarios but it is not applicable to more complex crash situations. There are situations, such as in the case of a vehicle rollover, where a combined model, with the ability to analyze in a coupled manner complex crash events and occupant dynamics, is necessary. In the case of small cars where the occupant masses become comparable to the vehicle mass, the presence of the occupants may have significant influence on the overall dynamics of the problem. Moreover, the intrusion effects, such as the case of a collapsing roof, may drastically influence the evaluation of severity indices. In such models, the force-deflection characteristics of the different contact surfaces must be provided and the treatment of contact conditions between the different segments of the biomechanical model and the surroundings must be taken into consideration.

To overcome this problem, in the present work detailed vehicle and occupant models are combined in integrated simulation environments, which can be applied with great efficiency in complex crash scenarios, such as vehicle rollovers (Day and Garvey, 2000; Parenteau *et al.*, 2001; Renfroe *et al.*, 1998). In this integrated environment, the interaction between the occupant, the seat and the vehicle's compartment are described within the framework of the proposed multibody dynamics formulation, using an appropriate non-linear contact/impact force model that accounts for the compliance of the contacting surfaces, energy dissipation effects and friction forces between contacting elements (Laananen *et al.*, 1983; Lankarani *et al.*, 1995). The geometry of possible contact surfaces is described analytically using rigid surfaces such as ellipsoids, cylinders and planes. Specific contact detection methods are applied for the detection of possible contact points and in the case of effective contact, to calculate the associated pseudo-penetration, pseudo-penetration velocity and several other important geometrical properties (Haug *et al.*, 1989; Klisch, 1997). The vehicle model, used

in the integrated simulation environment, includes a detailed suspension system with a comprehensive tire-terrain model (Gim, 1988), steering capabilities and a detailed description of the chassis with appropriate force-deflection characteristics for the potential points of contact between the chassis and the ground (Nikravesh *et al.*, 1990). A seat belt model with lap and shoulder straps is also included to restrain the occupants in their seated positions (Laananen, 1991). Due to the particular type of simulation and vehicle under analysis, no other types of restraint systems are included. Therefore, systems such as airbags are not modeled, although relevant work exists on this subject (Wang, 1989; Wang and Ngo, 1990).

The analysis of pedestrians' impact and run over is also an important application field for which the use of integrated multibody methodologies can be of utmost importance for the correct simulation and understanding of the biomechanics of impact and injury mechanics. Moreover, these type of tools also provide an efficient tool for more efficient vehicle designs in terms of pedestrian impact protection (Mackay, 1996; Silva and Ambrósio, 1999; Viano and King, 1996). Several studies indicate that car accidents involving pedestrians are estimated to be responsible for the death and injury of over a quarter of a million people annually worldwide (Mackay, 1996). Several statistics indicate that in the great majority of these accidents, the pedestrians are injured in single-vehicle and single-pedestrian impacts, with the probability of a pedestrian being struck by a bus six times more likely than by a private car, on a yearly basis. Moreover, the risk of a pedestrian being injured in a bus collision is twelve times greater than in a collision with a car (Mackay, 1996). This type of accidents usually involves multi-contact collisions between the pedestrian, the vehicle and the surrounding environment that can only be accurately modeled in an integrated multibody environment (Silva and Ambrósio, 1999). In order to demonstrate the application of the proposed methodologies to such scenarios, a run over simulation of a pedestrian by a bus, based on real events, is performed in this work.

1.2.5 Inverse Dynamics Analysis of Determinate Biomechanical Systems

The analysis of the human body very often requires the knowledge of the forces and moments-of-force developed by the musculoskeletal system during the execution of a

prescribed task (Blajer and Czaplicki, 2001; Hatze, 1981; Yang *et al.*, 1990). However, it is a well-known problem that the direct measurement of these forces raises several important issues, since most of the available methods require the use of force measuring devices and invasive techniques (Fujie *et al.*, 1995; Nigg and Herzog, 1995). In practical terms, this means that the use of invasive techniques is restricted to a reduced number of applications, such as laboratory research with human volunteers (Glos *et al.*, 1993), cadavers (Singerman *et al.*, 1995) and animals (Glos *et al.*, 1993; Prilutsky *et al.*, 1997), or in clinical cases (Lu *et al.*, 1997), where the introduction of such force measuring devices is strictly required. Conversely, multibody methodologies, such as the one proposed in this work, are successfully being applied to the analysis of general three-dimensional human movements, producing qualitative and quantitative results, without interfering with the subject or with its motion.

The analysis of prescribed human movements can be performed using inverse dynamics analysis (Bogert *et al.*, 1996; Kingma *et al.*, 1996; Ledesma and Bayo, 1994; Morecki *et al.*, 1981; Silva and Ambrósio, 2002a; Winter, 1990, 1991), or forward dynamics analysis (Eberhard *et al.*, 1999; Kaplan *et al.*, 2001; Rasmussen and Damsgaard, 1997; Shelburne and Pandy, 1997). The selection of the type of approach to adopt in the motion analysis should not be casual. It is reported in the literature that for many important human tasks, such as gait, the results produced by both types of analyses are practically equivalent (Anderson and Pandy, 2001b). Considering that, from the computational point of view, the inverse dynamics approach is far more efficient than the forward dynamics approach, the former should be adopted when the objectives of the analysis are exclusively the calculation of the joint reaction forces, muscle forces or their equivalent net moments-of-force around the joints. However, if the objective of the analysis is to predict a novel movement, or if no accurate kinematic or dynamic data is available, or in cases where time-dependency is an important issue, then the latter approach should be the one adopted (Anderson and Pandy, 2001b).

Independent of the type of approach selected, a large collection of input data is usually required. This data contains the kinematic and dynamic information necessary to perform the analysis of the system. The kinematic information is used to define the motion under analysis and it consists of the trajectories of a set of anatomical points located on important anatomical

landmarks such as joints and extremities (Allard *et al.*, 1995; Medved, 2001; Nigg and Herzog, 1995). The dynamic information is used to describe externally applied forces and inertial properties of each anatomical segment of the human body, and is in many cases obtained using force plates or other types of force measuring devices (Allard *et al.*, 1995; Medved, 2001; Nigg and Herzog, 1995). Each of these data sets is usually obtained experimentally and is therefore prone to errors and uncertainties (Ball and Pierrynowski, 1996; Leva, 1996; Silva *et al.*, 2001; Winter, 1990). Moreover, several studies show that the accuracy of the results is more crucially dependent on the accurate determination of the kinematics and kinetics of the model than on the type of methods used in the dynamic analyses (Patriarco *et al.*, 1981; Silva and Ambrósio, 2003b).

The transformation of a three-dimensional movement into a convenient kinematic data set, suitable for use in a computer program, is not straightforward. It requires the use of several numerical techniques such as digitization of images, three-dimensional motion reconstruction, data filtering and curve fitting. For the acquisition of the Cartesian coordinates of the anatomical points, a motion capture technique is applied in the present work using four cameras (Ambrósio *et al.*, 1999a; Ambrósio *et al.*, 1999b). The two-dimensional images captured by the four synchronized cameras are digitized and the 3D coordinates of the anatomical points are calculated using Direct Linear Transformations (DLT) (Addel-Aziz and Karara, 1971; Kwon and Fiaud, 2002). This procedure is considered to be one of the most popular reconstruction techniques, and is widely recognized for its simplicity, accuracy and robustness (Borghese *et al.*, 1997). The process of digitizing the images is error prone due to several problems that occur, namely, operator-picking errors in the case of manual digitization, errors in the positioning of the digitizing markers, hidden body segments or reduced image resolution. These problems introduce high frequency noise signals in the trajectories of the anatomical points that need to be attenuated using appropriate filtering techniques (Giakas and Baltzopoulos, 1997a, b). In this work, a 2nd Order Butterworth low-pass filter, with zero phase-lag is used in order to smooth the raw data curves (Winter, 1990). Other filtering techniques, such as the Optimally Regularized Fourier Series (Hatze, 1980), have also been shown to provide good results and are a good alternative to filter digitized

signals with different noise levels. The externally applied forces also need to be filtered. In fact, the process of acquisition and conversion of the analog signal, measured by the force transducers, into the digital signal, introduces high frequency components in the force curve that need to be attenuated. In the present work this is achieved using the Butterworth low-pass filter with properly chosen cutoff frequencies.

Either because the acquisition of the kinematic data is generally done independently of the biomechanical model used, or due to the filtering procedure, the processed kinematic data does not ensure that the kinematic constraints associated with the biomechanical model are fulfilled (Ambrósio *et al.*, 1999a; Celigüeta, 1996; Kaplan *et al.*, 2001). The lack of kinematic consistency is associated with the variation in the anthropometric link lengths, which occurs from time step to time step. These changes are due to errors in the digitization and motion reconstruction procedures, as well as to the modeling assumptions used, and are ultimately responsible for the introduction of errors in the kinematic constraint equations, associated with the anatomical joints. Moreover, the inverse dynamic analysis also requires that the system velocities and accelerations are known. A common process to obtain these involves the use a polynomial interpolation of the coordinates and their time derivatives (Lanshammar, 1982). This procedure does not ensure that the constraint velocity and acceleration equations are fulfilled, even if the position data is kinematically consistent. Consequently, spurious joint reaction forces and net moments-of-force, associated with the constraint violations, are generated in the solution of the inverse dynamic problem (Ambrósio *et al.*, 1999b). To ensure the consistency of the kinematic data with the constraints of the biomechanical model, it is proposed that the kinematic positions be modified in order to fulfill the constraint equations. Furthermore, the velocity and acceleration of the system are obtained using the velocity and acceleration constraint equations, respectively.

1.2.6 Inverse Dynamics Analysis of Indeterminate Biomechanical Systems

When performing an inverse dynamic analysis of a biomechanical system, depending on the process used to describe and model the skeletal muscles, two different types of problems can be identified: a determinate inverse dynamics problem, if the actions of different muscle

groups are lumped as resultant moments about the anatomical joints (Allard *et al.*, 1995; Celigüeta, 1996; Nigg and Herzog, 1995; Schaffner *et al.*, 1997; Silva and Ambrósio, 2002a; Winter, 1990, 1991); or an indeterminate inverse dynamics problem – also called the redundant problem in biomechanics (Yamaguchi *et al.*, 1995) – if each muscle of the muscle apparatus under analysis is introduced as an independent force generator actuator in the biomechanical model (Mow and Hayes, 1997; Seireg and Arvikar, 1989; Winters and Woo, 1990; Yamaguchi, 2001). From the physiological point of view, this indeterminacy is denoted by the fact that different muscle activation patterns can generate the same posture or movement of the human body. Indeterminate biomechanical problems can be resolved through the use of proper optimization tools, which estimate the muscle forces according to the minimization of some performance criteria, or cost functions, that simulate the decisions taken by the central nervous system when executing a prescribed task (Collins, 1995; Crowninshield and Brand, 1981; Glitsch and Baumann, 1997; Patriarco *et al.*, 1981; Seireg and Arvikar, 1975, 1989; Yamaguchi, 2001; Yamaguchi *et al.*, 1995). The optimal solution, calculated by the optimizer, must minimize the prescribed performance criteria while satisfying the equations of motion of the biomechanical system, i.e., the optimal solution must reproduce the observed motion, generating intersegmental resultant moments that are equal to the ones calculated as solution of the determinate inverse dynamics problem (Crowninshield and Brand, 1981; Patriarco *et al.*, 1981).

The selection of the most appropriate criterion to use in the optimization process depends upon several important aspects such as the type of motion under analysis, the objectives to achieve or the presence of any type of pathology. A cost function should be able to reflect the inherent physical activity or pathology and it should be able to include relevant physiological characteristics of the muscles, such as the maximum isometric force, penation angle or the physiological cross sectional area, and functional properties of the motion or posture such as the instantaneous moment arms or the electromyographic activity of the muscles (Collins, 1995; Tsirakos *et al.*, 1997). Additionally, from the computational point of view, a cost function should also be numerically stable and provide small evaluation periods. One of the most popular cost functions, from many that can be found in the literature, corresponds to the

minimization of the total muscle stress, which is generally accepted to be closely related to the minimization of muscular fatigue (Crowninshield and Brand, 1981). It can be shown, however, that this criterion and several others use the same base expression, with their major differences involving the type of weight-factors adopted (Raikova, 1999). Moreover, the latter study also points out the importance that the correct selection of these weight-factors has in the prediction of co-contraction of antagonistic muscles. Conversely, other authors defend that the prediction of co-contraction activity of antagonistic muscles does not depend on the type of cost functions used in the optimization process, but on the type of topology and joint description adopted for the biomechanical model (Li, 1999). Using a computer model of the knee joint with ten muscles, Li concludes that all the physiological criteria analyzed were able to predict similar antagonistic muscle activity if the knee joint is described in such a way that it allows motion in three dimensions. Although important research is still being carried out on this subject (Ait-Haddou *et al.*, 2000), the same conclusion is observed in the results obtained in the present work for the muscles crossing joints in which motion in three-dimensions is allowed.

Electromyographic data (EMG) can be included in the description of the physiological criteria, providing qualitative as well as temporal information regarding the activation of muscles or muscle groups (Tsirakos *et al.*, 1997). Over the last four decades, EMG has improved and is viewed by many authors as a valuable tool in many activities, such as in diagnostic and therapeutic applications (Merletti *et al.*, 1992; Winter, 1984). In particular, in activities related to gait analysis, EMG techniques have been used to predict and estimate joint moments-of-force (Olney and Winter, 1985), muscle activations (Vaughan *et al.*, 1992), stride-to-stride and inter-subject variability of gait patterns (Winter and Yack, 1987) for later use in the diagnosis of gait pathologies (Winter, 1984, 1991). However, it should be noted that although EMG is related to muscle forces, these are not proportional to the EMG signal. Consequently, EMG should not be used to estimate muscle forces, especially when large ranges of motion are considered (Tsirakos *et al.*, 1997). Moreover, from the experimental point of view, special care should be put into the setup of the experimental procedures used, since it is well known the high sensitivity of this technique to the skin preparation, the depth

of the muscle, their contractile or stretching condition and velocity, and to cross-talk problems (Tsirakos *et al.*, 1997). Regarding the latter problem, which basically can be described as the detection of the signal generated by a given muscle inside or above a different one, some authors defend that it can be considered irrelevant if indwelling electrodes are used (Merletti *et al.*, 1992). In the present work, no EMG data is used.

1.2.7 Dynamics of Muscle Tissue and Muscle Modeling

Skeletal muscles are highly complex organs made of excitable tissue, whose contractible and elastic properties are responsible for the production of movement. Due to their utmost importance in general human activity, important research has been conducted regarding their anatomy and physiology (Lieber, 1992; Mow and Hayes, 1997; Rouvière, 1924, 1943, 1954; Schneck, 1992; Winters and Woo, 1990). Another important aspect, crucial for an accurate simulation of muscular activity, is the correct definition of the dynamics of muscle tissue. According to several authors, the dynamics of muscle tissue can be divided into activation dynamics and contraction dynamics (Kaplan, 2000; Zajac, 1989). Activation dynamics describes the time lag between the neural signal and the correspondent muscle activation, while contraction dynamics describes the transformation of the muscle activation into the production of muscle force. Activation dynamics is usually accounted for when a forward dynamics approach is used to analyze the movement, and is frequently described by a first order differential equation that is assumed to approximate the kinetics associated with the intracellular process of calcium activation and deactivation of the contractile element (Kaplan, 2000; Riener *et al.*, 1996; Zahalak and Ma, 1990; Zajac, 1989). The process describing contraction dynamics is usually more intricate (Hatze, 1984). For that reason the use of specific mathematical models is required. Muscle models are often labeled as passive models or active models, depending on the inclusion of a contractile element (Yamaguchi, 2001). In the present work, an active Hill-type muscle model is used to describe the contraction dynamics of the muscles incorporated in the biomechanical model (Medved, 2001; Nigg and Herzog, 1995; Riener *et al.*, 1996; Winters and Woo, 1990; Yamaguchi, 2001; Zajac, 1989). The Hill model assumes that the total force produced in a muscle results from the contribution

of a passive element and a contractile element. In particular, the ability of the contractile element to represent the contractile characteristics of the muscle by means of the force-length and force-velocity relationships controlled by the muscle activation (Morrison, 1969; Nigg and Herzog, 1995; Yamaguchi, 2001; Zajac, 1989), makes this type of model the most widely used by researchers for intermuscular coordination (Zajac, 1989). Muscles are introduced in the biomechanical model using muscle actuators (Delp *et al.*, 1990; Silva and Ambrósio, 2002b, d), also called myoactuators (Hatze, 1984). A muscle actuator is defined by specifying its force generating properties, as described before, and its geometry (Riener *et al.*, 1996). Regarding their geometry, muscles are defined by a series of points connected by line segments. The first and last of these points correspond to the muscle origin and insertion points, respectively, while the remaining ones are the so-called via points. Muscles can be defined by using a straight line approach and, in that case, no via points are needed except in muscles that wrap around joints (Dostal and Andrews, 1981; Duda *et al.*, 1996; Seireg and Arvikar, 1973, 1975, 1989), or by using the centroid line approach, which considers that the force transmitted by a skeletal muscle acts along a line defined by the locus of the centroid of its transverse cross section (Carhart, 2000; Jensen and Davy, 1975; Winters and Woo, 1990; Yamaguchi, 2001).

1.2.8 Optimization Methods

Different optimization methods can be used to resolve the 'redundant problem in biomechanics'. Two of the methods most widely used are the Method of Feasible Directions (MFD) and the Gradient Projection method (GP) (Arora, 1989; Haftka and Gurdal, 1992; Vanderplaats, 1984). The first is one of the classical methods that can be applied to Non-Linear Programming (NLP) problems. However, since it uses linear approximations, it is difficult to maintain feasibility with respect to equality constraints (Arora, 1989). The second method uses a similar approach to the NLP problem but instead of calculating a feasible direction using a solution of a Linear Programming (LP) problem, which in many cases is time consuming, it uses an explicit expression that is obtained by projecting the search direction into the subspace tangent to the active constraints (Arora, 1989; Haftka and Gurdal,

1992). This method provides search directions that are very simple to calculate, although less accurate than the ones produced by the MFD.

Many of the previous methods are not able to distinguish between a local and a global minimum. Given an initial approximation, the method converges to the nearest optimal solution, which in many cases might not be the only one and, therefore, might not correspond to the global minimum. A procedure that is often applied, when an optimization problem is thought to have several local minimums, is to use several different initial approximations. However, for optimization problems with many state variables, not only the convergence to a global minimum is not fully guaranteed, but also it becomes computationally more expensive. To overcome this problem, several modifications were introduced in many classical optimization methods, bringing them closer to global convergent methods, at the same time that entirely new methods were developed. Examples of these developments are the following globally convergent methods: the Method of Moving Asymptotes (MMA) (Svanberg, 1987, 1999), Genetic Algorithms (GA) (Goldberg, 1989; Holland, 1992; Leal *et al.*, 2000; Madeira *et al.*, 2003; Raikova and Aladjov, 2002) and the Feasible Directions Interior Point Technique (FDIPT) (Herskovits, 1998). In the present work, three optimization software packages are applied to the optimization of the redundant muscle forces: the DOT 5.0 - Design Optimization Tools (Vanderplaats, 1999), the routine DNCONG from IMSL Library (Virtual Numerics, 1995) and the MMA – Method of Moving Asymptotes (Svanberg, 1987, 1999). The first package is a well-known optimization program, widely used in the structural design community, which offers three optimization methods to solve constrained NLP problems, namely the Modified Method of Feasible Directions (MMFD), the Sequential Linear Programming (SLP) method and the Sequential Quadratic Programming (SQP) method. The second package is a routine available in the IMSL-Mathematical and Statistical Library. This routine is based on a FORTRAN code by Schittkowski (1986), in which a SQP method is used to solve a NLP problem (Virtual Numerics, 1995). The method formulates and solves, iteratively, successive Quadratic Programming (QP) subproblems, which are obtained using a quadratic approximation of the Lagrangian and by linearizing the constraints. The third package is a FORTRAN code that uses the globally convergent method of moving

asymptotes with inner and outer iterations to solve a NLP problem (Svanberg, 1987, 1999). Analytical gradients of the cost function and optimization constraint equations are supplied to the three optimization routines, although the first and second ones also provide, if desired, numerical calculations of these quantities using finite differences.

1.3 Scope and Objectives

The purpose of this work is to develop and implement an integrated multibody methodology to be applied to the dynamic analysis of biomechanical systems in general and to the human body in particular. Two different types of dynamic analyses can be performed using the proposed methodology: forward dynamic analyses and inverse dynamic analyses. The first type of analysis predicts the dynamic response of the biomechanical system to external applied forces while the latter type predicts the internal and external forces developed at the joints and by biological actuators to produce an observed dynamic response.

Both types of analyses require the construction of the equations of motion of the biomechanical system and the accurate description of its kinematic structure. For that purpose, a multibody formulation using fully Cartesian coordinates is introduced and described in detail in Chapter 2. This formulation allows for general, three-dimensional, multibody systems to be modeled and for the respective equations of motion to be assembled and solved in a systematic way. This multibody methodology plays a very important role, since it is, from the mathematical point-of-view, the supporting structure used to describe and construct all the mechanical and biomechanical systems implemented in this work.

Common to almost every biomechanical analysis is the use of appropriate and accurate biomechanical models. These models are used to represent the human body in terms of its anthropometry, physiology and topology. Many biomechanical models have been developed, with different purposes and using different approaches, depending on the nature of the research, the objectives of the analysis and the expected results. In Chapter 3, two whole body response biomechanical models are defined using the multibody formulation described in detail in Chapter 2.

In Chapter 4, the methodologies and models presented in the two previous chapters are applied to five different illustrative test cases that not only demonstrate the possibilities of the application of the proposed formulation to a wide variety of situations but also allow for the verification of the biofidelity of the models, i.e., the overall behavior of the dynamic response of the models in terms of the displacements and motions obtained, which should be similar to average data generated with human volunteers or cadavers.

All the examples presented in Chapter 4 involve situations in which the main objective is to determine the human response to a particular external event involving impact. Depending on the example, this external event can be a football tackle, a pedestrian run-over or a sudden deceleration field produced by a car crash. Due to the nature and objectives of the simulations, a forward dynamics approach is used in all the analyses performed in this chapter.

Inverse dynamic analysis of a complex human task usually requires a large collection of input data. This input data is comprised of three distinct types of information: anthropometric information regarding the dimensions of the anatomical segments, the total body mass and height; kinematic information in which a set of trajectories of points, located in the joints and extremities of the biomechanical model, is used to describe its motion in a unique way; and dynamic information describing all the external applied forces to the biomechanical model. The information comprised in these three data sets is obtained either experimentally or from direct anthropometric measurements on the subject and, therefore, is prone to errors and uncertainties. These errors and uncertainties can drastically change the outcome of the analysis, producing poor quality results that might mislead the conclusions. The objectives of Chapter 5 are to identify the most common sources of uncertainties that affect the input data of an inverse dynamic analysis and to propose a set of numerical techniques that, when applied to this data, contribute to reducing this problem considerably. These techniques are: motion reconstruction methods that are used to reconstruct the three dimensional motion of the biomechanical model from two dimensional information, obtained from at least two video cameras; noise reduction procedures that are used to reduce the high frequency noise levels introduced during the digitization process; and kinematic consistency techniques that are used to ensure that the kinematic data is coherent with the anthropometric data, in any instant of

the inverse dynamic analysis. The methods and techniques described in Chapter 5 are general and can be applied to the inverse dynamic analysis of determinate or indeterminate problems.

Chapter 5 ends with a thorough analysis of the sensitivity of the results to imprecise input data. For this purpose, several inverse dynamic analyses are performed on the proposed gait application, with the following input parameters perturbed independently: masses of the head, hand, lower torso, upper and lower leg anatomical segments; Cartesian coordinates of anatomical points of the top of the head and knee; ground reaction force of the right foot; and coordinates of the application point of the ground reaction force of the right foot. This sensitivity analysis allows for the identification of the most relevant sources of error that lead to a decrease in the quality of the results.

In Chapter 6, the major issues involving the construction and solution of indeterminate biomechanical problems and the subsequent calculation of the redundant muscle forces are addressed in detail. A brief review of the muscle anatomy and physiology is carried out, in order to highlight the most relevant issues associated with the development of muscle models. Afterwards, the 'redundant problem in biomechanics' is identified and the concepts of muscle actuator and muscle actuator equations are introduced in the framework of the proposed multibody formulation. With each muscle actuator is associated a muscle model that simulates the muscle activation-contraction dynamics. In the present work, a Hill type muscle model is applied, with the force produced by the muscle contractile element calculated as a function of the muscle activation, maximum isometric peak force, muscle length and muscle rate of shortening.

The optimization problem is stated in Chapter 6, in the framework of multibody dynamics and it is subsequently applied to the solution of indeterminate biomechanical models with redundant muscle action. Different performance criteria are presented and their application to the calculation of the muscle forces developed in the locomotor apparatus of a subject during a normal cadence stride period is analyzed.

Finally, in Chapter 7, overall conclusions are drawn and several perspectives of future work and developments are described.

Chapter 2

Multibody Dynamics With Fully Cartesian Coordinates

The study and analysis of mechanical systems that undergo large displacements and rotations has always been a challenge for the scientific community due to the importance and relevance of the results they produce and also due to the complexity and non-linearity of the equations involved. The techniques and methods used in this type of analysis have evolved from a manual graphics art to a highly specialized research field where the kinematics and dynamics of complex mechanical systems are evaluated. With the growing development of computers, many elegant methods of analytical dynamics that were especially tailored to analyze specific mechanisms are being gradually substituted by efficient computer codes that, using multibody approaches, allow for the systematic formulation and solution of the equations of motion of general mechanical systems with high levels of complexity.

In this chapter, a multibody formulation, using fully Cartesian coordinates, is described (Jalón and Bayo, 1994; Silva, 1996). This formulation allows for general three-dimensional multibody systems to be modeled and the respective equations of motion to be assembled and solved in a systematic way. The proposed methodology plays a very important role since it is,

from the mathematical point-of-view, the supporting structure used to describe and construct all the mechanical and biomechanical systems implemented in this work.

2.1 Introduction to Fully Cartesian Coordinates

Before addressing the problem of modeling mechanical systems with fully Cartesian coordinates, it must be stated that, in the scope of the present work, a mechanical system (or multibody system), is a collection of rigid elements (or rigid bodies), interconnected by kinematic pairs (or joints) and acted upon by external applied forces, as depicted in Figure 2.1. Kinematic pairs are elements that are introduced in the mechanical system to constrain the relative motion between rigid bodies.

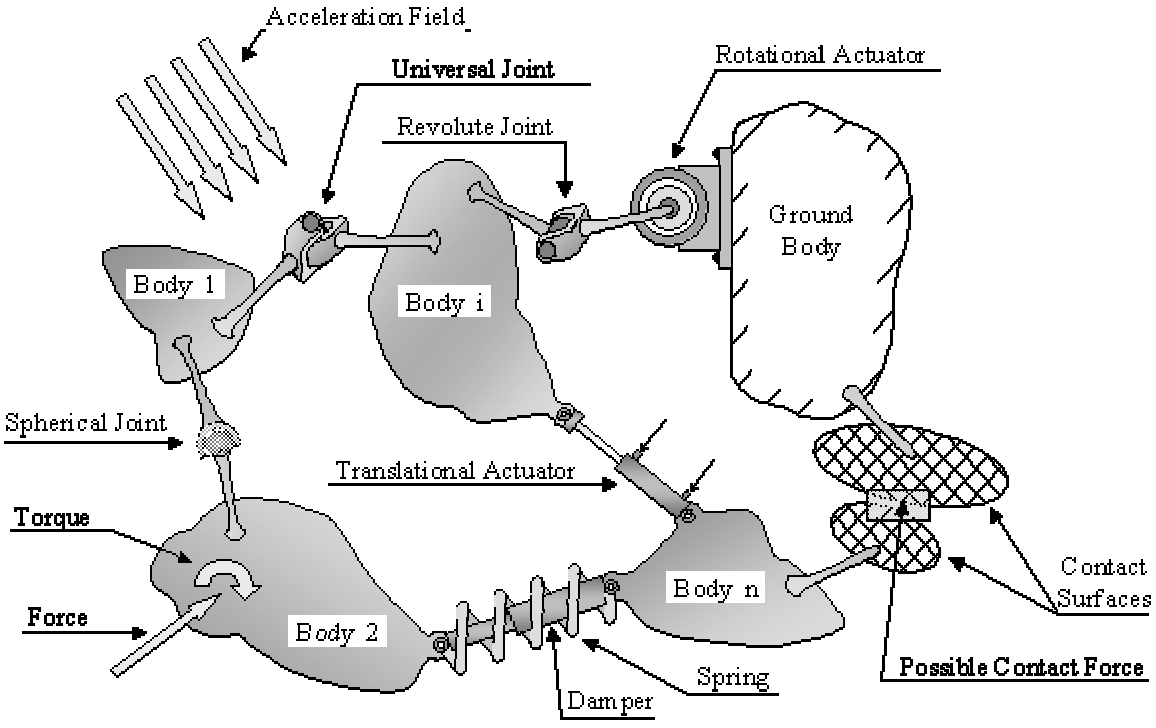

Figure 2.1: General mechanical system modeled using a multibody approach. The most significant elements are described as rigid bodies interconnected by kinematic joints. External applied forces, with different levels of complexity, are applied to rigid bodies in order to simulate the interactions among elements and between these and the surrounding environment. Driving actuators are also represented showing that the relative motion between rigid bodies can be prescribed.

Mathematically, kinematic pairs are algebraic equations that introduce kinematic relations between the coordinates describing the mechanical system, in such a way that the number of degrees-of-freedom between elements is reduced to the number of degrees-of-freedom allowed by the specific joint. External applied forces are represented by force elements that are applied to rigid bodies, modifying their dynamic response and the overall motion of the system. These force elements are introduced to express the interaction between rigid bodies and the surrounding environment. There are many types of external applied forces, depending on the type and level of complexity of the interactions to simulate. An external applied force can be as simple as a constant force or torque applied to an element or as complex as a non-linear force in which the magnitude, line-of-action and point-of-application depend not only on the actual configuration of the mechanical system – in terms of its position and velocity – but also on the geometry of rigid bodies and on the physical characteristics of the materials involved. Just to mention some of the applications to biomechanics and vehicle design, external applied forces can be used to model the contact between the biomechanical model and the ground or with the dashboard and interior trimmings of a car; to simulate the impact of a car with a wall or a rigid obstacle; to model the forces exerted by seat belts, airbags and seats on a vehicle occupant or to model the springs and dampers of a complex car suspension system.

When designing mechanical systems, there are essentially three types of analyses that can be performed: kinematic analyses, forward dynamic analyses and inverse dynamic analyses. Common to all types of kinematic and dynamic analyses, a set of coordinates must be specified to describe, in a unique way, the position and orientation of each element of the multibody system. There are many ways of describing the position and orientation of a mechanical system, or in other words, there are many types of coordinates capable of successfully performing that important task. As discussed in Chapter 1, advantages and drawbacks can be pointed out for any type of coordinates used. In the present work, the principal motivation for choosing fully Cartesian coordinates (also called natural coordinates)

(Jalón and Bayo, 1994), are some innovative aspects that are used with the biomechanical applications shown.

When using fully Cartesian coordinates, the position and orientation of a rigid body in a three-dimensional space are described using the Cartesian coordinates of a set of points and unit vectors. As shown in Figure 2.2(a), points are usually located in relevant positions of the mechanical system such as joints and extremities of rigid bodies, while vectors are typically used to define rotational and direction axes for kinematic joints. This process of describing rigid bodies, using the Cartesian coordinates of points and vectors, presents one of the major advantages of this formulation since there is no need to introduce any kind of angular variables such as Euler or Bryant angles or Euler parameters to define the rotation and orientation of each element. In fact, this important information is introduced implicitly with the Cartesian coordinates of the points and vectors.

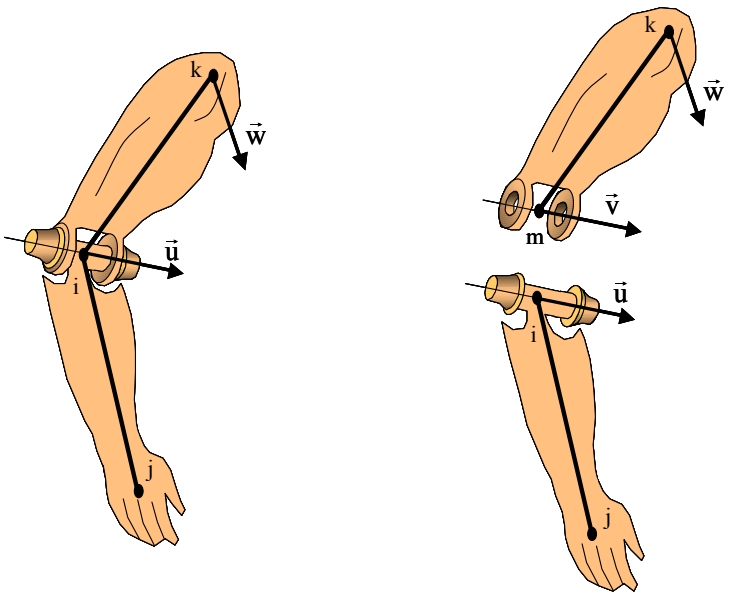

Figure 2.2: Example of a mechanical system described with fully Cartesian coordinates: rigid bodies are defined using the Cartesian coordinates of a set of points and vectors that are located at the joints and extremities of the elements. (a) Assembled mechanical system with a revolute joint created sharing point *i* and vector **u**. (b) The same mechanical system with the revolute joint created using independent points *i* and *m* and independent vectors **u** and **v**.

Another important aspect of this formulation, also shown in Figure 2.2(a), is the possibility of two adjacent rigid bodies sharing points and vectors. This unique characteristic has the advantage of reducing the number of coordinates necessary to describe the system as well as the number of algebraic equations needed to define kinematic pairs. The number of coordinates is reduced because when two bodies share, for instance, one point, its Cartesian coordinates contribute to the definition of the position and orientation of both rigid bodies. The number of algebraic equations is also reduced since some of the kinematic relations used in the definition of the system's topology – in terms of its kinematic pairs – are implicitly introduced and therefore there is no need to introduce them explicitly as new constraint equations.

This apparent advantage can later become a drawback if the internal reaction forces, developed in the joints, need to be known during the analysis. As will be seen later, if one of the objectives is to obtain the reaction forces at the joints of the mechanism, this feature should not be used since there is no explicit kinematic information describing part of the kinematic pairs. Consequently, an expanded multibody system, such as the one depicted in Figure 2.2(b), containing no shared points or vectors must be described instead.

In order to perform a kinematic or dynamic analysis of a general mechanical system, the Cartesian coordinates of every point and vector used in its description are grouped in column vector **q**. These coordinates are also designated by generalized coordinates since they define, in a unique way, the configuration of the system at any instant of time. The vector that holds these coordinates is named vector of generalized coordinates and is organized as follows:

$$\mathbf{q} = \left\{ \begin{array}{ccccccccccccc} x_{P_1} & y_{P_1} & z_{P_1} & \cdots & x_{P_n} & y_{P_n} & z_{P_n} & x_{V_1} & y_{V_1} & z_{V_1} & \cdots & x_{V_m} & y_{V_m} & z_{V_m} \end{array} \right\}^{\mathrm{T}} \tag{2.1}$$

where the index P refers to points, the index V refers to unit vectors and x, y and z represent either coordinates of a point or components of a vector in the three Cartesian directions. The subscripts n and m are respectively the total number of points and the total number of vectors used to describe the mechanism. Considering the organization of vector **q**, the total number

of generalized coordinates is given by $nc = 3(n+m)$, i.e., three times the sum of the number of points with the number of unit vectors of the system.

Depending on the type of coordinates that is being used and on the topology of the mechanical system under analysis, the general coordinates in vector $\mathbf{q}$ are said to be independent if they can vary independently; or dependent if they are related by algebraic expressions. In multibody formulations with fully Cartesian coordinates, the generalized coordinates describing the mechanical system are always dependent and, due to that reason, several algebraic equations need to be introduced to relate them. These equations usually arise from the description of the topology of the system, i.e., the type of joints and rigid bodies, and also from the description of the driver actuators used to guide the mechanism through the analysis. These algebraic equations are called kinematic constraint equations and they are gathered in column vector $\mathbf{\Phi}$. From the kinematic point of view, these equations must be fulfilled at every instant of time, giving rise to the following expression:

$$\mathbf{\Phi}(\mathbf{q},t) = \begin{Bmatrix} \mathbf{\Phi}_1(\mathbf{q}) \\ \vdots \\ \mathbf{\Phi}_{ns}(\mathbf{q}) \\ \mathbf{\Phi}_{ns+1}(\mathbf{q},t) \\ \vdots \\ \mathbf{\Phi}_{ns+nr}(\mathbf{q},t) \end{Bmatrix} = \mathbf{0} \tag{2.2}$$

where $\mathbf{\Phi}_i$ represent the i^{th} kinematic constraint equation, *ns* the total number of scleronomic constraints, *nr* the total number of rheonomic constraints and **0** the null vector. Considering the organization of vector $\mathbf{\Phi}$, the total number of holonomic constraints is given by $nh = ns + nr$, i.e., the number of scleronomic constraints plus the number of rheonomic constraints. Scleronomic constraints are kinematic constraints in which the time variable does not appear explicitly in the algebraic equation while in rheonomic constraints this dependency

is explicit. As will be seen later, scleronomic constraints are usually applied to express rigid body properties and to define kinematic pairs, while rheonomic constraints are associated with driver actuators. Both types are holonomic constraints, i.e., they result from Pfaffian forms that are perfect differentials (Meirovitch, 1970). Although multibody methodologies are capable of dealing with non-holonomic constraints – such as the ones often arising when modeling the rolling of a disc or a wheel on a surface – that type of kinematic restrictions is not used in this work.

2.2 Kinematic Analysis

When performing a kinematic analysis, the motion of the system is studied independently of the external forces that produce it. In particular, in a kinematic analysis the position, velocity and acceleration of every element of the system are obtained and analyzed. However, since forces are not considered, the motion of the system must be specified to some extent, i.e., the position, velocity and acceleration of some driving elements must be prescribed, while the position, velocity and acceleration of the remaining elements are obtained using the kinematic constraint equations that describe the topology of the system, its kinematic pairs and rigid body properties, expressed in the form of Equation (2.2).

The kinematic consistent positions, i.e., the positions acquired by the mechanical system that satisfy, in every instant of the analysis, the kinematic constraint equations, are obtained by solving Equation (2.2) in respect to the vector of generalized coordinates $\mathbf{q}$. Due to the non-linear nature of the kinematic constraints, Equation (2.2) represents a system of non-linear equations that, in the present work, is solved using the Newton-Raphson method. This iterative method achieves quadratic convergence near the solution and it involves the linearization of Equation (2.2), which results from its replacement by the first two terms of its expansion in a Taylor series, evaluated with an initial approximation vector $\mathbf{q}_i$. In this way, for a given time *t*, Equation (2.2) is rewritten as:

$$\boldsymbol{\Phi}(\mathbf{q},t) \cong \boldsymbol{\Phi}(\mathbf{q}_i,t) + \boldsymbol{\Phi}_{\mathbf{q}}(\mathbf{q}_i)(\mathbf{q}-\mathbf{q}_i) = \mathbf{0} \tag{2.3}$$

which represents a system of linear equations. The term $\mathbf{\Phi}_{\mathbf{q}}\left(\mathbf{q}_i\right)$ is the Jacobian matrix of the constraints, evaluated at the approximate solution $\mathbf{q}_i$.

Bearing in mind that the Newton-Raphson method is an iterative procedure, then $\mathbf{q}=\mathbf{q}_{i+1}$ represents an approximate solution of Equation (2.2) for the next iteration. Defining $\Delta\mathbf{q}_i=\mathbf{q}_{i+1}-\mathbf{q}_i$ as the residual for the actual iteration, then Equation (2.3) yields:

$$\mathbf{\Phi}_{\mathbf{q}}\left(\mathbf{q}_i\right)\Delta\mathbf{q}_i=-\mathbf{\Phi}\left(\mathbf{q}_i\right) \tag{2.4}$$

Equation (2.4) represents the iterative scheme used in the Newton-Raphson method, which is used repeatedly until the norm of the residual $\Delta\mathbf{q}_i$ is less than a specified tolerance. The Jacobian matrix of the constraints is defined as the matrix that contains the partial derivatives of each kinematic constraint with respect to the vector of generalized coordinates. Mathematically, this matrix is expressed as:

$$\mathbf{\Phi}_{\mathbf{q}}\left(\mathbf{q}\right)=\frac{\partial\Phi_m}{\partial q_n}=\begin{bmatrix} \dfrac{\partial\Phi_1}{\partial q_1} & \dfrac{\partial\Phi_1}{\partial q_2} & \cdots & \dfrac{\partial\Phi_1}{\partial q_{nc}} \\ \dfrac{\partial\Phi_2}{\partial q_1} & \ddots & & \\ \vdots & & \ddots & \vdots \\ \dfrac{\partial\Phi_{nh}}{\partial q_1} & \cdots & \cdots & \dfrac{\partial\Phi_{nh}}{\partial q_{nc}} \end{bmatrix} \tag{2.5}$$

In multibody formulations using fully Cartesian coordinates, the Jacobian matrix of the constraints does not depend explicitly on the time variable and it is, for the large majority of mechanical systems, a sparse matrix containing partial derivatives that are very simple to calculate and evaluate. This important characteristic can be exploited from the computational point-of-view, using appropriate sparse matrix solvers that reduce the total allocation size and increase the overall performance of the computer code.

Before addressing the calculation of the velocities and accelerations of the mechanical system, a remark must be made on the problem arising from the existence of redundant

constraints in the vector $\mathbf{\Phi}(\mathbf{q},t)$. Due to the automatic generation of the kinematic constraint equations in a multibody code or because the mechanism under analysis is over constrained, many multibody formulations generate redundant constraint equations that physically express the same topological restrictions. Mathematically, these redundant constraints contribute with linearly dependent lines to the Jacobian matrix, making this matrix rank-deficient. With a rank deficient Jacobian matrix, Equation (2.4) no longer allows for the calculation of the generalized coordinate vector and the kinematic analysis cannot proceed. Different methods can be applied to overcome this difficulty. In the present work, the least-squares formulation is used with its iterative scheme defined as (Jalón and Bayo, 1994):

$$\mathbf{\Phi}_{\mathbf{q}}^{\mathrm{T}}\left(\mathbf{q}_i\right)\mathbf{\Phi}_{\mathbf{q}}\left(\mathbf{q}_i\right)\Delta\mathbf{q}_i = -\mathbf{\Phi}_{\mathbf{q}}^{\mathrm{T}}\left(\mathbf{q}_i\right)\mathbf{\Phi}\left(\mathbf{q}_i\right) \tag{2.6}$$

which represents a system of linear equations obtained from the pre-multiplication of Equation (2.4) by the transpose of the Jacobian matrix. The leading matrix in Equation (2.6) is no longer rank-deficient and the algorithm converges to a solution that satisfies all the constraint equations. Computationally, the product $\mathbf{\Phi}_{\mathbf{q}}^{\mathrm{T}}\left(\mathbf{q}_i\right)\mathbf{\Phi}_{\mathbf{q}}\left(\mathbf{q}_i\right)$ represents an additional calculation effort that can be minimized considering that the matrices involved are sparse and that the resulting matrix is symmetric.

The velocities of the elements describing the mechanical system are calculated using the velocity constraint equations. These equations, obtained differentiating Equation (2.2) with respect to time, are:

$$\dot{\mathbf{\Phi}}\left(\mathbf{q},\dot{\mathbf{q}},t\right) = \frac{d\mathbf{\Phi}(\mathbf{q},t)}{dt} = \frac{\partial\mathbf{\Phi}(\mathbf{q},t)}{\partial t} + \frac{\partial\mathbf{\Phi}(\mathbf{q},t)}{\partial\mathbf{q}}\frac{d\mathbf{q}}{dt} = \mathbf{0} \tag{2.7}$$

where the term $\partial\mathbf{\Phi}(\mathbf{q},t)/\partial t$ is the vector containing the partial derivatives of the constraints with respect to time, the term $\partial\mathbf{\Phi}(\mathbf{q},t)/\partial\mathbf{q}$ is the Jacobian matrix of the constraints, already defined in Equation (2.5), and the term $d\mathbf{q}/dt$ is the vector of generalized velocities $\dot{\mathbf{q}}$, containing the velocities of each point and unit vector used in the definition of the mechanical

system. Defining vector $\mathbf{v}(t)$ as the right-hand-side of the velocity equation, the previous expression is rewritten as follows:

$$\mathbf{\Phi}_{\mathbf{q}}\dot{\mathbf{q}} = \mathbf{v} \tag{2.8}$$

where

$$\mathbf{v}(t) = -\frac{\partial \mathbf{\Phi}(\mathbf{q}, t)}{\partial t} \tag{2.9}$$

Only rheonomic constraints, associated with driver equations, contribute with non-zero entries to this vector. Moreover, it is assumed that this vector does not present any explicit dependency on the vector of generalized coordinates.

The calculation of the generalized acceleration vector, i.e., the vector that contains the accelerations associated with all the points and unit vectors defining the mechanical system under analysis, is performed following the same steps used in the velocity analysis. The equations that express the accelerations of the components of the mechanical system are obtained by differentiating the velocity constraint equations, given in Equation (2.8), with respect to time. The resulting acceleration constraint equations are:

$$\ddot{\mathbf{\Phi}}(\mathbf{q}, \dot{\mathbf{q}}, \ddot{\mathbf{q}}, t) = \frac{d\dot{\mathbf{\Phi}}(\mathbf{q}, \dot{\mathbf{q}}, t)}{dt} = \mathbf{\Phi}_{\mathbf{q}}\ddot{\mathbf{q}} + \left(\mathbf{\Phi}_{\mathbf{q}}\dot{\mathbf{q}}\right)_{\mathbf{q}}\dot{\mathbf{q}} + \mathbf{v}_t = \mathbf{0} \tag{2.10}$$

where $\mathbf{v}_t$ is the vector containing the partial derivatives of vector $\mathbf{v}$ with respect to time. Introducing vector $\boldsymbol{\gamma}$ as the right-hand-side of the acceleration equation, then previous expression is rewritten as:

$$\mathbf{\Phi}_{\mathbf{q}}\ddot{\mathbf{q}} = \boldsymbol{\gamma} \tag{2.11}$$

where

$$\boldsymbol{\gamma}(\mathbf{q}, \dot{\mathbf{q}}, t) = \mathbf{v}_t - \left(\mathbf{\Phi}_{\mathbf{q}}\dot{\mathbf{q}}\right)_{\mathbf{q}}\dot{\mathbf{q}} \tag{2.12}$$

A closer observation of Equations (2.8) and (2.11) shows that both expressions represent systems of linear equations, with the same leading matrix and different right-hand side vectors. Moreover, since both expressions share the same leading matrix – the Jacobian matrix of the constraints, evaluated with the latest calculated configuration of the system – then this matrix only needs to be factorized one time. In the presence of redundant constraint equations, the procedure described in Equation (2.6) is also applied to velocity and acceleration analysis, in order to allow for the solution of the systems of equations involved.

2.3. Constraint Equations

In the previous section the general form of the equations used in kinematic analyses of mechanical systems were provided. The terms involved in these equations appear in a generic sense and do not yet reflect the type of coordinates in use. It is the purpose of this section to introduce the most common types of kinematic constraints arising with fully Cartesian coordinates as well as to calculate their respective contribution to the Jacobian matrix of the constraints and to the right-hand side of the velocity and acceleration equations. Not all types of kinematic constraints, used in fully Cartesian coordinates, are described here. In this section only the kinematic constraints relevant to the work now presented are discussed. For the description of other types of kinematic constraints, the interested reader is referred to the work of other authors (Jalón and Bayo, 1994).

When analyzing mechanical systems with fully Cartesian coordinates there are essentially three types of kinematic constraints to be considered: rigid body constraints that are responsible for maintaining the rigid body characteristics of each element of the mechanical system; joint constraints that are applied in the definition of the kinematic pairs and topology of the mechanism; and driver constraints that are used to prescribe the motion of the system's driving elements.

The kinematic constraint equations required to define the rigid body characteristics and rotational drivers' constraint equations are similar from the mathematical point of view. Accordingly, both types of constraint equations are presented together in the next section.

2.3.1 Rigid Body Constraints and Rotational Driver Constraints

Rigid body constraints are introduced in the analysis to preserve rigid body properties. For a given element, the number of rigid body constraints is equal to the difference between the number of Cartesian coordinates defining it and the number of degrees-of-freedom of a general unconstrained rigid body in space, i.e., six degrees-of-freedom. Considering that a rigid body is described with fully Cartesian coordinates by a collection of points and unit vectors, its rigid body properties are associated with the preservation of constant distances between any two points of the element or with the preservation of constant angles between any two vectors. For instance, consider the rigid body depicted in Figure 2.3(a), which is used to define the feet of one of the biomechanical models used in this work. This rigid body is defined with twelve generalized coordinates associated with the three points (i, j and k) and unit vector **a**. Therefore, the kinematic description of this body is completed with the introduction of six constraint equations. These equations are responsible for maintaining the unit norm of vector **a**, the constant length of segments $\overline{ij}$ and $\overline{ik}$, and the constant angle between segments $\overline{ij}$ and $\overline{ik}$ and between vector **a** and segments $\overline{ij}$ and $\overline{ik}$.

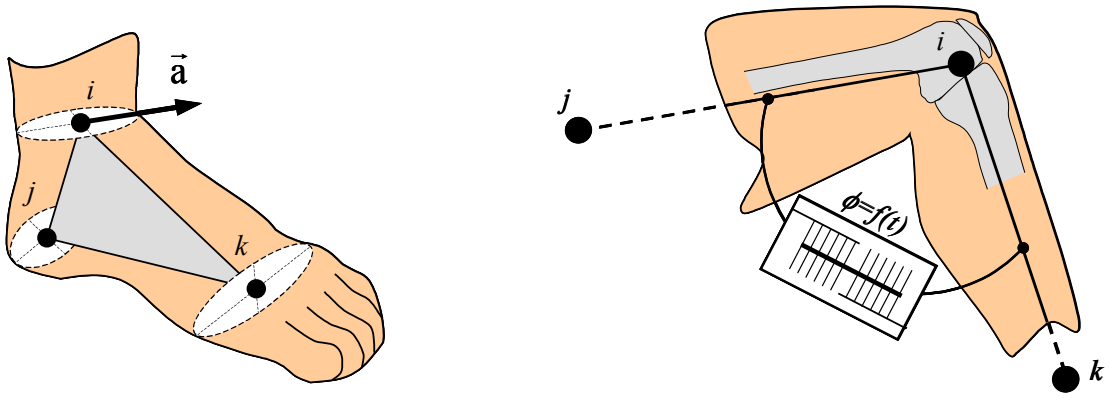

(a) (b)

Figure 2.3: Rigid body and rotational driver constraints. (a) Rigid body constraints used to define the kinematics of a rigid body described by 3 points and 1 unit vector. (b) Rotational driver constraint used to guide the knee joint. The function $\phi=f(t)$ describes the evolution in time of the angle formed by the rigid bodies defining the femur and tibia.

Although having different physical meanings, all of these kinematic restrictions can be defined mathematically with the same algebraic equation, i.e., with the equation describing the scalar product between two generic vectors **u** and **v**, given by:

$$\mathbf{\Phi}^{\mathrm{SP}}(\mathbf{q},t) = \mathbf{v}^{\mathrm{T}}\mathbf{u} - L_{\mathrm{v}}L_{\mathrm{u}}\cos\left(\langle \mathbf{v},\mathbf{u}\rangle(t)\right) = 0 \tag{2.13}$$

where L_{v} and L_{u} are the lengths of vectors **v** and **u** and $<\mathbf{v},\mathbf{u}>(t)$ is the angle defined between them. It should be noted that Equation (2.13), in this general form, expresses a rheonomic constraint in which the angle $<\mathbf{v},\mathbf{u}>(t)$ can vary in time. This equation can be used not only to express rigid body constraints, in which the angle between the vectors is kept constant throughout the analysis, but also to apply to the definition of rotational driver actuators, such as the one presented in Figure 2.3(b), which is used to drive the degree-of-freedom of the knee joint of one of the biomechanical models described in this work.

In Table 2.1 a full description of the possible applications of the scalar product constraint is presented. Each line contains an application of this constraint equation together with the values that the terms appearing in Equation (2.13) must assume in order to express the desired physical meaning.

As seen in Equation (2.13), the scalar product constraint presents a quadratic dependency on the generalized coordinates. Consequently, the contribution of this constraint equation to the Jacobian matrix of the constraints is linear. This feature produces partial derivatives that are very simple to evaluate, contributing to increases in the numerical and computational efficiency of the proposed multibody methodology. Referring again to Equation (2.5), the contribution of the scalar product constraint to the Jacobian matrix is given by:

$$\mathbf{\Phi}_{\mathbf{q}}^{\mathrm{SP}} = \frac{\partial(\mathbf{v}^{\mathrm{T}}\mathbf{u})}{\partial\mathbf{q}} = \mathbf{u}^{\mathrm{T}}\frac{\partial\mathbf{v}}{\partial\mathbf{q}} + \mathbf{v}^{\mathrm{T}}\frac{\partial\mathbf{u}}{\partial\mathbf{q}} = \begin{bmatrix}\mathbf{0}^{\mathrm{T}} & \cdots & \mathbf{u}^{\mathrm{T}} & \cdots & \mathbf{0}^{\mathrm{T}} & \cdots & \mathbf{v}^{\mathrm{T}} & \cdots & \mathbf{0}^{\mathrm{T}}\end{bmatrix} \tag{2.14}$$

where the only non-zero entries are those associated with the generalized coordinates used in the calculation of vectors **v** and **u**.

Table 2.1: The most common applications of the scalar product constraint and their respective physical meaning. Vectors $\mathbf{r}_i$, $\mathbf{r}_j$, $\mathbf{r}_k$ and $\mathbf{r}_l$ are the Cartesian coordinates of points i, j, k and l and unit vectors **a** and **b**, used in the definition of rigid bodies.

Constraint Description	**v**	**u**	L_v	L_u	<**v**,**u**>	Graphical representation
Constant distance between points i and j.	$(\mathbf{r}_j-\mathbf{r}_i)$	$(\mathbf{r}_j-\mathbf{r}_i)$	L_{ij}	L_{ij}	0	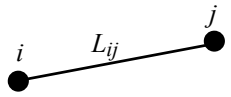
Unit vector.	**a**	**a**	1	1	0	
Constant angle between unit vectors **a** and **b**.	**a**	**b**	1	1	α	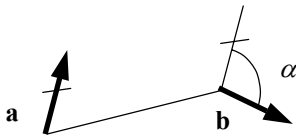
Constant angle between segment $\mathbf{r}_{ij}$ and unit vector **a**.	$(\mathbf{r}_j-\mathbf{r}_i)$	**a**	L_{ij}	1	β	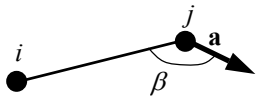
Constant angle between segments $\mathbf{r}_{ij}$ and $\mathbf{r}_{kl}$.	$(\mathbf{r}_j-\mathbf{r}_i)$	$(\mathbf{r}_l-\mathbf{r}_k)$	L_{ij}	L_{kl}	γ	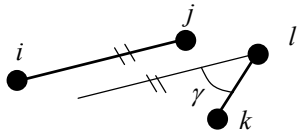
Orthogonal unit vectors.	**a**	**b**	1	1	$\pi/2$	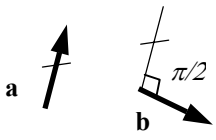
Rotational driver about a revolute joint located in point i, using segments $\mathbf{r}_{ij}$ and $\mathbf{r}_{ik}$.	$(\mathbf{r}_j-\mathbf{r}_i)$	$(\mathbf{r}_k-\mathbf{r}_i)$	L_{ij}	L_{ik}	$\phi=f(t)$	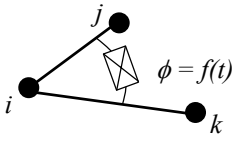
Translational driver defined between point i and point j belonging to different rigid bodies.	$(\mathbf{r}_j-\mathbf{r}_i)$	$(\mathbf{r}_j-\mathbf{r}_i)$	$L=f(t)$	$L=f(t)$	0	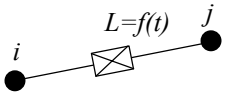

In the case of having **v** or **u** associated with two-point segments, the Jacobian entries must reflect that dependency, i.e., considering that $\mathbf{v} = \mathbf{r}_j - \mathbf{r}_i$, then Equation (2.14) becomes:

$$\mathbf{\Phi}_{\mathbf{q}}^{\mathrm{SP}} = \mathbf{u}^{\mathrm{T}} \left(\frac{\partial \mathbf{r}_j}{\partial \mathbf{q}} - \frac{\partial \mathbf{r}_i}{\partial \mathbf{q}} \right) + \mathbf{v}^{\mathrm{T}} \frac{\partial \mathbf{u}}{\partial \mathbf{q}} = \begin{bmatrix} \mathbf{0}^{\mathrm{T}} & \cdots & -\mathbf{u}^{\mathrm{T}} & \cdots & \mathbf{u}^{\mathrm{T}} & \cdots & \mathbf{0}^{\mathrm{T}} & \cdots & \mathbf{v}^{\mathrm{T}} & \cdots & \mathbf{0}^{\mathrm{T}} \end{bmatrix} \quad (2.15)$$

The contributions of the scalar product constraint to the right-hand side of the velocity and acceleration constraint equations are respectively given by:

$$\nu^{\mathrm{SP}}(t) = -L_{\mathbf{v}} L_{\mathbf{u}} \sin\left(\langle \mathbf{v}, \mathbf{u} \rangle (t) \right) \frac{\partial \langle \mathbf{v}, \mathbf{u} \rangle (t)}{\partial t} \quad (2.16)$$

and

$$\gamma^{\mathrm{SP}}(\dot{\mathbf{q}}, t) = \nu_t^{\mathrm{SP}}(t) - 2\left(\dot{\mathbf{v}}^{\mathrm{T}} \dot{\mathbf{u}} \right) \quad (2.17)$$

where

$$\nu_t^{\mathrm{SP}}(t) = -L_{\mathbf{v}} L_{\mathbf{u}} \left[\cos\left(\langle \mathbf{v}, \mathbf{u} \rangle (t) \right) \left(\frac{\partial \langle \mathbf{v}, \mathbf{u} \rangle (t)}{\partial t} \right)^2 + \sin\left(\langle \mathbf{v}, \mathbf{u} \rangle (t) \right) \frac{\partial^2 \langle \mathbf{v}, \mathbf{u} \rangle (t)}{\partial t^2} \right] \quad (2.18)$$

For rigid body constraints, in which there is no explicit dependency on time, Equations (2.16) and (2.17) are simplified considering that $\nu^{\mathrm{SP}}(t) = \nu_{\mathrm{t}}^{\mathrm{SP}}(t) = 0$.

2.3.2 Linear Combination Constraints

In most mechanical systems modeled with fully Cartesian coordinates, the kinematic structure of rigid bodies is defined using the procedure described in the previous section. However, there are applications in which the rigid bodies have a much more complex kinematic structure that needs to be defined using a wider collection of points and unit vectors. That is the case, for instance, of rigid bodies describing vehicles' chassis, where many points and unit vectors need to be introduced to define the complex structure of points' attachments used to define the front and rear suspensions.

For these complex bodies, a two-step procedure is used to describe their rigid body properties. First, three vectors (or a combination of vectors and segments) are selected, from the set of points and vectors defining the body, to form a vector base. The rigid body properties of the base vectors are described using the standard procedure with the scalar product constraint. Second, the positions and orientations of all other points and vectors are described as linear combination constraints of the vectors defining the base.

To demonstrate this procedure, consider again the rigid body describing the foot of the biomechanical model but, at this time, instead of using the kinematic structure depicted in Figure 2.3(a), a new structure is proposed, as presented in Figure 2.4, which allows for simulation of the metatarsal-phalangeal joint, after the introduction of an additional point and rigid body.

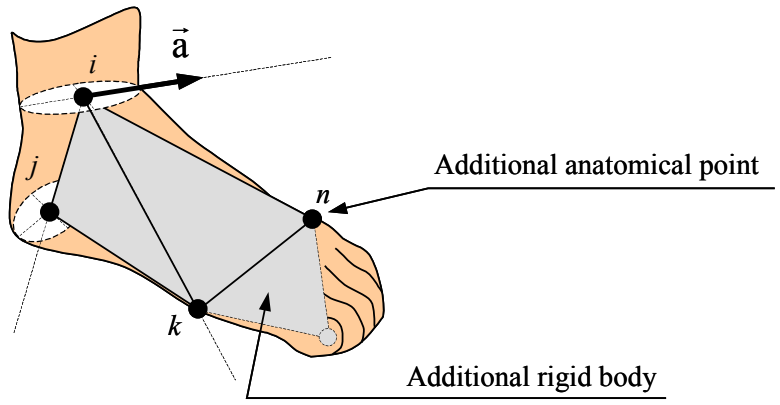

Figure 2.4: Rigid bodies defined with more complex kinematic structures. In the present example, point *n* is expressed as a linear combination of the vectors forming the reference frame defined by the dashed lines.

Using this new kinematic structure, the rigid body describing the foot is defined using four points (*i*, *j*, *k* and *n*) and unit vector **a**. The procedure proposed for describing complex rigid bodies is applied and a vector base is created using vector **a** and segments $\overline{ij}$, $\overline{ik}$. The rigid body properties of those vectors and segments are exactly the same as the ones introduced in the previous section for the rigid body describing the foot. Finally, the position of the

additional point n is defined as a linear combination of the vector base expressed by the following constraint equation:

$$\mathbf{\Phi}^{\mathrm{LC}}\left(\mathbf{q}\right) = \mathbf{r}_{in} - \alpha_1 \mathbf{r}_{ij} - \alpha_2 \mathbf{r}_{ik} - \alpha_3 \mathbf{a} = \mathbf{0} \tag{2.19}$$

where the coefficients α_i represent the coordinates of point n in the vector base, which are calculated in the beginning of the analysis and maintained constant thereafter. It should be noted that Equation (2.19) represents three algebraic equations, with a linear dependency on the generalized coordinates. This linear dependency is also the main reason that justifies the use of this constraint to describe the kinematics of complex rigid bodies, since it introduces constant coefficients in the Jacobian matrix of the constraints and it leads to null right-hand sides in the velocity and acceleration constraint equations.

2.3.3 Kinematic Joint Constraints

Kinematic joint constraints are used to describe the relative motion between the different elements of a mechanical system. Joint kinematic constraints are algebraic equations that relate the generalized coordinates of two different rigid bodies, constraining their relative motion and reducing their number of allowable degrees-of-freedom. In mechanical systems described with fully Cartesian coordinates, many of these kinematic restrictions arise naturally by being described implicitly by sharing points and unit vectors between different rigid bodies. If the calculation of joint reaction forces is not required for the analysis, this feature, inherent to the proposed multibody formulation, is considered an advantage since it significantly reduces the number of joint constraint equations of the system.

In the present work, only the kinematic joints used in the construction of the forthcoming biomechanical models are described in this section. These joints are the spherical joint, the revolute joint and the universal joint, as schematically represented in Figure 2.5. For the formulation and construction of other types of joints, procedures similar to the ones presented hereafter can be adopted (Jalón and Bayo, 1994).

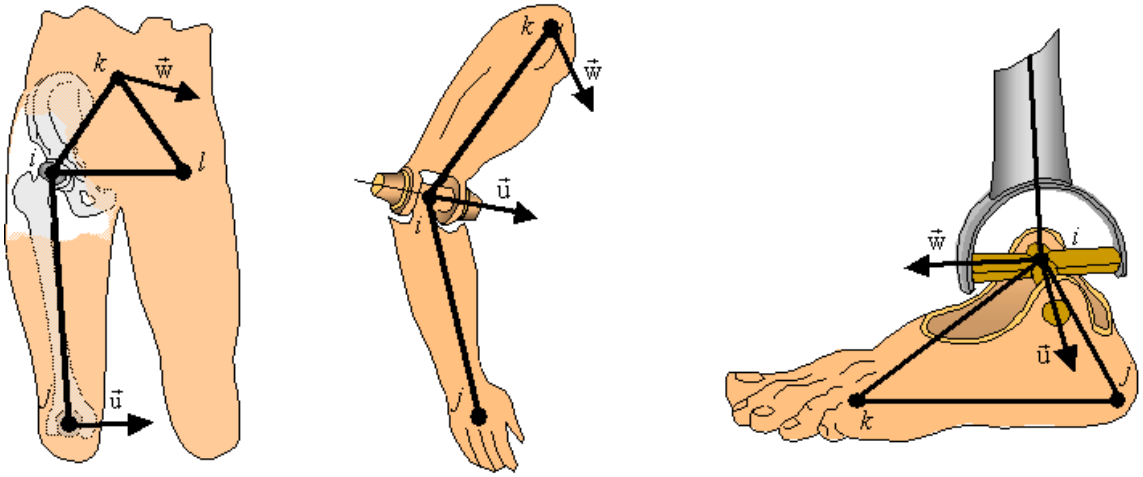

Figure 2.5: Kinematic joints definitions. Examples of application to biomechanics: (a) The spherical joint applied to the description of a hip joint; (b) The revolute joint applied to the description of the elbow and of the upper arm joints; (c) The universal joint applied to the definition of the ankle joint.

The Spherical Joint

The spherical joint is a ball and socket type of joint that restrains the motion between two rigid bodies (the three translations), only allowing three degrees-of-freedom (the three rotations), as depicted in Figure 2.5(a) for the hip joint. This type of joint can be modeled without introducing any joint constraint equations, just by sharing point *i* between two rigid bodies, as shown in Figure 2.5(a), or alternatively, by introducing proper joint kinematic constraints. In the second case, the kinematic constraint equations describing the spherical joint assume that there are two different points, each one belonging to a different rigid body, that share the same position in space. Hence, replacing point *i*, in Figure 2.5(a), by equivalent points *n* and *m* – with point *n* belonging to the femur and point *m* belonging to the pelvis – the following joint constraint equation is obtained to define the latter type of spherical joint:

$$\mathbf{\Phi}^{\mathrm{SPH}}\left(\mathbf{q}\right) = \mathbf{r}_n - \mathbf{r}_m = \mathbf{0} \tag{2.20}$$

where vectors $\mathbf{r}_n$ and $\mathbf{r}_m$ express the position of points *n* and *m* in the global reference frame. Equation (2.20) has a linear dependency on the generalized coordinates, leading to the

introduction of constant coefficients in the Jacobian matrix of the constraints and to null right hand sides for the associated velocity and acceleration constraint equations.

The Revolute Joint

The revolute joint restrains the motion between two rigid bodies in such a way that only one degree-of-freedom is allowed. This degree-of-freedom corresponds to the rotation of the rigid bodies around the unit vector used to describe the joint axis, as presented in Figure 2.5(b) for the elbow joint. This joint can be defined by sharing point *i* and vector **u** between two different rigid bodies or, alternatively, by using proper joint kinematic constraints. When the second definition is used, the first set of joint constraints is equivalent to those that describe the spherical joint, given by Equation (2.20). This set of constraints is responsible for ensuring that two different points *n* and *m*, with *n* belonging to the lower arm and *m* belonging to the upper arm, share the same position in space. The second set of constraints arises considering that vector **u**, depicted in Figure 2.5(b), is substituted by two different unit vectors **a** and **b** that belong to different rigid bodies but have the same components in space. This second set of equations is expressed by the following joint constraint equation:

$$\mathbf{\Phi}^{\mathrm{REV}}\left(\mathbf{q}\right) = \mathbf{b} - \mathbf{a} = \mathbf{0} \tag{2.21}$$

As before, Equation (2.21) also presents a linear dependency on the generalized coordinates and, therefore, it introduces constant contributions to the Jacobian matrix of the constraints and null right-hand-sides in the velocity and acceleration constraint equations.

An alternative procedure is also used in this work to define revolute joints that describe axial rotations between elements. As depicted in the example presented in Figure 2.6, the revolute joint describing the rotation of the upper arm can be defined without any additional constraint equations, just using two points that are shared between two different rigid bodies, or, if needed, using proper joint constraint equations. In the latter case, the joint constraint equations result from applying Equation (2.20) to point *i* and to point *k*.

Independently of the type of the revolute joint definition, six constraint equations are always introduced to describe a kinematic joint that restrains five degrees-of-freedom. This

means that in this set of six constraints there is one redundant equation. Consequently, the methods described in Section 2.2 must be applied to avoid numerical difficulties.

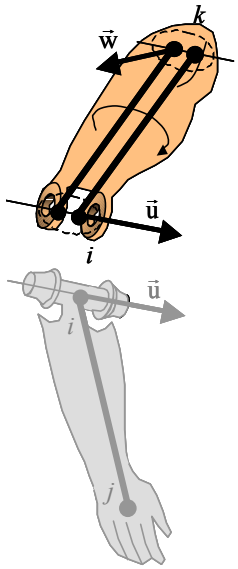

Figure 2.6: Revolute joint defined using two points. Two different rigid bodies share points *i* and *k* in order to define the revolute joint that describes the medial/lateral rotation of the upper arm.

The Universal Joint

The universal joint restrains the motion between two rigid bodies to only two degrees-of-freedom, corresponding to the rotations of the rigid bodies around two orthogonal vectors, each one belonging to a different rigid body. In the example depicted in Figure 2.5(c), the ankle joint is described using a universal joint. Vector **u** belongs to the rigid body describing the foot and vector **w** belongs to one of the rigid bodies describing the lower leg. Point *i* can be shared by both rigid bodies or, if needed, a specific joint kinematic constraint, of the type given in Equation (2.20), can be introduced.

The description of this joint is completed with the introduction of an additional joint kinematic constraint that assures the orthogonality of vectors **u** and **w**. This additional kinematic restriction is introduced using the scalar-product constraint presented in Equation (2.13) and described in Table 2.1.

2.4 Forward Dynamic Analysis

The forward dynamic analysis provides a way of calculating the dynamic response of a constrained multibody system due to the effect of external applied forces. The motion of the system is generally not prescribed, which makes its calculation one of the principal objectives of the analysis. The forward dynamic analysis also provides a way to estimate external forces that depend on the relative position between the system's elements, such as the forces generated by springs, dampers and actuators, as well as to estimate external forces that are generated as a consequence of the system's interaction with the surrounding environment, such as contact and friction forces. Another significant result provided by this type of dynamic analysis is the calculation of the internal reaction forces, generated in the kinematic pairs, which represent the forces that the system has to develop during the analysis to prevent the occurrence of motion in the degrees-of-freedom constrained by the kinematic joints.

2.4.1 Equations of Motion of a Constrained Multibody System

The equations of motion of a constrained multibody system can be obtained using one of several formulations, such as the application of Lagrange's equations; the principle of virtual work; or in the present case, the principle of virtual power (Jalón and Bayo, 1994). This principle establishes that the sum of the virtual power produced by the inertial and external forces acting in a mechanical system, must be zero in any instant in time. Mathematically, this is expressed as:

$$\mathcal{P}^* = \dot{\mathbf{q}}^{*\mathrm{T}} \left(\mathbf{M}\ddot{\mathbf{q}} - \mathbf{g} \right) = 0 \tag{2.22}$$

where $\dot{\mathbf{q}}^*$ is a virtual velocity vector, belonging to the null space of the Jacobian matrix, i.e., a vector containing, at any given time, a set of fictional velocities that are consistent with the velocity constraint equations, given by Equation (2.8), in the homogeneous form. The term $\mathbf{M}\ddot{\mathbf{q}}$ represents the inertial forces, with $\mathbf{M}$ defined as the global mass matrix and $\ddot{\mathbf{q}}$ the vector of generalized accelerations. The term $\mathbf{g}$ represents the generalized force vector, containing

the external applied forces and the velocity-dependent inertial forces, in which the centrifugal and Coriolis forces are included.

It must be noted that the internal forces, i.e., the forces associated with the kinematic constraints, are not included in the previous equation because they do not produce virtual power. However, these forces can be added to Equation (2.22) using the Lagrange multipliers method with the expression (Haug, 1989; Nikravesh, 1988):

$$\mathbf{g}^{\mathbf{\Phi}} = \mathbf{\Phi}_{\mathbf{q}}^{\mathrm{T}}\boldsymbol{\lambda} \tag{2.23}$$

where $\mathbf{g}^{\mathbf{\Phi}}$ is a generalized force vector containing the internal constraint forces, and $\boldsymbol{\lambda}$ is the vector of Lagrange multipliers. From the physical point of view, the rows of the Jacobian matrix provide the direction of the constraint forces and the vector of Lagrange multipliers their magnitude. Hence, the internal constraint forces, as described by Equation (2.23), are linear combinations of the rows of the Jacobian matrix. Considering the properties of the virtual velocity vector and according to the homogeneous form of Equation (2.8), the product $\dot{\mathbf{q}}^{*\mathrm{T}}\mathbf{\Phi}_{\mathbf{q}}^{\mathrm{T}}\boldsymbol{\lambda}$ belongs to the null space of the Jacobian matrix and, therefore, can be added to Equation (2.22), resulting in:

$$\mathcal{P}^{*} = \dot{\mathbf{q}}^{*\mathrm{T}}\left(\mathbf{M}\ddot{\mathbf{q}} - \mathbf{g} + \mathbf{\Phi}_{\mathbf{q}}^{\mathrm{T}}\boldsymbol{\lambda}\right) = 0 \tag{2.24}$$

Assuming that the system has *nc* generalized coordinates and *nh* holonomic constraints, it is always possible to find *nc–nh* arbitrary virtual velocities and *nh* Lagrange multipliers that make, in Equation (2.24), the term in brackets to be null. This term represents the equations of motion (EOM) describing a constrained multibody system and it is rewritten in is final form as:

$$\mathbf{M}\ddot{\mathbf{q}} + \mathbf{\Phi}_{\mathbf{q}}^{\mathrm{T}}\boldsymbol{\lambda} = \mathbf{g} \tag{2.25}$$

Note that Equation (2.25) represents a system of *nc* second-order ordinary differential equations (ODEs) with *nc*+*nh* unknowns corresponding to the generalized acceleration vector $\ddot{\mathbf{q}}$ and to the vector of the Lagrange multipliers $\boldsymbol{\lambda}$. In order to obtain a solution for the

previous equation, *nh* additional equations are required. Ideally, these additional equations should be provided by the constraint equation described in Equation (2.2) in order to ensure that both the equations of motion and the kinematic restrictions are fulfilled. However, proceeding in this way a system of *nc*+*nh* differential algebraic equations (DAEs) of index[1] *3* would be obtained with the inherent difficulties to achieve a solution (Haug, 1989; Jalón and Bayo, 1994; Nikravesh, 1988; Shabana, 1994). Instead, the acceleration equations given in Equation (2.11) are used, resulting in the system of *nc*+*nh* DAEs of index *1*, rearranged in matrix form as:

$$\begin{bmatrix} \mathbf{M} & \boldsymbol{\Phi}_{\mathbf{q}}^{\mathrm{T}} \\ \boldsymbol{\Phi}_{\mathbf{q}} & \mathbf{0} \end{bmatrix} \begin{Bmatrix} \ddot{\mathbf{q}} \\ \boldsymbol{\lambda} \end{Bmatrix} = \begin{Bmatrix} \mathbf{g} \\ \boldsymbol{\gamma} \end{Bmatrix} \tag{2.26}$$

Equation (2.26) can be transformed in a system of second order ODEs, once the Lagrange multipliers vector is eliminated from it. The resulting system of ODEs is expressed in terms of the generalized acceleration vector and can be integrated in time, given initial conditions for the position and velocity vectors. These initial conditions need to be consistent with kinematics of the multibody system, i.e.:

$$\boldsymbol{\Phi}\left(\mathbf{q}_0\right) = \mathbf{0} \tag{2.27}$$

$$\boldsymbol{\Phi}_{\mathbf{q}}\dot{\mathbf{q}}_0 = \boldsymbol{\nu}\left(t_0\right) \tag{2.28}$$

2.4.2 Lagrange Multipliers and Internal Forces

As was seen in Section 2.4.1, the internal forces developed in a mechanical system represent the forces that the system has to generate internally in order to satisfy the kinematic constraints, introduced to define the rigid bodies and to describe the topology of the system. These forces, represented by Equation (2.23), are obtained by multiplying the columns of the Jacobian matrix by the vector of the Lagrange multipliers. The columns of the Jacobian

[1] The index of a DAE represents one plus the number of differentiations of the constraints that are needed in order to eliminate the Lagrange multipliers vector (Ascher *et al.*, 1995).

matrix provide the direction in which these forces are applied, while the Lagrange multipliers vector provides their magnitude.

When kinematic joints are modeled using shared points and unit vectors, the kinematic restrictions defining those joints are imposed implicitly without using explicit kinematic constraints and, therefore, the calculation procedure described previously is not able to provide explicit results for the reaction forces associated with these joints. In order to solve this problem, two procedures can be applied: the first procedure establishes, for each reporting time step, the dynamic equilibrium equations of each rigid body, and obtains the reaction forces as the solution of these equations (Jalón and Bayo, 1994). This procedure has a complex implementation and it has the disadvantage of requiring additional information of the topology of the mechanical system under analysis. The second procedure consists in creating an expanded mechanical system in which there are no shared points or vectors. In this expanded system, additional points and unit vectors are defined in order to allow all kinematic joints to be explicitly defined, using the method described in Section 2.3.3. However, the expanded system is computationally less efficient than the original one, since it uses a much higher number of generalized coordinates and kinematic constraints. Consequently, this expanded system should only be used when the calculation of the reaction forces at the joints is necessary, in which case it must only be assembled and solved during reporting time steps or when the value for these forces is required.

2.4.3 Augmented Lagrange Formulation

From the numerical point of view, the solution of Equation (2.26) and the subsequent numerical integration of the generalized accelerations can present some difficulties since the kinematic constraint equations were substituted by the kinematic acceleration equations. The solution of Equation (2.26) and the subsequent integration of the generalized acceleration vector leads to generalized coordinates and velocity vectors that no longer exactly satisfy the kinematic equations (2.8) and (2.11), introducing in this way a drift in the position constraints. Moreover, the acceleration equations are differential equations of the type $\ddot{\mathbf{\Phi}} = \mathbf{0}$, which are known to be numerically unstable. This means that small integration and round-off errors

will easily grow, causing the occurrence of inevitable violations in the position and velocity constraint equations.

Stabilization methods are applied in the solution of the equations of motion, leading to more stable integration procedures and less constraint violations. The Baumgarte stabilization method is an extension of the feedback control theory to multibody analyses and it is probably the most well-known and applied method to stabilize the equations of motion of multibody systems (Baumgarte, 1972). This method is very efficient when redundant constraint equations are not present and the solution is not close to singular positions. However, this method fails to obtain a solution to Equation (2.26) whenever one of the situations just referred to occurs (Jalón and Bayo, 1994).

In the present work, the Augmented Lagrange Formulation is used to stabilize the equations of motion of a constrained mechanical system (Avello and Bayo, 1992; Jalón and Bayo, 1994). This is a penalty type formulation that does not fail near singular positions or in the presence of redundant constraints. Moreover, the Augmented Lagrange Formulation is an iterative method that leads to the reduction of the number of equations to solve from *nc*+*nh* equations, as in Equation (2.26), to *nc* equations. Therefore, only the accelerations of the system are calculated. The Lagrange multipliers evaluation is optional and performed only if required.

The Augmented Lagrange Formulation first introduces in the virtual power expression, given by Equation (2.24), an additional corrective term that is a function of the Jacobian matrix, hence not producing virtual power:

$$\mathscr{P}^* = \dot{\mathbf{q}}^{*\mathrm{T}} \left(\mathbf{M}\ddot{\mathbf{q}} - \mathbf{g} + \boldsymbol{\Phi}_{\mathbf{q}}^{\mathrm{T}} \bar{\boldsymbol{\lambda}} + \boldsymbol{\Phi}_{\mathbf{q}}^{\mathrm{T}} \boldsymbol{\beta} \right) = 0 \tag{2.29}$$

where $\boldsymbol{\beta}$ is a vector that penalizes the constraint violations and therefore controls the system response by enforcing that there are no constraint violations. Analytically vector $\boldsymbol{\beta}$ is expressed as:

$$\boldsymbol{\beta} = \alpha \left(\ddot{\boldsymbol{\Phi}} + 2\omega\mu\dot{\boldsymbol{\Phi}} + \omega^2 \boldsymbol{\Phi} \right) \tag{2.30}$$

If there are no constraint violations, $\boldsymbol{\beta}$ is a null vector since the position, velocity and acceleration constraint equations are fulfilled. From another point of view, if constraint violations occur, vector $\boldsymbol{\beta}$ is a penalizing term that grows with the increase of the constraint violations. Coefficients α, μ and ω are penalizing terms that contribute to a fast elimination of the constraint violations. In most applications involving rigid body dynamics these coefficients assume values that are within the following ranges (Avello and Bayo, 1992):

$$\begin{cases} 10^4 \leq \alpha \leq 10^7 \\ 0.0 \leq \mu \leq 1.0 \\ 1.0 \leq \omega \leq 10.0 \end{cases} \tag{2.31}$$

Comparing Equations (2.29) and (2.24), it can be concluded that they are equivalent when:

$$\boldsymbol{\lambda} = \bar{\boldsymbol{\lambda}} + \boldsymbol{\beta} \tag{2.32}$$

This expression is used to establish the iterative process of the Augmented Lagrange Formulation, i.e.:

$$\boldsymbol{\lambda}_{i+1} = \boldsymbol{\lambda}_i + \boldsymbol{\beta}_i \tag{2.33}$$

where *i* represent the iteration number. This iterative scheme is used until the difference between the vectors of the Lagrange multipliers of two consecutive iterations is less than a specified tolerance, i.e., when the term $\boldsymbol{\beta}_i$ vanishes. Introducing the iterative process given by Equation (2.33) in the equations of motion (2.25) for iteration *i+1*, the following expression is obtained:

$$\mathbf{M}\ddot{\mathbf{q}}_{i+1} + \boldsymbol{\Phi}_{\mathbf{q}}^{\mathrm{T}} \left(\boldsymbol{\lambda}_i + \boldsymbol{\beta}_i \right) = \mathbf{g} \tag{2.34}$$

The vector of Lagrange multipliers is eliminated from Equation (2.34) using the equations of motion (2.25), but this time rewritten for iteration *i*. Hence:

$$\mathbf{M}\ddot{\mathbf{q}}_{i+1} + \boldsymbol{\Phi}_{\mathbf{q}}^{\mathrm{T}} \boldsymbol{\beta}_i = \mathbf{M}\ddot{\mathbf{q}}_i \tag{2.35}$$

Equations (2.8) and (2.11) are now substituted in Equation (2.30), for iteration *i*, yielding:

$$\boldsymbol{\beta}_i = \alpha\left[\boldsymbol{\Phi}_{\mathbf{q}}\ddot{\mathbf{q}}_{i+1} - \boldsymbol{\gamma}_i + 2\omega\mu\left(\boldsymbol{\Phi}_{\mathbf{q}}\dot{\mathbf{q}}_i - \boldsymbol{\nu}_i\right) + \omega^2\boldsymbol{\Phi}_i\right] \tag{2.36}$$

where, for convenience, the generalized acceleration vector is expressed for iteration *i+1*. Substituting this result in Equation (2.35) and rearranging the terms, the following expression is obtained:

$$\left[\mathbf{M} + \boldsymbol{\Phi}_{\mathbf{q}}^{\mathrm{T}}\alpha\boldsymbol{\Phi}_{\mathbf{q}}\right]\ddot{\mathbf{q}}_{i+1} = \mathbf{M}\ddot{\mathbf{q}}_i + \boldsymbol{\Phi}_{\mathbf{q}}^{\mathrm{T}}\alpha\left(\boldsymbol{\gamma}_i - 2\omega\mu\left(\boldsymbol{\Phi}_{\mathbf{q}}\dot{\mathbf{q}}_i - \boldsymbol{\nu}_i\right) - \omega^2\boldsymbol{\Phi}_i\right) \tag{2.37}$$

Equation (2.37) represents the iterative scheme of the Augmented Lagrange Formulation that is used until the difference between the generalized acceleration vectors of two consecutive iterations is less than a specified tolerance. Equation (2.37) represents a system of *nc* ODEs, with the leading matrix $\left[\mathbf{M} + \boldsymbol{\Phi}_{\mathbf{q}}^{T}\alpha\boldsymbol{\Phi}_{\mathbf{q}}\right]$ always positive definite. An initial approximation for vector $\mathbf{q}_0$ can be obtained from Equation (2.25) considering that in the initial iteration there are no constraint violations, i.e., $\mathbf{M}\ddot{\mathbf{q}} = \mathbf{g}$.

The penalizing coefficient α does not affect the solution of Equation (2.37) but only the convergence rate of the method, which is usually obtained after two to four iterations. From the computational point of view, it is not very expensive to calculate matrix $\left[\mathbf{M} + \boldsymbol{\Phi}_{\mathbf{q}}^{T}\alpha\boldsymbol{\Phi}_{\mathbf{q}}\right]$ since it only needs to be evaluated once in the beginning of the iterative process. Regarding the matrix product $\boldsymbol{\Phi}_{\mathbf{q}}^{T}\alpha\boldsymbol{\Phi}_{\mathbf{q}}$, it should be noted that the Jacobian matrix is a sparse matrix and therefore appropriate methods can be used to take computational advantage of this fact.

As was seen before, the Lagrange multipliers are eliminated from the iterative process. This leads to a reduction in the number of equations to solve, in which the generalized accelerations are the only unknowns. However, if the values of the Lagrange multipliers are needed for the analysis, these can be calculated by solving the equation of motion (2.25), with respect to this vector, in the end of the iterative process.

2.4.4 Integration of the Equations of Motion

In Sections 2.4.2 and 2.4.3, the equations of motion of a constrained multibody system were introduced as well as specific methods that allow for their stabilization and consequent calculation of the generalized acceleration vector, associated with current time step. In order to advance the analysis in time, the equations of motion need to be integrated. Considering the high level of complexity of these equations, analytical solutions are impractical to obtain and, consequently, numerical integration algorithms must be applied.

The integration of the equations of motion plays a key role in the quality of the results and influences the computational costs involved in the solution process. Seeking real-time analysis and the possibility of introducing the concept of man-in-the-loop, many researchers have targeted their work to the development of more accurate and stable algorithms that integrate the equations of motion with larger time steps. In particular, for the case of first-order ODEs, several efficient integration algorithms can be used to compute their solution for specified initial conditions, i.e., the so-called first-order initial-value problems (Haug, 1989; Nikravesh, 1988).

In order to use such an algorithms, the DAE system expressed by Equation (2.26) or the associated system of second-order ODEs, needs to be transformed into a first-order initial-value problem. This transformation is accomplished within a numerical integration process called direct integration (Nikravesh, 1988), in which the vectors $\mathbf{y}$ and $\dot{\mathbf{y}}$ are defined in such a way that vector $\dot{\mathbf{y}}$ contains the generalized velocities and accelerations for actual time step t and vector $\mathbf{y}$ contains the generalized coordinates and velocities for the next time step $t+\Delta t$. Hence:

$$\dot{\mathbf{y}}_t = \begin{bmatrix} \dot{\mathbf{q}} \\ \ddot{\mathbf{q}} \end{bmatrix}_t \quad \text{and} \quad \mathbf{y}_{t+\Delta t} = \begin{bmatrix} \mathbf{q} \\ \dot{\mathbf{q}} \end{bmatrix}_{t+\Delta t} \tag{2.38}$$

The flow-chart describing the direct integration algorithm is presented in Figure 2.7 and the method develops according to the following steps:

i) Using the generalized coordinates and velocities of the current time step, solve the equations of motion and calculate the generalized accelerations using the methodologies described in Section 2.4.3. For the initial time step, the generalized coordinates and velocities are given as specified initial conditions that must fulfill the position and velocity constraint equations.

ii) With the generalized velocities and accelerations, obtained for the current time step t, assemble vector $\dot{\mathbf{y}}_t$ and carry out the numerical integration routine for time step $t+\Delta t$.

iii) Once the integration is successfully completed, extract from the newly calculated vector $\mathbf{y}_{t+\Delta t}$ the values of the generalized positions and velocities for time step $t+\Delta t$.

iv) Update the time variable and proceed to the new time step. Perform these steps while the final time for the analysis is not reached.

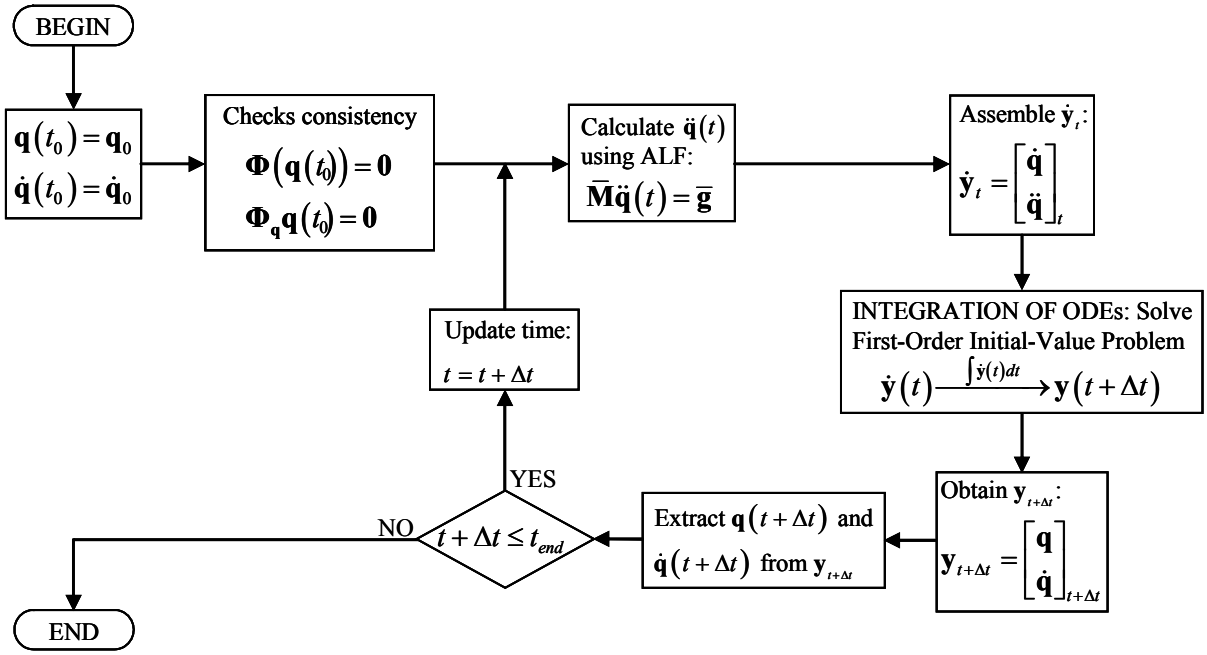

Figure 2.7: Direct Integration Algorithm. Flow-chart of the process used to numerically integrate the equations of motion of mechanical systems. A standard integration routine is used to solve the first-order initial-value problem, with the accelerations calculated using the Augmented Lagrange Formulation.

In this work a standard general-purpose integrator is used to perform the integration of the first-order initial-value problem. This integrator is based on the predictor-corrector Adams-Moulton-Bashforth methods, which use the implicit Adams-Moulton method as corrector and the explicit Adams-Bashforth method as predictor (Jalón and Bayo, 1994). This is a multi-step method, where the information of previous time steps is used to calculate the next step. In terms of its stability, this method is conditionally stable, i.e., the ideal time step is chosen depending on the characteristics of the problem, meaning that for some types of problems this method can become unstable and a solution may not be obtained. Moreover, the selected method is implicit, meaning that the solution for the next iteration is approximated using a guess of its value, obtained by an explicit procedure known as predictor step. This initial approximation is afterwards corrected using an implicit procedure known as corrector step and the final solution of the time step is obtained. This type of methods is much more accurate than general explicit methods, in which the solution for the next time step depends only on the solution obtained in the previous ones.

2.4.5 Mass Matrix for the Basic Rigid Body

In previous sections, general expressions were obtained for the complete set of equations of motion of a constrained mechanical system, which can be applied to any type of Cartesian coordinates. In this section, the methodologies described before are applied to fully Cartesian coordinates.

As shown in Sections 2.1 and 2.3, when using fully Cartesian coordinates, the rigid bodies can be described by different kinematic structures, which depend on the topology of the system and on the type of kinematic joints to which they are attached. At first sight, it can appear that many different mass matrices are required to express the mass and inertial properties of each different type of rigid body. That is not the case. In fact, each rigid body has its own mass matrix that differs according to its specific kinematic configuration. However, all of these possible mass matrices can be obtained from the mass matrix of a basic rigid body by means of a coordinate transformation. Therefore, the determination of this basic mass matrix requires the definition of the basic rigid body and its kinematic structure.

The basic rigid body, presented in Figure 2.8, has a kinematic structure made of two points, *i* and *j*, and two non-coplanar unit vectors, **u** and **v**. Consequently, a total number of twelve generalized coordinates, corresponding to the Cartesian coordinates of the two points and two vectors, are used in its definition. According to Section 2.3.1, six kinematic constraint equations of rigid body type need to be introduced. These kinematic constraints are described using Equation (2.13) and specified for some of the cases presented in Table 2.1. The six kinematic constraints are: the constant length between points *i* and *j*, the unit norms of vectors **u** and **v**, the constant angle between these vectors and the constant angles between these vectors and segment $\mathbf{r}_{ij}$.

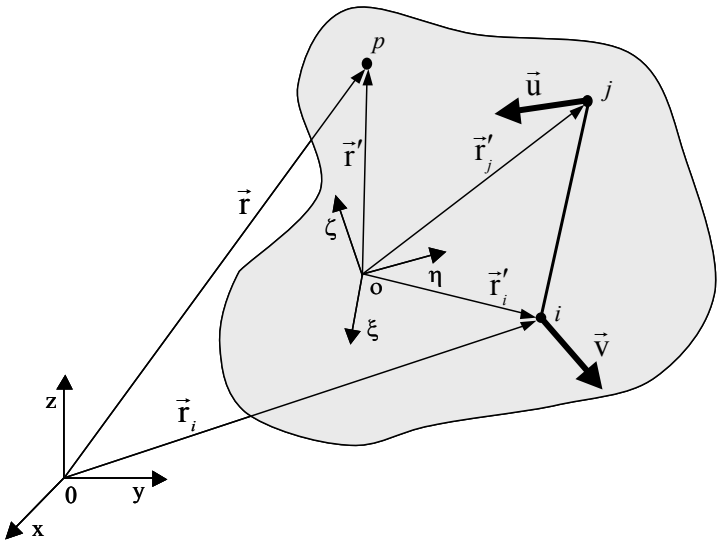

Figure 2.8: Basic rigid body. The kinematic structure of the basic rigid body is made of two points (*i* and *j*) and two non-coplanar unit vectors (**u** and **v**). Point *p* represents a generic point belonging to this rigid body. A local reference frame (oξηζ) is rigidly attached to the body, having its origin in point o, which is not necessarily its center-of-mass. The reference frame (xyz) represents the inertial reference frame.

A local reference frame is rigidly attached to the basic rigid body. This reference frame has its origin at point *o* and orientation given by the orthogonal axes ξ, η and ζ. The origin of this reference frame does not necessarily need to be coincident with the body's center-of-mass, and the direction of its reference axes does not need to be coincident with the body's principal inertial directions.

The virtual power generated within the rigid body by the inertial forces is expressed in its integral form by:

$$\mathcal{P}^* = -\rho \int_{\Omega} \dot{\mathbf{r}}^{*\mathrm{T}} \ddot{\mathbf{r}} \; d\Omega \tag{2.39}$$

where ρ is the density of the rigid body and $\dot{\mathbf{r}}^*$ and $\ddot{\mathbf{r}}$ are respectively the virtual velocity and acceleration vectors of the generic point *p*, belonging to the rigid body and represented in Figure 2.8. These vectors can be written in terms of the rigid body's generalized velocity and acceleration vectors by means of an appropriate coordinate transformation. This coordinate transformation is obtained considering that vector **r**, defining the global position of point *p*, can be expressed by the Cartesian coordinates of segment $\mathbf{r}_{ij}$ and unit vectors **u** and **v**, as:

$$\mathbf{r} - \mathbf{r}_i = c_1 \left(\mathbf{r}_j - \mathbf{r}_i \right) + c_2 \mathbf{u} + c_3 \mathbf{v} \tag{2.40}$$

where c_1, c_2 and c_3 are the coordinates of segment $\mathbf{r}_{ip}$ in the three-dimensional base formed by vectors $\mathbf{r}_{ij}$, **u** and **v**. Rearranging Equation (2.40) in matrix form, it becomes:

$$\mathbf{r} = \begin{bmatrix} (1-c_1)\mathbf{I}_3 & c_1\mathbf{I}_3 & c_2\mathbf{I}_3 & c_3\mathbf{I}_3 \end{bmatrix} \begin{Bmatrix} \mathbf{r}_i \\ \mathbf{r}_j \\ \mathbf{u} \\ \mathbf{v} \end{Bmatrix} \tag{2.41}$$

or in a more compact form:

$$\mathbf{r} = \mathbf{C}\mathbf{q}_e \tag{2.42}$$

where **C** is a transformation matrix, independent of the motion of the body and therefore constant in time, and $\mathbf{q}_e$ represents the vector of generalized coordinates describing the basic body. Equation (2.42) is differentiated twice with respect to time, yielding the expressions:

$$\dot{\mathbf{r}} = \mathbf{C}\dot{\mathbf{q}}_e \tag{2.43}$$

$$\ddot{\mathbf{r}} = \mathbf{C}\ddot{\mathbf{q}}_e \tag{2.44}$$

where $\dot{\mathbf{q}}_e$ and $\ddot{\mathbf{q}}_e$ are the generalized velocity and acceleration vectors of the basic rigid body.

The numerical values for coefficients c_1, c_2 and c_3 are obtained, rewriting Equation (2.40) in the local coordinate system of the rigid body, i.e.:

$$\mathbf{r}' - \mathbf{r}'_i = c_1 \left(\mathbf{r}'_j - \mathbf{r}'_i \right) + c_2 \mathbf{u}' + c_3 \mathbf{v}' \tag{2.45}$$

Equation (2.45) is rearranged in matrix form, yielding:

$$\left(\mathbf{r}' - \mathbf{r}'_i \right) = \begin{bmatrix} \mathbf{r}_{ij} & \mathbf{u}' & \mathbf{v}' \end{bmatrix} \begin{Bmatrix} c_1 \\ c_2 \\ c_3 \end{Bmatrix} = \mathbf{X}'\mathbf{c} \tag{2.46}$$

where matrix $\mathbf{X}'$ contains the local coordinates of segment $\mathbf{r}_{ij}$ and vectors $\mathbf{u}$ and $\mathbf{v}$ in the reference frame of the rigid body and, therefore, always has an inverse. Solving Equation (2.46) for vector $\mathbf{c}$, the following result is obtained:

$$\mathbf{c} = \mathbf{X}'^{-1} \left(\mathbf{r}' - \mathbf{r}'_i \right) \tag{2.47}$$

which allows for the evaluation of the coefficients.

Considering again the expression of the virtual power of the inertial forces, given by Equation (2.39), and substituting the Equations (2.43) and (2.44) that relate the velocity and acceleration of a generic point with the generalized coordinates of the rigid body to which it is attached, the following expression is obtained:

$$\mathcal{P}^* = -\rho \int_{\Omega} \dot{\mathbf{q}}_e^{*\mathrm{T}} \mathbf{C}^{\mathrm{T}} \mathbf{C} \ddot{\mathbf{q}}_e \; d\Omega \tag{2.48}$$

where vectors $\dot{\mathbf{q}}_e^*$ and $\ddot{\mathbf{q}}_e$ are independent of the body's volume and therefore can placed outside the integral, yielding the expression for the mass matrix of the basic rigid body:

$$\mathbf{M} = \rho \int_{\Omega} \mathbf{C}^T \mathbf{C} \; d\Omega \tag{2.49}$$

The term inside the integral can be evaluated using matrix **C**, described in Equation (2.41), yielding:

$$\mathbf{M} = \int_{\Omega} \rho \begin{bmatrix} 1-2c_1+c_1^2\mathbf{I}_3 & c_1-c_1^2\mathbf{I}_3 & c_2-c_1c_2\mathbf{I}_3 & c_3-c_1c_3\mathbf{I}_3 \\ c_1-c_1^2\mathbf{I}_3 & c_1^2\mathbf{I}_3 & c_1c_2\mathbf{I}_3 & c_1c_3\mathbf{I}_3 \\ c_2-c_1c_2\mathbf{I}_3 & c_1c_2\mathbf{I}_3 & c_2^2\mathbf{I}_3 & c_2c_3\mathbf{I}_3 \\ c_3-c_1c_3\mathbf{I}_3 & c_1c_3\mathbf{I}_3 & c_2c_3\mathbf{I}_3 & c_3^2\mathbf{I}_3 \end{bmatrix} d\Omega \tag{2.50}$$

A closer look into Equation (2.50) reveals that the following three integrals need to be calculated:

$$\begin{aligned} &\int_{\Omega} \rho \, d\Omega = m \\ &\int_{\Omega} \rho \mathbf{c} \, d\Omega = \mathbf{X}'^{-1} \int_{\Omega} \rho \left(\mathbf{r}' - \mathbf{r}_i' \right) d\Omega = m\mathbf{X}'^{-1} \left(\mathbf{r}_g' - \mathbf{r}_i' \right) = m\mathbf{a}_i \\ &\int_{\Omega} \rho \mathbf{c}\mathbf{c}^{\mathrm{T}} d\Omega = \mathbf{X}'^{-1} \left(\int_{\Omega} \rho \left(\mathbf{r}' - \mathbf{r}_i' \right) \left(\mathbf{r}' - \mathbf{r}_i' \right)^{\mathrm{T}} d\Omega \right) \mathbf{X}'^{-\mathrm{T}} = \mathbf{X}'^{-1} \mathbf{J}_i \mathbf{X}'^{-\mathrm{T}} = \mathbf{Z}_i \end{aligned} \tag{2.51}$$

where m is the total mass of the rigid body and $\mathbf{r}_g'$ is the vector containing the coordinates of the center-of-mass of the element in the local reference frame ($\xi\eta\zeta$). The vector $\mathbf{a}_i$ and the matrix $\mathbf{Z}_i$ are respectively the first and second area moments of the rigid body, calculated with respect to the reference frame with origin at point i and axes defined by the generalized coordinates of segment $\mathbf{r}_{ij}$ and unit vectors **u** and **v**. Matrix $\mathbf{J}_i$ is used in the calculation of matrix $\mathbf{Z}_i$ and it contains the information regarding the moments and products of inertia of the rigid body, with respect to a fictional reference frame with origin at point i and axes parallel to those of the local reference frame ($\xi\eta\zeta$). Matrix $\mathbf{J}_i$ is expressed as follows:

$$\mathbf{J}_i = \begin{bmatrix} \int_\Omega x'^2 d\Omega + m\left(x_i'^2 - 2x_g'x_i'\right) & \int_\Omega x'y' d\Omega + m\left(x_i'y_i' - x_g'y_i' - x_i'y_g'\right) & \int_\Omega x'z' d\Omega + m\left(x_i'z_i' - x_g'z_i' - x_i'z_g'\right) \\ & \int_\Omega y'^2 d\Omega + m\left(y_i'^2 - 2y_g'y_i'\right) & \int_\Omega y'z' d\Omega + m\left(y_i'z_i' - y_g'z_i' - y_i'z_g'\right) \\ \text{Symmetric} & & \int_\Omega z'^2 d\Omega + m\left(z_i'^2 - 2z_g'z_i'\right) \end{bmatrix} \quad (2.52)$$

where the integral expressions in matrix $\mathbf{J}_i$ can be expressed in terms of the moments and products of inertia of the rigid body with respect to the local reference frame ($\xi\eta\zeta$) as:

$$\begin{aligned} \int_\Omega x'^2 d\Omega &= \frac{1}{2}\left(I_{\eta\eta} + I_{\zeta\zeta} - I_{\xi\xi}\right) = \bar{I}_{\xi\xi} \\ \int_\Omega y'^2 d\Omega &= \frac{1}{2}\left(I_{\xi\xi} + I_{\zeta\zeta} - I_{\eta\eta}\right) = \bar{I}_{\eta\eta} \\ \int_\Omega z'^2 d\Omega &= \frac{1}{2}\left(I_{\xi\xi} + I_{\eta\eta} - I_{\zeta\zeta}\right) = \bar{I}_{\zeta\zeta} \\ \int_\Omega x'y'\, d\Omega &= I_{\xi\eta} \\ \int_\Omega x'z'\, d\Omega &= I_{\xi\zeta} \\ \int_\Omega y'z'\, d\Omega &= I_{\eta\zeta} \end{aligned} \quad (2.53)$$

The remaining terms in matrix $\mathbf{J}_i$ are additional inertial contributions that represent the application of the parallel-axis theorem to the calculation of the moments of inertia of the rigid body with respect to the fictional reference frame previously described. Substituting the results of Equation (2.53) in Equation (2.52), the final expression for matrix $\mathbf{J}_i$ is obtained:

$$\mathbf{J}_i = \begin{bmatrix} \bar{I}_{\xi\xi} + m\left(x_i'^2 - 2x_g'x_i'\right) & I_{\xi\eta} + m\left(x_i'y_i' - x_g'y_i' - x_i'y_g'\right) & I_{\xi\zeta} + m\left(x_i'z_i' - x_g'z_i' - x_i'z_g'\right) \\ & \bar{I}_{\eta\eta} + m\left(y_i'^2 - 2y_g'y_i'\right) & I_{\eta\zeta} + m\left(y_i'z_i' - y_g'z_i' - y_i'z_g'\right) \\ \text{Symmetric} & & \bar{I}_{\zeta\zeta} + m\left(z_i'^2 - 2z_g'z_i'\right) \end{bmatrix} \quad (2.54)$$

It should be noted that if the origin of the local reference frame ($\xi\eta\zeta$) is coincident with the center-of-mass of the body, the first area moment is zero and matrix $\mathbf{J}_i$ is simplified. Using the results provided by Equations (2.51) and (2.54) in Equation (2.50), the final expression for the mass matrix of the basic rigid body, described with two points and two non-coplanar unit vectors is obtained (Jalón and Bayo, 1994; Silva, 1996):

$$\mathbf{M}_e = \begin{bmatrix} (m - 2ma_1 + z_{11})\mathbf{I_3} & (ma_1 - z_{11})\mathbf{I_3} & (ma_2 - z_{12})\mathbf{I_3} & (ma_3 - z_{13})\mathbf{I_3} \\ (ma_1 - z_{11})\mathbf{I_3} & z_{11}\mathbf{I_3} & z_{12}\mathbf{I_3} & z_{13}\mathbf{I_3} \\ (ma_2 - z_{21})\mathbf{I_3} & z_{21}\mathbf{I_3} & z_{22}\mathbf{I_3} & z_{23}\mathbf{I_3} \\ (ma_3 - z_{31})\mathbf{I_3} & z_{31}\mathbf{I_3} & z_{32}\mathbf{I_3} & z_{33}\mathbf{I_3} \end{bmatrix} \quad (2.55)$$

This mass matrix is constant in time and for that reason needs to be evaluated and assembled in the global mass matrix only once in the beginning of the analysis. Moreover, this mass matrix depends only upon a set of ten different values. These values are the total mass of the rigid body, the coordinates of its center-of-mass in the local reference frame ($\xi\eta\zeta$) and the six different elements of the inertia tensor, also calculated with respect to the local reference frame.

2.4.6 Mass Matrix for Other Rigid Bodies

When fully Cartesian coordinates are used, many different types of rigid bodies can be obtained depending on the topology of the system under analysis. The degree of complexity of such bodies depends on the number of points and unit vectors used for their definition. Fortunately, in most cases, it is always possible to identify, among the set of points and unit vectors, two points and two non-coplanar unit vectors that can be used in the construction of the basic mass matrix introduced before. When such a collection of points and vectors cannot be found, other simple kinematic structures are used instead. These kinematic structures are associated with rigid bodies, whose mass matrices are obtained from the basic mass matrix by means of a coordinate transformation. These other rigid bodies are described here:

- Rigid body with a kinematic structure described by three non-collinear points and one unit vector, non-coplanar with the plane defined by the three points. This type of rigid body is represented in Figure 2.3(a) and it is used to describe the foot of the biomechanical model;
- Rigid body with a kinematic structure described by two points and one non-collinear unit vector. This type of rigid body is represented in Figure 2.6 and it is used to describe the upper arm of the biomechanical model;
- Rigid body with a kinematic structure described by four non-coplanar points;
- Rigid body with a kinematic structure described by three non-collinear points.

In this work, only the mass matrices for the first two rigid bodies are presented, considering their relevance in the construction of the biomechanical models presented in the next chapter. The remaining rigid bodies follow the same procedure to be described for the calculation of the mass matrices but, since they are not used in this work, their calculation is not presented here. The interested reader is referred to the work of Jalón and Bayo (1994) and Silva (1996) for more information.

Rigid Body with Three Points and One Unit Vector

This rigid body, presented in Figure 2.3(a), is defined with twelve generalized coordinates, corresponding to the Cartesian coordinates of the points *i*, *j* and *k* and of unit vector **a**. These coordinates are grouped together as:

$$\mathbf{q}_{3\text{p1v}} = \left\{ \mathbf{r}_i \quad \mathbf{r}_j \quad \mathbf{r}_k \quad \mathbf{a} \right\}^{\mathrm{T}} \tag{2.56}$$

In order to obtain the transformation matrix that relates the coordinates of the basic rigid body, introduced in the previous section, with the coordinates of the present body, a second unit vector, corresponding to vector **v** of the basic body, is defined as:

$$\mathbf{v} = \frac{\left(\mathbf{r}_k - \mathbf{r}_j \right)}{L_{jk}} \tag{2.57}$$

which has the same direction of the segment $\mathbf{r}_{jk}$. Using Equation (2.57), the following linear transformation of coordinates, is obtained:

$$\mathbf{q}_e = \begin{Bmatrix} \mathbf{r}_i \\ \mathbf{r}_j \\ \mathbf{u} \\ \mathbf{v} \end{Bmatrix} = \begin{bmatrix} \mathbf{I}_3 & \mathbf{0}_3 & \mathbf{0}_3 & \mathbf{0}_3 \\ \mathbf{0}_3 & \mathbf{I}_3 & \mathbf{0}_3 & \mathbf{0}_3 \\ \mathbf{0}_3 & \mathbf{0}_3 & \mathbf{0}_3 & \mathbf{I}_3 \\ \mathbf{0}_3 & -\frac{1}{L_{jk}}\mathbf{I}_3 & \frac{1}{L_{jk}}\mathbf{I}_3 & \mathbf{0}_3 \end{bmatrix} \begin{Bmatrix} \mathbf{r}_i \\ \mathbf{r}_j \\ \mathbf{r}_k \\ \mathbf{u} \end{Bmatrix} = \mathbf{V}_{3\text{p1v}}\mathbf{q}_{3\text{p1v}} \tag{2.58}$$

which transforms the coordinates representing the current body to those used by the basic rigid body. The transformation matrix $\mathbf{V}_{3\text{p1v}}$ is independent of the motion of the body and, therefore, constant in time. Differentiating Equation (2.58) twice with respect to time, the following results are obtained, relating the generalized velocity and acceleration vectors of the basic body with the generalized velocity and acceleration vectors of the current rigid body:

$$\dot{\mathbf{q}}_e = \mathbf{V}_{3\text{p1v}}\dot{\mathbf{q}}_{3\text{p1v}} \tag{2.59}$$

$$\ddot{\mathbf{q}}_e = \mathbf{V}_{3\text{p1v}}\ddot{\mathbf{q}}_{3\text{p1v}} \tag{2.60}$$

Substituting Equations (2.59) and (2.60) in Equation (2.48), leads to:

$$\mathcal{P}^* = -\dot{\mathbf{q}}_e^{*\mathrm{T}}\mathbf{M}_e\ddot{\mathbf{q}}_e = -\dot{\mathbf{q}}_{3\text{p1v}}^{*\mathrm{T}}\left(\mathbf{V}_{3\text{p1v}}^{\mathrm{T}}\mathbf{M}_e\mathbf{V}_{3\text{p1v}}\right)\ddot{\mathbf{q}}_{3\text{p1v}} \tag{2.61}$$

where the term between brackets represents the mass matrix of a rigid body with a kinematic structure made of three points and one non-coplanar unit vector, i.e.:

$$\mathbf{M}_{3\text{p1v}} = \mathbf{V}_{3\text{p1v}}^{\mathrm{T}}\mathbf{M}_e\mathbf{V}_{3\text{p1v}} \tag{2.62}$$

The mass matrix presented in Equation (2.62) is constant and, therefore, needs to be calculated and assembled only once at the beginning of the analysis.

Rigid Body with Two Points and One Unit Vector

This rigid body, presented in Figure 2.6, is defined using nine generalized coordinates that correspond to the Cartesian coordinates of the points *i*, and *j* and of unit vector **u**. The calculation of its mass matrix follows the same procedure described before for the rigid body with three points and one unit vector. However, since this body is defined with only nine generalized coordinates, the coordinate transformation obtained is no longer linear and, consequently, the resulting mass matrix for this rigid body is no longer constant.

The coordinates that describe the current rigid body are grouped in the vector:

$$\mathbf{q}_{2\text{p1v}} = \left\{ \mathbf{r}_i \quad \mathbf{r}_j \quad \mathbf{u} \right\}^{\mathrm{T}} \tag{2.63}$$

A transformation matrix, relating the coordinates of the current rigid body with the coordinates of the basic rigid body is obtained, introducing a second unit vector that simulates the vector **v** of the basic body. This vector is defined using the generalized coordinates of the present rigid body through the following cross product:

$$\mathbf{v} = \frac{\tilde{\mathbf{u}}\mathbf{r}_{ij}}{L_{\tilde{\mathbf{u}}\mathbf{r}_{ij}}} \tag{2.64}$$

where $\tilde{\mathbf{u}}$ is the skew-symmetric matrix associated with vector **u** and $L_{\tilde{\mathbf{u}}\mathbf{r}_{ij}} = L_{ij} \sin\left(\left\langle \mathbf{u}, \mathbf{r}_{ij} \right\rangle\right)$ the coefficient that normalizes vector **v**.

The resulting vector **v** is orthogonal to the plane defined by unit vector **u** and segment $\mathbf{r}_{ij}$. Using Equation (2.64), the following coordinate transformation is obtained:

$$\mathbf{q}_e = \begin{Bmatrix} \mathbf{r}_i \\ \mathbf{r}_j \\ \mathbf{u} \\ \mathbf{v} \end{Bmatrix} = \begin{bmatrix} \mathbf{I}_3 & \mathbf{0}_3 & \mathbf{0}_3 \\ \mathbf{0}_3 & \mathbf{I}_3 & \mathbf{0}_3 \\ \mathbf{0}_3 & \mathbf{0}_3 & \mathbf{I}_3 \\ -\dfrac{\tilde{\mathbf{u}}}{L_{\tilde{\mathbf{u}}\mathbf{r}_{ij}}} & \dfrac{\tilde{\mathbf{u}}}{L_{\tilde{\mathbf{u}}\mathbf{r}_{ij}}} & \mathbf{0}_3 \end{bmatrix} \begin{Bmatrix} \mathbf{r}_i \\ \mathbf{r}_j \\ \mathbf{u} \end{Bmatrix} = \mathbf{V}^*_{2\text{p1v}} \mathbf{q}_{2\text{p1v}} \tag{2.65}$$

The transformation matrix $\mathbf{V}_{2\text{p1v}}^{*}$ depends on the motion of the body and, therefore, is not constant in time. Differentiating Equation (2.65) twice with respect to time, the following expressions are obtained, relating the generalized velocity and acceleration vectors of the basic body with the generalized velocity and acceleration vectors of the present rigid body:

$$\dot{\mathbf{q}}_e = \mathbf{V}_{2\text{p1v}}^{*}\dot{\mathbf{q}}_{2\text{p1v}} + \dot{\mathbf{V}}_{2\text{p1v}}^{*}\mathbf{q}_{2\text{p1v}} = \left(\mathbf{V}_{2\text{p1v}}^{*} + \overline{\mathbf{V}}_{2\text{p1v}}^{*}\right)\dot{\mathbf{q}}_{2\text{p1v}} = \mathbf{V}_{2\text{p1v}}\dot{\mathbf{q}}_{2\text{p1v}} \tag{2.66}$$

$$\ddot{\mathbf{q}}_e = \mathbf{V}_{2\text{p1v}}\ddot{\mathbf{q}}_{2\text{p1v}} + \dot{\mathbf{V}}_{2\text{p1v}}\dot{\mathbf{q}}_{2\text{p1v}} \tag{2.67}$$

where the matrices $\mathbf{V}_{2\text{p1v}}$ and $\dot{\mathbf{V}}_{2\text{p1v}}$ are defined as:

$$\mathbf{V}_{2\text{p1v}} = \begin{bmatrix} \mathbf{I}_3 & \mathbf{0}_3 & \mathbf{0}_3 \\ \mathbf{0}_3 & \mathbf{I}_3 & \mathbf{0}_3 \\ \mathbf{0}_3 & \mathbf{0}_3 & \mathbf{I}_3 \\ -\dfrac{\tilde{\mathbf{u}}}{L_{\tilde{\mathbf{u}}\mathbf{r}_{ij}}} & \dfrac{\tilde{\mathbf{u}}}{L_{\tilde{\mathbf{u}}\mathbf{r}_{ij}}} & -\dfrac{\tilde{\mathbf{r}}_{ij}}{L_{\tilde{\mathbf{u}}\mathbf{r}_{ij}}} \end{bmatrix} \quad \text{and} \quad \dot{\mathbf{V}}_{2\text{p1v}} = \begin{bmatrix} \mathbf{0}_3 & \mathbf{0}_3 & \mathbf{0}_3 \\ \mathbf{0}_3 & \mathbf{0}_3 & \mathbf{0}_3 \\ \mathbf{0}_3 & \mathbf{0}_3 & \mathbf{0}_3 \\ -\dfrac{\dot{\tilde{\mathbf{u}}}}{L_{\tilde{\mathbf{u}}\mathbf{r}_{ij}}} & \dfrac{\dot{\tilde{\mathbf{u}}}}{L_{\tilde{\mathbf{u}}\mathbf{r}_{ij}}} & -\dfrac{\dot{\tilde{\mathbf{r}}}_{ij}}{L_{\tilde{\mathbf{u}}\mathbf{r}_{ij}}} \end{bmatrix} \tag{2.68}$$

Substituting Equations (2.66) and (2.67) in Equation (2.48), the following expression is obtained for the virtual power associated with the current rigid body:

$$\mathcal{P}^{*} = -\dot{\mathbf{q}}_e^{*\mathrm{T}}\mathbf{M}_e\ddot{\mathbf{q}}_e = -\dot{\mathbf{q}}_{2\text{p1v}}^{*\mathrm{T}}\left[\left(\mathbf{V}_{2\text{p1v}}^{\mathrm{T}}\mathbf{M}_e\mathbf{V}_{2\text{p1v}}\right)\ddot{\mathbf{q}}_{2\text{p1v}} + \left(\mathbf{V}_{2\text{p1v}}^{\mathrm{T}}\mathbf{M}_e\dot{\mathbf{V}}_{2\text{p1v}}\dot{\mathbf{q}}_{2\text{p1v}}\right)\right] \tag{2.69}$$

The first term in parentheses represents the mass matrix of the rigid body with a kinematic structure made of two points and one unit vector, while the second term in parentheses represents the velocity-dependent inertial forces that must be added to the generalized force vector **g**. Hence, the mass matrix and the generalized velocity-dependent force vector are defined as:

$$\mathbf{M}_{2\text{p1v}} = \mathbf{V}_{2\text{p1v}}^{\mathrm{T}}\mathbf{M}_e\mathbf{V}_{2\text{p1v}} \tag{2.70}$$

$$\mathbf{g}_{2\text{p1v}} = \mathbf{V}_{2\text{p1v}}^{\mathrm{T}}\mathbf{M}_e\dot{\mathbf{V}}_{2\text{p1v}}\dot{\mathbf{q}}_{2\text{p1v}} \tag{2.71}$$

The mass matrix and the velocity-dependent force vector presented in Equations (2.70) and (2.71) are not constant in time. Consequently, they need to be evaluated and assembled at each time step of the analysis.

2.4.7 External Applied Forces and Moments

When performing dynamic analyses of mechanical systems, it is often necessary to apply different types of external forces and moments to rigid bodies. When using fully Cartesian coordinates, it is necessary to transform these generic external forces or moments into generalized forces that can be assembled in the generalized force vector. The required steps to perform this transformation are described here for concentrated forces and moments applied to basic rigid bodies.

Concentrated Forces

In Figure 2.10 a generic force **f** is applied to a point *p* belonging to a basic rigid body with a kinematic structure defined with two points and two unit vectors, like the one described in Section 2.4.5. Considering that point *p* does not belong to the set of points that defines the rigid body, a coordinate transformation needs to be introduced in order to transform force **f** into an equivalent generalized force $\mathbf{g}_f$ distributed over the generalized coordinates of the rigid body.

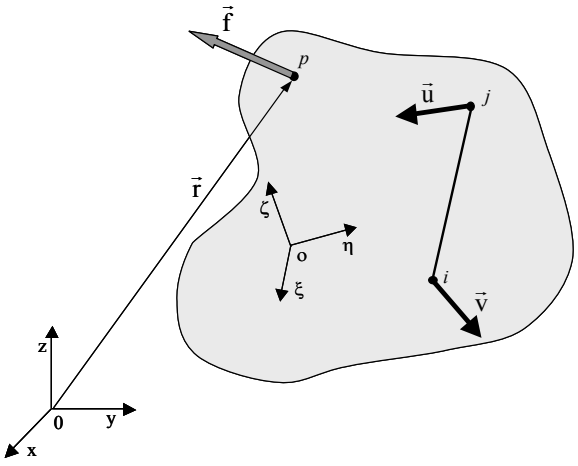

Figure 2.9: Application of a concentrated force **f** to point *p*, belonging to a basic rigid body. Point *p* may not be one of the points used in the description of the body.

Considering that the virtual work performed by the concentrated force **f** and the equivalent generalized force $\mathbf{g}_\mathrm{f}$ must be the same, the following expression is obtained:

$$\delta W = \delta \mathbf{r}_p^\mathrm{T} \mathbf{f} = \delta \mathbf{q}_e^\mathrm{T} \mathbf{g}_\mathrm{f} \tag{2.72}$$

where the position vector $\mathbf{r}_p$ is expressed in terms of the generalized coordinates of the rigid body, by means of the coordinate transformation given in Equation (2.42), i.e.:

$$\mathbf{r}_p = \mathbf{C}_p \mathbf{q}_e \tag{2.73}$$

Substituting Equation (2.73) in Equation (2.72) leads to:

$$\delta W = \delta \mathbf{q}_e^\mathrm{T} \mathbf{C}_p^\mathrm{T} \mathbf{f} = \delta \mathbf{q}_e^\mathrm{T} \mathbf{g}_\mathrm{f} \tag{2.74}$$

Comparing the second and third terms of Equation (2.74), it can be concluded that:

$$\mathbf{g}_\mathrm{f} = \mathbf{C}_p^\mathrm{T} \mathbf{f} \tag{2.75}$$

which represents the transformation of the generic force **f** into an equivalent generalized force $\mathbf{g}_\mathrm{f}$ distributed over the generalized coordinates that define the basic rigid body.

Force **f** can be applied to other types of rigid bodies, with different kinematic structures. Consequently, the coordinate transformation given in Equation (2.73) is no longer valid and a new coordinate transformation needs to be introduced. This additional coordinate transformation is identical to those presented by Equations (2.58) and (2.66), and is used to express the vector of generalized coordinates of the basic body in terms of the vector of generalized coordinates of other types of rigid bodies. Following an equivalent calculation procedure, the following expression is obtained:

$$\mathbf{g}_\mathrm{f} = \mathbf{V}^\mathrm{T} \mathbf{C}_p^\mathrm{T} \mathbf{f} \tag{2.76}$$

which represents the force transformation that need to be performed to generic forces applied over different types of rigid bodies.

Concentrated Moments

When using fully Cartesian coordinates there is no direct procedure to apply concentrated moments over the rigid bodies, because no rotational coordinates are explicitly used in the description of the system. When necessary, the concentrated moment **m** must be transformed into an equivalent pair of forces **f** and -**f** of equal magnitude and opposite directions, separated by a unit vector **b**, which act on a plane perpendicular to the direction of **m**, as illustrated in Figure 2.10. Proceeding in this way, the pair of forces can subsequently be applied to the rigid body using the procedures described before for concentrated forces.

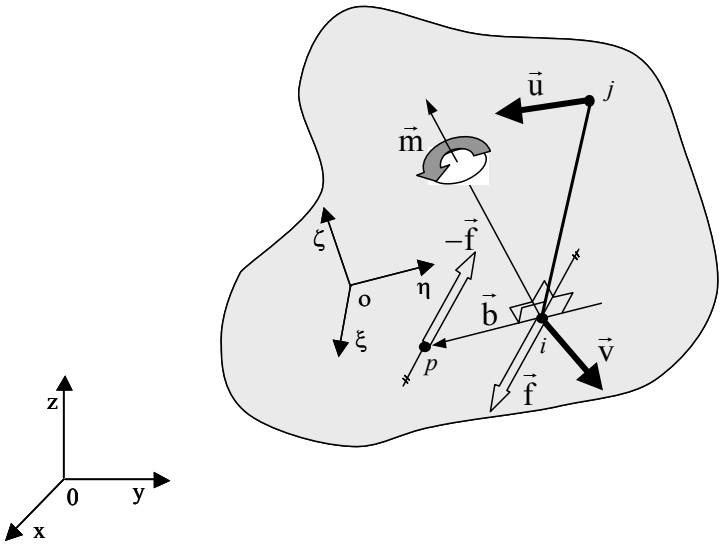

Figure 2.10:Concentrated torque **m** applied to a basic rigid body.

Let a pair of forces represent the concentrated moment **m** as:

$$\mathbf{m} = \tilde{\mathbf{b}}\mathbf{f} \tag{2.77}$$

where $\tilde{\mathbf{b}}$ is the skew-symmetric matrix associated with unit vector **b**, with origin at point *i* and defined as follows:

$$\mathbf{b} = \frac{\tilde{\mathbf{r}}_{ij}\mathbf{m}}{L_{\tilde{\mathbf{r}}_{ij}\mathbf{m}}} \tag{2.78}$$

where $L_{\tilde{\mathbf{r}}_{ij}\mathbf{m}}$ represents the norm of the vector resulting from the cross product of segment $\mathbf{r}_{ij}$ and moment **m**. With the concentrated moment **m** and the unit vector **b**, the generic pair of forces **f** can be calculated as:

$$\mathbf{f} = \tilde{\mathbf{b}}\mathbf{m} \tag{2.79}$$

Using Equation (2.79), the equivalent generalized force $\mathbf{g}_{\mathrm{m}}$ is obtained considering that the virtual work, performed by the concentrated pair of forces **f** and the generalized force $\mathbf{g}_{\mathrm{m}}$, must be the same, i.e.:

$$\delta W = \delta \mathbf{r}_i^{\mathrm{T}}\mathbf{f} - \delta \mathbf{r}_p^{\mathrm{T}}\mathbf{f} = \delta \mathbf{q}_e^{\mathrm{T}}\mathbf{g}_{\mathrm{m}} \tag{2.80}$$

where $\mathbf{r}_p=\mathbf{r}_i+\mathbf{b}$. Using the coordinate transformation given in Equation (2.42) and after some algebraic manipulations, the expression that allows for the calculation of the generalized force equivalent to concentrated moment **m** is obtained as:

$$\mathbf{g}_{\mathrm{m}} = (\mathbf{C}_i^{\mathrm{T}} - \mathbf{C}_p^{\mathrm{T}})\mathbf{f} \tag{2.81}$$

If the moment **m** is applied to other types of rigid bodies, defined with different sets of points and unit vectors, an expression similar to the one given by Equation (2.76) is obtained. Hence:

$$\mathbf{g}_{\mathrm{m}} = \mathbf{V}^{\mathrm{T}}\left(\mathbf{C}_i^{\mathrm{T}} - \mathbf{C}_p^{\mathrm{T}}\right)\mathbf{f} \tag{2.82}$$

where matrix **V** is the transformation matrix that expresses the generalized coordinates of other types of rigid bodies in terms of the generalized coordinates of the basic rigid body.

2.5 Inverse Dynamic Analysis

The inverse dynamic analysis of a mechanical system is a process that allows for the evaluation of the internal and external forces developed in the system and by the system, taking into consideration its topology, kinematic restrictions and observed motion. When applied to biomechanical systems, the inverse dynamic analysis plays a very important role since it provides a non-invasive method to calculate and evaluate the reaction forces and net-

moments of force developed in the joints and by the muscle apparatus of a biomechanical model, as a result of performing a task that has been previously observed. The equations of motion governing this type of analysis are exactly the same as the ones presented in Section 2.4, for forward dynamic analysis. Only the objectives of the analysis are different and, as a consequence, the unknown terms to calculate in those equations.

When performing an inverse dynamic analysis of a mechanical system, it is assumed that the motion corresponding to the task under analysis is known in advance and that it is consistent with the kinematic restrictions describing the system. Considering a mechanical system defined using fully Cartesian coordinates, this means that not only the coordinates of a set of points and unit vectors need to be obtained in a previous stage, but also that they need to be consistent with the kinematics of the system, fulfilling its kinematic constraint equations given by Equation (2.2). The calculation of this consistent motion requires the use of several methodologies, involving digitization techniques, filtering procedures and kinematic consistency methodologies that play a very important role in the quality and accuracy of the results of the analysis, as it will be seen in detail in Chapter 4.

The generalized velocity and acceleration vectors can be calculated from the generalized coordinates, describing the consistent motion, using two different procedures. The first procedure consists in applying the generalized coordinates to the kinematic equations describing the velocities and accelerations of the system, presented in Equations (2.8) and (2.11). The second procedure consists in interpolating the trajectories of each generalized coordinate using cubic splines and then obtaining their velocity and acceleration using spline differentiation techniques. Although experience shows that both procedures lead to very similar results, they are conceptually different. The first uses the velocity and acceleration equations to assure the kinematic consistency of the results, while the second assumes that the differentiation of kinematic consistent positions leads to kinematic consistent velocities and accelerations. When compared, the first procedure involves higher computational costs since it requires, for each time step, the assembly of the Jacobian matrix of the constraints and the solution of the two systems of linear equations given by Equations (2.8) and (2.11). The second procedure has smaller computational costs since it only involves spline manipulation

and differentiation. Nevertheless, the second procedure can present inaccuracies in the results when small sampling frequencies are used, and can present numerical instabilities in the velocities and accelerations calculated at the beginning and ending positions. Interpolation of the trajectory curves can be applied to both procedures if the evaluation of the position of the system is necessary in intermediate time steps.

At this stage, the kinematic data required to perform the inverse dynamic analysis is needed to be available and to be consistent with the kinematics of the mechanical system, i.e., it fulfils the constraint equations of position, velocity and acceleration given by Equations (2.2), (2.8) and (2.11), respectively. The next step involves the construction of the mass matrices and generalized force vectors of all the elements describing the mechanical system and their respective assemblage in the system's equations of motion, given by Equation (2.25).

The methods described in Sections 2.4.2 and 2.4.4, referring to the stabilization, solution and integration of the equations of motion are no longer needed since in this type of analysis the motion of the system is fully known. However, the methods described in Sections 2.4.5, 2.4.6 and 2.4.7, referring to the assembling of different types of mass matrices and externally applied forces, are still suitable and are applied to assemble the global mass matrix and the generalized force vector of the system.

There are several methods that can be used to solve the inverse dynamics problem and to obtain the values of the external and internal forces. These methods are basically equivalent and the advantages of using one method over another depends, in most cases, on the type of dependent coordinates used, on the type of results needed and on the multibody system under analysis (Jalón and Bayo, 1994). In this work two methods are considered to generate the equilibrium equations to solve: the Lagrange multipliers method and the Newton method.

The Lagrange multipliers method considers that with each external force is associated a kinematic driving actuator, similar to those described in Section 2.3.1. Such a driver is used to guide a specified degree-of-freedom, according to an initially prescribed kinematics or according to a known guiding function. Hence, a set of additional constraint equations is introduced in the Jacobian matrix of the constraints, equal in number to the degrees-of-

freedom of the multibody system. The equations of motion, given by Equation (2.25), are assembled and solved with respect to the augmented Lagrange multipliers vector, as follows:

$$\boldsymbol{\Phi}_{\mathbf{q}}^{\mathrm{T}}\boldsymbol{\lambda} = \mathbf{g} - \mathbf{M}\ddot{\mathbf{q}} \tag{2.83}$$

The Lagrange multipliers associated with the driving constraints are used to calculate the external forces associated with each degree-of-freedom of the mechanism. All other Lagrange multipliers are associated with kinematic constraints introduced to describe the kinematic topology of the mechanical system and, therefore, with the internal forces developed in the kinematic pairs and rigid bodies, as described in Section 2.4.2.

Conversely, the Newton method considers that with each degree-of-freedom is associated an external actuator that produces an unknown external force required for the system to reproduce the observed motion. To setup this procedure, the generalized force vector $\mathbf{g}$, in the right-hand-side of Equation (2.25), is divided in two terms: the term $\mathbf{g}_{\mathrm{e}}$ containing all the known external forces and the term $\mathbf{g}_{\mathrm{d}}$ associated with the unknown external forces produced by the external actuators:

$$\mathbf{g} = \mathbf{g}_{\mathrm{e}} - \mathbf{g}_{\mathrm{d}} \tag{2.84}$$

where the minus signal in Equation (2.84) is used for convenience of the calculations. The term $\mathbf{g}_{\mathrm{d}}$, is expressed as the product of matrix $\boldsymbol{\Gamma}$ by vector $\mathbf{f}_{\mathrm{d}}$, as follows:

$$\mathbf{g}_{\mathrm{d}} = \boldsymbol{\Gamma}^{\mathrm{T}}\mathbf{f}_{\mathrm{d}} \tag{2.85}$$

where matrix $\boldsymbol{\Gamma}$ contains geometrical information regarding the direction of the external forces produced by the actuators and is calculated using the generalized coordinates describing the multibody system. The vector $\mathbf{f}_{\mathrm{d}}$ contains the unknown magnitudes of these external forces. Substituting Equations (2.84) and (2.85) in the Equation (2.25) and rearranging the result, the following expression is obtained:

$$\begin{bmatrix} \boldsymbol{\Phi}_{\mathbf{q}}^{\mathrm{T}} & \boldsymbol{\Gamma}^{\mathrm{T}} \end{bmatrix} \begin{Bmatrix} \boldsymbol{\lambda} \\ \mathbf{f}_{\mathrm{d}} \end{Bmatrix} = \left\{ \mathbf{g}_{\mathrm{e}} - \mathbf{M}\ddot{\mathbf{q}} \right\} \tag{2.86}$$

that is rewritten in a more compact form as:

$$\bar{\mathbf{\Phi}}_{\mathbf{q}}^{\mathrm{T}}\bar{\boldsymbol{\lambda}} = \mathbf{g} - \mathbf{M}\ddot{\mathbf{q}} \tag{2.87}$$

As it can be observed, Equation (2.87) is analogous to Equation (2.83), which shows that both methods are similar. The only significant difference is that the Newton method leads directly to the determination of the magnitude of the external driving forces while the Lagrange multipliers method does not.

In the presence of over-constrained mechanisms, with or without redundant constraints, there are more unknowns than equations of motion. This means that an infinite set of solutions can be obtained from Equations (2.83) and (2.87). In order to obtain an unique solution for these equations, the minimum norm condition is used (Jalón and Bayo, 1994). When using the Lagrange multipliers method, this methodology considers that the best solution is the one orthogonal to the null-space of the matrix $\mathbf{\Phi}_{\mathbf{q}}^{\mathrm{T}}$, i.e., a solution that belongs to the column space of $\mathbf{\Phi}_{\mathbf{q}}$. This is written as:

$$\boldsymbol{\lambda} = \mathbf{\Phi}_{\mathbf{q}}\boldsymbol{\lambda}^{*} \tag{2.88}$$

Substituting Equation (2.88) in Equation (2.83), the resulting leading matrix is always invertible and, therefore, a unique solution can be found for $\boldsymbol{\lambda}^{*}$. The final value for $\boldsymbol{\lambda}$ is obtained by substituting the value calculated for $\boldsymbol{\lambda}^{*}$ in Equation (2.88).

2.5 Discussion

In this Chapter, a general-purpose multibody formulation was presented that allows the kinematic and dynamic analyses of three-dimensional mechanical systems to be performed. The proposed formulation uses fully Cartesian coordinates to describe the position and orientation of the rigid elements in space and, from the mathematical point of view, it is the supporting structure for all the biomechanical models and dynamic analyses that are presented in the forthcoming chapters.

The multibody formulation was introduced using a general approach to the analysis of multibody constrained mechanical systems using the virtual power method. Subsequently, the formulation was detailed for the type of coordinates adopted and expressions were obtained for the most common types of kinematic constraints, kinematic joints and mass matrices of rigid bodies. The formulation described here follows the basic steps proposed by Jalón and Bayo (1994). A different approach is suggested by Silva and Ambrósio (2003a) that introduces some alternative procedures to the definition of rigid bodies, mass matrices, kinematic joint constraints and kinematic drivers. This new perspective shortens the gap between multibody formulations using fully Cartesian coordinates and formulations using standard Cartesian coordinates, at the same time it preserves all the major advantages as well as the essence inherent to a formulation with fully Cartesian coordinates.

The Augmented Lagrange Formulation was adopted in this chapter as an alternative method to the Baumgarte constraint stabilization method. This method is an iterative procedure for the stabilization the equations of motion that does not fail to obtain a solution near singular positions or in the presence of redundant kinematic constraints.

Some remarks were also made regarding the type of differential equations that are obtained to describe the motion of constrained multibody systems and the methods that are applied for their solution. It was not the purpose of this chapter to make a detailed description of all the available methods and integration algorithms. For such purpose the interested reader is referred to a detailed review by Marsden and West (2001).

Finally, as biomechanics is a research field with different lines of thought and varied backgrounds, special attention was given to the examples presented in this chapter, in order to associate them and the described methodologies in the framework of biomechanics and biomechanical applications. Moreover, this Chapter should provide a starting point as well as a motivation for the use of multibody formulations in biomechanics and biomechanical applications.

Chapter 3

Biomechanical Models for Human Motion Simulation

The development of reliable mathematical models of the human body has been a major challenge for the biomechanics community over the last thirty years (Nigg and Herzog, 1995). The interest in the simulation of different human actions results from the need to predict, with sufficient accuracy, the mechanical behavior of the human body in various conditions of its activity. In fact, the computer simulation of several human capabilities has shown to be important in many different types of applications, including: athletic actions, where the aim to improve different sport performances and to optimize the design of sporting equipment; ergonomic studies, to assess operating conditions for comfort and efficiency in different aspects of human body interaction with the environment; orthopedics, to design and analyze prosthesis; and occupant dynamic analysis for crashworthiness and vehicle safety related research and design.

A common denominator to all of these applications is the use of biomechanical models to describe, from the mathematical point of view, the human body in terms of its anthropometry, physiology and topology. In the recent years and throughout the world, many biomechanical

models have been developed, with different purposes and using different approaches, depending on the nature of the research, the objectives of the analysis and the expected results. There are essentially two types of mathematical approaches that are used to construct and describe biomechanical models: multibody formulations and finite element methods. The multibody approach is usually applied in simulation cases where gross-motions are involved and when complex interactions with the surrounding environment are to be modeled and analyzed (Alvarez *et al.*, 1993b; Amirouche *et al.*, 1990; Anderson and Pandy, 2001b; Celigüeta, 1996; Hatze, 1984; Huang, 1995; Laananen *et al.*, 1983; Morecki *et al.*, 1984; Rasmussen *et al.*, 2002b; Reich *et al.*, 1999; Silva and Ambrósio, 2002a; Tno, 1997), while the finite element approach is applied in cases where localized structural deformations or soft tissues need to be described and analyzed in detail (Bandak *et al.*, 1996; Bedewi and Bedewi, 1996; Dinis *et al.*, 1999; Haug, 1996; Kan *et al.*, 2001; Miller and Chinzei, 1997; Saha *et al.*, 1991). The use of hybrid multibody and finite element models is another possible approach with a very high potential that is already being used by other research groups in an attempt to join together the advantages of both mathematical formulations and to construct more realistic models (Eberhard *et al.*, 1999; Maurel and Thalmann, 1999; T.N.O., 1997). However, the creation and simulation of finite element models can be computationally very expensive, making these methods less attractive in dynamic analyses where real-time is an issue or in optimization schemes that involve many function evaluations.

Biomechanical models can vary in detail, complexity and topology depending on the objectives of the analysis. When describing biomechanical models there are essentially two categories that can be distinguished: detailed partial models (Abdel-Rahman and Hefzy, 1993; Brelin-Fornari *et al.*, 1998; Engel *et al.*, 1997; Gilchrist and Winter, 1996; Horst *et al.*, 1997; Leardini *et al.*, 1999; Mommersteeg *et al.*, 1997; Sathasivam and Walker, 1997; Shelburne and Pandy, 1997; Tumer and Engin, 1993; Wismans, 1980; Wynarsky and Greenwald, 1983) and whole body response models (Aleshinsky and Zatsiorsky, 1978; Celigüeta, 1996; Hatze, 1984; Laananen *et al.*, 1983; Rasmussen *et al.*, 2002b; Reich *et al.*, 1999; Silva and Ambrósio, 2002a). The first ones usually correspond to partial representations of the human body in which a particular anatomical segment, joint, organ or physiological function is

represented with a high level of detail, while the second ones represent the human body as a whole, with the objective of capturing general characteristics rather than obtaining highly detailed information on particular component. However, with the increasing computer power and the continuous development of new and more efficient numerical methods and formulations, biomechanical models tend to be less partial and more detailed, i.e., biomechanical models tend to be whole body response models with detailed representations of particular components and functions.

In this work, two whole body response biomechanical models are defined using the multibody formulation described in detail in the previous chapter. Although different in many aspects, these models share a common structure of anatomical segments and use the same anthropometric model (Kroemer *et al.*, 1988) to describe the physical characteristics of each one of these segments.

3.1 The Anthropometric Model

In this work, an anthropometric model is considered to be a representation of the static body geometry, in which relevant dimensions and physical properties are described (Kroemer *et al.*, 1988). These relevant dimensions and physical properties include, among others, the body size, shape and proportion as well as the mass, inertia and center-of-mass location of the its principal anatomical segments.

Since the early studies of Braune and Ficher (Kroemer *et al.*, 1988) in the end of the nineteenth century, in which the concept of interconnected links was used to analyze and calculate the center of gravity of the German infantryman, many were the researchers that strongly contributed to the development of the actual anthropometric models of the human body. The fifties and the sixties were two decades of important and intense development of this research field. In 1954, Hertzberg et al. obtained the body size data regarding the anthropometry of flying personnel; one year later, in 1955, in a thorough study regarding the space requirements of the seated operator, Dempster calculates the center-of-mass locations and the density of the principal anatomical segments of the human body, using human cadavers; and two years later, in 1957, Barter establishes the mass-predictive equations for

seven anatomical segments as a percentage of the total body weight. During the sixties, several authors developed mathematical models for computing inertial parameters of living subjects. These models use known geometrical shapes to approximate the human body and to calculate approximated values for the moments of inertia of several anatomical segments. These models proved to be in a fairly close agreement with the experimental results obtained for living subjects (Seireg and Arvikar, 1989). A representative work in which this type of approach is used (Hanavan, 1964), describes the human body using fifteen anatomical segments. This personalized anthropometric model uses anthropometric data of the subject to calculate the moments of inertia for each anatomical segment, as well as it predicts the global center-of-mass location and the principal axes and moments of inertia of the entire body, for any specified posture.

These studies laid the foundations of the actual anthropometric models, although in some cases, substantial differences can be found when comparing the results reported by these authors. Many reasons justify these differences: the type of subject used in the study (in vivo, in vitro or mathematical analogues), the reduced number of subjects, different age ranges, gender, etc. Although differences exist between anthropometric models, these do not affect significantly the results obtained when inverse dynamic analyses are used. As it will be shown later in Chapter 5, the results produced by inverse dynamic analyses are not very sensitive to small variations in the anthropometric data. This justifies why, for so many models used in biomechanical research, the results obtained are in most cases consistent, correlated and comparable.

In this work, the anthropometric model used is based on the one presented in the computer simulation code SOM-LA (Laananen, 1991; Laananen *et al.*, 1983). The anthropometric data for this model was obtained from the work of Chandler, *et al.* (1981), regarding the uniform mass distribution and body size of the 50^{th} percentile aircrew member. The model considers the human body divided in sixteen anatomical segments, as presented in Figure 3.1 and briefly described in Table 3.1.

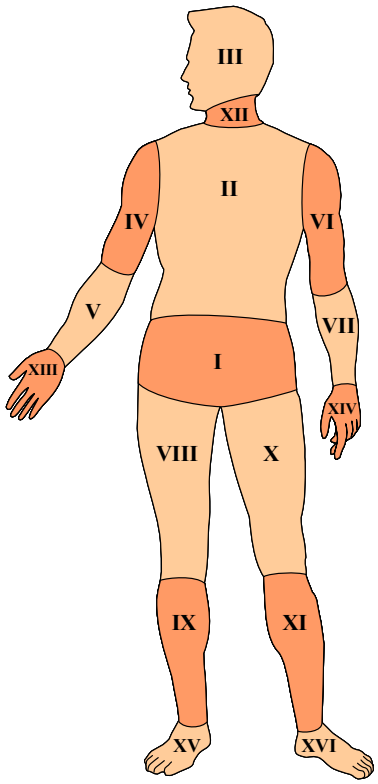

Figure 3.1: The anthropometric model based on the work of (Laananen *et al.*, 1983). The human body is divided in sixteen anatomical segments.

Table 3.1:Description of the anatomical segments of the anthropometric model.

Nbr.	Name	Description
I	Lower Torso	From the first lumbar vertebrae to the bony pelvis
II	Upper Torso	From the first thoracic joint to the twelfth
III	Head	Cranium, upper and lower jaws
IV	Right Upper Arm	From shoulder to elbow
V	Right Lower Arm	From elbow to wrist
VI	Left Upper Arm	From shoulder to elbow
VII	Left Lower Arm	From elbow to wrist
VIII	Right Upper Leg	From hip to knee
IX	Right Lower Leg	From knee to ankle
X	Left Upper Leg	From hip to knee
XI	Left Lower Leg	From knee to ankle
XII	Neck	From the first cervical vertebrae to the seventh.
XIII	Right Hand	From wrist to finger tips
XIV	Left Hand	From wrist to finger tips
XV	Right Foot	From ankle to toe
XVI	Left Foot	From ankle to toe.

3.1.1 Body Dimensions and Inertial Properties

In this section, the relevant anthropometric characteristics, required for the construction of the biomechanical models, are presented. Considering the sixteen anatomical segments depicted in Figure 3.1, these characteristics are: length, mass, center-of-mass location and the moments of inertia. It should be noted that, as illustrated in Figure 3.2, the lengths of the anatomical segments are considered to be the straight-line distance between adjacent joint centers of rotation, and not anthropometric dimensions based on external measurements.

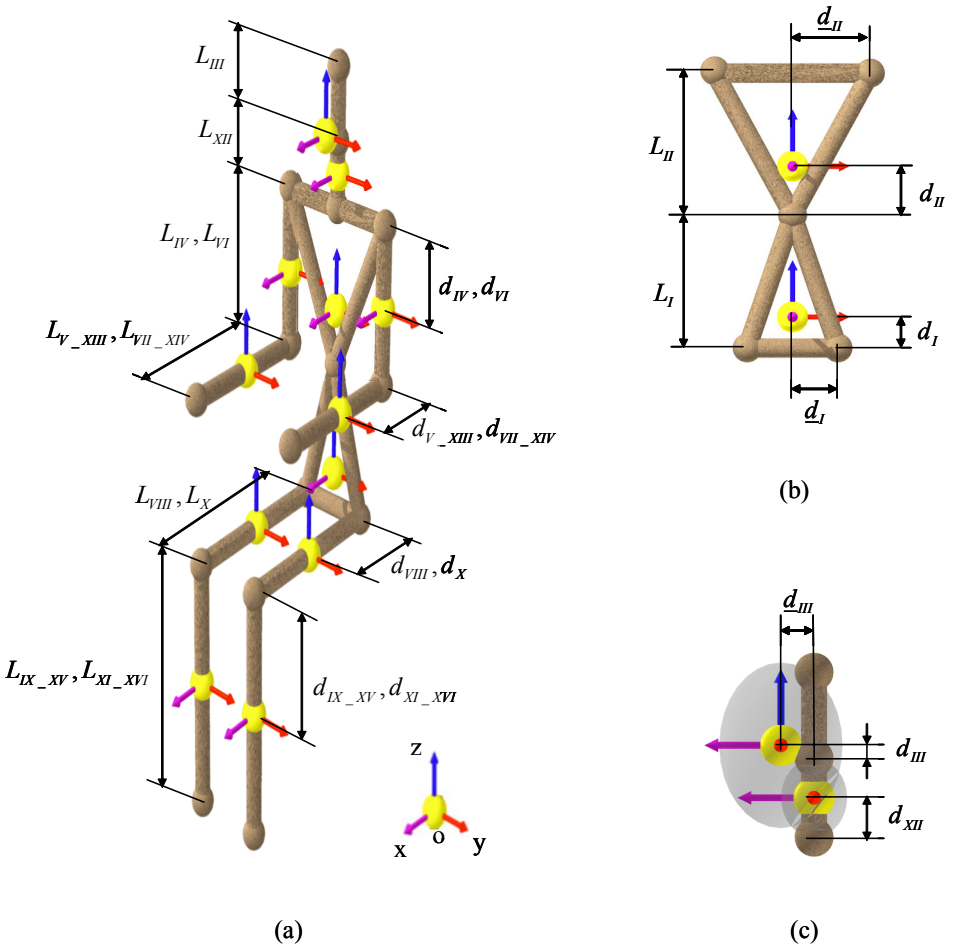

Figure 3.2: Anthropometric model. Representation of the major dimensions, reference frames and center of mass locations. (a) Perspective view in the reference seated position. (b) Frontal view of the principal dimensions of the lower and upper torso. (c) Sagittal view of the principal dimensions of the head and neck.

Regarding the specification of the moments of inertia of each anatomical segment, a local reference frame is rigidly attached to its center-of-mass, as depicted in Figure 3.2. It is assumed that these reference frames are orientated according to the principal axes of each anatomical segment, which means that the moments of inertia are the principal moments, calculated with respect to the axes of this local reference frame. In Figure 3.2, the model is presented in the seated position, in which the orientation of each local reference frame is assumed to be coincident with the orientation of the global reference frame (xyz) also represented in the figure. The center-of-mass locations, as indicated in Figure 3.2, are given with respect to the proximal joint for all segments, except for the center-of-mass locations of the lower and upper torsos that are given with respect to the distal joint. In some cases, such as for the lower and upper torsos and head, an additional dimension is provided to locate their center-of-mass.

In the anthropometric data presented in Table 3.2, the characteristics of the hands and feet, described by segments *XIII*, *XIV*, *XV* and *XVI*, are combined with the characteristics of the lower arms and lower legs respectively, as if the joints of the wrist and ankle were rigid.

Table 3.2: Anthropometric data for the sixteen anatomical segments represented in the model of Figure 3.1 (Laananen *et al.*, 1983). The lengths L_i and center-of-mass locations d_i and $\underline{d}_i$ are schematically represented in Figure 3.2.

Description	Seg.	Length	CM Location		Mass	Principal Moments of Inertia		
	I	L_i [m]	d_i [m]	$\underline{d}_i$ [m]	m_i [Kg]	$I_{\xi i}$ [10^{-2} Kg.m^2]	$I_{\eta i}$ [10^{-2} Kg.m^2]	$I_{\zeta i}$ [10^{-2} Kg.m^2]
Lower Torso	I	0.275	0.064	0.094	14.200	26.220	13.450	26.220
Upper Torso	II	0.294	0.101	0.161	24.950	24.640	37.190	19.210
Head	III	0.128	0.020	0.051	4.241	2.453	2.249	2.034
R Upper Arm	IV	0.295	0.153	–	1.991	1.492	1.356	2.487
R Lower Arm R Hand	V_XIII	0.376	0.180	–	1.892	0.192	2.871	2.204
L Upper Arm	VI	0.295	0.153	–	1.991	1.492	1.356	0.249
L Lower Arm L Hand	VII_XIV	0.376	0.180	–	1.892	0.192	2.871	2.204
R Upper Leg	VIII	0.434	0.215	–	9.843	1.435	15.940	9.867
R Lower Leg R Foot	IX_XV	0.467	0.230	–	4.808	10.480	13.220	5.708
L Upper Leg	X	0.434	0.215	–	9.843	1.435	15.940	9.867
L Lower Leg L Foot	XI_XVI	0.467	0.230	–	4.808	10.480	13.220	5.708
Neck	XII	0.122	0.061	–	1.061	0.268	0.215	0.215

3.1.2 Body Physique

In this work, the geometry of the human body – or the body physique – is approximated using surfaces of known geometric shapes, such as spheres, ellipsoids and cylinders. These surfaces, with simple analytical representations, are used in the following chapter to detect and calculate the contact forces generated among impacting anatomical segments and between these and the surrounding environment. This set of contact surfaces is represented in Figure 3.3, and it describes the body physique of the standard 50th percentile human male. Complementary dimensions, as well as the type of each surface, are provided in Table 3.3.

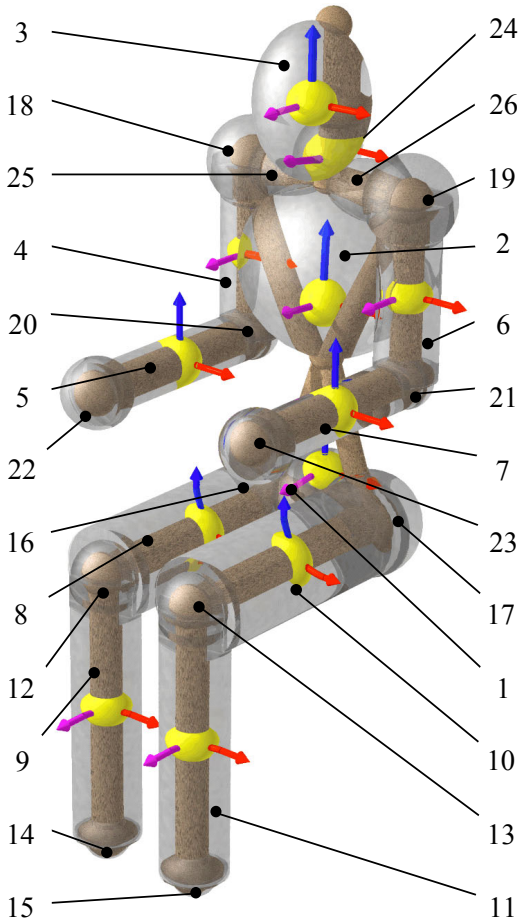

Figure 3.3: Body physique. Approximation of the human body geometry using known geometric shapes, such as spheres, ellipsoids and cylinders. The dimensions of the surfaces, as well as their type, are listed in Table 3.3. The anthropometric model represented in Figure 3.2 is visible underneath the contact surfaces.

Table 3.3: Complementary dimensions used to define the contact surfaces describing the human body geometry. The data presented in this table refers to the physical dimensions of the standard 50th percentile human male. Refer to Figure 3.3 for a schematic representation of each surface.

Nbr	Description	Type	Dimension [m]	Nbr.	Description	Type	Dimension [m]
1	Lower Torso	ELLIPSOID	0.102	14	R Foot	SPHERE	0.041
2	Upper Torso	ELLIPSOID	0.127	15	L Foot	SPHERE	0.041
3	Head	ELLIPSOID	0.095	16	R Hip	SPHERE	0.091
4	R Upper Arm	CYLINDER	0.053	17	L Hip	SPHERE	0.091
5	R Lower Arm	CYLINDER	0.042	18	R Shoulder	SPHERE	0.076
6	L Upper Arm	CYLINDER	0.053	19	L Shoulder	SPHERE	0.076
7	L Lower Arm	CYLINDER	0.042	20	R Elbow	SPHERE	0.047
8	R Upper Leg	CYLINDER	0.083	21	L Elbow	SPHERE	0.047
9	R Lower Leg	CYLINDER	0.057	22	R Hand	SPHERE	0.059
10	L Upper Leg	CYLINDER	0.083	23	L Hand	SPHERE	0.059
11	L Lower Leg	CYLINDER	0.057	24	Neck	ELLIPSOID	0.051
12	R Knee	SPHERE	0.058	25	R Scapula	ELLIPSOID	0.051
13	L Knee	SPHERE	0.058	26	L Scapula	ELLIPSOID	0.051

3.1.3 Scaling Anthropometric Data

The anthropometric data presented in previous sections refers to the standard 50th-percentile human male. However, in the majority of the cases, the stature, segment lengths, body masses and body physique of the subject under analysis are different from the anthropometric data presented before. In order to improve the similarity of the anthropometric model with respect to the body of the subject being examined, the anthropometric data is submitted to a scaling procedure. The detail and complexity of a scaling procedure is dependent of the amount of available data on the subject under analysis. Hanavan (1964) defined a minimum set of twenty-five dimensions required to calculate the masses, center-of-mass locations and inertias of any given subject. However, such parametric information is not often accessible and more straightforward scaling procedures are required.

In the present work, the scaling procedure used calculates for each anatomical segment, non-dimensional scaling factors, based on measured data from the subject and equivalent data from the 50th percentile human male. These scaling factors are defined as (Laananen, 1991):

$$\chi_{L_i} = \frac{L_i^{n^{th}}}{L_i^{50^{th}}}$$
$$\chi_{m_i} = \frac{m_i^{n^{th}}}{m_i^{50^{th}}} \tag{3.1}$$
$$\chi_{I_i} = \chi_{m_i} \cdot \chi_{L_i}^2$$

where χ_{L_i}, χ_{m_i} and χ_{I_i} are respectively the scaling factors of the length, mass and moments of inertia calculated for segment *i*. It should be noted that if the length and mass of each segment of the subject are not available, the calculation of χ_{L_i} and χ_{m_i} can be performed using the ratio between statures and the ratio between total body weights, respectively. The length scaling factor is used to scale all the dimensions, including center-of-mass location and body-shape surfaces. The scaled anthropometric data is obtained multiplying the calculated scaling factors by the corresponding values in Table 3.2 and Table 3.3. This procedure should only be used to scale subjects of the same gender and with anthropometric characteristics not far from the reference model.

3.1.4 Joint Range of Motion

In this section, the limits of human joint motion are presented for the joints interconnecting the anatomical segments of the model shown in Figure 3.1. The anthropometric data used in the description of the range of motion of the joints is mainly reported in SOMLA and is based on the works of Dempster and Glanville (Laananen *et al.*, 1983). Additional data, describing the range of motion of the wrist and ankle joints is obtained from the work of Panero and Zelnik (1987). Complementary information regarding this subject is also obtained from Kapandji (1973; 1974a; 1974b) and Rouvière (1924; 1943; 1954). Significant differences can be found in the literature regarding the joint range of motion. This variability reflects the fact that most of the data describing the range of motion of the human joints is obtained in

particular conditions, using cadavers or well-trained volunteers. Moreover, in most cases, this data does not reflect many important aspects that may contribute to restrict the human body range of motion, such as: age, sex and body geometry, or even the type of the clothes and foot-ware that is being used.

Table 3.4: Range of motion of the human body joints. This table contains the description, representation and quantification of the most important motions described by eight gross-motion joint complexes of the human body. Data reported by (Laananen *et al.*, 1983; Panero and Zelnik, 1987)

Joint Name	Motion Name	Representation	Rotation [deg]
Head-Neck-Torso	Flexion	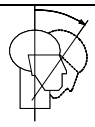	60
	Hyperextension	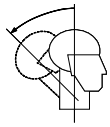	60
	Lateral Flexion	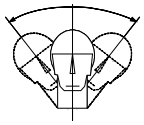	40
	Rotation	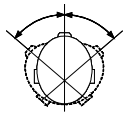	78
Shoulder	Flexion	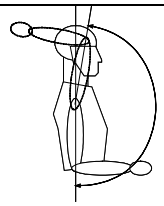	180
	Hyperextension	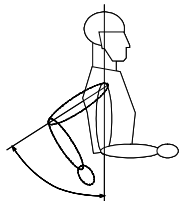	58
	Abduction	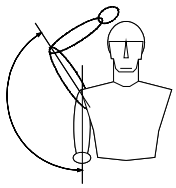	130

Joint Name	Motion Name	Representation	Rotation [deg]
Elbow	Flexion		141
	Pronation / Supination	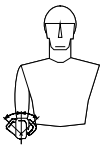	90 / 90
Wrist	Flexion/Extension	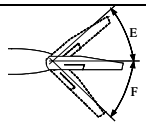	70 / 65
	Deviation Radial/Ulnar	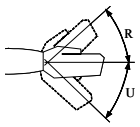	15 /30
Upper-Lower Torso	Flexion	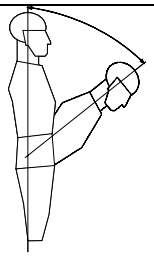	70
	Hyperextension	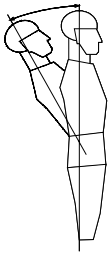	30
	Lateral Flexion	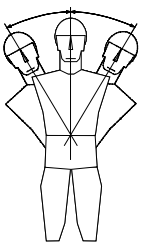	35
	Rotation	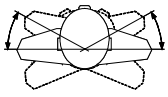	35

Joint Name	Motion Name	Representation	Rotation [deg]
Hip	Flexion	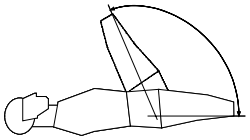	102
	Hyperextension		45
	Abduction/Adduction	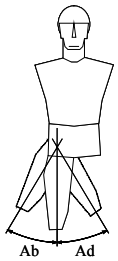	53 / 31
	Medial/Lateral Rotation	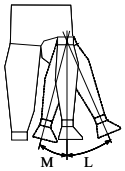	39 / 34
Knee	Flexion	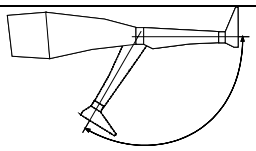	125
Ankle	Flexion / Dorsiflexion	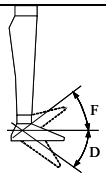	20 / 35
	Inversion / Eversion	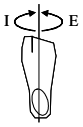	35 / 25
	Abduction/Adduction	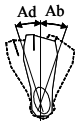	5 / 5

3.2 Biomechanical Models

In the present work two whole-body response biomechanical models of the human body are implemented, using the multibody formulation described in Chapter 2. The models share the same anthropometric model introduced in Section 3.1, although they have considerably different kinematic structures.

There are essentially two main reasons justifying the implementation of two different biomechanical models: the type of dynamic analysis to perform and the type of situation/task to simulate. The first biomechanical, due to its very simple and straightforward kinematic structure, is to be used in forward dynamic analyses only and preferably in impact simulations modeling a pedestrian or a vehicle occupant. This biomechanical model is not suitable to be used in inverse dynamic analyses. Conversely, the second biomechanical model has a much more complex kinematic structure, especially developed for inverse dynamic analyses of human motion, in a wide variety of situations and tasks. This second biomechanical model can also be used in forward dynamic analyses although, in the majority of the applications, due to its more complex kinematic structure, it presents a reduced computational efficiency, when compared with the first one. Considering the main features described before, the first model is hereafter designated as *forward biomechanical model* or simply *forward model*, while the second model is referred to as *inverse biomechanical model* or simply *inverse model*.

Both biomechanical models can be viewed as a collection of rigid bodies interconnected by kinematic joints, in which the rigid bodies are used to describe the anatomical segments represented in Figure 3.1. However, while in the forward model a rigid body can be used to represent one or more anatomical segments, in the inverse model more than one rigid body is usually required to represent an anatomical segment.

Regarding the type of joints used in both models to interconnect the rigid bodies, and according to the definition given by Zatsiorsky (1998), these are considered to be *nominal* joints or *geometrically ideal* joints. Considering the schematic representation provided in Figure 3.4, the following simplifying assumptions are considered:

- The joint movement is of pure rotation about one or more fixed joint axes;
- The translational joint motion can be neglected;
- For joints with two or three degrees-of-freedom, the axes of rotation are orthogonal and intersect each other at the joint center.

This approach is commonly used to simulate gross motor activities such as walking and running, although it is considered to be too much superficial when specific details of the joint motion are an issue (Zatsiorsky, 1998).

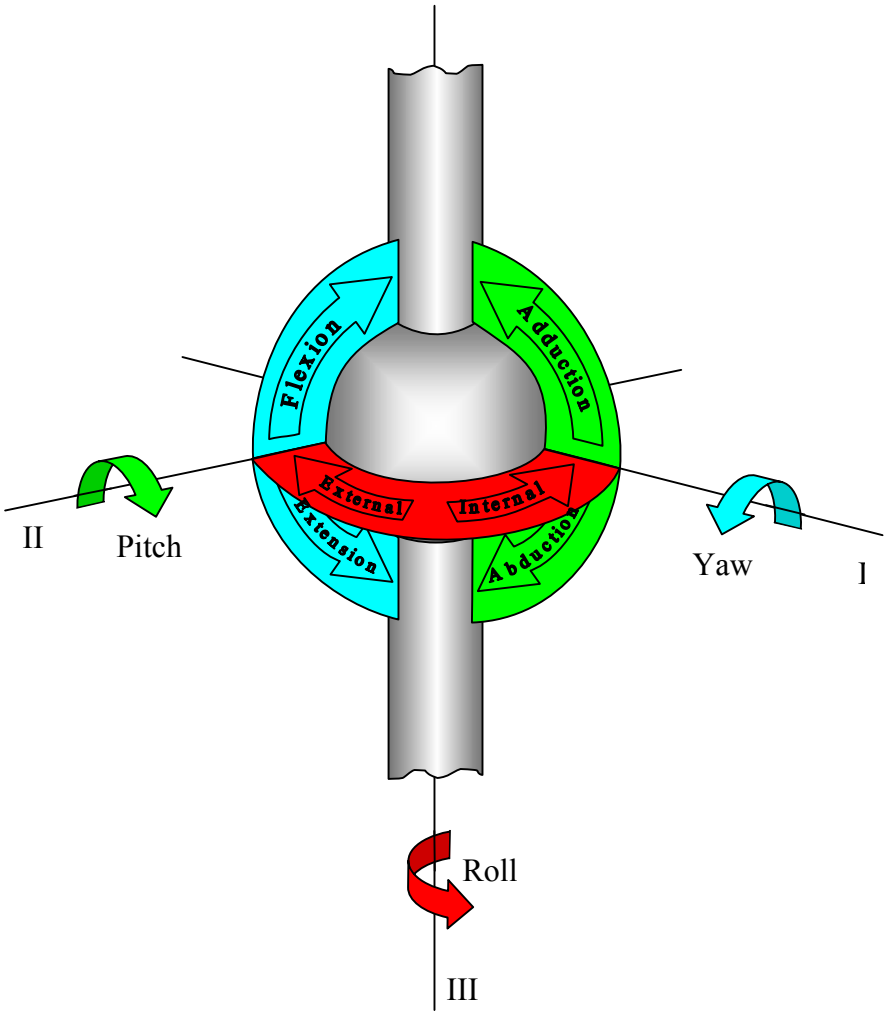

Figure 3.4: Schematic representation of a *nominal* or *geometrically ideal* joint with three degrees-of-freedom (for instance the right hip joint). The joint rotation axes (flexion-extension, abduction-adduction and internal-external rotation) intersect each other at the fixed joint center.

In geometrically ideal joints, the axes of rotation of the joint are called *nominal joint axes*. It is often observed in the literature that the rotations, performed by the segments in turn of these axes, are classified differently depending on the research background. Therefore, referring once more to Figure 3.4, it should be noted that while from the engineering stand point these rotations are typically known as yaw, pitch and roll; from the physiological point of view, these rotations are classified as flexion-extension, abduction-adduction and internal-external rotation. Moreover, if the extension of a joint exceeds its normal position it is often designated by hyperextension. In some anatomical segments such as the head and foot, the extension of the joint is often designated as dorsiflexion. Regarding the internal-external rotation of a joint, a different designation can be found depending on the anatomical segment in analysis. For instance, it is often used the term pronation-supination to describe the internal-external rotation of the lower arm; and the term inversion-eversion to describe the internal-external rotation of the foot.

3.2.1 Forward Biomechanical Model

The forward biomechanical model has a kinematic structure made of twelve rigid bodies interconnect by eleven kinematic joints, as depicted in Figure 3.5(a). These twelve rigid bodies are considered to be the minimum set of rigid elements required to model with accuracy the whole-body response of the human body (Laananen *et al.*, 1983). The model also considers that the joints defining the wrists and ankles are rigid, which allows for the hands and lower arms as well as the feet and lower legs to be defined using only one rigid body. However, due to this simplification, this model should only be used in simulations where the relative motion between these joints is of no importance for the results.

A local reference frame is rigidly attached to each rigid body. The criteria used to locate the origin and orientation of these frames are the same used in Section 3.1, when defining the anthropometric model, i.e., the origin is located in the center-of-mass of each rigid body and the orientation is coincident with the global reference frame (xyz), for the reference seated position. Using these criteria, the application of the anthropometric data, provided in Section 3.1, to define the characteristics of the rigid bodies is a straightforward procedure.

In Table 3.5, a detailed description of the rigid bodies is presented. This table also includes the points and unit vectors used in the definition of the set of generalized coordinates of each rigid body.

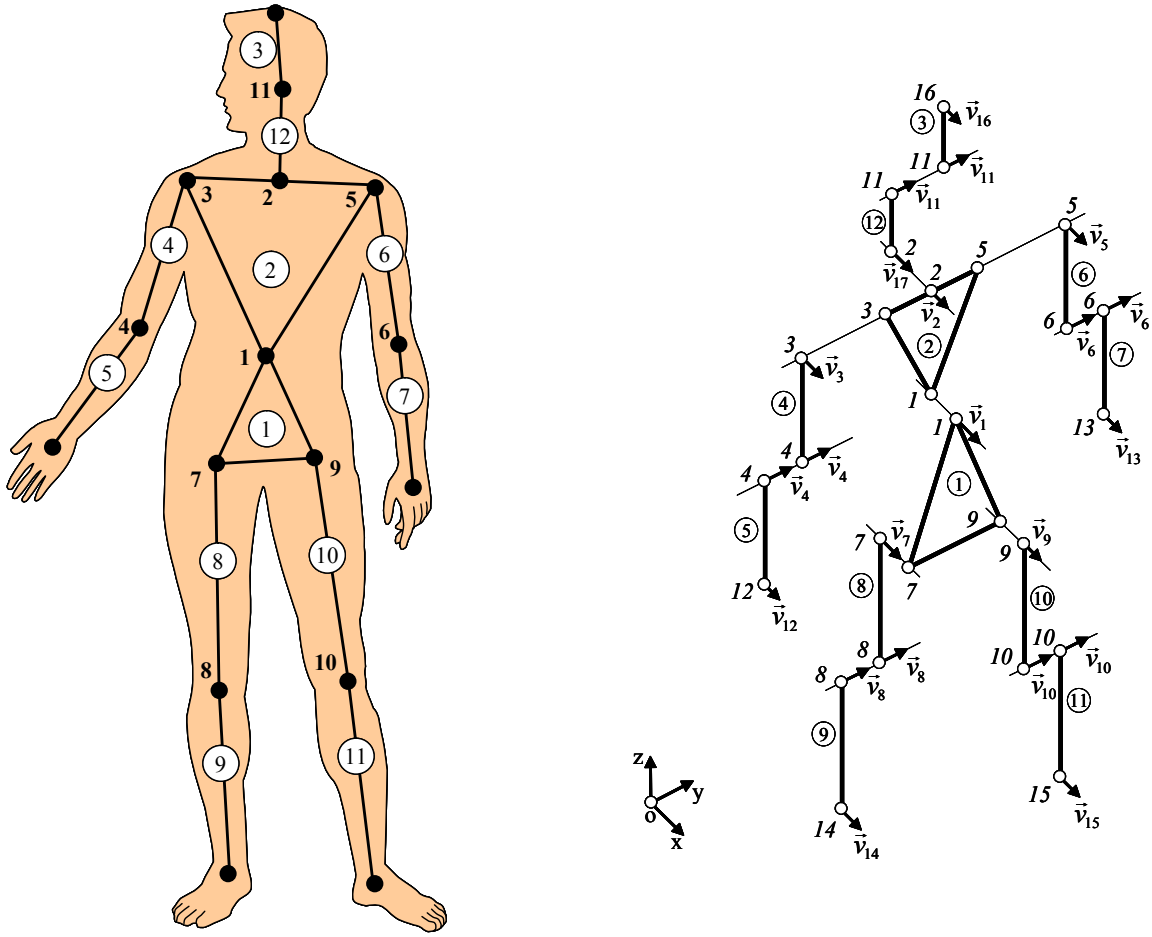

Figure 3.5: Forward biomechanical model: (a) Structure of twelve rigid bodies (body numbers are inside a circle) used to model the sixteen anatomical segments depicted in Figure 3.1, and the eleven kinematic joints (joint numbers are in bold) described in detail in Table 3.6; (b) The exploded view of the kinematic structure of the biomechanical model with indication of the points (represented in italic) and unit vectors. Shared points and shared vectors are represented more than once in the exploded view.

Table 3.5: Rigid bodies used to describe the forward biomechanical model. The local coordinates are used to locate the position and orientation of points and vectors with respect to the local reference frame of each rigid body (as specified in Figure 3.2). Refer to Table 3.2 for the values of L_i, d_i and $\underline{d}_i$.

Name	Body i	Type	Points	Vectors	Local Coordinates		
					ξ_i [m]	η_i [m]	ζ_i [m]
Lower Torso	1	3 points 1 vector (see Sec 2.4.6)	1		0.0	0.0	$L_I - d_I$
			7		0.0	$-\underline{d}_I$	$-d_I$
			9		0.0	$\underline{d}_I$	$-d_I$
				1	1.0	0.0	0.0
Upper Torso	2	3 + 1 points 1 vector (see Sec 2.3.2 and Sec 2.4.6)	1		0.0	0.0	$-d_{II}$
			2		0.0	0.0	$L_{II} - d_{II}$
			3		0.0	$-\underline{d}_{II}$	$L_{II} - d_{II}$
			5		0.0	$\underline{d}_{II}$	$L_{II} - d_{II}$
				2	1.0	0.0	0.0
Head	3	2 points 2 vectors (see Sec 2.4.5)	11		$-\underline{d}_{III}$	0.0	$-d_{III}$
			16		$-\underline{d}_{III}$	0.0	$L_{III} - d_{III}$
				11	0.0	1.0	0.0
				16	1.0	0.0	0.0
Upper Arm	4 (6)	2 points 2 vectors (see Sec 2.4.5)	3 (5)		0.0	0.0	d_{IV} (d_{VI})
			4 (6)		0.0	0.0	$d_{IV} - L_{IV}$ ($d_{VI} - L_{VI}$)
				3 (5)	1.0	0.0	0.0
				4 (6)	0.0	1.0	0.0
Lower Arm	5 (7)	2 points 2 vectors (see Sec 2.4.5)	4		$-d_{V\_XIII}$ ($-d_{VII\_XIV}$)	0.0	0.0
			12 (13)		$L_{V\_XIII} - d_{V\_XIII}$ ($L_{XII\_XIV} - d_{XII\_XIV}$)	0.0	0.0
				4 (6)	0.0	1.0	0.0
				12 (13)	0.0	0.0	1.0
Upper Leg	8 (10)	2 points 2 vectors (see Sec 2.4.5)	7 (9)		$-d_{VIII}$ ($-d_X$)	0.0	0.0
			8 (10)		$L_{VIII} - d_{VIII}$ ($L_X - d_X$)	0.0	0.0
				7 (9)	0.0	0.0	1.0
				8 (10)	0.0	1.0	0.0
Lower Leg	9 (11)	2 points 2 vectors (see Sec 2.4.5)	8 (10)		0.0	0.0	d_{IX_XV} (d_{XI_XVI})
			14 (15)		0.0	0.0	$L_{XI\_XVI} - d_{XI\_XVI}$ ($L_{XI\_XVI} - d_{XI\_XVI}$)
				8 (10)	0.0	1.0	0.0
				14 (15)	1.0	0.0	0.0
Neck	12	2 points 2 vectors (see Sec 2.4.5)	2		0.0	0.0	$-d_{XII}$
			11		0.0	0.0	$L_{XII} - d_{XII}$
				2	1.0	0.0	0.0
				11	0.0	1.0	0.0

The complete set of rigid bodies is described using a collection of sixteen points and seventeen unit vectors, located at the joints and extremities of the anatomical segments, to which corresponds a total number of ninety-nine generalized coordinates. The local coordinates, presented in Table 3.5, are used to locate the points and unit vectors with respect to the local reference frame of each rigid body, as represented in Figure 3.2. The anthropometric link-lengths (L_i) and center-of-mass locations (d_i and $\underline{d}_i$) that appear in this table refer to the ones presented in Table 3.2 for the standard 50th percentile human male.

As it can be observed in Figure 3.5 and on Table 3.5, a same point or unit vector can be used to describe the kinematics of more than one rigid body. This process of sharing points and unit vectors allows simple kinematic joints, such as revolute and spherical, to be defined in a natural way, as pointed out on the previous chapter.

The joints used in the biomechanical model are of two types: revolute joints with one degree-of-freedom (usually the flexion-extension of an anatomical segment) and spherical joints with three degrees-of-freedom (the three rotations as represented in Figure 3.4). In Figure 3.6, the revolute and spherical joints used to describe the model's elbow and hip joints are presented respectively.

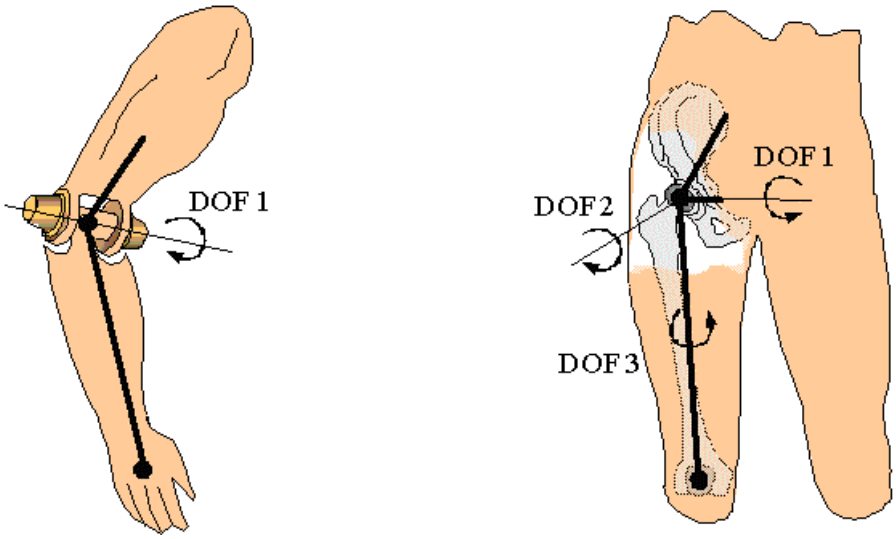

Figure 3.6: Example of application of a 1 DOF revolute joint and a 3 DOF spherical joint to model the nominal joints of the elbow and hip respectively. A similar approach, using revolute and spherical joints, is used to model the remaining joints of the forward biomechanical model.

A detailed description of the joints is presented in Table 3.6. There, the joint type, the location of the joint center and the points and unit vectors used in their definition are identified. The forward biomechanical model has twenty-nine degrees-of-freedom, in which five are associated with revolute joints, eighteen with spherical joints and six with rigid body motion.

Table 3.6: Nominal joints used in the forward biomechanical model. Description of the joints used to interconnect the rigid bodies of the forward biomechanical model. Indication of the type of joint, number of degrees-of-freedom, points and vectors used in their construction and location of the joint center.

Nbr.	Joint	Type	DOF	Shared		Joint Center Location
				Point	Vector	
1	Back	Spherical	3	1	–	†Between 12th thoracic and 1st lumbar
2	Torso/Neck	Spherical	3	2	–	†Between 7th cervical and 1st thoracic
3 (5)	Shoulder	Spherical	3	3 (5)	–	‡At the center of the humeral head.
4 (6)	Elbow	Revolute	1	4 (6)	4 (6)	‡Center of a transverse section of the humerus at the level of the medial humeral epicondyle.
7 (9)	Hip	Spherical	3	7 (9)	–	‡At the center of the femoral head.
8 (10)	Knee	Revolute	1	8 (10)	8 (10)	‡Midpoint between the maximal protrusions of the femoral epicondyles.
11	Head/Neck	Revolute	1	11	11	†At occipital condyles.

†from (Laananen *et al.*, 1983); ‡from (Zatsiorsky, 1998).

3.2.2 Inverse Biomechanical Model

The inverse biomechanical model, presented in Figure 3.7, is a general-purpose model based on the work of Celigüeta (1996). The model can be used to simulate a wide variety of situations and human tasks, in forward or inverse dynamic analyses. However, its kinematic structure of rigid bodies and nominal joints is especially suitable to be applied to the inverse dynamic analysis of the human body.

The major objective of an inverse dynamic analysis is to calculate the external forces that need to be applied to the elements of the system in order to produce a previously observed motion. In biomechanical applications, these external forces are usually the net moments-of-force, developed by the muscular apparatus about the nominal joint axes (see Figure 3.4), that produce a prescribed joint posture, i.e., that produce a specified combination of flexion/extension, adduction/abduction and internal/external rotation. For this purpose, in

biomechanical models for inverse dynamic analysis, it is essential to have a set of nominal axes associated to each joint.

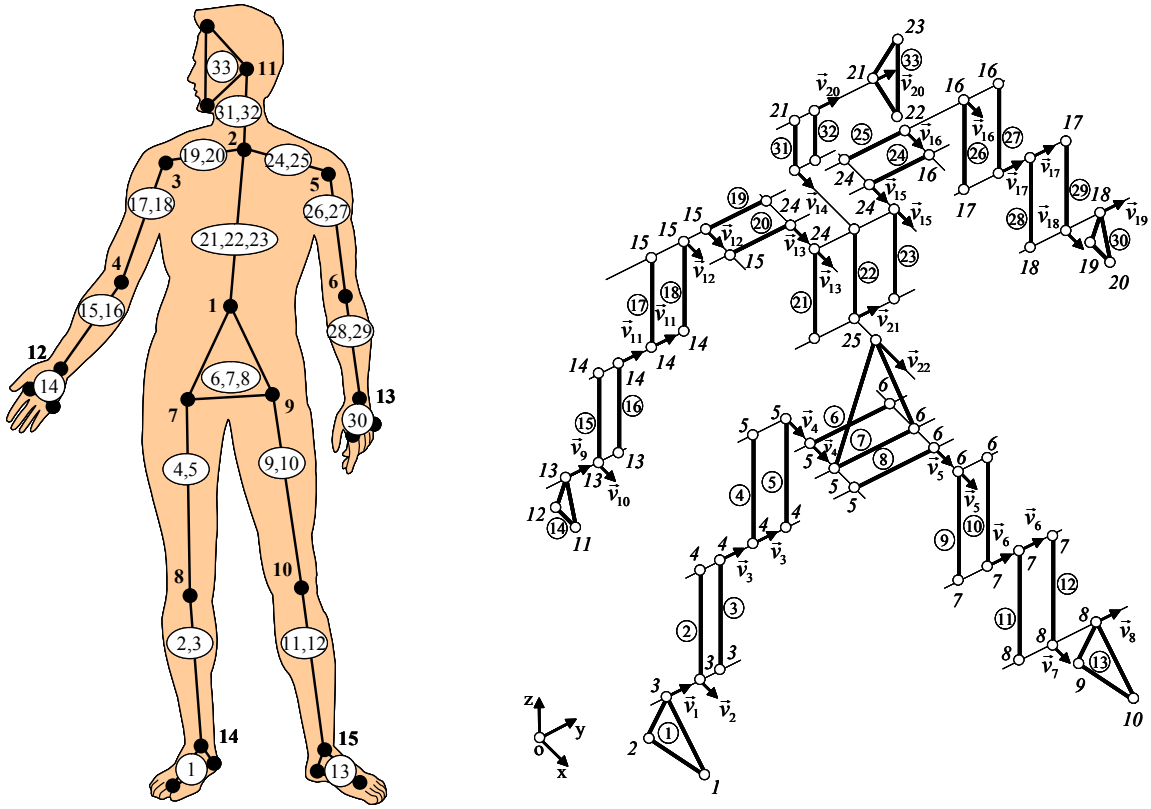

Figure 3.7: Inverse biomechanical model. (a) Structure of thirty-three rigid bodies (body numbers are inside a circle) used to model the sixteen anatomical segments depicted in Figure 3.1, and the fifteen kinematic joints (joint numbers are in bold) described in detail in Table 3.7; (b) The exploded view of the kinematic structure of the biomechanical model with indication of the points (represented in italic) and unit vectors. Shared points and shared vectors are represented more than once in the exploded view.

Considering the kinematics of a revolute joint, it is always possible to associate the nominal joint axis to the unit vector used in its definition. However, in the case of a spherical joint, this procedure cannot be used anymore since there are no unit vectors to which associate the nominal joint axes. In order to solve this problem, every spherical joint of the forward model is substituted by an equivalent joint set made of a revolute and a universal joint, as illustrated in Figure 3.8. This equivalent joint set allows the same three rotations of a

spherical joint but in this case, the rotations are perfectly defined about the fixed axes of the three unit vectors used in the joint construction. It is now possible to associate the nominal joint axes to each one of these joint vectors and to use them to measure and describe any joint posture.

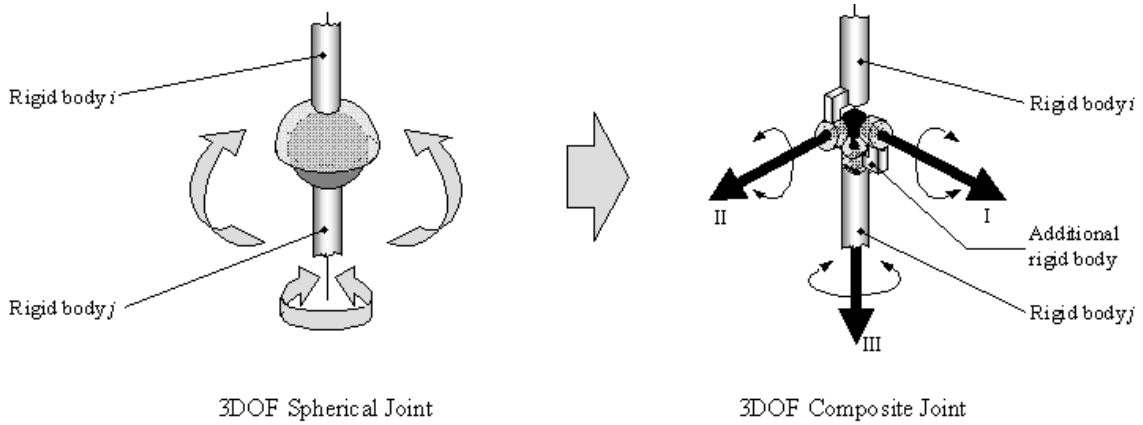

Figure 3.8: Replacement of a spherical joint by an equivalent composite joint made with a revolute and a universal joint.

Although necessary, this procedure has some drawbacks. For each composite joint a new additional rigid body must be introduced, as depicted in Figure 3.8. Consequently, there is a substantial increment in the number of rigid bodies necessary to describe the model, as it can be observed in Figure 3.7, and also in the number of generalized coordinates and kinematic constraints. This is the main reason why, in this model, it is usually required more than one rigid body to describe each one of the anatomical segment of the anthropometric model introduced in Section 3.1.

Additionally, there are many situations and tasks in which the calculation of the moments-of-force at the ankle and wrist joints is required. Therefore, the hands and feet of the inverse model are described using independent rigid bodies. The wrist and ankle joints are no longer rigid, like in the forward model, but instead, are described using the composite joint represented in Figure 3.8.

Some changes are also introduced to describe the kinematics of the upper torso and head. Instead of one single rigid body, the upper torso is now defined using seven rigid bodies, which allow the shoulders to have independent motions. With respect to the head segment,

this is modeled using a rigid body with three points and one unit vector rather than using a basic rigid body with two points and two vectors. For inverse dynamic analyses, this change allows the position of the head, in terms of its internal/external rotation, to be determined with a higher precision level.

The result is an inverse biomechanical model with a kinematic structure made of thirty-three rigid bodies interconnected by the fifteen geometrically ideal joints, represented in Figure 3.7(a). The rigid bodies are described using a collection of twenty-five points and twenty-two unit vectors located at the joints and extremities of the model, making a total number of 141 generalized coordinates. In Table 3.7 a detailed description of the joints is presented, in which the joint type, the location of the joint center and the points and unit vectors used are identified. The inverse biomechanical model has forty-four degrees-of-freedom, in which nine are associated with revolute joints, thirty with composite and universal joints and six with rigid body motion.

Table 3.7: Joints of the inverse biomechanical model. Description of the joints used to interconnect the rigid bodies of the inverse biomechanical model, with the indication of their type, number of degrees-of-freedom, points and vectors used in their construction and location of their joint centers.

Nbr.	Joint	Type	DOF	Shared		Joint Center Location
				Point	Vector	
1	Back	Universal	2	25	–	†Between 12th thoracic and 1st lumbar
2	Torso/Neck	Composite	3	24	–	†Between 7th cervical and 1st thoracic vertebrae.
	Torso/Scapula	Rev + Rev	2	24,25	13 (15)	
3 (5)	Shoulder	Composite	3	15 (16)	–	‡At the center of the humeral head.
4 (6)	Elbow	Revolute	1	14 (17)	11 (17)	‡Center of a transverse section of the humerus at the level of the medial humeral epicondyle.
7 (9)	Hip	Composite	3	5 (6)	–	‡At the center of the femoral head.
8 (10)	Knee	Revolute	1	4 (7)	3 (6)	‡Midpoint between the maximal protrusions of the femoral epicondyles.
11	Head/Neck	Revolute	1	21	20	†At occipital condyles.
12 (13)	Wrist	Composite	3	13 (18)	–	‡Center of a transverse section of the capitate bone, at the level of the grove between the lunate and capitate bones.
14 (15)	Ankle	Composite	3	3 (8)	–	‡Center of a transverse section of the talus, at the level of the distal tip of the fibula.

†from (Laananen *et al.*, 1983); ‡from (Zatsiorsky, 1998).

Due to the complexity of the kinematic structure of the inverse model, special attention must be put in the association of the anthropometric data, provided in Section 3.1, to the rigid bodies describing the model. The association process is not as straightforward as it is for the forward model and, therefore, some additional anthropometric information needs to be calculated, from the initial anthropometric data, to fit the kinematic structure of the inverse model. It should be noted that although the anthropometric model described in Section 3.1 supports both biomechanical models, some of its anthropometric characteristics need to be expanded considering the increased number of rigid bodies and joints of the inverse model.

In Figure 3.9 the anthropometric model is presented in its original and expanded forms. As it can be observed, the reference position with respect to the global reference frame is still the same in the expanded form, although some new centers-of-mass can be identified in the anatomical segments describing the hands, feet, upper and lower torso. As a result, the center-of-mass locations of the lower arms, lower legs, upper and lower torso need to be recalculated, in order to preserve the original anthropometric data.

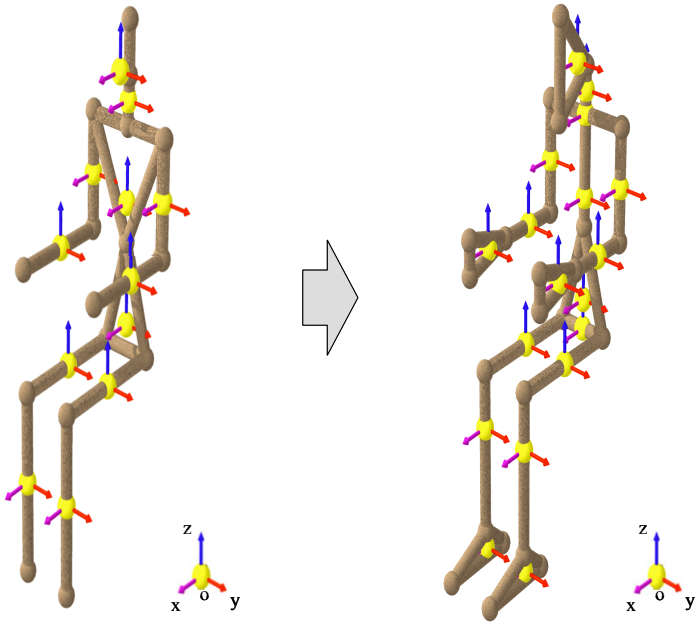

Figure 3.9: Expansion of the anthropometric data to fit the inverse model. In the expanded representation, the center-of-mass of the hands and feet is detached from the center-of-mass of the lower arm and lower leg, respectively.

A local reference frame is rigidly attached to each rigid body. The criteria used to locate the origin and orientation of these frames are the same used in Section 3.1, i.e., the frame origin is located in the center-of-mass of each rigid body and its orientation is coincident with the global reference frame (xyz), in the reference seated position. The principal dimensions that characterize the sixteen anatomical segments of the standard 50th percentile human male, in its expanded form, are illustrated in Figure 3.10.

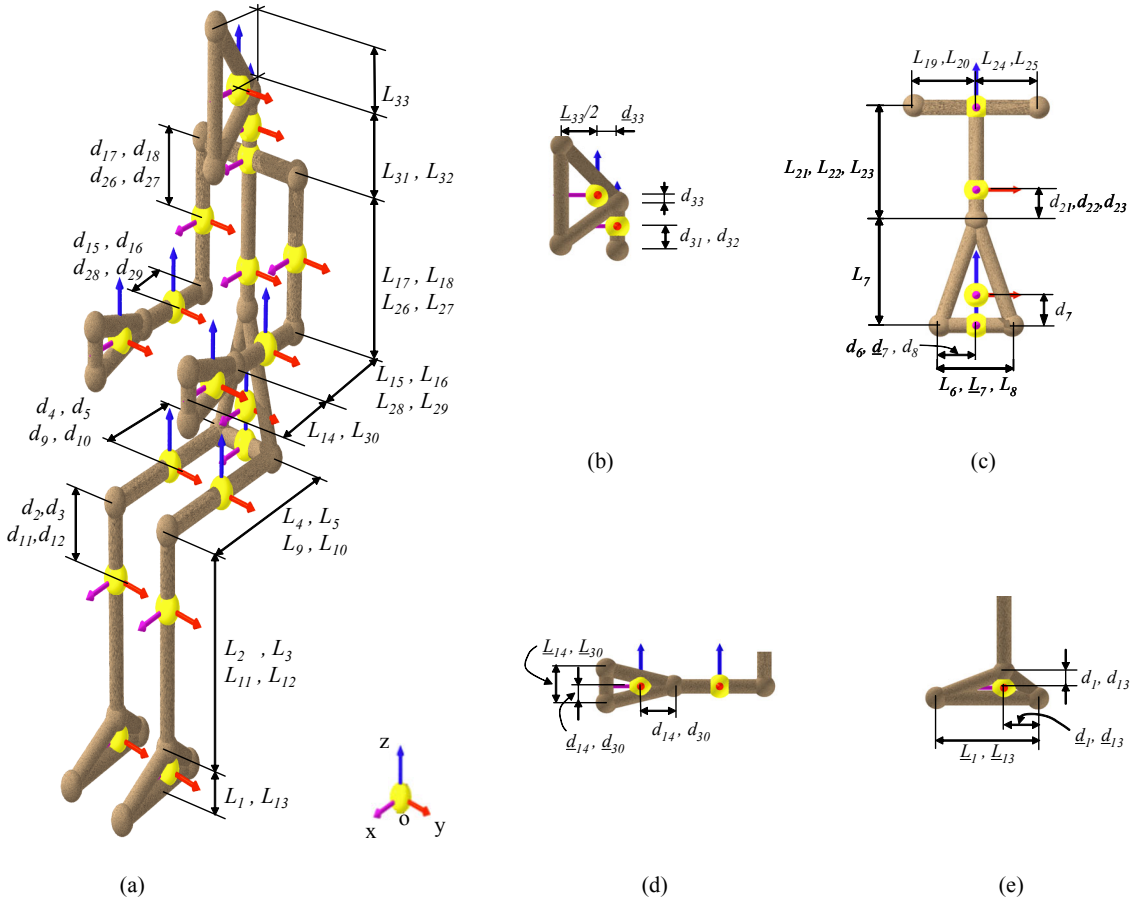

Figure 3.10: Expanded form of the anthropometric model. Representation of the major dimensions, reference frames and center of mass locations. (a) Perspective view in the reference seated position. (b) Sagittal view of the principal dimensions of the head and neck. (c) Frontal view of the principal dimensions of the lower and upper torso. (d) Sagittal view of the principal dimensions of the hand. (d) Sagittal view of the principal dimensions of the foot.

In Table 3.8 the expanded anthropometric data is presented. In this table, the index i specifies the rigid body number of the rigid bodies used to describe the kinematic structure of the inverse biomechanical model represented in Figure 3.8. It is assumed that the orientation of the local reference frames is coincident with the principal axes of each rigid body.

Table 3.8: Expanded anthropometric data referring the sixteen anatomical segments represented in the model of Figure 3.1. The lengths L_i and $\underline{L}_i$ and the center-of-mass locations d_i and $\underline{d}_i$ are schematically represented in Figure 3.10.

Description	Seg.	Body	Length		CM Location		Mass	Principal Moments of Inertia		
		i	L_i [m]	$\underline{L}_i$ [m]	d_i [m]	$\underline{d}_i$ [m]	m_i [Kg]	$I_{\xi i}$ [10^{-2} Kg.m^2]	$I_{\eta i}$ [10^{-2} Kg.m^2]	$I_{\zeta i}$ [10^{-2} Kg.m^2]
		6	0.188	–	0.094	–	1.420	2.622	1.009	2.622
Lower Torso	I	7	0.275	0.188	0.079	0.094	11.360	19.550	10.010	20.980
		8	0.188	–	0.094	–	1.420	2.622	1.009	2.622
		19	0.161	–	0.000	–	0.624	1.417	1.395	1.393
		20	0.161	–	0.000	–	0.624	1.417	1.395	1.393
		21	0.294	–	0.079	–	7.485	2.875	7.066	4.546
Upper Torso	II	22	0.294	–	0.079	–	7.485	2.875	7.066	4.546
		23	0.294	–	0.079	–	7.485	2.875	7.066	4.546
		24	0.161	–	0.000	–	0.624	1.417	1.395	1.393
		25	0.161	–	0.000	–	0.624	1.417	1.395	1.393
Head	III	33	0.128	0.191	0.020	0.051	4.241	2.453	2.249	2.034
R Upper Arm	IV	17	0.295	–	0.153	–	0.996	0.746	0.678	0.124
		18	0.295	–	0.153	–	0.996	0.746	0.678	0.124
R Lower Arm	V	15	0.250	–	0.123	–	0.701	0.062	0.482	0.149
		16	0.250	–	0.123	–	0.701	0.062	0.482	0.149
R Hand	XIII	14	0.185	0.090	0.093	0.045	0.489	0.067	0.146	0.148
L Upper Arm	VI	26	0.295	–	0.153	–	0.996	0.746	0.678	0.124
		27	0.295	–	0.153	–	0.996	0.746	0.678	0.124
L Lower Arm	VII	28	0.250	–	0.123	–	0.701	0.062	0.482	0.149
		29	0.250	–	0.123	–	0.701	0.062	0.482	0.149
L Hand	XIV	30	0.185	0.090	0.093	0.045	0.489	0.067	0.146	0.148
R Upper Leg	VIII	4	0.434	–	0.215	–	4.922	0.718	7.970	4.934
		5	0.434	–	0.215	–	4.922	0.718	7.970	4.934
R Lower Leg	IX	2	0.439	–	0.151	–	1.813	0.543	1.915	1.570
		3	0.439	–	0.151	–	1.813	0.543	1.915	1.570
R Foot	XV	1	0.069	0.271	0.035	0.091	1.182	0.129	0.128	2.569
L Upper Leg	X	9	0.434	–	0.215	–	4.922	0.718	7.970	4.934
		10	0.434	–	0.215	–	4.922	0.718	7.970	4.934
L Lower Leg	XI	11	0.439	–	0.151	–	1.813	0.543	1.915	1.570
		12	0.439	–	0.151	–	1.813	0.543	1.915	1.570
L Foot	XVI	13	0.069	0.271	0.035	0.091	1.182	0.129	0.128	2.569
Neck	XII	31	0.122	–	0.061	–	0.531	0.134	0.107	0.107
		32	0.122	–	0.061	–	0.531	0.134	0.107	0.107

A detailed description of the rigid bodies as well as the points and unit vectors used in their construction is presented in Table 3.9. The local coordinates locate the points and vectors in the local reference frame of each body and are therefore invariant throughout the analysis.

Table 3.9: Description of the rigid bodies used to construct the inverse biomechanical model. The local coordinates are used to locate the position and orientation of points and vectors with respect to the local reference frame of each rigid body (as specified in Figure 3.10). Refer to Table 3.8 for the values of L_i, $\underline{L}_i$, d_i and $\underline{d}_i$.

Name	Body i	Type	Points	Vector(s)		Local Coordinates		
				nbr	in body	ξ_i [m]	η_i [m]	ζ_i [m]
Lower Torso	7	3 points	5			0.0	$-\underline{d}_7$	$-d_7$
			6			0.0	$\underline{L}_7 - \underline{d}_7$	$-d_7$
		1 vector	25			0.0	0.0	$L_7 - d_7$
				22	7	1.0	0.0	0.0
	6 (8)	2 points	5			0.0	$-d_6$	0.0
			6			0.0	$L_6 - d_6$	0.0
		1 vector		4 (5)	6 (8)	0.0	0.0	1.0
Upper Torso	21,22 (23)	2 points	24			0.0	0.0	$L_{22} - d_{22}$
			25			0.0	0.0	$-d_{22}$
		1 vector		13 (15)	21 (23)	1.0	0.0	0.0
				21	22	0.0	1.0	0.0
	19 (20)	2 points	15			0.0	$d_{19} - L_{19}$	0.0
			24			0.0	d_{19}	0.0
		1 vector		12 (13)	19 (20)	1.0	0.0	0.0
	24 (25)	2 points	16			0.0	$L_{24} - d_{24}$	0.0
			24			0.0	$-d_{24}$	0.0
		1 vector		15 (16)	24 (25)	1.0	0.0	0.0
Head	33	3 points	21			$-\underline{d}_{33}$	0.0	$-d_{33}$
			22			$\underline{L}_{33}/2 - \underline{d}_{33}$	0.0	$-L_{33}$
		1 vector	23			$\underline{L}_{33}/2 - \underline{d}_{33}$	0.0	L_{33}
				20	33	0.0	1.0	0.0
Upper Arm	17,18 (27,26)	2 points	14 (17)			0.0	0.0	$d_{17} - L_{17}$ $(d_{26} - L_{26})$
			15 (16)			0.0	0.0	d_{17} (d_{26})
		1 vector		11 (17)	17 (27)	0.0	1.0	0.0
				12 (16)	18 (26)	1.0	0.0	0.0
Lower Arm	15,16 (29,28)	2 points	13 (18)			$L_{15} - d_{15}$ $(L_{28} - d_{28})$	0.0	0.0
			14 (17)			$-d_{15}$ $(-d_{28})$	0.0	0.0
		1 vector		10 (18)	15 (29)	0.0	0.0	1.0
				11 (17)	16 (28)	0.0	1.0	0.0

Table 3.9 (Continued)

Name	Body *i*	Type	Points	Vectors		Local Coordinates		
				nbr	in body	ξ_i [m]	η_i [m]	ζ_i [m]
Hand	14 (30)	3 points 1 vector	11 (20)			$L_{14} - d_{14}$ ($L_{30} - d_{30}$)	0.0	$\underline{L}_{14} - \underline{d}_{14}$ ($\underline{L}_{30} - \underline{d}_{30}$)
			12 (19)			$L_{14} - d_{14}$ ($L_{30} - d_{30}$)	0.0	$-d_{14}$ ($-d_{30}$)
			13 (18)			$-d_{14}$ ($-d_{30}$)	0.0	0.0
				9 (19)	14 (30)	0.0	1.0	0.0
Upper Leg	4,5 (9,10)	2 points 1 vector	4 (7)			$L_4 - d_4$ ($L_9 - d_9$)	0.0	0.0
			5 (6)			$-d_4$ ($-d_9$)	0.0	0.0
				3 (6)	4 (10)	0.0	1.0	0.0
				4 (5)	5 (9)	0.0	0.0	1.0
Lower Leg	2,3 (12,11)	2 points 1 vector	3 (8)			0.0	0.0	$d_2 - L_2$ ($d_{11} - L_{11}$)
			4 (7)			0.0	0.0	d_2 (d_{11})
				2 (9)	2 (12)	1.0	0.0	0.0
				3 (6)	3 (11)	0.0	1.0	0.0
Foot	1 (13)	3 points 1 vector	1 (10)			$\underline{L}_1 - \underline{d}_1$ ($\underline{L}_{13} - \underline{d}_{13}$)	0.0	$d_1 - L_1$ ($d_{13} - L_{13}$)
			2 (9)			$-\underline{d}_1$ ($-\underline{d}_{13}$)	0.0	$d_1 - L_1$ ($d_{13} - L_{13}$)
			3 (8)			0.0	0.0	$-d_1$ ($-d_{13}$)
				1 (8)	1 (13)	0.0	1.0	0.0

3.3 Joint Resistance

In the human body, all joints have a limited range of motion, as described in Section 3.1.4. However, when using geometrically ideal joints, the admissible range of motion, prescribed for each one of these joints, can be easily violated since no additional kinematic restrictions are introduced that prevent those joints from acquiring unfeasible positions, such as knee or elbow hyper-extensions.

Joint resistance moments are introduced in the biomechanical models to prevent unfeasible joint positions to occur and also to simulate the passive muscle action, introducing some energy dissipation at the joint level. Consequently, two terms contribute to the calculation of these moments-of-force: a dissipative term modeled using a viscous torsional damper and a motion-limiting term – also called penalty term – modeled as a nonlinear torsional spring. This is described by :

$$\mathbf{m}_i^{(\mathrm{r})} = \mathbf{m}_i^{(\mathrm{d})} + \mathbf{m}_i^{(\mathrm{p})} \tag{3.2}$$

It should be noted that joint resistance moments are applied to the models only when these are used for forward dynamic simulations. According to Winter (1991), in inverse dynamic analyses the joint angles do not reach their extreme limits, the friction forces are minimal and, therefore, no joint resistance moments need to be applied in this type of analysis.

3.3.1 Joint Dissipative Moment

The joint dissipative moment is introduced to simulate the passive muscle action and to allow some energy dissipation at the joint level. This moment acts to resist the motion of the joint and is calculated using a viscous torsional damper as:

$$\mathbf{m}_i^{(\mathrm{d})} = -j_i \dot{\boldsymbol{\beta}}_i \tag{3.3}$$

where $\dot{\boldsymbol{\beta}}_i$ is the relative angular velocity vector calculated between the bodies interconnected by joint i and j_i is the associated damping coefficient, which differs from joint to joint.

3.3.2 Joint Motion-Limiting Moment

The calculation of the magnitude and direction of the joint motion-limiting moment follows a general procedure that can be applied to restrict the range of motion of any type of joints used in the construction of the biomechanical models. This penalty moment has a nonlinear behavior that is null during normal joint rotation and increases rapidly from zero until a maximum value, specified for each joint, whenever an unfeasible position of the joint is detected. The shoulder joint is used next to illustrate the description of this general procedure, since it is considered to be the most mobile joint of the human body (Kapandji, 1974a).

The first step towards the calculation of the joint penalty moment is the determination of the circumduction cone of each joint (Kapandji, 1974a), i.e., the three-dimensional surface inside which any joint position is considered to be a feasible position. In Figure 3.11 the circumduction cone of the shoulder joint is illustrated. The tip of this cone is always located in the joint center.

It should be noted that a circumduction cone is specified for every joint, independently of the number of its degrees-of-freedom. Even in joints with only one degree-of-freedom, such as the elbow or the knee, this cone is used regardless of their planar type of motion. The only difference is that in this type of joints there are parts of the cone that are never reached due to the intrinsic kinematic structure of these joints.

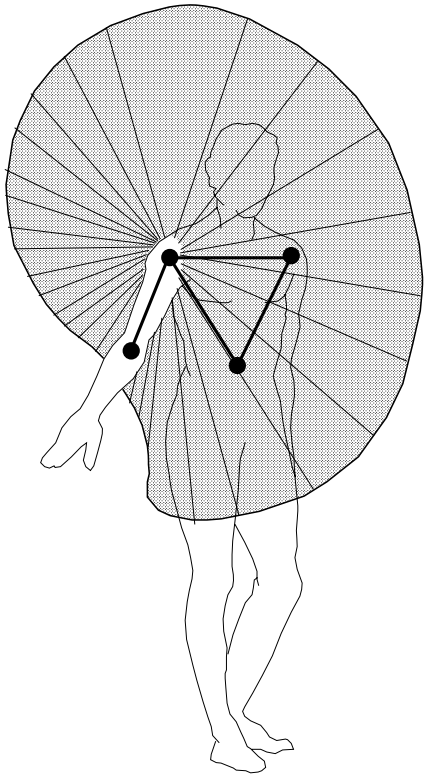

Figure 3.11: Cone of circumduction of the shoulder joint. The cone has the origin located in the shoulder joint center and describes the sector of accessibility, wherein the arm can move without displacement of the upper and lower torso.

The circumduction cone is described using a local reference frame with origin located in the joint center and rigidly attached to the reference body. The axes of the reference frame are calculated using points and unit vectors already defined in the construction of the reference body. In the case of the shoulder joint depicted in Figure 3.12, the unit vectors defining the axes u_ξ and u_η of the local reference frame are built using the points and unit vectors of the upper torso as:

$$\mathbf{u}_{\xi} = \mathbf{u}_{n} \tag{3.4}$$

and

$$\mathbf{u}_{\eta} = \frac{\mathbf{r}_j - \mathbf{r}_i}{\left\| \mathbf{r}_j - \mathbf{r}_i \right\|} \tag{3.5}$$

The third base vector is calculated as the result of the cross product of the first two:

$$\mathbf{u}_{\zeta} = \tilde{\mathbf{u}}_{\xi} \mathbf{u}_{\eta} \tag{3.6}$$

After the construction of the reference frame, a position unit vector $\mathbf{u}_r$ (also represented in the previous figure) with the same direction of the upper arm, is calculated using the two points describing this body:

$$\mathbf{u}_{r} = \frac{\mathbf{r}_k - \mathbf{r}_o}{\left\| \mathbf{r}_k - \mathbf{r}_o \right\|} \tag{3.7}$$

In order to determine whether the actual position of the joint is inside or outside its circumduction cone, the spherical coordinates expressing vector $\mathbf{u}_r$ in the local reference frame ($\mathbf{u}_\xi$, $\mathbf{u}_\eta$, $\mathbf{u}_\zeta$), are calculated. These coordinates are respectively the longitude θ and the latitude β of the actual joint position, as illustrated in Figure 3.13(a), and are used for convenience considering the shape of the circumduction surface.

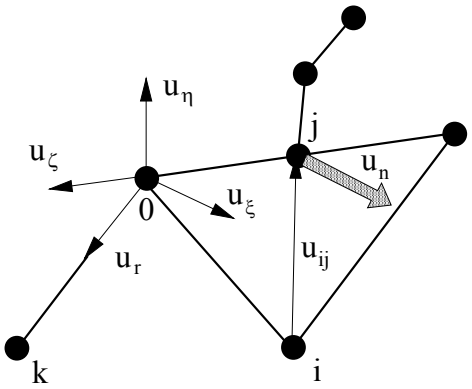

Figure 3.12: Local reference frame ($\mathbf{u}_\xi$, $\mathbf{u}_\eta$, $\mathbf{u}_\zeta$) used to define the circumduction cone of the shoulder joint. The position vector $\mathbf{u}_r$, describing the position of the joint with respect to the local reference frame, is also represented.

The circumduction cone is defined, in a similar way, specifying for any given longitude θ, the maximum allowable latitude β_{max}. As illustrated in Figure 3.13(b), an interpolation curve, expressing β_{max} as a function of θ, is constructed using the information collected from Table 3.4, which contains the aperture of the shoulder joint in positions I to IV.

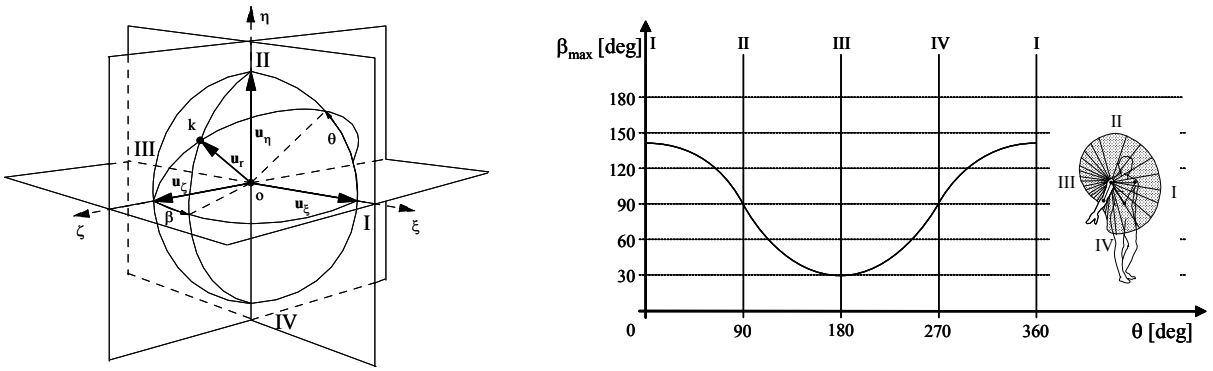

Figure 3.13: Spherical coordinates describing the latitude and longitude of the actual joint position.

If for the actual longitude θ, the associated latitude β exceeds the maximum allowable latitude β_{max} of the joint, then an unfeasible position is occurring and a penalty moment is applied. The penalty moment has a nonlinear behavior that can be described as being zero for any feasible position of the joint and to increase rapidly with the increase of penetration in zones outside the circumduction cone. The direction of the penalty moment is calculated as being orthogonal to the plane described by vectors u_ζ and vector u_r:

$$\begin{cases} \mathbf{m}_i^{(p)} = 0 & \text{if} \quad \beta \le \beta_{\max} \\ \mathbf{m}_i^{(p)} = m_{p_i}\left[3\left(\dfrac{\beta_i - \beta_{i_{\max}}}{\Delta\beta_i}\right)^2 - 2\left(\dfrac{\beta_i - \beta_{i_{\max}}}{\Delta\beta_i}\right)^3\right]\tilde{\mathbf{u}}_\zeta \mathbf{u}_r & \text{if} \quad \beta > \beta_{\max} \end{cases} \tag{3.8}$$

where the term inside brackets is a polynomial of the third degree with the behavior depicted in Figure 3.14. The direction of the resistance moment depicted in Equation (3.8) is accurate for circumduction cones with a circular base. Otherwise, the direction of the moment must be set to be tangent to the generalized cone base in the point of contact with u_r.

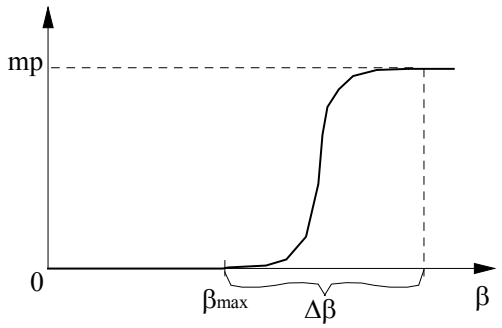

Figure 3.14: Nonlinear behavior of the joint penalty moment. The joint penalty moment is zero for joint apertures less than β_{max} (i.e. inside the circumduction cone) and increase rapidly along a third degree curve for apertures greater than β_{max} (i.e. outside the circumduction cone) until a maximum value m_p is reached.

Table 3.10 describes the values for the limiting angles for the different joints of the human body. The range of motion is obtained from Table 3.4.

Table 3.10: Joint resistance data.

Joint	$\beta_{i\ I}$[°]	$\beta_{i\ II}$[°]	$\beta_{i\ III}$[°]	$\beta_{i\ IV}$[°]	$\Delta\beta_i$[°]	m_i[g]	m_{pi}[Nm]	j_i[Nms]
1	40.0	35.0	30.0	35.0	11.5	2.0	226.0	16.950
2	60.0	40.0	60.0	40.0	15.0	2.0	678.0	3.390
3-5	140.0	90.0	30.0	90.0	11.5	1.0	226.0	3.763
4-6	90.0	-	45.0	-	11.5	1.0	226.0	3.390
7-9	10.0	120.0	50.0	45.0	11.5	2.0	452.0	5.650
8-10	-	90.0	-	45.0	11.5	1.0	226.0	5.650
11	19.0	-	2.0	-	15.0	2.0	452.0	16.950
12-13								
14-15								

3.4 Conclusions

In this Chapter, two whole body response biomechanical models of the human body were presented. These models provide useful simulation tools that allow for a wide variety of situations involving gross-motion human tasks to be analyzed in detail. Although having quite different kinematic structures both models share the same anthropometric data provided by an anthropometric model with sixteen anatomical segments, which is also presented and described in detail in this Chapter. The models are constructed using the multibody formulation presented in Chapter 2. The range of motion of the biomechanical segments was kept in a prescribed zone of feasible motion using joint resisting moments anytime the relative position of two adjacent segments started to violate that region.

Two main reasons can be pointed out, justifying the implementation of two different biomechanical models: the type of dynamic analysis to perform and the type of situation/task to simulate. The first biomechanical model, due to its very simple and straightforward kinematic structure, is to be used in forward dynamic analyses only and preferably in impact simulations as a pedestrian or as a vehicle occupant. The second biomechanical model has a much more complex kinematic structure and it is specially developed for inverse dynamic analyses of human motion, in a wide variety of situations and tasks.

Finally, it was seen that for the type of applications foreseen, in which gross-motion activities are expected, the use of *nominal* joints – also called *geometrically ideal* joints – is preferred to more detailed joint descriptions. However, it was also pointed out that when specific joint details are an issue for the simulation objectives, the type of joints adopted in both biomechanical models may be too simplistic.

Chapter 4

Injury and Impact Biomechanics

In the present chapter, the methodologies and models presented in Chapters 2 and 3 are used to study a set of six illustrative test-cases that demonstrate the application of the proposed multibody formulation and biomechanical models to simulate and analyze a wide variety of situations involving the motion of the human body. The biofidelity of the models, i.e., the correlation between the human behavior and the overall dynamic response of the models in terms of their kinematics and kinetics, are also discussed in the framework of independent data generated with human volunteers or cadavers, in applications to impact biomechanics (Wismans *et al.*, 1994).

All the examples presented in this chapter involve situations in which the main objective is to determine the human response to a particular external event. Depending on the case, these external events illustrate sports impacts, road user accidents and the kinematics of occupants in car crashes. Due to the nature and objectives of the simulations, the forward dynamics approach is used in all the analyses performed. The application examples are:

- Simulation of a frontal and a lateral football tackle;
- Simulation of a car accident using a deceleration sled;

- Simulation of a rollover test using an integrated occupant-vehicle environment;
- Simulation of a rollover test with multiple occupants (belted and unbelted);
- Simulation of real pedestrian run-over (accident reconstruction).

Along with the proposed examples, a set of interface models is also presented in this chapter. The interface models play a very important role in all the simulations, allowing for the interaction between the biomechanical models and the surrounding environment to be accurately described (Kroemer *et al.*, 1988). These interface models are specially tailored to be used in forward dynamic analyses only and are characterized as:

- Contact/impact model;
- Rigid seat model;
- Seat belt model.

Together with these interface models, some injury criteria are also presented. These criteria provide information regarding the severity of the injuries produced in specific anatomical segments of the biomechanical model as a consequence of the external event and subsequent body response. The criteria implemented in this work are:

- The Head Injury Criterion (HIC);
- The chest Severity Index (SI).

The results obtained using these criteria can be subsequently related with real physiological alterations or with real structural failure of human body anatomical segments using known tolerance levels such as the Wayne State Tolerance Curve (WSTC) and injury scales such as the Abbreviated Injury Scale (AIS) (Wismans *et al.*, 1994).

4.1 Application Case to Sports Impact

Many athletic activities involve severe body impacts that eventually lead to serious injuries or even disabilities, as demonstrated by the pictures presented in Figure 4.1. This problem is recognized to be a serious source of injury in many different sports, such as tackle football, rugby, boxing or even cycling, being the use of protective equipment mandatory in all of these activities.

Many of the techniques used in these sport activities are characterized by high impact loads during a short period of time. Due to the lack of previous indication that contact will take place and due to the short impact periods, no active muscle reaction is observed in the impacted human subject. The estimation of injury measures and their relation to injury mechanisms is decisive for a better design of body protective equipment, field pavements or furniture protections. Moreover, the quantification of the injury potential can also be of utmost importance for setting up new rules and to define specific training procedures.

(a) (b) (c)

Figure 4.1: Example of athletic activities that, due to severe body impacts, can induce serious injuries to the human body. Biomechanical models such as the ones presented in Chapter 3 represent a tool for the design of more efficient protective equipment. (a) Example of a football tackle. (b) and (c) Examples of injuries produced during athletic activities.

4.1.1 Initial Conditions

The cases of a frontal and an offside tackle of a player by another one are simulated here to demonstrate the application of the proposed methodologies to sports scenarios involving body impact. No special attention is paid in this application example to issues related to the technical correctness of the tackle.

The athlete subjected to the tackle is a 50th percentile human male that is standing in an upright posture. The incoming player, with a total mass of 75 Kg, is moving with a velocity of 3 m/s until the impact occurs at the level of the lower torso of the standing athlete, as represented in Figure 4.2.

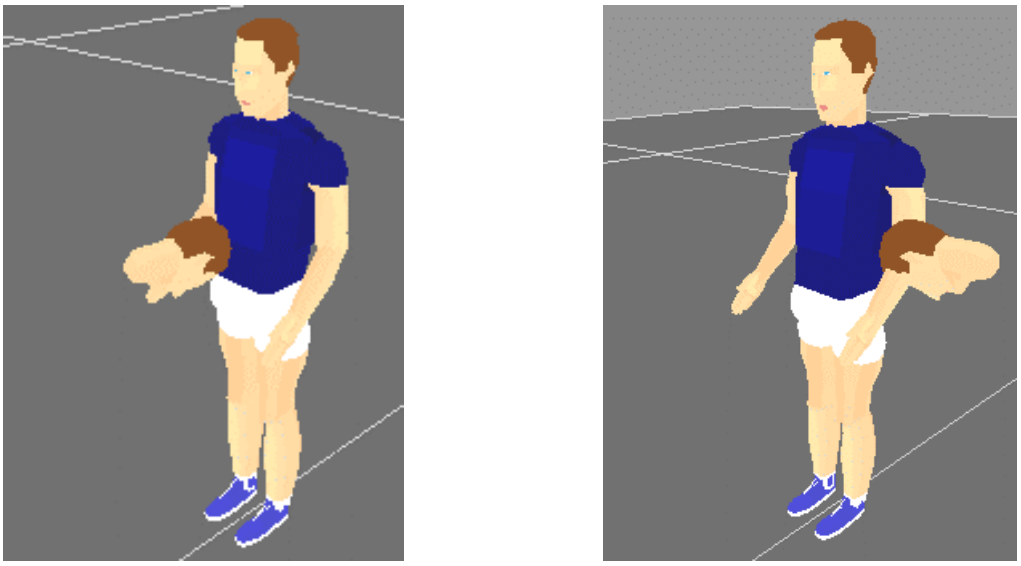

(a) (b)

Figure 4.2: Initial conditions for the simulation scenario. The initial position and velocity of the biomechanical models are specified. (a) Frontal tackle. (b) Offset tackle.

In this type of simulations, where multiple contacts and impacts may occur, it is essential the use of an accurate and numerically efficient contact/impact force model. Besides the biofidelity of the models, the correct treatment of the contact/impact conditions between the different segments of the biomechanical model and the surrounding contact surfaces must be taken into account. Many studies have been carried on, using three-dimensional models, in the area of body impact biomechanics (Bartz, 1971; Bosio and Bowman, 1986; Wismans *et al.*, 1982). In all of them, the problem of modeling the contact/impact forces was addressed with great detail. In the framework of general rigid body impact, Lankarani (1995) provided a detailed discussion of the problem and proposed a continuous contact/impact force model based on the Hertz contact theory (Hertz, 1895) that also includes energy dissipation due to localized deformation effects. This is the model adopted in the present work to describe the

contact/impact involving biomechanical anatomical segments. A detailed description of this contact/impact force model is provided in Section 4.1.2.

Another important aspect that helps analysts to evaluate the levels of potential injury is the definition of appropriate injury criteria. The most commonly used injury criteria are presented in Section 4.1.3.

4.1.2 Continuous Contact/Impact Force Model

Regardless of the formulation used to describe the motion of the biomechanical model, it is necessary to describe the forces resulting from several contact/impact situations. The contact/impact between two bodies is characterized by forces that develop and disappear over a short period of time. The physics of the contact and the relation between geometry and material properties of the surfaces must be described, while the force model should not disrupt the stability of the numerical integration of the equations of motion.

A classical approach to solve this problem as a discontinuous event is based on the momentum balance impulse equations. This methodology provides the velocity jump that results from the collision of the bodies (Lankarani and Nikravesh, 1992).

Alternatively, the model described here, treats the deformations and contact/impact forces as continuous events. It also allows for the introduction of energy dissipation due to localized deformations, as illustrated in Figure 4.3(a). The contact/impact forces, represented in Figure 4.3(c), are calculated as function of the pseudo-penetration of contact surfaces δ and the pseudo-penetration velocity $\dot{\delta}$, using the expression:

$$\mathbf{f}_{c/i} = \left(K\delta^{n} + D\dot{\delta} \right) \mathbf{u}_{\perp} \tag{4.1}$$

where K is the relative stiffness coefficient between the contacting surfaces, D is the hysteresis damping coefficient and $\mathbf{u}_{\perp}$ is a unit vector normal to the surfaces at the contact point. The coefficient n is responsible for the non-linearity of the equation and it usually takes the value of $n=1.5$ for the type of contact surfaces modeled in this work (Lankarani and Nikravesh, 1992).

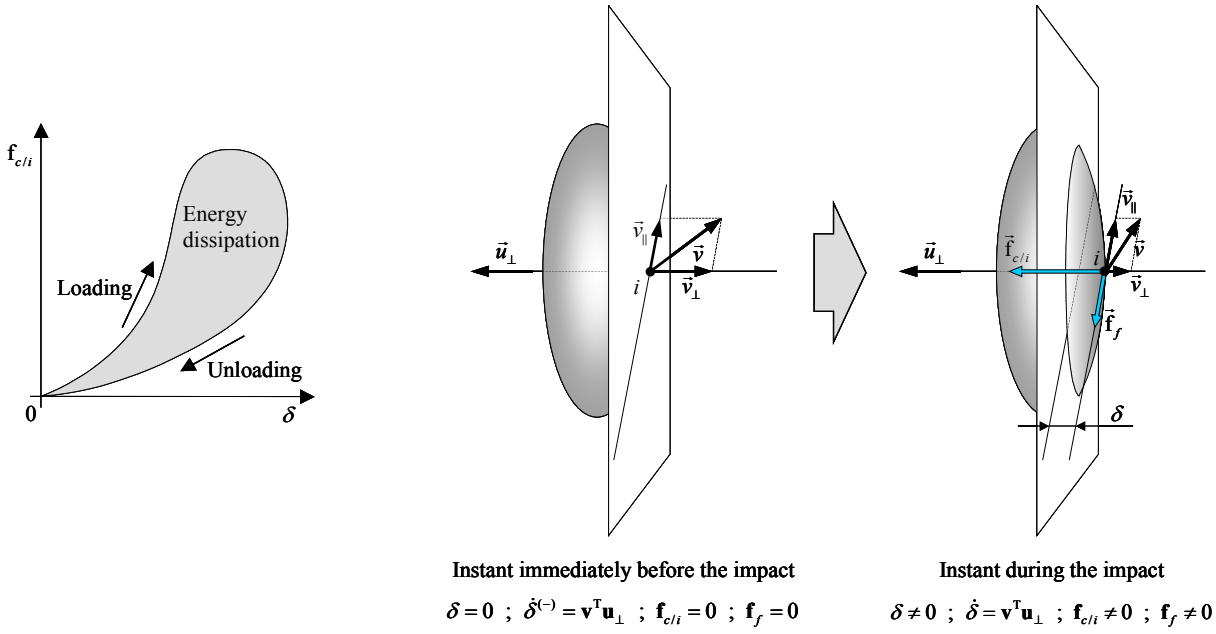

Figure 4.3: Continuous contact/impact model. (a) Representation of the load cycle of a generic contact/impact force. The gray area represents the energy dissipation due to hysteretic damping and localized deformations of the contact surfaces. (b) Representation of the instant immediately before contact between the two surfaces (an ellipsoid and a plane). Vector **v** represents the relative velocity of the contact point *i*. Vectors $\mathbf{v}_\perp$ and $\mathbf{v}_\parallel$ represent the normal and tangential projections of vector **v** in the tangential plane to the surfaces. (c) Representation of an instant during contact. The pseudo-penetration δ is represented as well as the contact/impact and friction forces applied at the contact point associated with the ellipsoid surface.

The relative stiffness *K* depends on the geometry of the surfaces in contact as well as their material properties. Regarding the hysteretic damping, it can be shown that the coefficient *D* depends on the impact velocity $\dot{\delta}^{(-)}$, represented in Figure 4.3(b), on the relative stiffness *K* and on the restitution coefficient *e*. This relation is expressed as (Lankarani *et al.*, 1995):

$$D = \frac{3\left(1-e^2\right)}{4\dot{\delta}^{(-)}}\dot{\delta} \tag{4.2}$$

The substitution of Equation (4.2) in Equation (4.1) leads to the expression for the continuous contact/impact force, given by:

$$\mathbf{f}_{c/i} = K\,\delta^{n}\left[1+\frac{3\left(1-e^{2}\right)}{4}\frac{\dot{\delta}}{\dot{\delta}^{(-)}}\right]\ \mathbf{u}_{\perp} \tag{4.3}$$

It should be noted that the restitution coefficient *e* reflects the type of impact. For a fully elastic contact *e=1*, while for a fully plastic contact *e=0*. Moreover, this equation is valid for impact velocities lower than the propagation speed of elastic waves across the bodies, i.e., for $\dot{\delta}^{(-)} \le 10^{-5}\sqrt{E/\rho}$, where the coefficient *E* is the Young modulus of the materials in contact and ρ their respective mass density (Lankarani *et al.*, 1995). In all applications considered here this criterion is fulfilled.

At this point, it should be noted that the values for the coefficients *K* and *n*, published in the available literature concern rigid body impact. In particular, the relative stiffness coefficient is based on the Hertz contact theory, which is far from being applicable to human body contact. Though it has been found that no major differences in the outcome of the impact response of the biomechanical model is observed for a wide variations of this coefficient, further studies are yet to be done to identify physically realistic values for the relative stiffness *K*.

Together with the contact/impact force, a friction force is also calculated according to the Coulomb's friction theory, and applied to the bodies in contact. The direction of this force, as represented in Figure 4.3(c), is calculated as being opposite to the projection of the velocity vector of the contact point, in the tangent plane to the contact surfaces, i.e.:

$$\mathbf{f}_{f} = -\mu \mathrm{f}_{c/i}\frac{\mathbf{v}_{\parallel}}{\left\|\mathbf{v}_{\parallel}\right\|} \tag{4.4}$$

where the μ is the friction coefficient specified between the contacting surfaces.

The contact surfaces used to describe the body shape of the biomechanical model used in this simulation are schematically represented in Figure 3.3, being their dimensions provided

in Table 3.3. The dimensions of these surfaces can be scaled or changed, whenever necessary, in order to reflect with a better accuracy the actual dimensions of the subject or, when protective equipment is used, the actual dimensions of the body equipped with such protective gear. Regarding the surfaces describing the surrounding environment, these are described using planes, cylinders and second or higher order ellipsoids, as represented in Figure 4.4.

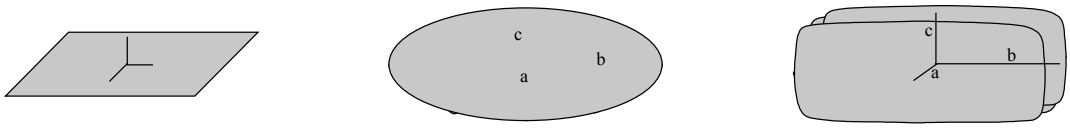

(a) (b) (c)

Figure 4.4: Contact surfaces used to describe the environment surrounding the biomechanical model. (a) Planar. (b) 2nd order ellipsoid. (c) nth order ellipsoid.

The use of higher order ellipsoids enables the representation of objects with cylinder and cube like geometries. The n^{th} order ellipsoid is described by:

$$\left(\frac{|x|}{a}\right)^n + \left(\frac{|y|}{b}\right)^n + \left(\frac{|z|}{c}\right)^n = 1 \tag{4.5}$$

where a, b and c are the dimensions represented in Figure 4.4(b) and (c), while n is now the degree of the ellipsoid.

4.1.3 Head Injury Criteria and Severity Index

Due to tight safety requirements, the aerospace and automotive industries use measures of the human tolerance to impact and to large accelerations (Steele and Lankarani, 1991). Regarding head injuries, the criteria commonly used are the Head Injury Criteria and the Severity Index, which are based on integral measures of the head acceleration during a period of time (Hutchinson *et al.*, 1998). Although initially applied to aerospace and automotive crashworthiness cases, these indicators can also be applied in other areas of activity, such as the one presented in the current case of a sports activity involving frontal and offside tackles of athletes.

Historically, one of the first criteria established to quantify the head injury was the Severity Index (SI). This criterion is based on another criterion called the Wayne State Tolerance Curve (WSTC), which establishes a relationship between the average acceleration, measured in the back of the head, and the time duration in which this average acceleration occurs. The resulting tolerance curve, illustrated in Figure 4.5, indicates the potential for a given acceleration pulse to cause severe head injuries (when above the tolerance curve) or to be within the human tolerance levels (if below the tolerance curve). The injury potential associated to this curve was established as a result of extensive testing.

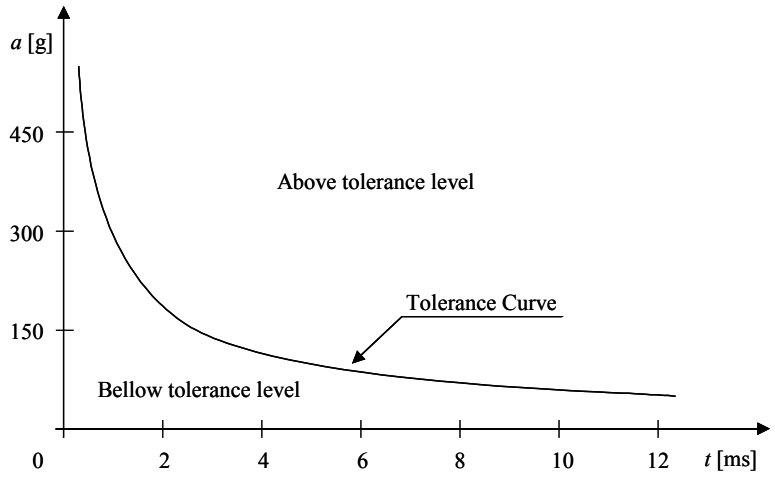

Figure 4.5: Wayne State Tolerance Curve (WSTC). This tolerance curve indicates the potential for a given acceleration pulse to cause severe head injuries (when above the tolerance curve) or to be within the human tolerance levels for the head (if below the tolerance curve).

The Severity Index appears as a weighted acceleration criterion, based on a straight-line approximation to the WSTC in a log-log scale, for impact durations between 2.5 and 50.0 ms. The Severity Index (SI) is evaluated using the expression:

$$SI = \int_0^T a(t)^{2.5}\, dt \tag{4.6}$$

where 2.5 is the weighting coefficient for the head segment, $a(t)$ is the head acceleration in g's, T is the pulse duration and t is the time in seconds. The tolerance level of concussion for frontal impact is 1000 while for non-contact impact conditions the threshold is 1500.

Another criterion with the same nature, generally used to measure the probability of head injuries, is the Head Injury Criterion (HIC), calculated as:

$$HIC = \left\{ (t_2 - t_1) \left[\frac{1}{t_2 - t_1} \int_{t_1}^{t_2} a(t)dt \right]^{2.5} \right\}_{\max} \tag{4.7}$$

where $a(t)$ is the resultant head acceleration in g's, measured in the center-of-mass of the head, and $(t_2\text{-}t_1)$ represents the time interval during which the *HIC* reaches its maximum value. It is considered that the maximum allowable time interval that produces suitable HIC values is 36.0 ms for acceleration pulses not involving direct head impact and 15.0 ms for acceleration pulses involving hard head impacts (Wismans *et al.*, 1994). A tolerance level of 1000 is used in this criterion as the threshold for permanent head injuries.

4.1.4 Simulation Results

The simulation results of the cases presented in Section 4.1.1 are depicted in Figure 4.6, using sequences of four images. These sequences show that the observed motion, for both simulations, is within the qualitative dynamic response expected for the human body in similar situations. The motion of the joints is within their feasible range, which shows that the joint penalty moments are properly applied.

During the simulation, the displacements, velocities, accelerations and forces acting upon the anatomical segments are calculated. However, only the results referring the forward acceleration of the head are presented in Figure 4.7 for both simulations, considering their importance for the calculation of the injury criteria described in previous section.

In both simulations, it is observed that the head of the player collides with the pavement approximately 0.63s after the initial impact produced by the tackle. Maximum acceleration peaks of 1.20g and 140g are obtained respectively for the frontal and offset tackles. Based on these results a Severity Index of 2170 and a Head Injury Criteria of 873 are obtained for the offset tackle. These results suggest that though the action simulated is within the head injury threshold the SI and HIC values are very high. Therefore, head protective equipment is

recommended to preserve the player's physical integrity. Concurrently, the compliance of the field surface can be set within a given range to lower the injury potential.

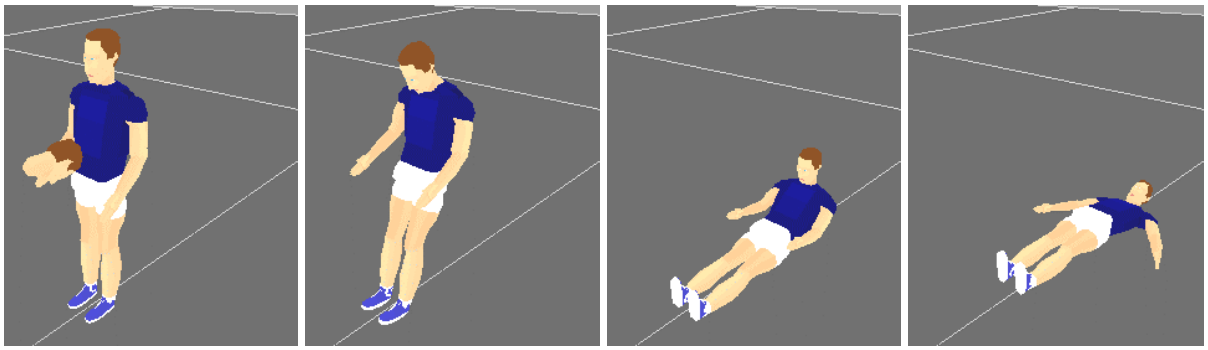

(a)

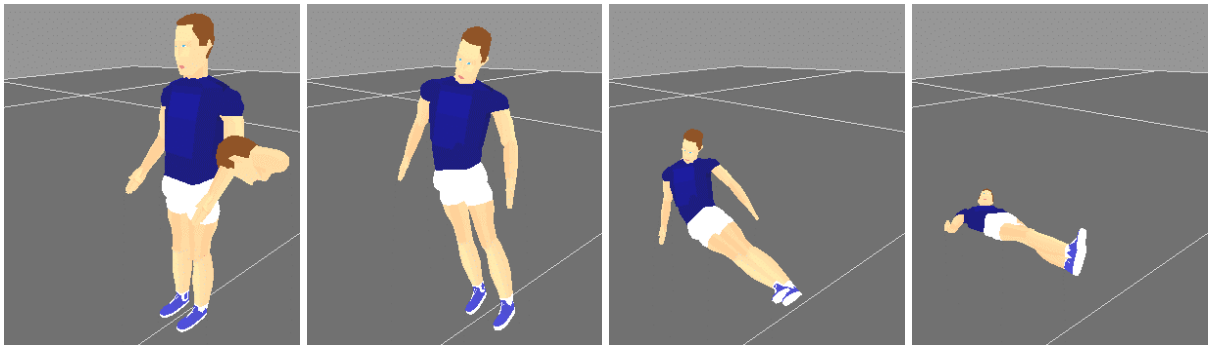

(b)

Figure 4.6: Sequence of four images obtained from the results produced during the simulations of football tackles. (a) Frontal tackle. (b) Offset tackle.

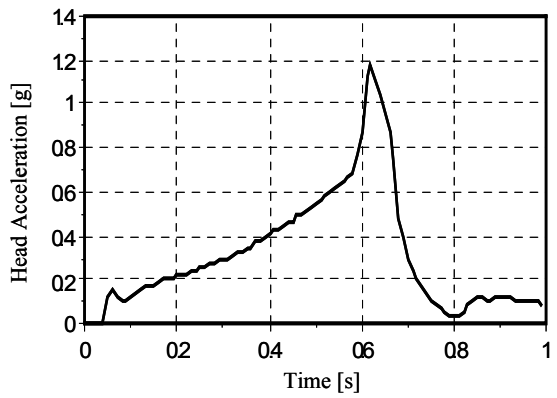

(a)

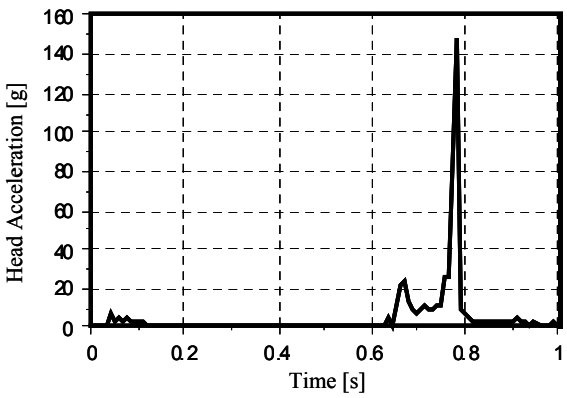

(b)

Figure 4.7: Forward acceleration of the biomechanical model's head in the first second of analysis. (a) Frontal tackle. (b) Offset tackle.

The contact between the shoulders and the ground is also monitored. Based on the compliance between the surfaces in contact and any protective equipment, conclusions can be drawn on how the athlete withstands the impact and on the potential for injury. The contact force obtained in the right shoulder of the athlete during the offset tackle is presented in Figure 4.8.

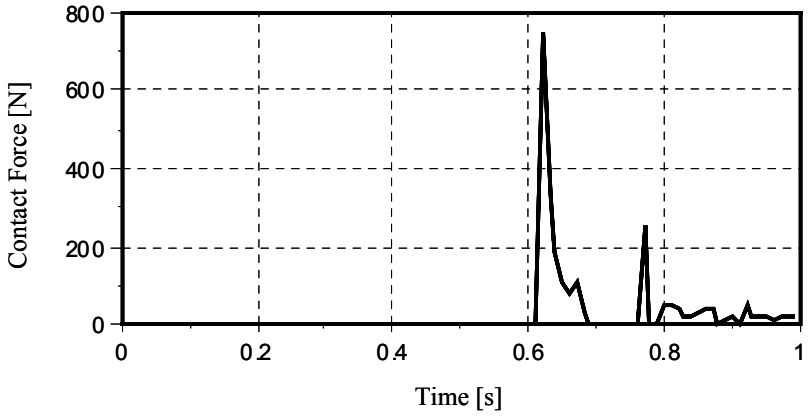

Figure 4.8: Contact force generated during the simulation of the offset tackle, between the right shoulder and the pavement.

4.1.5 Discussion

The biomechanical computer model of the athlete was applied in the simulation of frontal and offset tackles of an athlete by another player. The interaction of the biomechanical model with the surrounding environment is effectively modeled and related with the material and geometric characteristics of the impacting bodies. In the process of describing this interaction, measures for the injury potential were obtained, showing that the injury criteria for head impact, used in the aerospace and automotive industries, are still suitable for application in sports activities. However, further investigation must be carried in terms of the quantification of the threshold of various levels for different injuries. More detailed models of the head-neck complex and of the spine must also be considered for a better measure of the injury potential of athletes, especially if these are used to evaluate a wider range of athletic actions.

4.2 Application Case to a Seated Vehicle Occupant

Deceleration sleds have been widely used in the aerospace and automotive industries over the past fifty years, as illustrated in Figure 4.9. These devices allow for the simulation of a wide variety of crash/impact situations in a controlled environment. Deceleration sleds can be highly and easily instrumented in order to provide significant information regarding the sled it self and the passenger in the seat. Regarding the passenger, this can be represented by human volunteers, human cadavers or crash-test dummies.

Deceleration sled tests are often applied to the simulation of frontal and lateral car crashes as well as in the simulation of complex airplane crash scenarios. The valuable information they provide can be used in different phases of the design of seats, airbags and seat belts. From a different point of view, these devices can also be used to measure human tolerance levels, whole body dynamic responses or to test and validate crash-test dummies.

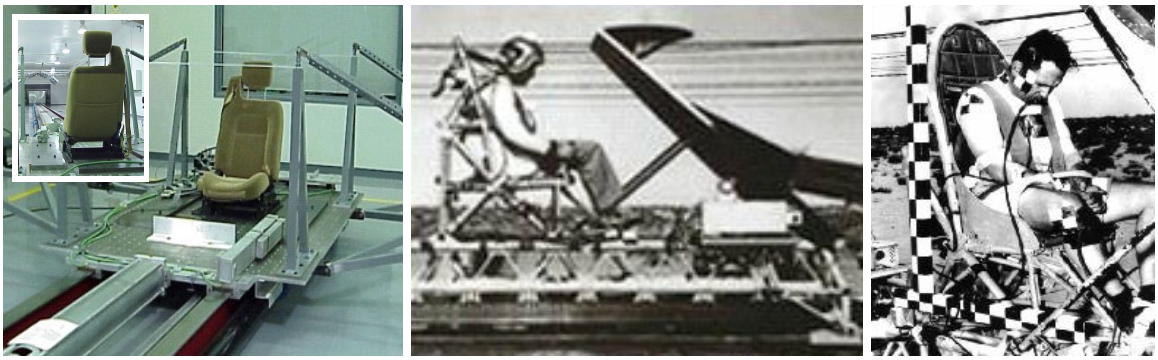

(a) (b) (c)

Figure 4.9: Deceleration sleds. (a) Example of an actual lab apparatus. Notice the sled rail represented in the small detail on the left upper corner of the picture (*in* http://www.via-systems.com). (b) and (c) Earlier sled tests performed by Col. Stapp, with human volunteers, in the mid fifties (*in* http://www.spacefame.org).

This type of scenarios is commonly used in computer simulations since it allows for the numerical results, produced during the analysis, to be compared, qualitatively and quantitatively with the experimental results obtained in a lab environment. Therefore, the application case presented here not only serves to analyze the behavior of the biomechanical model in a crash/impact scenario but it also serves to test and evaluate the numerical

performance of the interface between the biomechanical model and the rigid seat and seat belt models that are described in the forthcoming Sections 4.2.2 and 4.2.3, respectively.

4.2.1 Initial Conditions

In this application example, a vehicle frontal crash/impact simulation is performed using a combined multibody description of a deceleration sled and an integrated biomechanical model, as illustrated in Figure 4.10. The anthropometric model of the standard 50% human male is used to represent the dimensions of the occupant. The simulation scenario consists in a sled that is moving along a rail with a forward velocity of 20 Km/h towards a rigid barrier. The impact is simulated using an energy absorbing device located in the front part of the sled that deforms when the contact with the rigid wall occurs (Ambrósio *et al.*, 1996). For simplicity, neither the rigid barrier nor the energy-absorbing device are represented in Figure 4.10, although they exist in the mathematical model simulated.

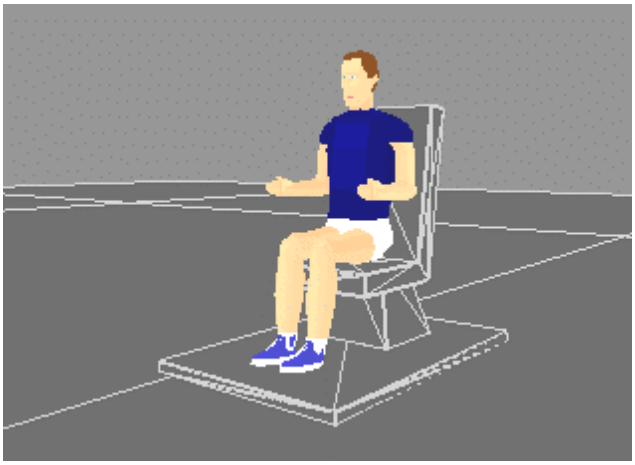

Figure 4.10: Initial simulation scenario. The initial position of the occupant and the initial velocity of the sled are specified for the purpose of the analysis.

In order to simulate this impact case, models of a rigid seat and a seat-belt are required to support and restrain the biomechanical model in its seated position. These components are the most important devices that ensure a comfortable and secure interaction between the occupant and the vehicle during normal use, as well as they contribute greatly for the occupant's passive protection. Such protection, in case of accident, is achieved by preventing

the whiplash phenomena and consequent ejection of the passenger from the seat, during the impact. Considering their importance in the simulation of this type of impact scenarios, it is fundamental to develop and include mathematical models of these components in the numerical simulation tool, proposed in the present work. The rigid seat and seat belt models, introduced in the following sections, are based in the models proposed in SOMLA (Laananen *et al.*, 1983).

4.2.2 Rigid Seat Model

The rigid seat model presented here consists in the application of a set of contact and friction forces, that result from the contact detected between the anatomical segments of biomechanical model and the seat pan cushion, seat back cushion and the floor. This set of forces is schematically represented in Figure 4.11.

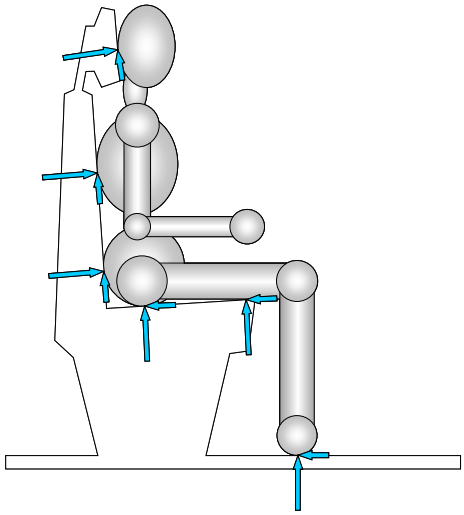

Figure 4.11: Rigid seat model. The set of forces illustrated in this figure, represent the contact and friction forces generated in the interface between the biomechanical model, the rigid seat and the floor. The forces represented are applied to the biomechanical model. A set of forces opposite to this one is applied to the rigid body to which the rigid seat and floor are attached to.

The process used, in the rigid seat model, to detect possible contact points and to calculate the associated pairs of contact force and friction force, is identical to the procedure used for the continuous contact/impact force model, presented in Section 4.1.2. The contact force is

considered to be normal to the tangent plane at the contact point, while the friction force is calculated using the Coulomb's friction model, being its direction opposite to the projection of the pseudo-penetration velocity vector in the tangential plane. The most significant difference between the seat contact model and the continuous force model is the type of constitutive law relating the contact force with the pseudo-penetration between the anatomical segments and the seat cushions or floor. For this model, the constitutive equation is given by:

$$\mathbf{f}_c = \left[A\left(e^{B\delta} - 1\right) + C\dot{\delta} \right] \mathbf{u}_\perp \tag{4.8}$$

where A and B are two numerical coefficients that characterize the stiffness properties of the seat cushion and C is the damping coefficient that allows some energy dissipation. The unit vector $\mathbf{u}_\perp$ represents the vector normal to the tangent plane at the contact points, which in the case of the rigid seat model is a unit vector normal to the planar surfaces defining the seat pan and seat back, as represented in Figure 4.12. The pseudo-penetration δ and the pseudo-penetration velocity $\dot{\delta}$ are evaluated using the geometrical characteristics of the seat, displayed in Figure 4.12, and the geometrical characteristics of the contact surfaces of the biomechanical model presented in Table 3.3. The geometrical characteristics and the material properties of the seat model used in this application case are presented in Table 4.1.

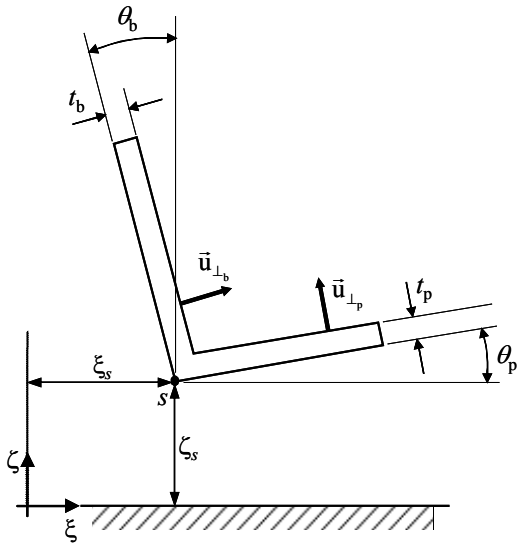

Figure 4.12: Geometric characteristics of the seat model. The seat attachment point to the base body is represented by s, while t_p and t_b are the seat cushions thickness.

Table 4.1: Geometrical characteristics and material properties of the rigid seat model used in the present application case (refer to Figure 4.12). The coordinates of the seat's attachment point *s* are given with respected to the local reference frame of the seat's base body. *A*, *B* and *C* are the numerical coefficients used in the force/displacement relationship given by Equation (4.8), and μ is the friction coefficient used to calculate the friction forces.

Seat nbr	Seat Geometrical Characteristics			Cushion Material Properties			
	$\xi_s/\eta_s/\zeta_s$ [m]	θ_p/θ_b [deg]	t_p/t_b [m]	*A* [N]	*B* [1/m]	*C* [N.s/m]	μ
1	0.414 / 0.419 / 0.062	10 / 20	0.07 / 0.07	3380.0	19.7	420.0	0.3

4.2.3 Seat Belt Model

The seat belt model described here simulates the restraining action of the three-point lap/shoulder belt shown in Figure 4.13. The belt has three attachment points that not only define part of the belt geometry but also represent the point of application of the seat-belt loads on the base body. In the present example the base body corresponds to the sled. Depending on the coordinates specified for the third attachment point a_3, the shoulder strap describes a left shoulder belt, as represented in the figure, or a right shoulder belt. If the application case only requires the use of a lap belt, then no coordinates need to be specified for the third attachment point. In Table 4.2, the local coordinates of the three attachment points, used in the present application case, are described.

Table 4.2: Coordinates of the attachment points of the seat belt to the base body (points a_1 to a_3), given with respect to the local reference frame of the base body.

Attachment Points	Local Coordinates on Base Body
	ξ / η / ζ [m]
a_1	-0.477 / 0.113 / -0.124
a_2	-0.477 / 0.725 / -0.124
a_3	-0.663 / 0.092 / 0.580

The path described by the seat belt over the biomechanical model is defined using four contact points (c_1 to c_4) that are located in specific points of the model's contact surfaces, as illustrated in Figure 4.13. The contact points c_1 and c_2 are located at the outermost point of the hip contact surfaces, point c_3 is located at the top-middle point of the scapula contact

surface and point c_4 is located at the extreme-posterior point of the upper torso contact surface.

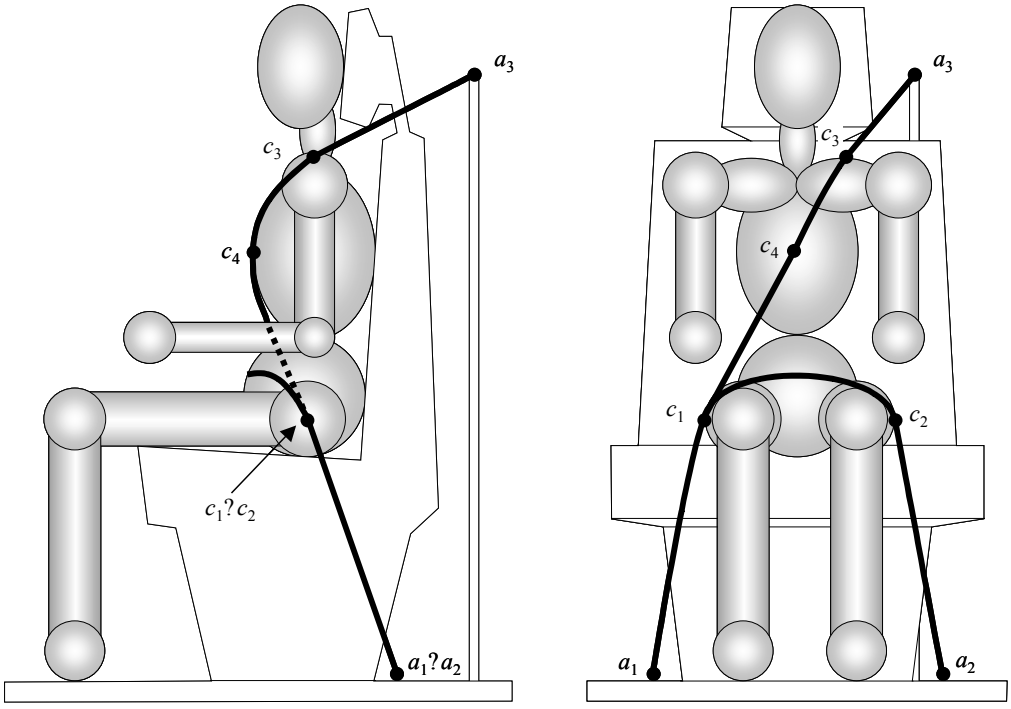

Figure 4.13: Seat belt model. The seat belt model consists on a restraining system made with a lap strap and a diagonal shoulder strap. Points a_1 to a_3 represent the attachment points of the seat belt to the base body, while points c_1 to c_4 represent specific control points located on the contact surfaces of the biomechanical model.

The set of seven points, described by the attachment and contact points, is used to calculate the lengths of the seat belt segments, i.e., the lap strap length and shoulder strap length. Hence, the length of the lap belt is calculated as the sum of the lengths of the straight line straps going from a_1 to c_1 and from a_2 to c_2, with the length of the arc described by the contact surfaces between c_1 and c_2. The length of the straight line straps is most probable to vary during the analysis, according to changes in the position of the biomechanical model, while the length of the curved strap is kept constant during the simulation period.

Using a similar procedure, the length of the shoulder belt is calculated as the sum of the straight line straps going from a_3 to c_3 and from c_1 to c_4, with the length of the arc described by the contact surfaces between c_3 and c_4. Once again the length of the arc is considered to

remain constant throughout the simulation period, while the length of the straight line straps is most probable to vary during the analysis, as a consequence of changes in the position of the biomechanical model.

In order to calculate the seat belt forces, a reference configuration for the restraint system needs to be considered. In that configuration it is assumed that no loads are being transmitted by the seat belt to the biomechanical model. This reference configuration corresponds to the initial position of the occupant in the seat with the seat belt on, as depicted in Figure 4.10. If during the analysis a configuration is detected, in which the lengths of the lap and shoulder belt straps exceed those calculated in the reference configuration, then a tensile state of stress is occurring in the belt and a tensile force is applied according to a force/strain relationship, obtained experimentally. In the present case, the force/strain relationship describing the seat belt material is presented in Figure 4.14 (Laananen, 1991).

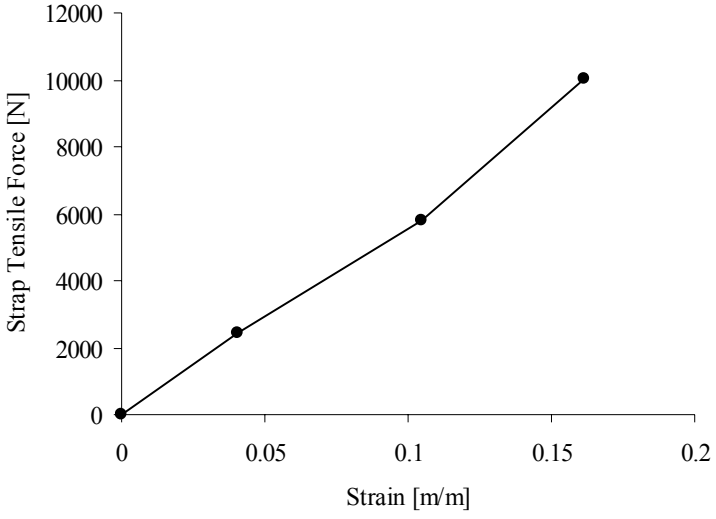

Figure 4.14: Force/strain relationship describing the material properties of the seat belt straps (Laananen, 1991).

The effective forces produced by the interaction between the biomechanical model and the seat belt are calculated from the tensile force in the seat belts, obtained previously. In a first step, the lap belt force and the shoulder belt force are calculated independently using the

tension force obtained for each belt and the directions provided by the straight line segments described before. In a second step a force balance is performed in which the lap belt force is recalculated in order to include an additional reaction term that balances the shoulder belt load at the buckle point, which is coincident with point c_1 in the present application case.

The calculated seat belt forces are applied to the biomechanical model and to the base body to which the seat belt is attached. The seat belt forces, transmitted to the base body, are applied in the fixed attachment points a_1 to a_3, while the seat belt forces transmitted to the occupant are applied in the attachment points c_1 and c_2 and to a non-fixed attachment point, located between points c_3 and c_4. The coordinates of this point are calculated such that the seat belt force, applied in this point, is perpendicular to surface of the ellipsoid describing the geometry of the upper torso. In the present work, no friction forces are considered to exist between the seat belt and the contact surfaces of the biomechanical model.

4.2.4 Simulation Results

The kinematics of the vehicle occupant, obtained from the simulation, is presented in Figure 4.15 in a sequence of four images collected from the graphical animation of the analysis outcome. For simplicity, only the biomechanical model, the sled and the rigid seat are represented in the figure. The rigid barrier, the energy absorber device and the seat belt are not displayed, although they are represent in the mathematical model.

The results presented in Figure 4.15, reveal that the integration of the occupant, rigid seat and seat belt models was successfully accomplished. Qualitatively, the biomechanical model presents a human-like dynamic response. Moreover, the motion obtained is consistent with the expected dynamic response for this particular case. The sequence shows that when the sled impacts with the rigid barrier the occupant moves forward and stretches the seat belt. Due to the lack of symmetry of the shoulder belt the torso of the occupant has a rotation about the axis of the spine while bending forward. After the impact, the occupant retains the seated position in the car. Its final posture reflects the fact that there is no active muscle action. The graphics sequence also reveals that the normal range of human motion is maintained, meaning that the joint motion-limiting moments are properly defined and implemented.

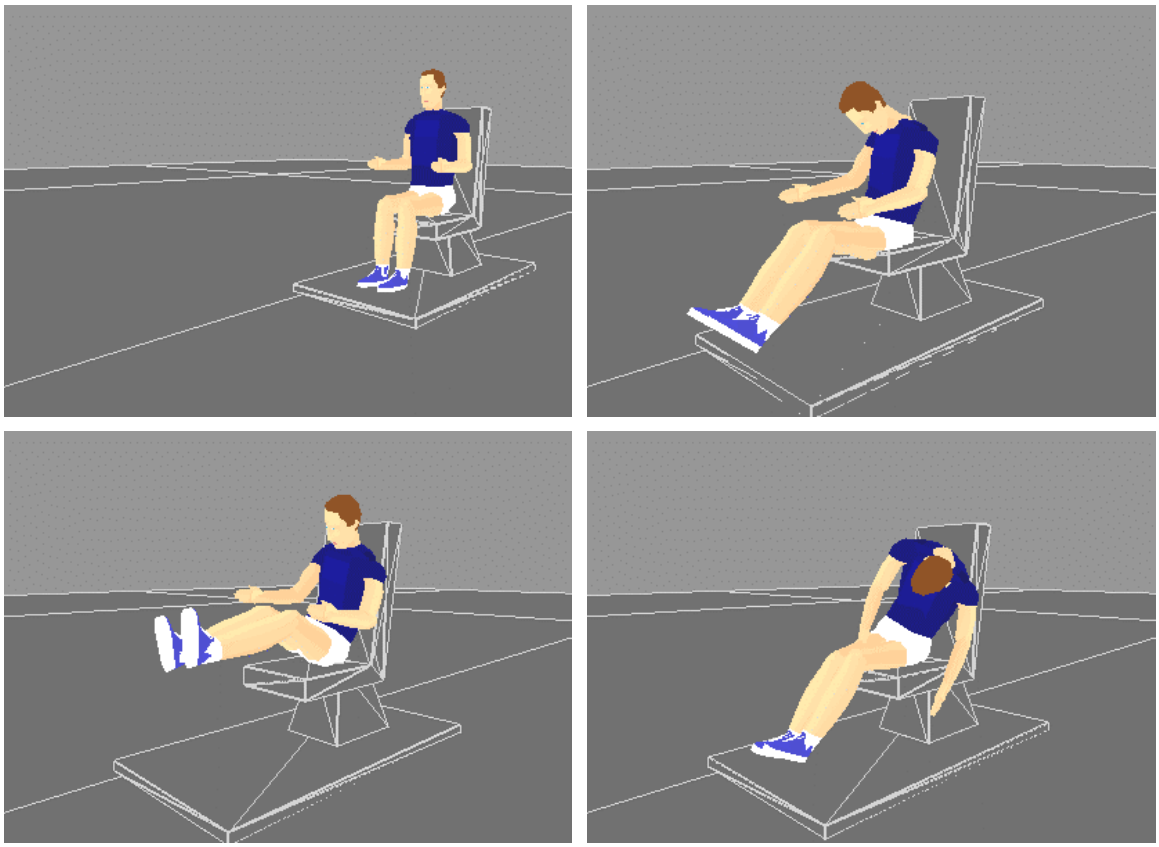

Figure 4.15: Sequence of four images obtained from the results produced during the simulation of the impact of a deceleration sled with a rigid barrier. Although not represented in the figure, a seat belt is used in the mathematical model to restrain the biomechanical model in the rigid seat.

In Figure 4.16(a), the acceleration registered in the center-of-mass of the head, during the simulation, is presented. The reported acceleration levels are produced by the deceleration of the sled and by the forces exerted over the occupant by the seat belt and rigid seat, since no direct impact was detected between the head and other contact surfaces. The acceleration levels, registered in the center-of-mass of the head, are clearly bellow the injury tolerance level for this anatomical segment, for cases where no direct impact is detected.

From the observation of the graphical sequence, presented in Figure 4.15, it is clear that the limit of motion in the joint between the neck and the upper torso is reached and that joint motion-limiting moments are applied to this joint to prevent infeasible human positions to occur. In Figure 4.16(b), the resistance moment for the neck-torso joint is presented.

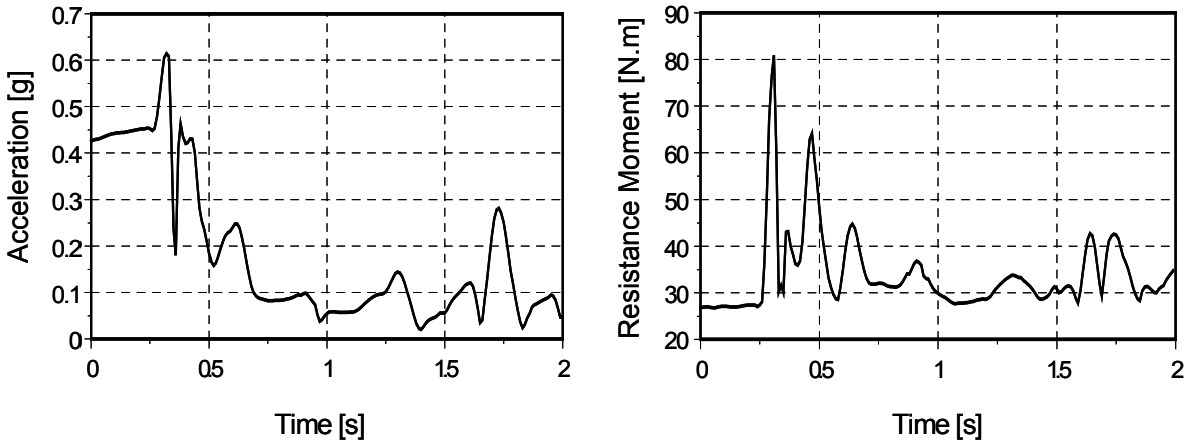

Figure 4.16: Numerical results for the occupant in a frontal crash. (a) Acceleration registered at the center-of-mass of the head segment during the simulation. (b) Joint resistance moment applied to the neck-torso joint during the simulation period.

4.2.5 Discussion

In this application case, a simulation of a deceleration sled with an integrated occupant model was performed. The purpose of the simulation, widely used in several research fields, is the qualitative model validation. Moreover, this application case also provided a natural viewpoint for the introduction of the mathematical models that are used in the present work to describe the interaction between the biomechanical model and a rigid seat and between the biomechanical model and the seat belt restrain system. It is clear, from the analysis of the reported results that, these two models are required in almost every simulation involving the crash dynamics of vehicles and occupants.

The dynamic response obtained for the biomechanical model is within the expected results, showing that the proposed mathematical models for the rigid seat and the seat belt presented a good aptitude to describe the interaction between them and the biomechanical model. The relative motion between the body segments was also monitored. It was observed that the relative motion between anatomical segments is kept within feasible regions of human motion by applying motion-limiting moments to the joints whenever their limits of relative motion are reached.

4.3 Application Case to a Vehicle Rollover with an Integrated Occupant

The safety of occupants and their potential survival in crash events in transportation systems involve many different aspects, including structural crashworthiness, restraint systems efficiency and adequate interior trimming of the passenger compartment. The analysis of such aspects is currently an important issue in modern automobile, aircraft and passenger train design, particularly in the early design stages. In order to support the design of such complex systems, some well known simulation programs are available. For structural impact analyses, reference should be made to the simulation programs PAM CRASH (Haug and Ulrich, 1988), and DYNA 3D (Halquist, 1982), while for occupant dynamics a reference is due to the simulation program MADYMO (T.N.O., 1997). These computer codes are able to simulate with relative detail frontal, rear and side impact scenarios. In most cases these programs treat separately the structural impact and the occupant dynamics. This is normally done by retrieving from the structural crashworthiness analysis the relevant accelerations pulses which are subsequently used in the occupant analysis phase where injury indices such as HIC and SI can be directly used to access design performances.

This procedure may be valid for some impact scenarios but it is not applicable to crash situations in which the occupant kinematics may interfere with the vehicle motion. In situations such as the case of a vehicle rollover, a combined model with the ability to analyze in a coupled manner complex crash events and occupant dynamics is necessary. In particular, for the case of small cars, where the occupant masses become comparable to the vehicle mass, the presence of the occupants may influence in a visible manner the overall dynamics of the system. Moreover the intrusion effects, such as the case of a collapsing roof, may drastically influence the evaluation of severity indices. In such models the force-deflection characteristics of the different contact surfaces must be provided and the treatment of contact conditions between the different segments of the biomechanical model and the surroundings must be taken into consideration.

The present application case is carried out because it combines two important aspects: it shows the applicability of the proposed methodologies to a real design process and it allows

the comparison of the simulation results with the outcome of the experimental test performed to a real vehicle with similar initial conditions.

The simulation proposed here attempts to characterize the behavior of a Military Unit Tactical Truck (MUTT) in a rollover scenario. The vehicle under analysis is the M151-A2 jeep model, depicted in Figure 4.17. This vehicle was initially designed by Ford in the late thirties and it is still being used in the present as a small transportation system.

(a) (b)

Figure 4.17:The M151-A2 Military Unit Tactical Truck (MUTT). (a) Overall appearance. (b) Detailed views of the rear-end and dashboard.

All the versions of the M151 truck, including the A2 version modeled in the present application case, use a four-wheel independent *A*-arm suspension system with coil springs. Due to the intrinsic nature of the type of suspension system adopted, a tendency to roll over during high speed turns is observed in the M151 truck, even after some design changes have being introduced in the rear suspension system of the A2 version, by changing the rear *A*-arms from pivot on the inside of the wheel to pivot front-to-back.

Due to this tendency to roll over, it was found necessary to introduce in the structure safety devices, such as a roll bar protection system (ROPS), which provides the occupants with a survival cell in case of accident. The design of this roll bar kit required the test of several M151 with the ROPS in a roll over scenario (Nikravesh *et al.*, 1990). The results of one of those tests are presented in Figure 4.18.

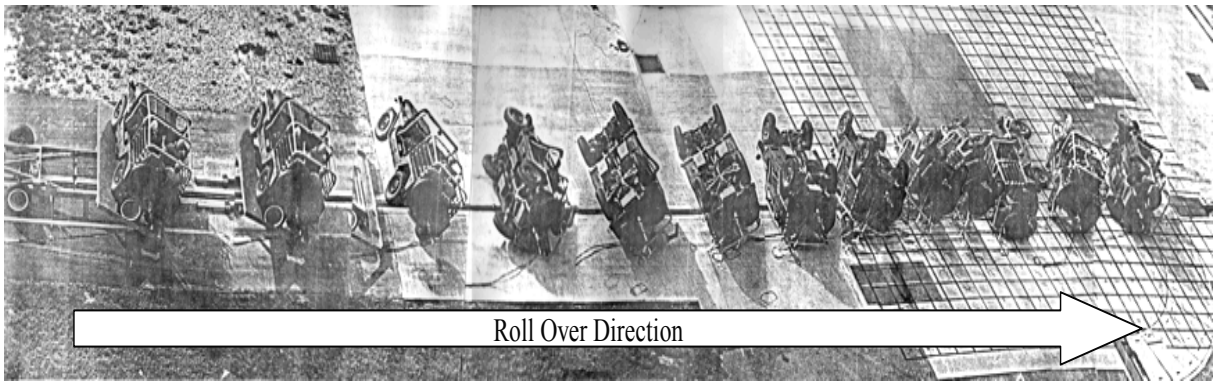

Figure 4.18: Experimental roll over sequence of the M151-A2 with the roll bar protection system (ROPS). The vehicle moves on a cart with a velocity of 13.41 m/s (30 mph) until the impact with a water-filled decelerator system occurs. The vehicle is ejected with an initial roll angle of 23 degrees. The initial velocity of the vehicle, when ejected, is approximately 11.75 m/s (25 m.p.h.) while its initial angular roll velocity is 1.5 rad/s.

The objective of the computer simulation is to reproduce the real roll over test, using a vehicle-occupant integrated model and also to analyze the interaction between the biomechanical model and the vehicle in this complex crash environment.

4.3.1 Initial Conditions

A fully coupled vehicle-occupant model and the interaction between the compartment and the occupant are described using the continuous contact/impact force model, the rigid seat model and the seat belt model described previously in Sections 4.1.2, 4.2.2 and 4.2.3 respectively. The vehicle model includes a detailed suspension system, a tire-terrain contact representation (Gim, 1988), steering capabilities and a spatial description of the chassis with appropriate force-deflection characteristics for the potential points of contact between the chassis and the ground.

The initial conditions of the simulations are schematically represented in Figure 4.19. The depicted initial conditions are obtained from the experimental setup where the vehicle moves on a cart with a velocity of 13.41 m/s (30 mph) until the impact with a water-filled decelerator system occurs. The vehicle is ejected with an initial roll angle of 23 degrees. The initial velocity of the vehicle, when ejected, is approximately 11.75 m/s (25 m.p.h.) while its initial angular roll velocity is 1.5 rad/s.

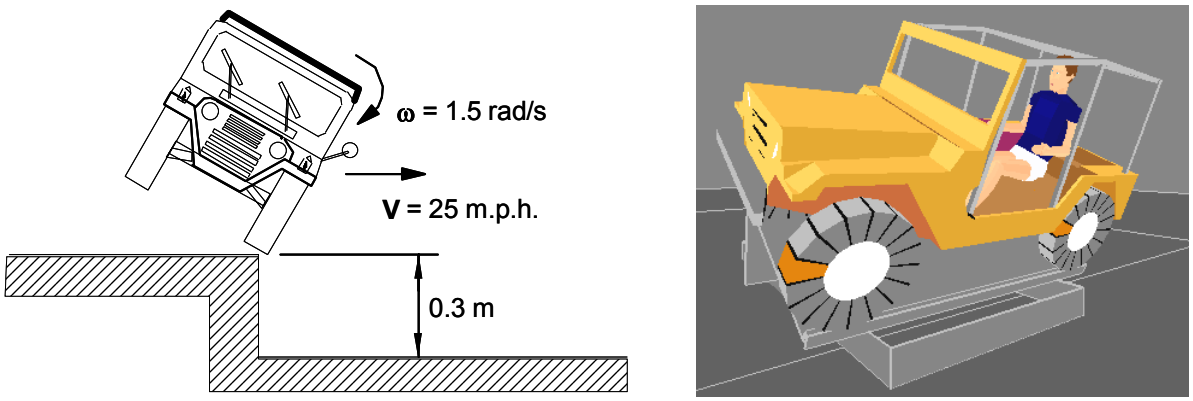

Figure 4.19: Initial conditions of the computational roll over simulation. The initial conditions for the several rollover tests are obtained from experimental measurements made during the real rollover test depicted in Figure 4.18.

4.3.2 Vehicle Model

A detailed description of the M151-A2 is presented in this section. The vehicle is equipped with the roll over protection system (ROPS) for the occupant protection. The additional weight of this structure is accounted for in the total weight of the vehicle. Thus, the truck fully equipped has a total mass of 1470 Kg that corresponds to a weight of 7840 N in the front axle and 6580 N in the rear axle. The most relevant external dimensions of the vehicle are presented in Figure 4.20. The vehicle height is 1.803 m while its length and width are 1.633 m and 3.371 m respectively. The center of mass is located 0.650 m above the ground and 1.232 m to the rear of the centerline of the front axle. The truck has a four wheel independent *A*-arm suspension system, with coil springs. More specifically, the suspension system uses a double *A*-arm in the front axle and a single *A*-arm in the rear axle (Nikravesh *et al.*, 1990).

The truck is modeled with thirteen rigid bodies, as represented in Figure 4.21(a). In Table 4.3, the mass and inertia for each system component is presented. Though the masses of the main chassis and wheels are known, the moments of inertia have been approximated according to the components shapes. The bodies of the suspension system have negligible masses as compared to the mass of the wheels and chassis. For computational purposes, these masses have been assumed to be 1 Kg for each component.

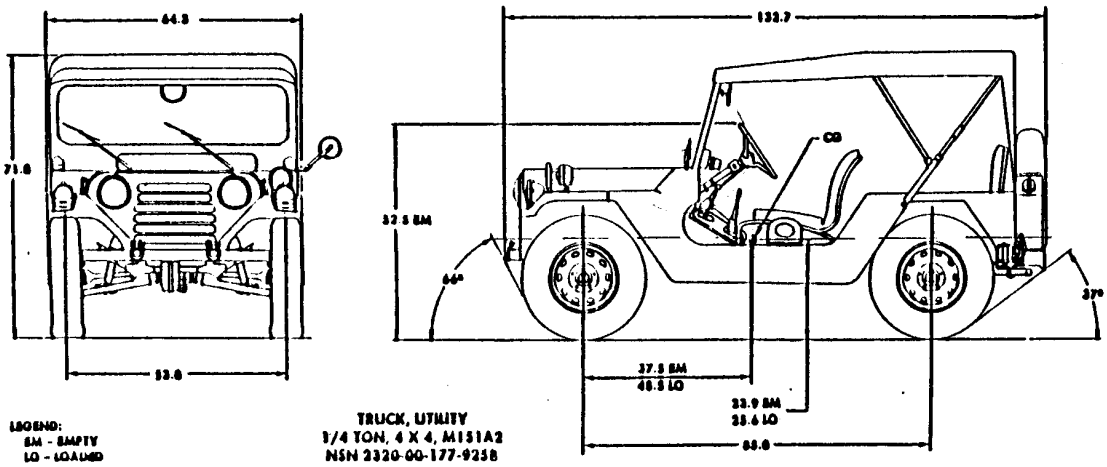

Figure 4.20: Schematic representation of the general external dimensions of the M151-A2. The dimensions in the figure are in inches.

Table 4.3: Description of the thirteen rigid bodies used to construct the multibody model of the M151-A2. In this table, the mass and inertial characteristics of each rigid body are also indicated.

Body nbr.	Description	Mass [Kg]	$I_{\xi\xi}/I_{\eta\eta}/I_{\zeta\zeta}$[Kg.m^2]
1	Chassis	1368.00	1300/2500/2000
2 (6)	Left (Right) Front-Upper '*A*-arm'	1.00	1.0/1.0/1.0
3 (7)	Left (Right) Front Hub	1.73	0.6/1.0/0.6
4 (8)	Left (Right) Front-Lower '*A*-arm'	1.00	1.0/1.0/1.0
5 (9)	Left (Right) Rear '*A*-arm'	1.73	0.6/1.0/0.6
10 (12)	Left (Right) Front Wheel	22.70	1.0/1.9/1.0
11 (13)	Left (Right) Rear Wheel	22.70	1.0/1.9/1.0

According to the characteristics inherent to type of coordinates used to describe the vehicle, a total number of twenty points and seventeen unit vectors is used to support the construction of the rigid bodies and to define the kinematic of the joints. In Figure 4.21(b) the schematic representation of this underlying structure of points and unit vectors is presented. The coordinates of the points and vectors are presented in Table 4.4. These coordinates are given with respect to the local reference frame of the bodies in which they are defined. Due to the symmetry of the model, only the left side points and vectors are shown in this table.

Table 4.4: Local coordinates of the points and vectors used to construct the rigid bodies. These coordinates locate each point or vector with respect to the center-of-mass of the rigid body to which they are attached. If a point or unit vector presents local coordinates in more than one rigid body this means that it is being shared by two bodies and used to describe a kinematic joint. Due to the symmetry of the model, only the left side points and vectors are presented.

Pt	$\xi_1/\eta_1/\zeta_1$	$\xi_2/\eta_2/\zeta_2$	$\xi_3/\eta_3/\zeta_3$	$\xi_4/\eta_4/\zeta_4$	$\xi_5/\eta_5/\zeta_5$	$\xi_{10}/\eta_{10}/\zeta_{10}$	$\xi_{11}/\eta_{11}/\zeta_{11}$
1	1.232/.319/-.102	0.0/0.0/0.0					
2	1.232/.195/-.256			0.0/0.0/0.0			
3	-.502/.484/-.257				.432/-.189/-.013		
4	-.608/.102/-.239				.326/-.572/.005		
9		0.0/.260/-.017	0.0/-.094/.125				
10			0.0/-.067/-.095	0.0/.412/-.083			
11			0.0/0.0/0.0			0.0/0.0/0.0	
12						0.0/0.0/-.406	
13					0.0/0.0/0.0		0.0/0.0/0.0
14							0.0/0.0/-.406
Vt	$\xi_1/\eta_1/\zeta_1$	$\xi_2/\eta_2/\zeta_2$	$\xi_3/\eta_3/\zeta_3$	$\xi_4/\eta_4/\zeta_4$	$\xi_5/\eta_5/\zeta_5$	$\xi_{10}/\eta_{10}/\zeta_{10}$	$\xi_{11}/\eta_{11}/\zeta_{11}$
1	1.0/0.0/0.0	1.0/0.0/0.0		1.0/0.0/0.0			
2		0.0/0.0/1.0					
3			1.0/0.0/0.0				
4			0.0/1.0/0.0			0.0/1.0/0.0	
5				0.0/0.0/1.0			
6						-1.0/0.0/0.0	
7					0.0/0.0/1.0		
8					0.0/1.0/0.0		0.0/1.0/0.0
9							-1.0/0.0/0.0

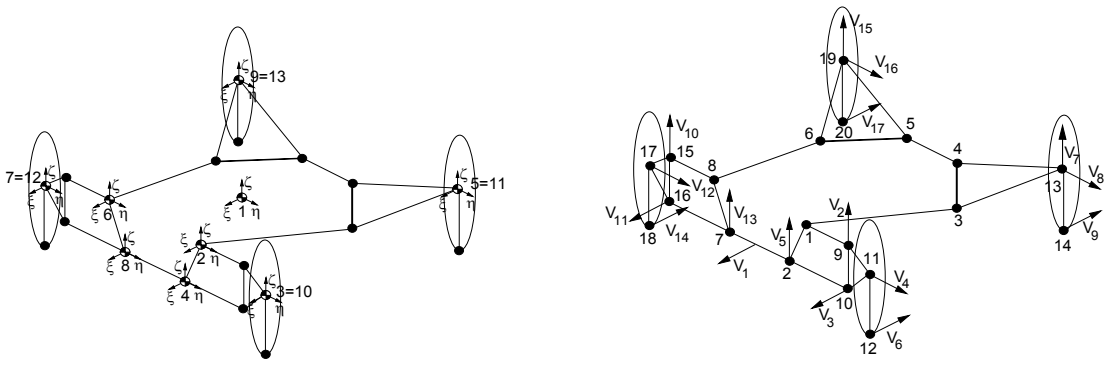

(a) (b)

Figure 4.21: Schematic representation of the multibody model of the vehicle M151-A2. (a) Kinematic structure of the thirteen rigid bodies used to setup the multibody model, with indication of the center-of-mass location of each body and overall topology. (b) Structure of points and unit vectors used in the construction of the rigid bodies.

4.3.3 Suspension Spring-Damper and Tire Models

The suspension system of the M151-A2 includes four independent assemblies of a coil spring and damper. These assemblies are introduced between the lower *A*-arm and the chassis, for the front suspension system; and between the single *A*-arm and the chassis, for the rear suspension system. The local coordinates of the respective attachment points, with respect to the center of mass of the bodies where they are defined, are presented in Table 4.5.

Table 4.5: Local coordinates of the attachment points of the coil spring and damper assemblies of the M151-A2 vehicle. Due to the symmetric properties of the model, only the local coordinates of the left side attachment points are presented.

Assembly	Attachment Bodies	$\xi^p/\eta^p/\zeta^p$ [m]
Left-Front	1	1.329/0.377/-0.094
	4	0.097/0.236/-0.038
Left-Rear	1	-0.840/0.476/-0.089
	5	0.093/-0.197/-0.090

The most important physical characteristics that describe the behavior of the coil spring and damper were obtained experimentally (Nikravesh *et al.*, 1990). During experimental tests, both spring and damper revealed a non-linear behavior that can be approximated by the non-linear force-displacement and force-velocity relationships presented in Figure 4.22(a) and (b), respectively. Table 4.6 presents the numerical values used to define the non-linear spring-damper behavior illustrated in Figure 4.22.

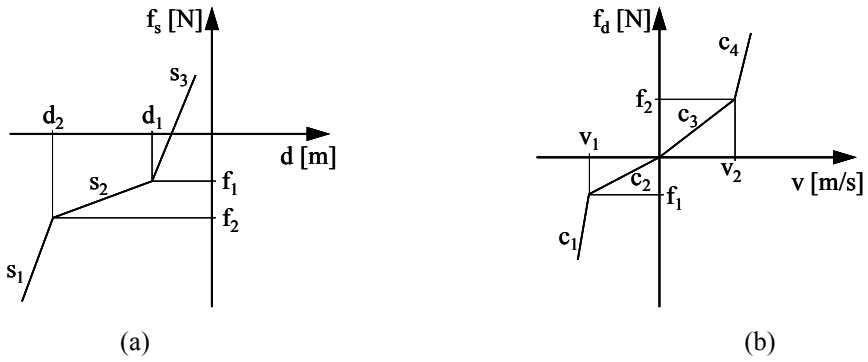

Figure 4.22: Non-linear behavior of the spring and damper assembly. (a) Non-linear force-displacement relationship used to model the coil spring. (b) Non-linear force-velocity relationship used to model the damper.

Table 4.6: Physical characteristics of the non-linear spring-damper assemblies used to model the M151-A2 vehicle. The non-linear behavior of these spring-damper assemblies is illustrated in Figure 4.22.

Spring	L_0 [m]	d_1 [m]	d_2 [m]	f_1 [N]	f_2 [N]	s_1 [N/m]	s_2 [N/m]	s_3 [N/m]
Front	0.279	-0.0987	-0.0212	-9041.0	-1945.0	2521700.0	91600.0	1251.2
Rear	0.328	-0.1173	-0.0519	-6893.0	-3052.0	898619.0	58766.0	2093.4
Damper	v_1 [m/s]	v_2 [m/s]	f_1 [N]	f_2 [N]	c_1 [N.s/m]	c_2 [N.s/m]	c_3 [N.s/m]	c_4 [N.s/m]
Front	-0.3391	0.3391	-489.0	1757.0	1180.0	1443.0	5181.0	1082.0
Rear	-0.3391	0.3391	-556.0	2113.0	590.0	1640.0	6230.0	2164.0

A comprehensive tire model is used to describe the interaction between the vehicle and the ground (Gim, 1988). This model includes traction, braking and lateral forces due to steering, and depends on the normal force, slip angle, camber angle, stiffness and geometry of the tires. The tire data for the vehicle model is described in Table 4.7.

Table 4.7: Tire characteristics used by the comprehensive tire model (Gim, 1988) to describe the interface between the vehicle and the ground.

Tire Characteristics	Value	Units
Radius	0.406	[m]
Radial stiffness	5.84×10^5	[N/m]
Longitudinal stiffness	1.0×10^5	[N/rad]
Cornering stiffness	1.0×10^5	[N/rad]
Maximum friction coefficient	0.80	
Minimum friction coefficient	0.60	

4.3.4 Roll Over Protection System Model

The vehicle rollover has been extensively analyzed with the purpose of studying the influence of the rollover protection system, or roll bar cage, in the vehicle stability and to evaluate its structural integrity (Nikravesh *et al.*, 1990). There, the roll bar cage is modeled as a nonlinear flexible body, experiencing large plastic deformations. Here, the structural deformations of this safety device are not included in the model, though up to a certain extend its deformations are implicitly described by the contact/impact force model. Regarding to its geometrical characteristics, the roll bar cage is a flexible frame made of steel bars that are mounted over the structure of the chassis, as illustrated in Figure 4.23. The bars have an annular cross-sectional area with an outer radius of 2.54 cm and are made of a 1025-1030 steel.

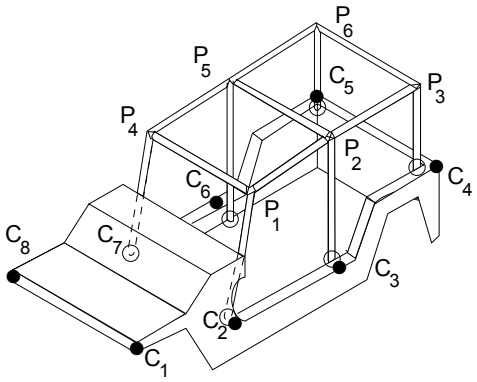

Figure 4.23: Roll over protection system mounted on the vehicle. This device is a flexible frame made of steel bars with annular cross-sectional area.

The interaction between the vehicle, the roll bar cage and the ground is described by controlling the coordinates of fourteen potential contact points: six points in the roll bar cage (P_1 through P_6) and eight points on the vehicle structure for possible ground contact (C_1 through C_8). These points are illustrated in Figure 4.23 and have their local coordinates, with respect to the center-of-mass of the chassis, described in Table 4.8. When contact is detected, a force is applied on the contact points in the direction normal to the ground surface. This force is calculated using the model described in Section 4.1.2. In addiction to this normal force, a friction force is also applied using the Coulomb friction model. The direction of the friction force is opposite to the direction of the projected velocity of the contact point on the ground. For the rollover simulation, the values of n=1.5, K=1.05×10^7 N/m$^{1.5}$, e=0.75 and a friction coefficient of μ=0.75 are used in this continuous force model.

Table 4.8: Local coordinates of the potential contact points between the vehicle and the protection system with the ground. These points are illustrated in Figure 4.23.

Points on the Roll Bar Cage		Points on the Chassis	
Pt	ξ_P /η_P/ζ_P [m]	Pt	ξ_C/η_C/ζ_C [m]
P_1	0.303/0.708/1.001	C_1	1.457/0.692/0.319
P_2	-0.483/0.692/1.045	C_2	0.589/0.692/-0.231
P_3	-1.387/0.692/0.995	C_3	-0.432/0.692/-0.088
P_4	0.303/-0.708/1.001	C_4	-1.387/0.692/0.244
P_5	-0.483/-0.692/1.045	C_5	1.457/-0.692/0.319
P_6	-1.387/-0.692/0.995	C_6	0.589/-0.692/-0.231
		C_7	-0.432/-0.692/-0.088
		C_8	-1.387/-0.692/0.244

4.3.5 Simulation Results

Three simulations are performed: the first one to the vehicle model without occupants, and the others to the integrated vehicle-occupant model using occupants with different sizes. In the simulations with occupant, this is positioned in the driver seat and restrained to the vehicle using the rigid seat and the seat belt models introduced in Sections 4.2.2 and 4.2.3. The vehicle, with and without occupants, is then simulated in the rollover scenario with the initial conditions described in Section 4.3.1. For each one of the three simulations, a sequence of six images is collected from the graphical results and presented in Figure 4.24 to illustrate the type of dynamic response obtained.

From the simulations outcomes, it can be observed that the results obtained are qualitatively comparable with the results obtained in the real experimental roll over test, depicted in Figure 4.18. The integration of the biomechanical model with the vehicle model is successfully accomplished, being the overall behavior of the biomechanical model, in both simulations, within the expected range of dynamic response.

The first contact of the vehicle's wheels with the ground occurs at 0.3 s, for all simulations, causing the vehicle to bounce from the ground with an increasing roll velocity. At about 0.8 s the truck impacts the ground with the roll bar cage and continues its rolling motion with the contact of different points of the roll bar. It is noticeable that the vehicle with occupant rolls more than the empty vehicle. Finally, the vehicle is upside down from 1.6 s until 2 s. In Figure 4.25, the vertical acceleration of the vehicle's center of mass is presented.

The occupant motion is constrained by the seat belts and by the contact of the different biomechanical segments with the vehicle floor, interior trimmings and dashboard. In Figure 4.26 the head and chest accelerations for both occupants are shown. There, high acceleration peaks, resulting from the direct contact of the head and chest with the vehicle interior, appear shortly after the contact of the vehicle with the ground has occurred.

Injury tolerance levels are calculated for the simulations where occupants are included. Values higher than 5400 are obtained for the Head Injury Criteria, as a result of the extremely severe head contact/impact with the vehicle side and top panels.

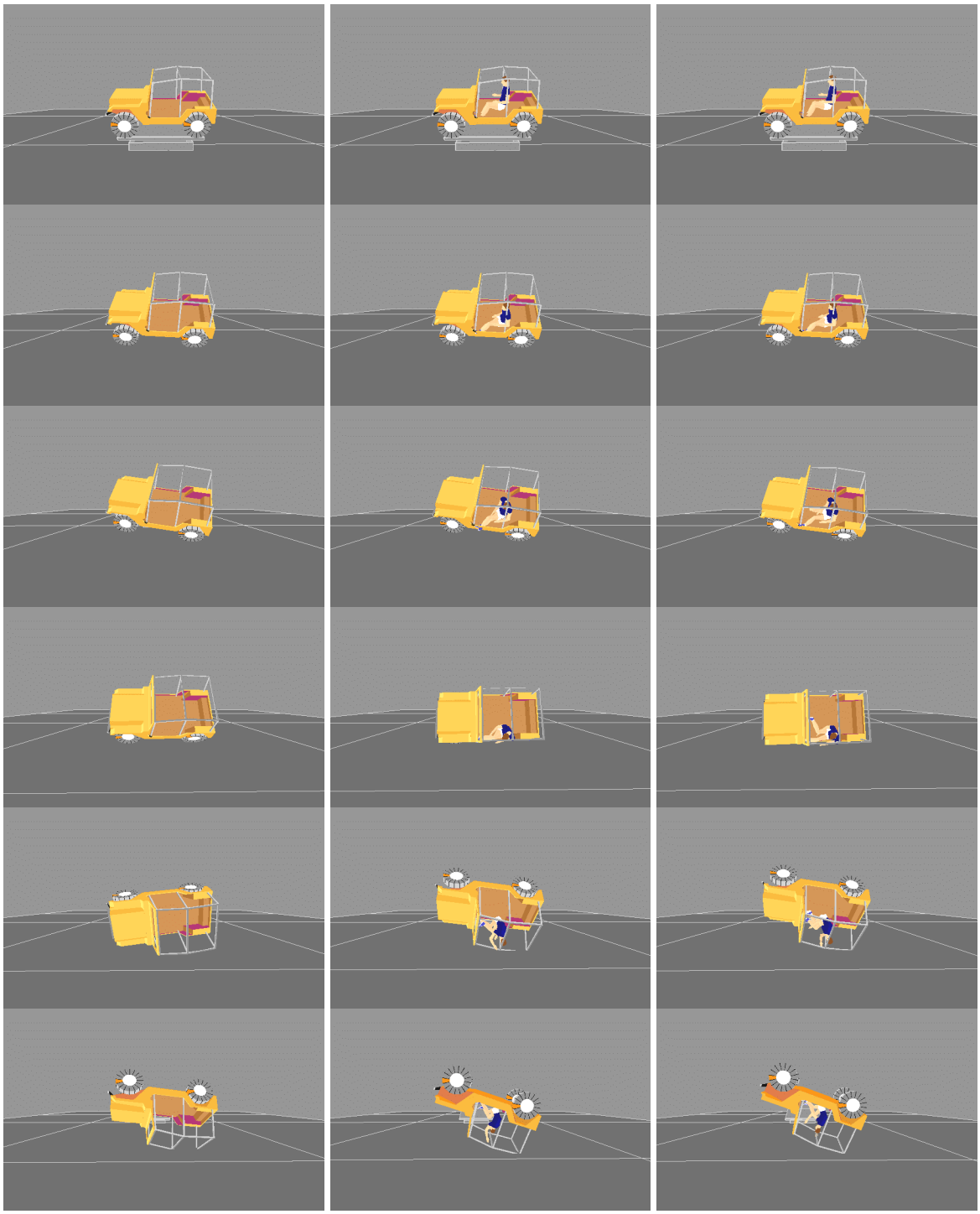

(a) (b) (c)

Figure 4.24:Sequences of the three rollover simulations. (a) Vehicle without occupant. (b) Vehicle with the 50%ile human model. (c) Vehicle with the 95%ile human model.

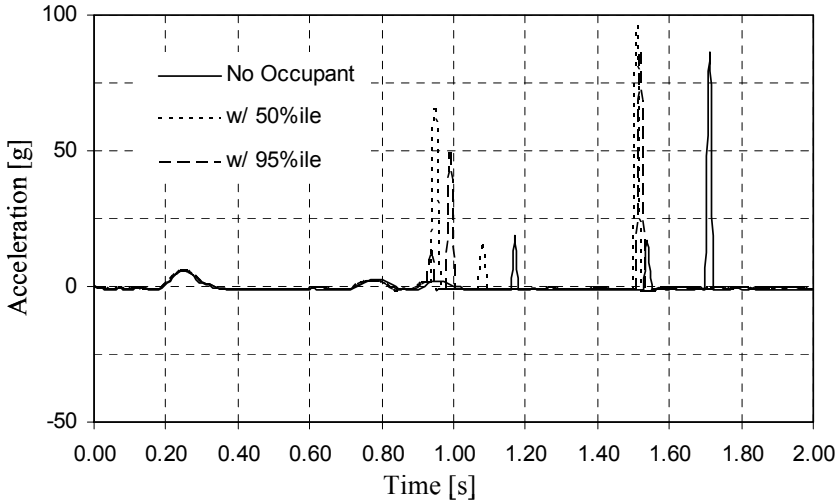

Figure 4.25: Vertical acceleration measured in the center-of-mass of the vehicle during the three simulations.

Observing the forces on the seat belts, presented in Figure 4.27, it is noticeable that the lap belt plays the most important role in keeping the vehicle occupant in place during the rollover. Load peaks of 8000 N and 9500 N are observed in the lap belt when the vehicle impact with the ground starts. While the upside-down position is maintained, forces on the lap belts increase to 35000 N in both simulations. During the impact, the shoulder belt plays a minor role comparatively to the role played by the lap belt, which indicates that the passenger ejection is mostly prevented by the lap belt.

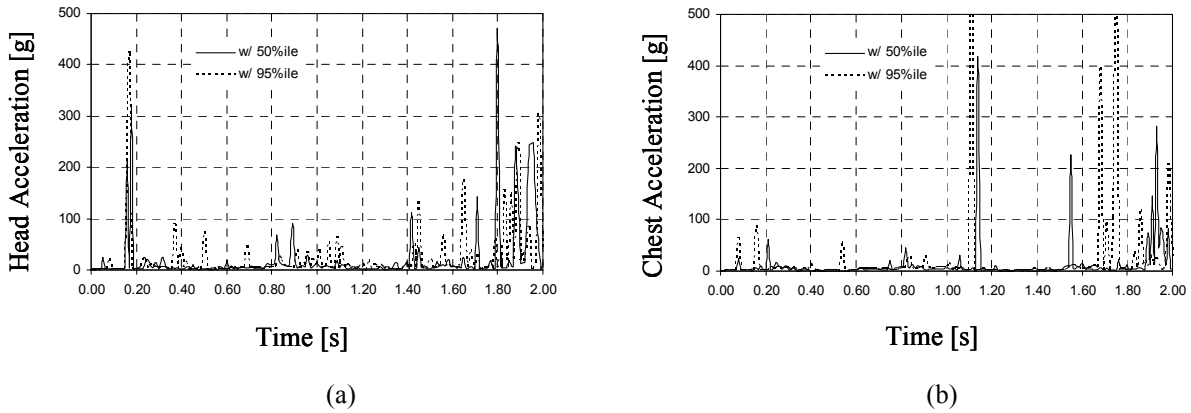

Figure 4.26: Acceleration levels measured in different anatomical segments of both biomechanical models during the simulations. (a) Acceleration in the head's center-of-mass. (b) Acceleration in the chest's center-of-mass.

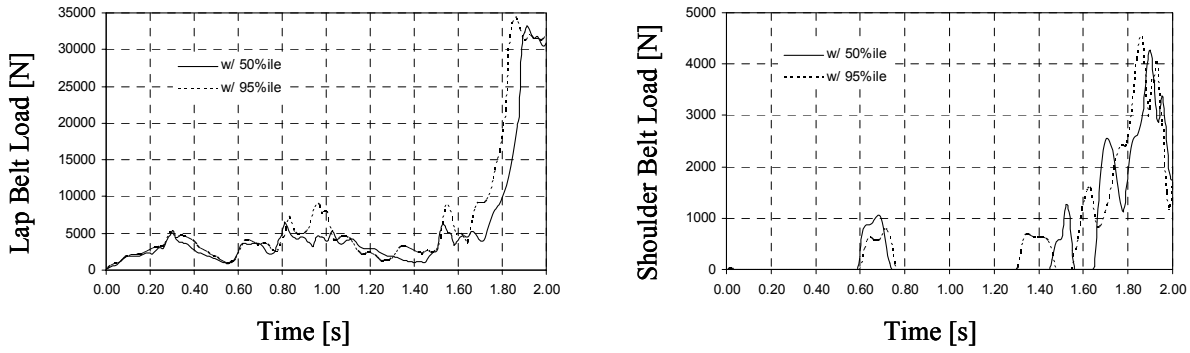

(a) (b)

Figure 4.27: Seat belt forces applied in both biomechanical models during the simulations. (a) Lap belt. (b) Shoulder belt.

4.3.6 Discussion

An integrated vehicle-occupant model, based on a multibody dynamics methodology that effectively describes the coupling between the vehicle and occupant motion, was presented in this application case. Models of a 50%ile and a 95%ile standard human male were seated and belted in the driver's position in the two simulations of the vehicle's rollover. Contact between the vehicle and the ground and between the occupant and the vehicle interior is modeled using a continuous contact/impact force model.

Three simulations of the vehicle, with and without occupants, in a rollover motion were carried on for a period of 2 seconds. The results predict a realistic motion for the occupant and vehicle as well as force and acceleration levels comparable to those reported in the literature. Moreover, it is observed that there is an effective coupling between the vehicle and the occupant behavior, revealing that the simulation tool presented proved to be adaptable and numerically efficient to simulate the coupled motion of the vehicle and occupant under severe impact conditions. However, improved results and more insight on the rollover consequences can be obtained with a better characterization of the geometry and properties of the surfaces where contact with the occupants occurs.

The results showed that differences can be found between the dynamic responses of the vehicle with or without occupants. This suggests that the use of integrated models to simulate the dynamic response of light weight vehicles with occupants is of importance.

4.4 Application Case to a Vehicle Rollover with Multiple Occupants

The forward dynamics analysis of mechanical systems requires, as input data, the initial positions and velocities of the bodies used in its description and also the external forces applied to the mechanism in that particular instant. Hence, the dynamic response of the system can be significantly affected by the quality of this initial input data. This is particularly important for biomechanical applications in which, due to the complexity and sensitivity of the biomechanical models, there is a strong dependence of the results on the quality of the input data.

In this application case, a methodology for the evaluation of the full spatial position of real occupants or pedestrians is addressed. For that purpose, the spatial positions of a seated occupant, adopting different attitudes, are evaluated and used as initial positions for the simulation of the dynamics of three out-of-position vehicle occupants, i.e., vehicle occupants that may take positions different from those for which the conventional restraint systems have been developed. This methodology uses the images collected by four synchronized video cameras and a motion reconstruction technique, called Direct Linear Transformation (DLT) (Addel-Aziz and Karara, 1971), to perform the special reconstruction of the recorded initial position. The DLT technique is commonly used with inverse dynamic analysis for the reconstruction of three-dimensional motions. Due to this affinity, the complete description of this technique is not provided in this section, but later in Section 5.2.1. The complex vehicle rollover scenario presented in the previous example is used again in this application case.

4.4.1 Initial Conditions

Three 50%tile occupants are integrated in the vehicle model using three rigid seats, which are described using the model presented in Section 4.2.2. The two occupants in the front seats are restrained in the seat using shoulder and lap seat belts, described with the model proposed in Section 4.2.3, while the occupant in the back seat is unrestrained. The initial positions of the occupants correspond to a normal seated driver, a front passenger that is bent to check the ‘glove compartment’ and a rear occupant with a ‘relaxed’ position, as showed in Figure 4.28.

Figure 4.28: Initial position of the vehicle and occupants for the rollover. This initial position corresponds to a normal seated driver, a front passenger that is bent forward to check out the 'glove compartment' and a rear occupant with a 'relaxed' position.

4.4.2 Evaluation of the Initial Position of Occupants

The process of recording the motion of the human body and the extraction from this data of the thee-dimensional position of its anatomical segments is designated by spatial reconstruction. Hence, the problem of evaluating the positioning of the out-of-position occupant is solved using spatial reconstruction methods. The most common techniques used for the spatial motion reconstruction are found in gait and sports motion analysis (Winter,1990 ; Nigg and Herzog, 1999 ; Allard, Stokes and Blanchi, 1995). However, contrary to gait or sports applications, in which the motion of the subject occurs inside a large open volume, out-of-position occupants applications are characterized by developing in small and closed volumes where these are seated. Therefore, the use of spatial reconstruction automated techniques is very limited and all the data processing has to be handled differently from normal gait analysis. Moreover, in this type of applications only the initial position, corresponding to a single frame, is required. Hence, four video cameras are used to capture a series of frames out of which the initial position is to be reconstructed.

The laboratory apparatus of cameras is schematically represented in Figure 4.29. The cameras have a 60 Hz sampling frequency and are synchronized during the trials.

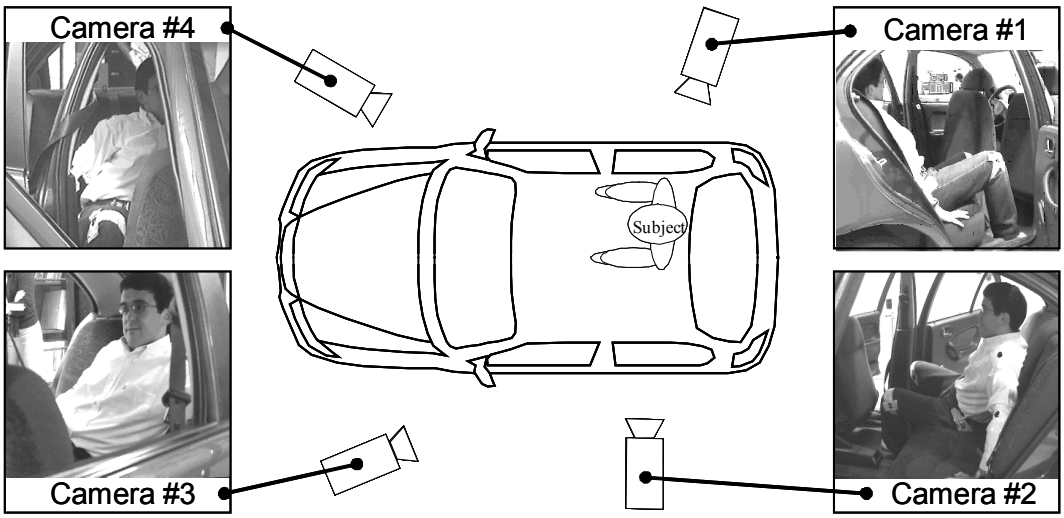

Figure 4.29: Vehicle and video cameras for the recording of the out-of-position occupants.

The spatial position and orientation of the anatomical segments of the biomechanical model are obtained from the spatial positions of a set of reconstructed points, using the Direct Linear Transformation technique described later in Section 5.2.1. Taking advantage of the fact that the reconstructed points coincide with the biomechanical model points used in the definition of the anatomical segments, the transformation matrix that positions each body of the system with respect to a given referential is evaluated. The next step in defining the initial position of the occupant consists in finding the position of an insertion point of the biomechanical model in the vehicle model, which is the mathematical equivalent of 'seating the occupant in the proper vehicle's seat. As the transformation matrix of this root body is available at this time, the initial position and orientation of the segment becomes fully known. The final step in the definition of the biomechanical model initial position is to position the remaining anatomical segments of the model according to its topological structure. Notice that, due to the use of natural coordinates, the anatomical joints are formed by making two adjacent bodies to share a point between them. Therefore, in a biomechanical branch, the insertion of an anatomical segment with respect to the previous one is done automatically,

being its orientation known from the spatial reconstruction process. Then the initial values for the generalized coordinates become fully known using this process.

From Figure 4.29 it is clear that using standard video cameras for a vehicle occupant does not allow observing all anatomical points necessary for the reconstruction process in all cameras. The problems in the reconstruction process can eventually be solved with a larger number of smaller cameras. However, this alternative introduces other sources of errors, such as large distortions of the video images and the need to develop a procedure that takes into account that not all anatomical points are visible in all images. To demonstrate the methodology presented here, instead of a complete vehicle it is used a vehicle seat and steering column and wheel to seat the occupant, as presented in Figure 4.30. Although this setup prevents several meaningful positions for the occupant from being obtained, it still allows for the identification of a large collection of out-of-position occupants.

Figure 4.30: Vehicle seat used in the experimental setup to find the occupant initial conditions

With the setup described in Figure 4.29 and the vehicle seat presented in Figure 4.30, a seated occupant is asked to adopt seated positions similar to those that would be used when riding a car in different situations. Among those, that are videotaped and reconstructed, the positions presented in Figure 4.31 are selected and used in the application of the methodology to the vehicle rollover analysis.

(a) (b) (c) (d) (e)

Figure 4.31:(a)-(d) Out-of-position occupants as viewed by the cameras and (e) spatial reconstructions.

4.4.3 Simulation Results

The vehicle and occupants are simulated in the rollover situation described in Section 4.3.1 and represented in Figure 4.19. The results of this simulation are pictured in Figure 4.32, where several frames of the animation of the vehicle rollover with occupants are presented, as observed from two different points of view. It is noticeable in these sequences that the vehicle first impacts the ground with its left tires. At this point the rear occupant is ejected. The rollover motion of the vehicle proceeds with an increasing angular velocity, mainly due to the ground-tire contact friction forces. The occupants in the front of the vehicle are hold in place by the seat belts. Upon continuing its roll motion, the vehicle impacts the ground with its roll bar cage, while the ejection of the rear occupant is complete. Bouncing from the inverted position the vehicle completes another half turn and impacts the ground with the tires again.

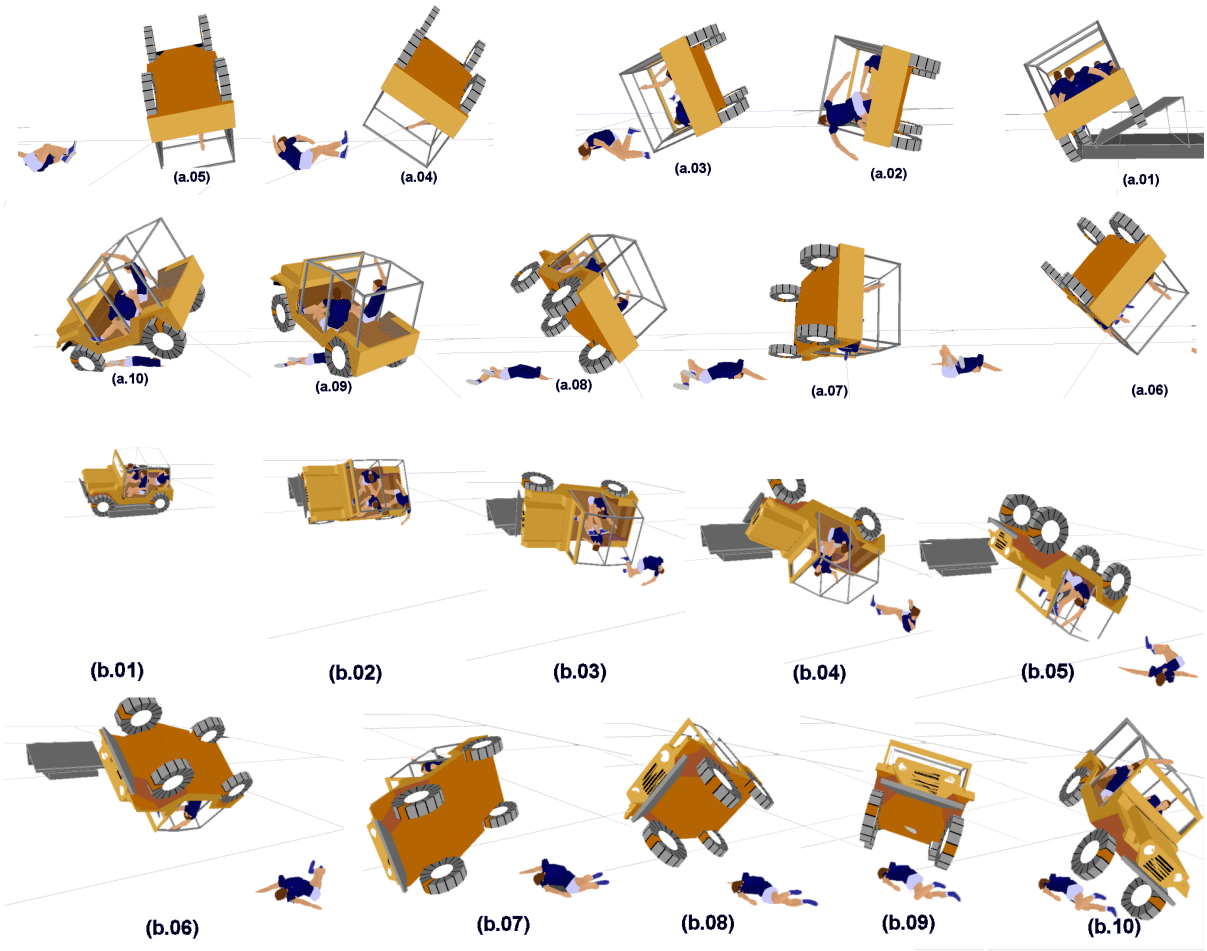

Figure 4.32:Two views of the outcome of the rollover simulation of a vehicle with three occupants

The Severity Index given by Equation (4.6) and displayed in Figure 4.33 reaches values largely exceeding the threshold, indicating a very high probability of fatal injuries for the occupants under the conditions simulated. The accelerations for the occupants' heads are presented in Figure 4.34, as an illustration of the results that are readily available by using the formulation proposed. Notice that the model has rigid seats, interior trimming for the dashboard, side and floor panels, and that the ground is also considered to be rigid. It is expected that the head accelerations are lower if some compliance is included in the vehicle interior. However, the ejected occupant would certainly face a fatal outcome, as the Severity Index that indicates potential death is reached on the first impact of the head with the ground.

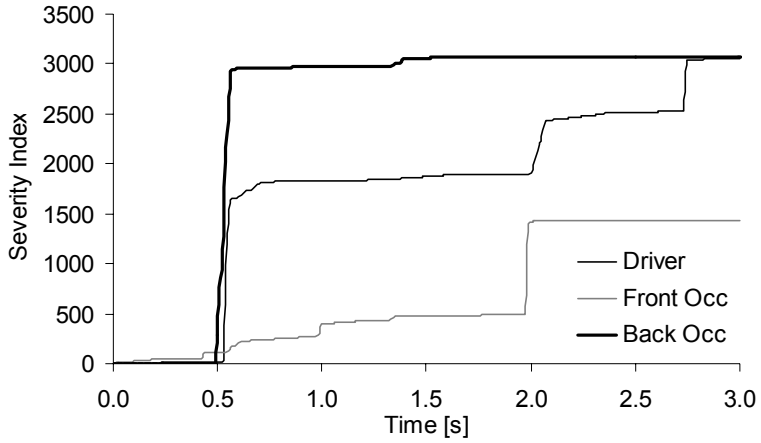

Figure 4.33: Severity Index for the vehicle occupants.

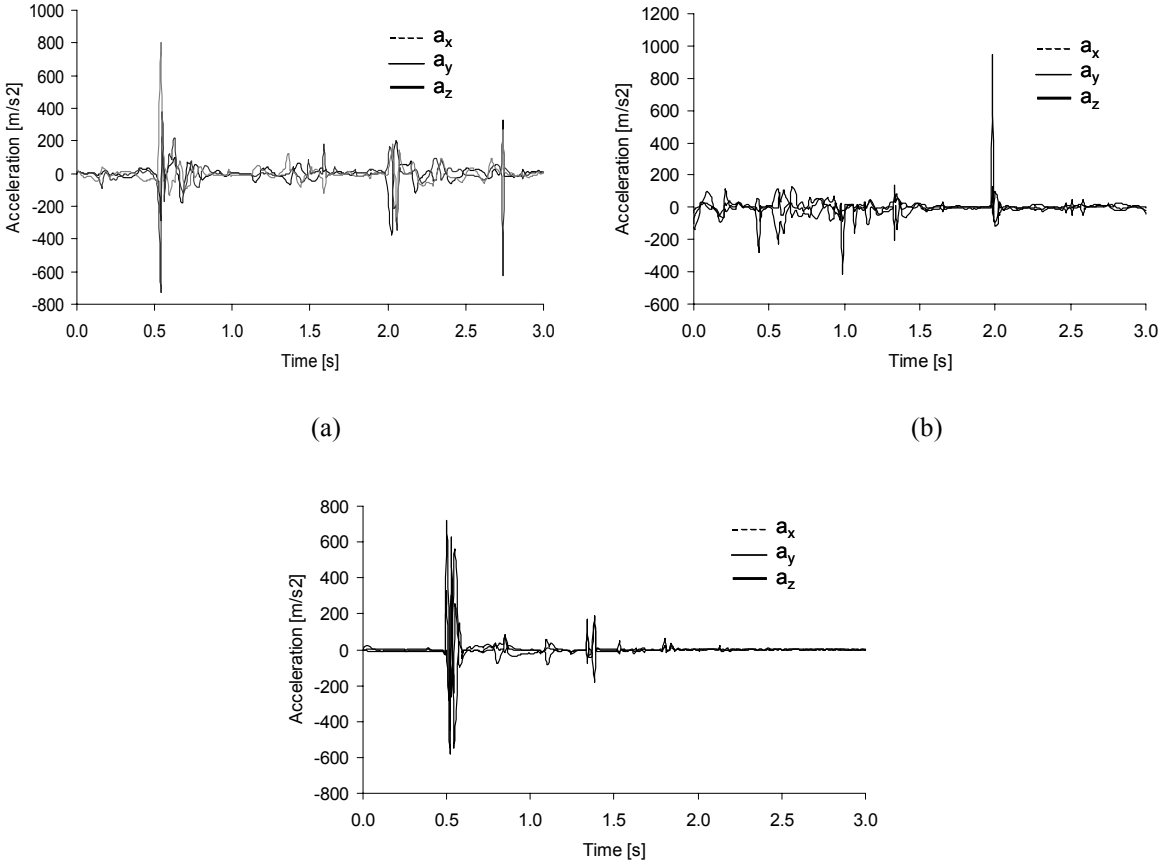

Figure 4.34: Head accelerations during the rollover (a) Driver; (b) Front passenger; (c) Back passenger.

4.4.4 Discussion

An integrated multibody methodology for the simulation of vehicles with one or more occupants inside, in complex crash scenarios, has been proposed and demonstrated here. It has been shown that the formulation presented has all the major ingredients necessary for the simulation of vehicle and occupant impact. Contrary to other applications to vehicle rollover presented in the literature, it is possible to identify in the formulation proposed all the parameters used in the model whose values are ultimately responsible for the large variability of the rollover simulation results. To support the definition of the initial conditions for the biomechanical models a procedure for the spatial reconstruction of biomechanical systems is also proposed in this work. The formulation is based in the existence of a whole body response biomechanical model and uses the Direct Linear Transformations to evaluate the initial positions of a given set of anatomical points. Special care is used in the reconstruction process in order to obtain the system initial positions and velocities consistent with the kinematic constraints. The application of the vehicle and occupants in a rollover crash scenario showed the feasibility of the models and the potential to use realistic evaluations of the occupants' initial positions. Though the vehicle model used in the rollover simulation is fully validated, the results obtained for the kinematics of the biomechanical model lack validation, as they do not correspond to any situation experimentally analyzed in great detail. Nevertheless, provided that the vehicle model can include airbags and/or intelligent restraint systems, the models proposed and the techniques associated to them are valuable tools to evaluate the performance of such systems in face of out-of-position occupants. Moreover, due to the ease and flexibility in reconstructing different out-of-position occupants' initial conditions, the methodologies proposed are also suitable to evaluate the sensitivity of the smart systems developed to the change in occupants' positions.

Some shortcomings of the proposed methodology are also identified. These include the difficulties on using the sets of multiple synchronized cameras in small closed space as the passenger compartments in a normal vehicle, and the sensitivity of the simulation results to the contact law parameters used in the models.

4.5 Application Case to a Pedestrian Run Over

Car crash accidents involving pedestrians are estimated to be worldwide responsible for the death and injury of over a quarter of a million people annually (Mackay, 1996). The statistics also show that in the great majority of these accidents, the pedestrians are injured in single-vehicle and single-pedestrian impacts. The involvement rate in a vehicle base, shows that the probability of a pedestrian to be struck by a bus is six times more likely than by a private car, in a yearly basis. Moreover, the risk of a pedestrian to be injured in a bus collision is twelve times more then by a car (Mackay, 1996).

The study of this type of accidents is important to understand of the mechanisms of injury of the pedestrian and also to achieve more efficient vehicle designs in terms of pedestrian impact protection. Due to the high complexity of the accidents, involving multi-contact collisions between the pedestrian, the vehicle and the surrounding environment, multibody methodologies appear as very attractive and powerful tools for a complete and accurate accident modeling. With these methodologies, engineers are able to model and simulate both vehicle and pedestrian in an integrated environment, estimating the potential risk of injury for the pedestrian through the calculation of several injury criteria.

In this application case, the simulation of the impact and run over of a pedestrian by a bus is presented. This simulation is based on a real event, demonstrating the use of integrated multibody methodologies, such as the one presented in this work, as accident reconstruction tools. The correct interaction between the bus and the pedestrian and between the pedestrian and the ground is accomplished using the continuous contact/impact force model described in Section 4.1.2. Rigid contact surfaces are used to model the shape of the bus and pedestrian in a precise manner. A parametric study of the model is performed for a given impact scenario using different initial velocities and relative positions between the bus and the pedestrian.

4.5.1 Initial Conditions

The model setup indicated in Figure 4.35 represents a real event in which the bus hit the pedestrian in a street crosswalk. As illustrated in the figure, impact occurred between the

front right corner of the bus and the left hip of the pedestrian. The initial position of the pedestrian, the impact angle and the bus forward velocity are defined according to witness testimonials and data collected on the field.

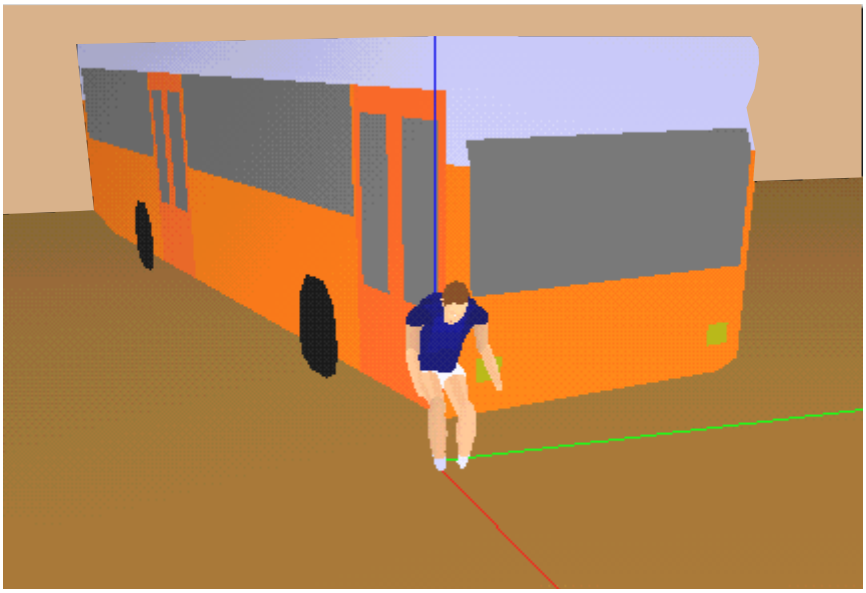

Figure 4.35:Pedestrian run over scenario. The initial position of the pedestrian and the initial position and velocity of the bus are specified.

According to these testimonials, the pedestrian detects the bus instants before the impact and, with an instinctive reaction, tries to avoid the eminent contact by spinning and turning his back to the bus. With this information, an initial angle of 80 degrees between the bus longitudinal direction and the pedestrian shoulder line is used as reference. The velocity of the bus, calculated after measurements made at the local, is within a range of 20 to 40 km h^{-1}. After impact, the pedestrian spinning motion is expected to continue until contact with the ground occurs. The pedestrian is modeled using the biomechanical model described in Chapter 3, with the biomechanical data scaled to the dimensions and weight of the real subject. The bus is modeled using a twelve-ton rigid body with a constant forward motion.

4.5.2 Simulation Results

Several simulations of the run over are performed, considering different initial relative positions between the bus and the pedestrian, as well as different initial impact velocities for

the bus. These initial positions, as illustrated in Figure 4.36, are obtained moving the bus closer to the pedestrian, controlling in this form the amount of penetration of the initial sideswipe, which enables the simulation of different levels of impact between the front of the bus and the pedestrian. For each initial position, five different impact velocities are considered. These impact velocities are respectively 20, 25, 30, 35 and 40 km/h, with the direction represented in Figure 4.36.

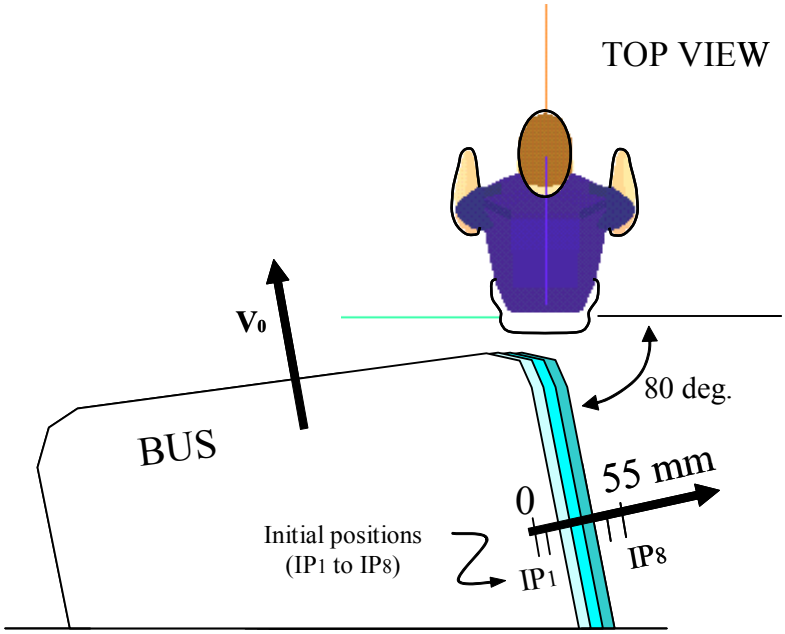

Figure 4.36: Description of the different simulation scenarios used in the accident reconstruction. Eight different relative initial positions are used (IP1 to IP8) and each initial position is simulated with five different impact velocities (20 km/h, 25 km/h, 30 km/h, 35 km/h and 40 km/h).

This set of simulations, provided the results for the parametric study of the accident, which include the monitoring of the relative position of the biomechanical model's foot with respect to the rear wheel of the bus, as presented in Figure 4.37 and Figure 4.38. These results show that the probability of the rear wheel to run over the pedestrian's foot is very high, in particular for velocities below 30 Km h^{-1}. Moreover, a spinning motion is observed for the pedestrian, in particular for small pseudo-penetrations between the bus and the pedestrian. These correspond to initial positions IP1 to IP3, which suggest that the impact is characterized

by a sideswipe of the pedestrian. This particular set of results is emphasized since in the real accident the foot of the pedestrian was in fact run over by the bus.

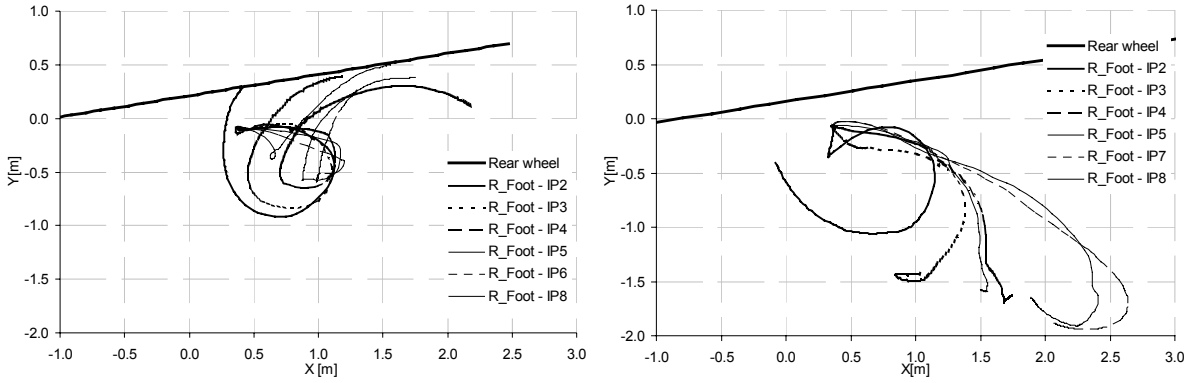

(a) (b)

Figure 4.37: Relative position of the foot with respect to the bus' rear wheel for different initial positions of the bus and: (a) a bus incoming velocity of 20 km/h. (b) a bus incoming velocity of 40 km/h.

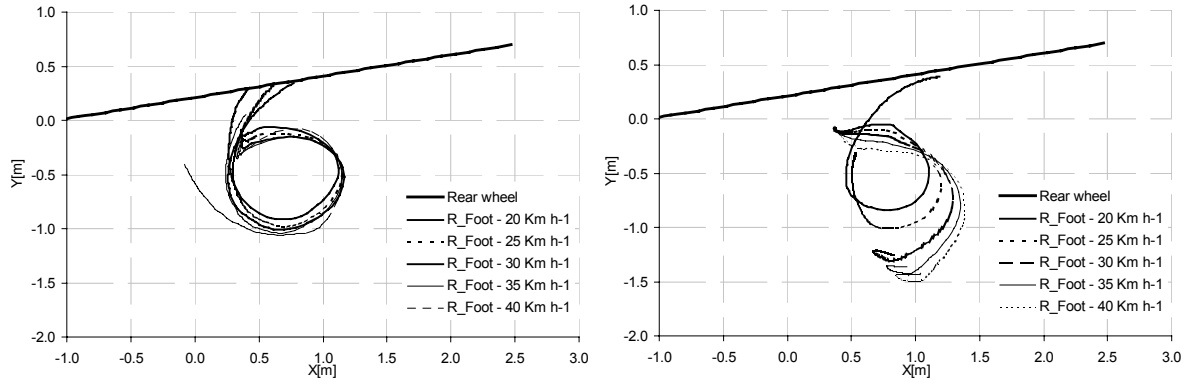

(a) (b)

Figure 4.38: Relative position of the foot with respect to the bus' rear wheel for different incoming velocities and: (a) bus initial position IP2. (b) bus initial position IP3.

In order to evaluate potential for head injuries in the pedestrian, the Head Injury Criteria (HIC) is evaluated. This severity index has a threshold of 1000, which means that there is a potential hazard of head injury for values of HIC superior to this value. In Figure 4.39, a carpet plot with the values of HIC as function of the initial velocity and penetration is

presented. From the analysis of the carpet plot, it is concluded that the risk of direct head impact is relatively small, as observed from the values of HIC close to zero. When direct head impact actually occurs, the values of HIC are still relatively small. Only for the case of an impact velocity of 30 km/h and for initial position IP_8, a value of HIC greater than the threshold is observed.

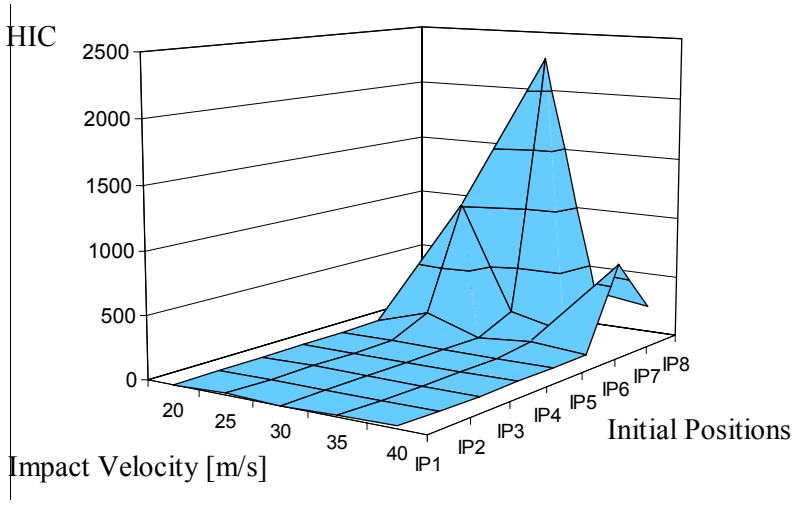

Figure 4.39: Plot of the Head Injury Criteria (HIC) for the pedestrian's head, as a function of the bus incoming speed and the relative initial position between the pedestrian and the bus.

A typical dynamic response of the biomechanical model to the sideswipe impact of the bus is presented in Figure 4.40, by a sequence of six images obtained from the graphical animation produced by one of the simulations performed. From the close analysis of this sequence, a very good correlation is observed between these results and the accident description made by the witness. Moreover, a common pattern can be identified in all the simulations performed and in the accident description, which is characterized by a spin over of the pedestrian just after the impact that continues until the contact with the ground occurs. Once in the ground, the rest of the pedestrian's kinetic energy, due to the impact, is dissipated by friction with the ground. These results are in conformity with the accident reported, in which, besides the foot injuries resulting from the run over by the bus' rear wheel, only bruises due to friction contact have been reported.

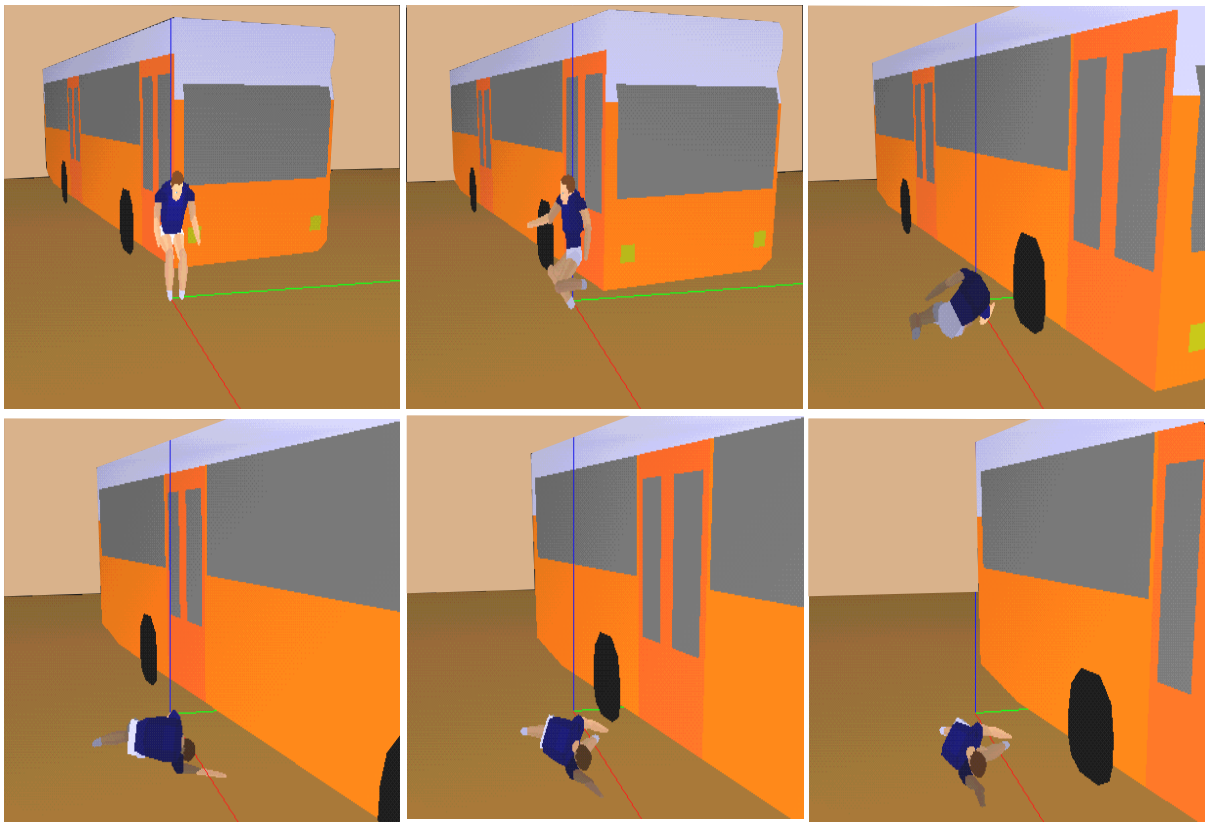

Figure 4.40: Sequence of images showing a run over of a pedestrian by a bus. This sequence presents a very good correlation between the simulation results and the accident report made by the witness.

4.5.3 Discussion

In this application case, an accident involving the run over of a pedestrian by a bus was simulated using the general multibody formulation presented in Chapter 2 and the biomechanical model described in Chapter 3. The bus and the pedestrian are modeled together in an integrated environment, being the contact between them represented using the continuous contact/impact force model described in Section 4.1.2. The initial position of the pedestrian and the impact velocity of the bus were estimated from witness testimonials and measurements made on the field. The results obtained show a very good correlation with the description of the real accident, confirming the ability of these methodologies for the simulation of complex multi-impact scenarios. Moreover, this application case showed that multibody simulation tools have in accident reconstruction a natural field for their application.

4.6 Conclusions

In this Chapter, several illustrative examples of the application of the multibody formulation described in Chapter 2 and the biomechanical models introduced in Chapter 3 were presented. The examples covered a wide range of applications that included sports activities and car crash simulations with occupants and pedestrians. These cases clearly showed that the proposed multibody formulation and biomechanical models can be viewed as powerful analysis tools in many application fields, due to the relevance of the results they provide and the simplicity in which complex simulation scenarios are described and simulated.

The application cases presented in this chapter were also used to introduce, in a natural context, a collection of mathematical models that are fundamental for the accurate description of the interaction between the biomechanical model and the surrounding environment. These models are a continuous contact/impact force model, a rigid seat model and a seat belt model. These models not only provide a way to calculate the contact forces generated due to the interaction between the biomechanical model and the exterior, but also contribute for the stability of the equations of motion since they introduce damping, which accounts for the energy dissipation.

Finally, the most commonly injury criteria used to evaluate the potential risk of permanent injuries to occur in different anatomical segments of the human body were also introduced in this Chapter. The calculation and evaluation of these injury levels can be particularly important in the early phases of design of protective equipment, when the shape of an impact surface or a specific material characteristic are still being investigated.

Chapter 5

Inverse Dynamic Analysis of Determinate Biomechanical Systems

The study of human motion and the calculation of reaction forces and net moments-of-force developed at the joints of a subject during the execution of specified physical tasks are of major importance in many areas of research such as biomedical engineering, physical rehabilitation, ergonomics and implant design. However, it is well known that from the experimental point of view, the measurement and evaluation of these forces poses a large number of difficulties, since most of the available techniques are invasive and, therefore, only applied to experienced volunteers or to human cadavers. Moreover, many of the experimental techniques used with human volunteers produce mainly qualitative results, with which is difficult to quantify the real value of the forces and moments involved in the task. In order to overcome these limitations, computational methods are being successfully used in the evaluation of these forces, producing not only qualitative but also quantitative results. Some of these methods are able to perform inverse dynamic analyses of complex human tasks, in general three-dimensional environments, without using invasive techniques or highly specialized equipment.

An inverse dynamic analysis of a complex human task usually requires a large collection of input data. This input data usually comprises three distinct types of information: anthropometric information regarding the dimensions of the anatomical segments, the total body mass and height; kinematic information in which a set of trajectories of points, located in the joints and extremities of the biomechanical model, are used to described its motion in a unique way; and dynamic information describing all the external applied forces to the biomechanical model and their respective points of application. The information comprised in these three data sets is obtained either experimentally or from direct anthropometric measurements on the subject and therefore is prone to errors and uncertainties. These errors and uncertainties can drastically change the outcome of the analysis, producing poor quality results that might mislead the conclusions.

It is the objective of this chapter to identify the most common sources of uncertainties that affect the input data of an inverse dynamic analysis and to suggest and propose a set of numerical techniques that, when applied to this data, contribute to considerably reduce this type of problems. These techniques are: motion reconstruction methods used to reconstruct the three dimensional motion of the biomechanical model from two dimensional information obtained from, at least two, video cameras; filtering techniques that are used to reduce the high frequency noise levels introduced during the digitization process; and kinematic consistency enforcing procedures that are used to ensure that the kinematic data is consistent with the anthropometric data, at any instant of the inverse dynamic analysis.

The methods and techniques described in this chapter are general and can be applied to the inverse dynamic analysis of determinate or indeterminate problems, i.e., to problems where the number of unknowns is equal to the number of equations of motion or to problems where the number of unknowns is higher than the number of available equations of motion. However, for the clearness of the description of the methods and straightforwardness of the chapter, only determinate inverse dynamic cases are used to support the proposed methods. Regarding the inverse dynamic analysis of indeterminate problems, this issue is addressed in detail in Chapter 6.

Throughout the chapter, an application example of an inverse dynamic analysis of a normal cadence stride period is used to demonstrate the application of the numerical techniques, and to evaluate the effect of their application in the quality of the results. The input data required to carry out this example was acquired on the Laboratório de Marcha do Centro de Medicina e Reabilitação do Alcoitão. In this application case, the action of the different muscles and muscle groups is lumped, as net moments-of-force about the joints of the biomechanical model, leading to a determinate inverse dynamics problem.

The chapter ends with a thorough analysis of the sensitivity of the results to perturbed input data. This analysis is carried out in order to investigate what are the items in the input data that most contribute to the quality of the simulation results. For this purpose, several inverse dynamic analyses are performed using the input data of the referred gait application case, with the following input parameters perturbed independently: masses of the head, hand, lower torso, upper and lower leg anatomical segments; Cartesian coordinates of anatomical points of the top of the head and knee; ground reaction force of the right foot; and coordinates of the application point of the ground reaction force of the right foot.

5.1 Description of the Application Case

The study of the human locomotion and in particular the inverse dynamic analysis of human gait provides valuable information that can be used to improve the diagnostic and treatment of pathologies of the locomotor apparatus, gait disturbances or the development of more efficient artificial joints and prosthesis. Other areas such as sport activities, ergonomics or robotics can also benefit from such type of analysis since it provides a way to calculate, using non-invasive methods, the net moments and reaction forces at the joints of the human body.

However, as it was mentioned before, the experimental process that leads to the acquisition of the required input data for this type of analysis is prone to errors and uncertainties that can be substantially reduced using proper numerical methods. In the present chapter, an application example of a normal cadence stride period is chosen with the purpose of demonstrating the applicability of the referred methods and to present the improvements obtained in the results produced by the inverse dynamic analysis.

5.1.1 Anthropometric Data

The subject used to perform this analysis is a twenty-five years old male, with a normal gait pattern. As depicted in Figure 5.1, the height and weight of the subject were measured as well as all the necessary anthropometric dimensions that are needed to construct the inverse biomechanical model introduced in Section 3.2.2. The subject has 1.70 m height and 70.250 kg of total body mass. The remaining physical characteristics of the subject, namely the moments of inertia of each anatomical segment and their respective center of mass location, were scaled from the anthropometric data of the 50th percentile standard human male, presented in Table 3.2, using the scaling procedure described in Section 3.1.3.

(a) (b)

Figure 5.1: Detail of the experimental procedure used to measure the input anthropometric data describing the subject under analysis. (a) The shoulder height with footwear. (b) The average body weight in each foot, with footwear included.

5.1.2 Kinematic Data

In inverse dynamic analyses, the kinematic input data refers to the information used to describe the motion of the system during the analysis period. In gait related studies, the analysis period is usually given by one or more stride periods, which are defined as the period of time measured from an initial event of one foot to the subsequent occurrence of the same event in the same foot (Winter, 1990, 1991). Moreover, it is also suggested that this initial event should be determined by the initial contact of the foot with the ground, which, in a

normal gait analysis, is described by the contact of the heel of the foot or shoe with the ground. In the present case, the analysis period is equal to one stride period and the initial event is characterized by the contact of the right shoe heel with the ground.

Considering the kinematic structure of the inverse biomechanical model, the kinematic input data for this application case consists in the set of trajectories describing the evolution in time of the twenty-five points and twenty-two unit vectors depicted in Figure 3.7. However, since the coordinates describing the biomechanical model are not independent, the required set of trajectories that needs to be acquired is, in fact, smaller than the initially described. This smaller set of trajectories contains the evolution in time of the Cartesian coordinates of the twenty-three anatomical points illustrated in Figure 5.2.

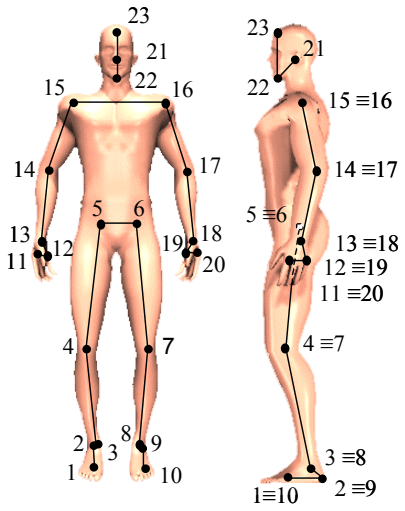

Figure 5.2: Set of anatomical points used to describe, in a unique way, the motion of the biomechanical model during the execution of the specified task.

These points are located at the joints and extremities of the subject under analysis and, as it can be observed from the comparison of Figure 3.7 with Figure 5.2, there is a straightforward equivalence between these points and the points used to construct the rigid bodies of the biomechanical model. This convenient mapping, in which the Cartesian coordinates of these points can be used, without additional calculations, in the construction of the rigid bodies of the biomechanical model is pointed out as one of the most important advantages of using fully Cartesian coordinates in the dynamic analyses of biomechanical systems.

The trajectories of the rest of the points and unit vectors that define the biomechanical model are calculated from the trajectories of these twenty-three anatomical points. In order to illustrate this calculation procedure, a couple of examples is provided: the trajectory of point *24*, represented in Figure 3.7, is calculated as being the midpoint between points *15* and *16*, while the components of unit vector $\mathbf{v}_1$, also represented in Figure 3.7, are calculated as being orthogonal to the plane described by points *1*, *2* and *3*.

Several different techniques that can be used to acquire the motion of the system and the trajectories of the points illustrated in Figure 5.2 (Allard *et al.*, 1995; Nigg and Herzog, 1995; Winter, 1990). In the present work, the motion is captured using four synchronized video cameras. The cameras have a 60 Hz sampling frequency and are positioned with respect to the subject as represented in Figure 5.3.

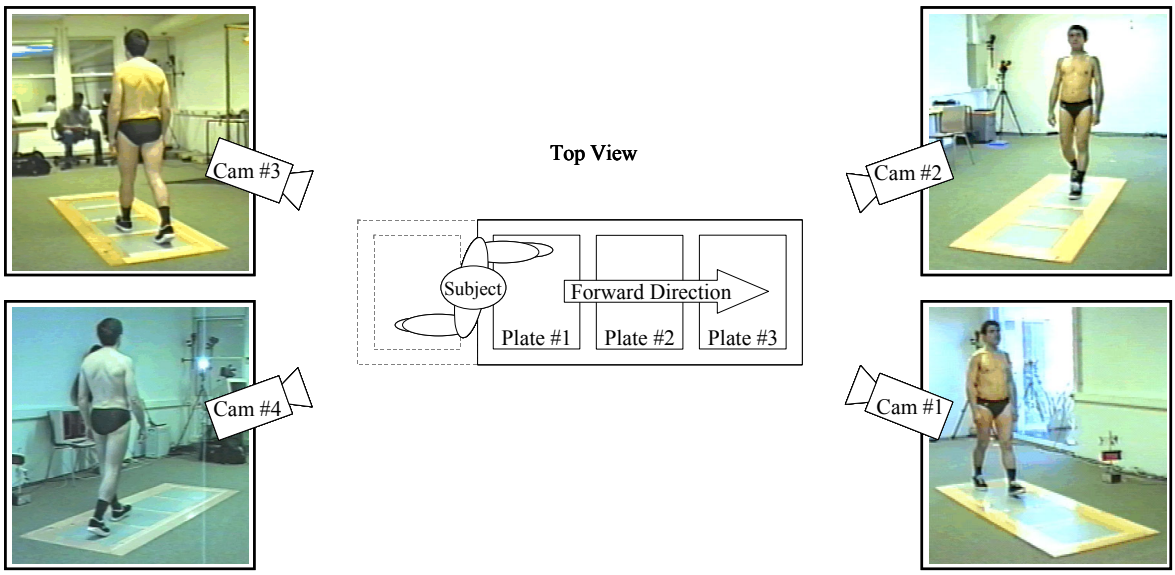

Figure 5.3: Representation of the set of four video cameras used to acquire the motion of the biomechanical system and their location with respect to the subject. Representation of the three force plates used to acquire the ground reaction forces measured during the stride period in the subject's feet.

For each camera, 66 images are collected in time intervals of 1/60 s, which corresponds to a stride period of 1.083 s and a walking cadence of approximately 111 steps per minute. This cadence is within the range of values reported in the literature for normal cadence stride periods (Winter, 1991).

The images collected by each one of these cameras (two-dimensional in nature) are manually digitized and the coordinates of each one of the points are obtained with respect to the view plane of each camera. Once having these coordinates, a motion reconstruction technique, designated by Direct Linear Transformation (Addel-Aziz and Karara, 1971), is applied in order to reconstruct the three-dimensional Cartesian coordinates of each point and the subsequent motion of the biomechanical model. This reconstruction technique is addressed in detail in Section 5.2.1.

To demonstrate the type of kinematic data obtained as result of the digitization process and the subsequent application of the motion reconstruction technique, the Cartesian coordinates of the right ankle, knee and hip (respectively points 3, 4 and 5 of the biomechanical model) are presented in Figure 5.4. This unprocessed kinematic data is usually designated as raw data.

It is clear from the observation of Figure 5.4, in particular in what concerns the Y coordinate, that a considerable amount of undesired high frequency noise is introduced in the coordinates of the points during the digitization process. If this high frequency noise is not attenuated from the digitized raw data, it will be amplified during the calculation of the velocities and accelerations of the anatomical points, with the consequent reduction of the quality of the results. In order to reduce these noise levels, a proper filtering technique is described in detail in Section 5.2.2.

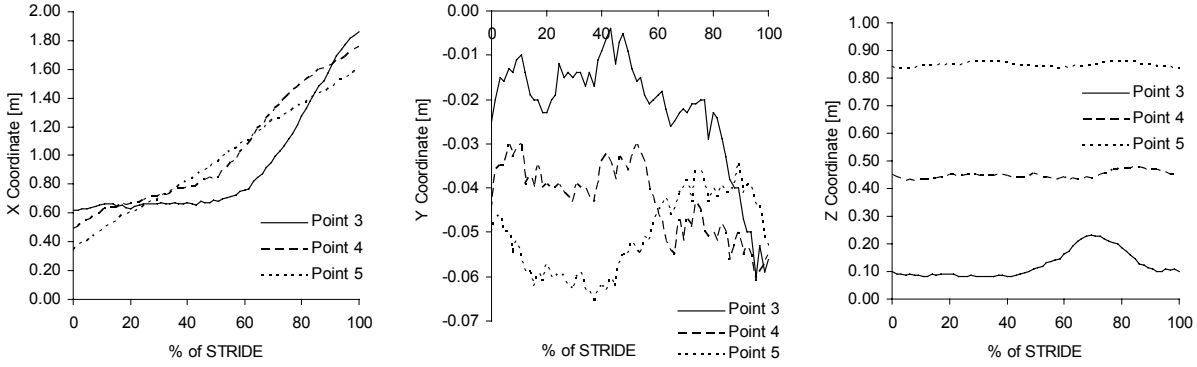

Figure 5.4: Raw kinematic data. In this figure, the Cartesian coordinates of the right ankle, knee and hip are presented. It is noticeable that high frequency noise levels are introduced in the coordinates as a consequence of the digitization process.

5.1.3 Kinetic Data

The dynamic data in inverse dynamic analyses corresponds to the determination of the externally applied forces over the anatomical segments of the subject being studied as well as their respective points of application. Some of these forces, such as the gravity acceleration field, are known in advance and therefore can be added to the equations of motion without any prior measurement. However, depending on the task being analyzed, many are the types of externally applied forces that can be exerted over the biomechanical model. Some of these forces cannot be measured at all, and in such cases an estimation procedure is performed using force models with different degrees of complexity (Blajer and Czaplicki, 2001). In other circumstances, such as in the case of gait analysis or in other types of sport activities such as running and jumping, the subject or the surrounding environment can be instrumented with proper force measuring devices, that are able to acquire the external forces and their respective points of application. That is the procedure used in the present case, where three AMTI (OR6-6) force plates, represented schematically in Figure 5.3, are used to measure the ground reaction forces and their respective points of application on the subject's feet. The three force plates are synchronized with the four video cameras and acquire the force data with a 600 Hz sampling frequency, which is multiple of the cameras' sampling frequency. The process of acquisition and conversion of the analog signal, measured by the force plates, into the digital signal, introduces high frequency components in these forces, which need to be attenuated using filtering techniques similar to the ones applied to the kinematic data.

The ground reaction forces and the center-of-pressure curves, which are the curves that provide the coordinates of the points of application for the external forces to the feet of the biomechanical model, are obtained for the right and left feet using the three force plates. The three components of these forces are presented in Figure 5.5 for the right and left feet and the respective center-of-pressure curves are shown in Figure 5.6. The values obtained for these forces and respective center-of-pressure curves are within the values reported in the literature for these quantities in applications related to normal cadence gait analysis (Vaughan *et al.*, 1992; Winter, 1991).

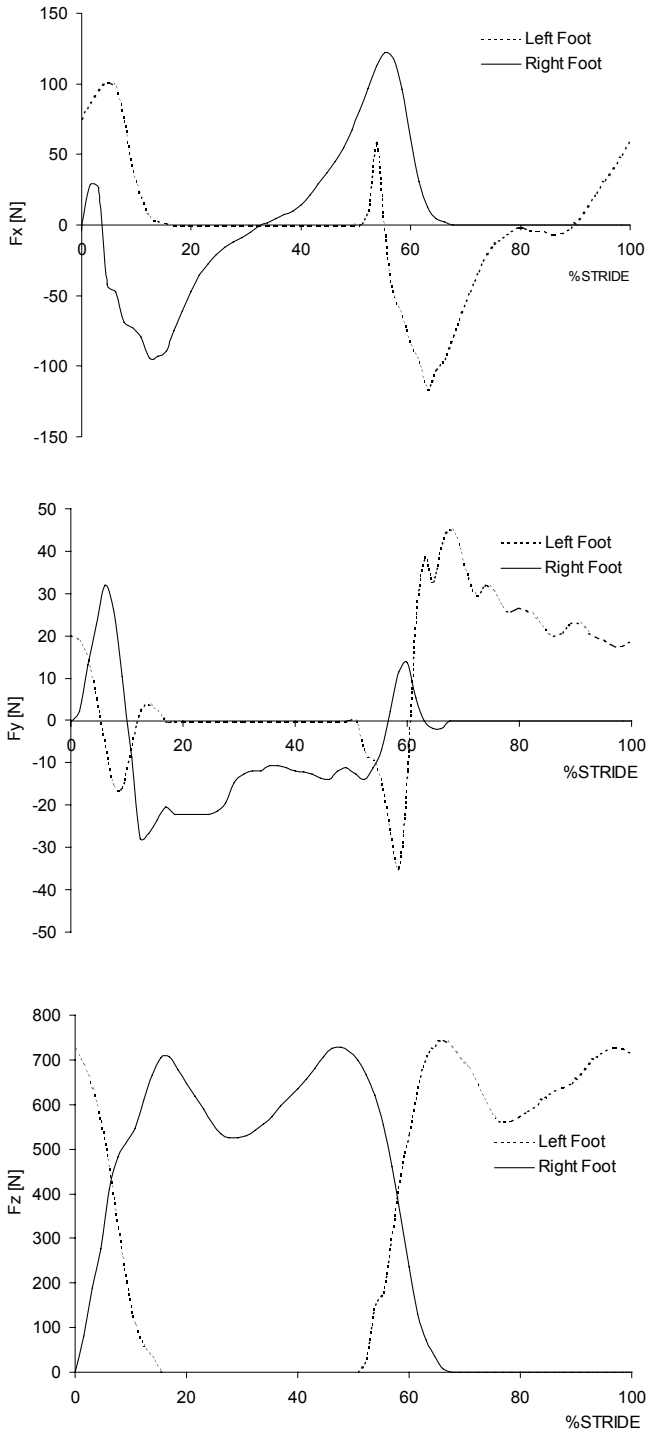

Figure 5.5: Ground Reaction Forces. Representation of the three raw components of the ground reaction forces measured in the right and left feet by the three force plates, during the normal cadence stride period.

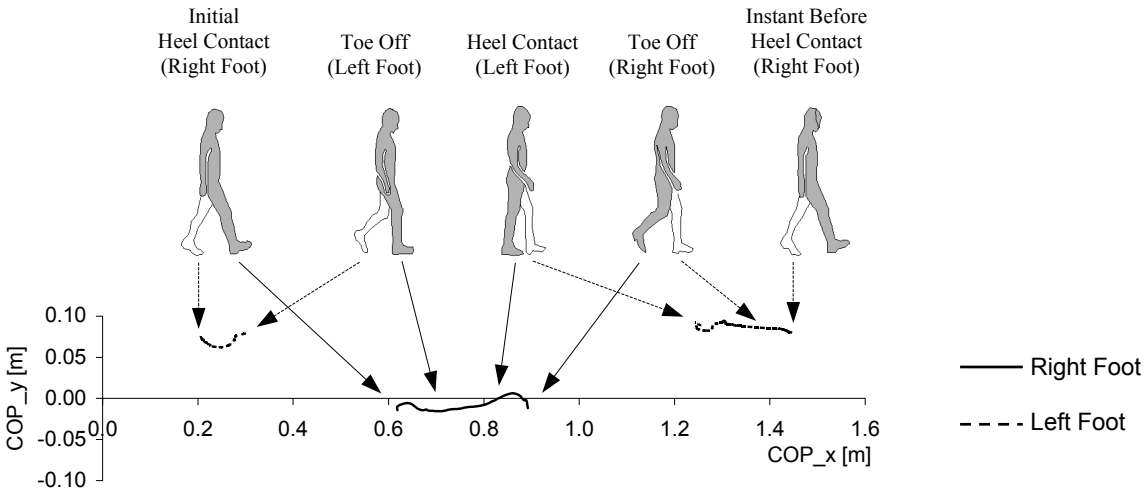

Figure 5.6: Center-of-pressure curves. Representation of the center-of-pressure curves (COP) measured in the force plates, for the right and left feet, during the execution of the normal cadence stride period.

5.1.4 Joint Moments-of-Force and Joint Actuators

In inverse dynamic analyses of determinate human tasks the main objectives are the calculation of the net moments-of-force and the joint reaction forces in the joints of the subject performing the task. Regarding the reaction forces, it was seen in Section 2.4.2 that these forces are associated to the Lagrange multipliers of the constraint equations describing the kinematic structure of the expanded (bio)mechanical system. Therefore, the values of these forces can be obtained using the procedure already described in Section 2.5, i.e., solving the equations of motion of the system with respect to the vector of Lagrange multipliers.

The Lagrange multipliers method is also applied to the calculation of the moments-of-force at the joints of the biomechanical model. The application of this method to the calculation of the joints moments-of-force requires the introduction of a kinematic driving actuator for each degree-of-freedom of the model. The purpose of these actuators is to describe the motion of each degree-of-freedom during the task under analysis and also to provide additional constraint equations, to which are associated the Lagrange multipliers that represent the joints moments-of-force.

In the present application case, the inverse biomechanical model is used. This model has forty-four degrees-of-freedom, as it can be observed in Figure 5.7, which means that an equal number of joint driving actuators is required for the calculation of an unique solution for the joint moments-of-force.

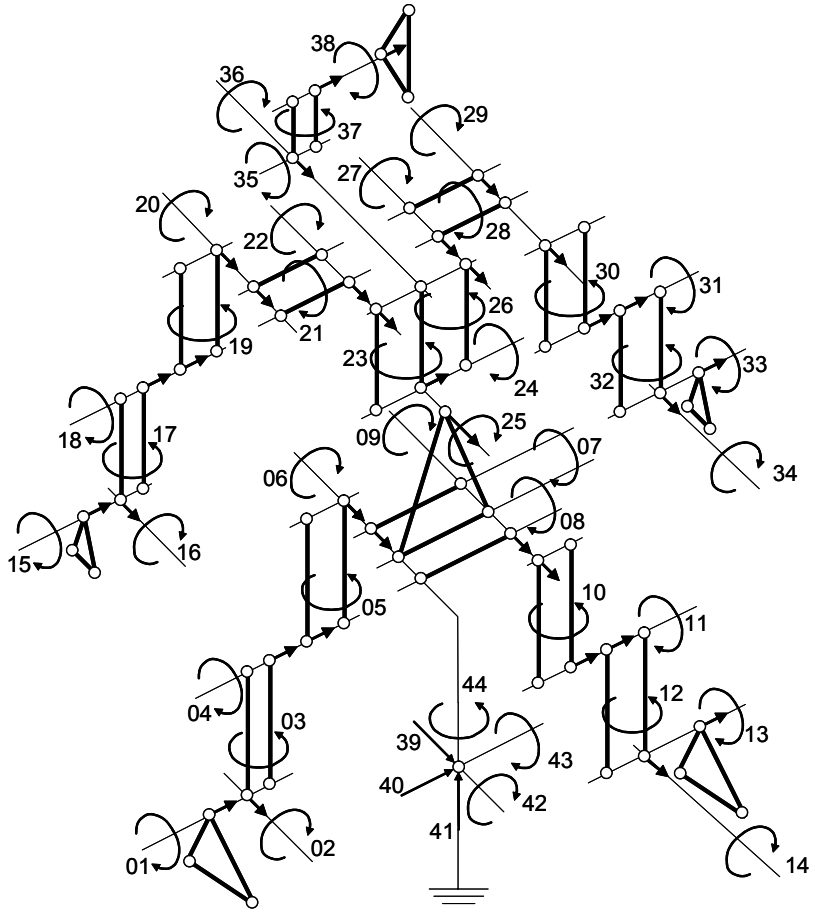

Figure 5.7: Schematic representation of the forty-four degrees-of-freedom of the inverse biomechanical model. To each one of these degrees-of-freedom is associated a driving constraint that is responsible to drive the model throughout a prescribed kinematic law. To each driving constraint is associated a moment-of-force that represents the external moments generated by the muscles to produced the observed motion.

The degrees-of-freedom 39 to 44 represent the three translations and three rotations of the biomechanical model as a whole rigid body. The driving constraints associated to these six degrees-of-freedom are called base body constraints and are responsible to drive the so-called

base body – the lower torso in the present model – through the observed motion. The forces and moments associated with these base body constraints are residual forces and moments that can be associated to the inconsistencies existing between the anthropometric data, kinematic data and kinetic data (Kaplan *et al.*, 2001). Hence, these terms can be regarded as a set of external corrective forces that, together with the kinematic and kinetic data obtained experimentally, are added to the equations of motion in order for these to be fulfilled. However, these corrective forces and moments would be zero if completely consistent input data could be obtained.

The driving constraint equations used to prescribe the motion of each joint of the biomechanical model are of scalar product type as described by Equation 2.13. For each rotational actuator equation, the evolution of angle $\phi(t)$, represented in Figure 2.1(b) for the case of the knee joint, is calculated using the kinematic data acquired in Section 5.1.2. In Figure 5.8 the evolution curves of the angles used to drive the degrees-of-freedom that control the flexion of the ankle, knee and hip are presented. The results presented in this figure correlate well with similar results presented by other authors (Vaughan *et al.*, 1992; Winter, 1991), although it is noticeable that a substantial amount of high frequency noise is presented in these curves as the result of the use of noisy kinematic data in the calculation of the joint angles.

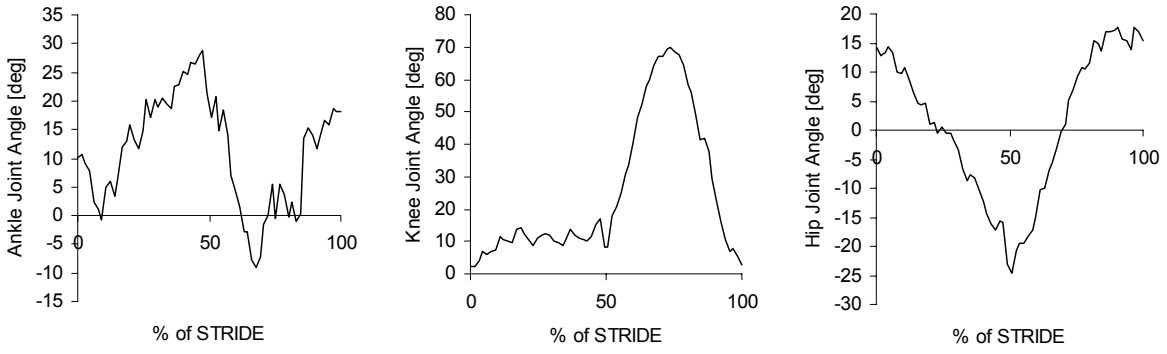

Figure 5.8: Driving angles for degrees-of-freedom 1, 4 and 7, to which correspond respectively the flexion of the ankle, knee and hip.

The results presented in Figure 5.8 support the idea that the use of proper filtering techniques is essential to reduce the noise levels and to improve the consistency of the input data. Moreover, it must be taken in account that the first and second derivatives of these curves are required for the construction of the right-hand-sides of the velocity and acceleration equations, as described in detail in Section 2.3.1. If an effective reduction of the noise levels is not achieved and considering that differentiation intrinsically amplifies the noise levels, then angular velocity and angular acceleration curves with poor quality are to be expected.

5.2 Three-Dimensional Motion Reconstruction and Data Filtering

The transformation of a three-dimensional movement into a convenient kinematic data set, suitable for use in a computer program, is not a straightforward process. It requires the use of several numerical techniques such as digitization of images, three-dimensional motion reconstruction and data filtering. In the present section a detailed description of the motion reconstruction techniques and filtering methods used in this work is presented.

5.2.1 Motion Recording and Reconstruction

There are several possible techniques for recording a three-dimensional motion (Allard *et al.*, 1995; Nigg and Herzog, 1995; Winter, 1990). The selection of a technique depends upon several factors such as the purpose of the analysis, the type of movement to be studied, the available time to obtain the results and the costs involved. Photogrammetry is the most frequently used technique. Video cameras are used, being the process of acquiring and digitizing images easily automated if proper markers, located at the anatomical joints and extremities, are applied (Nigg and Herzog, 1995).

The use of markers can be of great help in the digitization process to locate and identify different anatomical points. There are essentially two types of markers: passive markers, made of reflective materials, with different shapes and colors that reflect the light beams to the camera and active markers that emit a signal that is captured by the video camera (Nigg and Herzog, 1995). Though markers allow for an automatic spatial reconstruction process,

they do not eliminate digitization errors, because they cannot be positioned exactly in the anatomical joints and because of skin movements. Moreover, the use of markers has additional drawbacks. In sport activities this type of device can interfere, either physically or psychologically, with the performance of the athlete during the execution of the task. In a large number of activities, it is counterproductive the use markers and the motion has to be reconstructed based on manual digitization of video images. In this work, four video cameras are used to capture the motion, as illustrated in Figure 5.3. No passive or active markers are used and the digitization process is done manually.

The images collected by a single camera are a collection of two-dimensional information, resulting from the projection of a three-dimensional space into a two-dimensional one. The sequence of transformations that describe this projection is known in computer graphics as Virtual Camera (Allard *et al.*, 1995), which is the mathematical equivalence of projecting a three-dimensional object into the plane of the camera, as shown in Figure 5.9 for the anatomical point of the elbow joint.

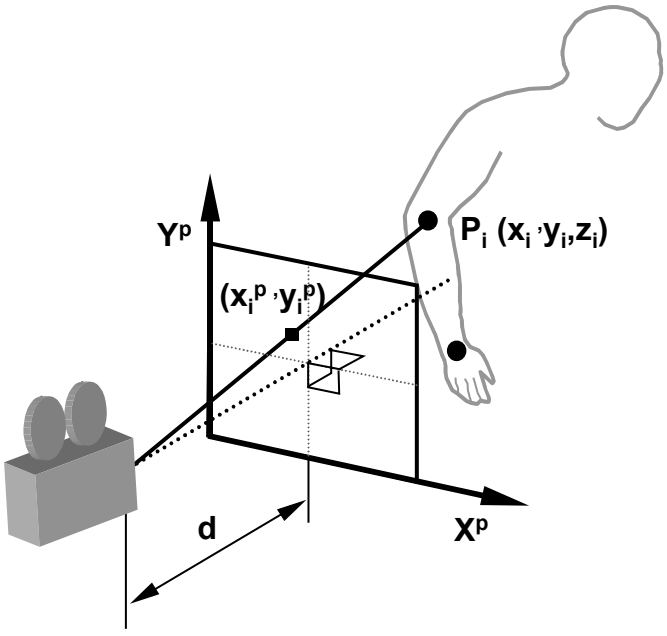

Figure 5.9: Camera projection plane. Coordinates (x_i^p, y_i^p) represent the position of point P_i in the projection plane of the camera. Coordinates (x_i, y_i, z_i) represent the Cartesian coordinates of this point in the three-dimensional space. The distance d is called focal length.

Mathematically, due to the lost of one dimension – the depth – the inverse of the transformation described in Figure 5.9 does not exist, i.e., from the mathematical point of view it is not possible to reconstruct the three-dimensional coordinates of a point in space from its two-dimensional projection in a single frame.

In order to solve this problem, Addel-Aziz and Karara, proposed a reconstruction process called Direct Linear Transformation (DLT) (Addel-Aziz and Karara, 1971), in which the two-dimensional information, collected by a set of two or more cameras, is used to reconstruct the three-dimensional coordinates of the anatomical points in space. Using the Direct Linear Transformation method, for every anatomical point, each camera introduces a set of two equations, written as:

$$\begin{cases} x_i = \dfrac{a_{1i}X + a_{2i}Y + a_{3i}Z + a_{4i}}{a_{9i}X + a_{10i}Y + a_{11i}Z + 1} \\ \\ y_i = \dfrac{a_{5i}X + a_{6i}Y + a_{7i}Z + a_{8i}}{a_{9i}X + a_{10i}Y + a_{11i}Z + 1} \end{cases} \tag{5.1}$$

where X, Y, and Z are the unknown Cartesian coordinates of the anatomical point in space, x_i and y_i are the coordinates of the projected point in the projection plane of camera i. Coefficients a_{1i} through a_{11i} are camera calibration parameters, which define the camera position, orientation, focal length and also account for distortion factors (Allard *et al.*, 1995). These coefficients are calculated through an initial calibration procedure in which a reference structure, with known position and dimensions, is recorded and the image coordinates of at least six of its points are acquired. As the spatial positions of the calibration points are known in advance, the only unknowns of Equation (5.1) are the calibration parameters.

Since at least two cameras must be used, the number of available equations for the reconstruction of the Cartesian coordinates of a given anatomical point is larger than the number of unknowns. The spatial reconstruction of each anatomical point is obtained by minimizing the mean square deviation of the solution of the two sets of Equations (5.1), for the three unknown coordinates.

5.2.2 Data Filtering and Cut-off Frequency Estimation

Errors in the coordinates of the reconstructed anatomical points are introduced due to the finite precision of the equipment, operator picking errors and the inability to locate exactly the anatomical points. After the process of motion reconstruction has been accomplished, the coordinates of the anatomical points must be filtered in order to reduce the noise due to digitization errors. This noise is inherent in the digitization process and also occurs when location markers are used. Consequently, the filtering process is important since it smoothes the coordinates, reducing the noise levels, making them suitable to be used in the kinematic analysis.

Different filtering methods can be used in the experimental data filtering, for noise reduction. Among these, the Butterworth 2nd order filters (Winter, 1990) and the Fourier series with optimal regularization (Hatze, 1980) are the most commonly used. The selection of the best filter for each type of application is a question not completely settled (Giakas and Baltzopoulos, 1997a). Taking into account the type of applications foreseen in the present work, a low-pass Butterworth 2nd order filter, with a zero-phase lag, is used (Winter, 1990). This filter has a frequency response curve that does not affect the signal below a specified cut-off frequency but, for frequencies above this cut-off, it leads to a rapid attenuation of the noise, as schematically illustrated in Figure 5.10(b).

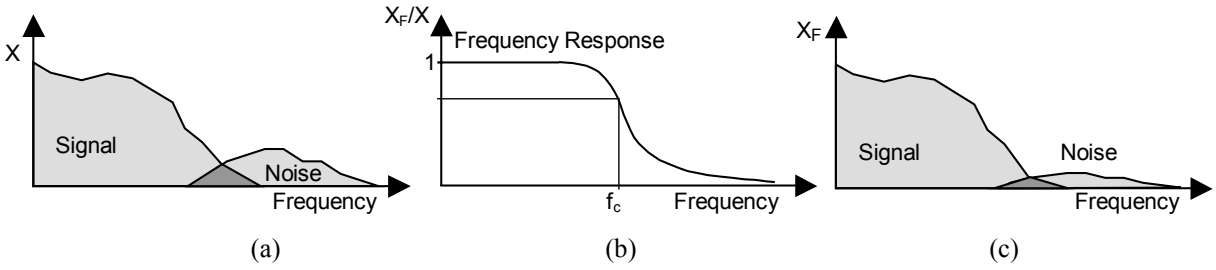

Figure 5.10: Representation of the filtering procedure using the Butterworth 2nd order, low pass filter. (a) The unfiltered signal. (b) The frequency response curve. (c) The filtered signal.

For gait analysis, the values of these cut-off frequencies typically range from 2 to 6 Hz, depending of the motion cadence and on the location of the anatomical points to filter. Faster

cadence movements and points located in the limbs need higher cut-off frequencies than slower cadence movements and points located on the trunk.

The filtered signal is calculated using an expression that weights non-filtered signals with filtered signals from previous frames in the following way:

$$x_i^F = a_0 x_i + a_1 x_{i-1} + a_2 x_{i-2} + b_1 x_{i-1}^F + b_2 x_{i-2}^F \tag{5.2}$$

where x^F represent filtered coordinates, x represent non-filtered coordinates and the indexes i, $i-1$ and $i-2$ indicate frame numbers. The coefficients a_0, a_1, a_2, b_1 and b_2 have constant values and are calculated using the following expressions (Winter, 1990):

$$a_0 = \frac{a_1}{2} = a_2 = \frac{k_2}{(1 + k_1 + k_2)} \tag{5.3}$$

$$b_1 = -2a_0 + k_3 \tag{5.4}$$

$$b_2 = 1 - 2a_0 - k_3 \tag{5.5}$$

where $k_1 = \sqrt{2}\omega_c$, $k_2 = \omega_c^2$ and $k_3 = 2a_0/k_2$, with $\omega_c = \tan(\pi f_c / f_s)$. The coefficients f_c and f_s are respectively the cut-off frequency of the filter and the sampling frequency of the capture device.

When applying the Butterworth 2nd order filter to an unfiltered signal, a phase-lag is introduced in the neighborhood of the cut-off frequency. In order to eliminate this undesired phase-lag, the zero-phase lag technique is used to prevent possible distortions of the signal. This performs a second filtering of the signal in the reverse order of frames. In this form, a symmetric phase-lag that cancels the first one is introduced, eliminating the distortion of the signal. However, it should be noted that when using this technique, the value of the cut-off frequency is modified and becomes only 80.2% of its initial value. Therefore, in order to obtain the correct value for this parameter, the initial value of the cut-off frequency must be divided by 0.802.

Usually, the selection of an appropriate value for the cut-off frequency is not an easy task. Either the value is too high and there is undesired noise passing to the filtered signal or the

value is too low and important characteristics of the signal can be lost in the filtered signal. In many situations, the selection of the appropriate value for the cut-off frequency starts as an initial guess, based on experience, which is afterwards tuned up for its final value by trial and error. However, there are several useful methods that can be used to support the selection of the appropriate cut-off frequencies that not only simplify the selection process but also improve the reliability of the filtered signals. In the present work, a method called Residual Analysis is used for that purpose (Winter, 1990). This method calculates the residual value between the filtered and the non-filtered signals for a specified range of cut-off frequencies, using the expression:

$$R(f_c) = \sqrt{\frac{\sum_{i=1}^{N} (x_i - x_i^F)^2}{N}} \tag{5.6}$$

where $R(f_c)$ is the residual, calculated for a cut-off frequency f_c and N is the number of recorded frames. After this calculation, a plot of the residual versus the cut-off frequencies is constructed computationally. This plot always present the typical behavior illustrated in Figure 5.11. The curves depicted in this figure are the result of the application of this method to the *X* coordinate of points *3*, *4* and *5*, which are located in the ankle, knee and hip joints of the subject, respectively. The reconstructed Cartesian coordinates of these points are presented in Figure 5.4.

Regarding the results presented in Figure 5.11, it is observed that each curve can be divided in two distinctive parts: an initial part in which the residual is characterized by a non-linear behavior that increases with the decrease of the cut-off frequency and a second part in which the residual decreases linearly with the cut-off frequencies. The initial non-linear part of the residual curve corresponds to a signal distortion introduced by the use of excessively low cut-off frequencies that not only are attenuating the noise but also important signal information. In the linear part of the residual curve there is no distortion of the signal, only an attenuation of the noise levels, which increase with the decrease of the cut-off frequency.

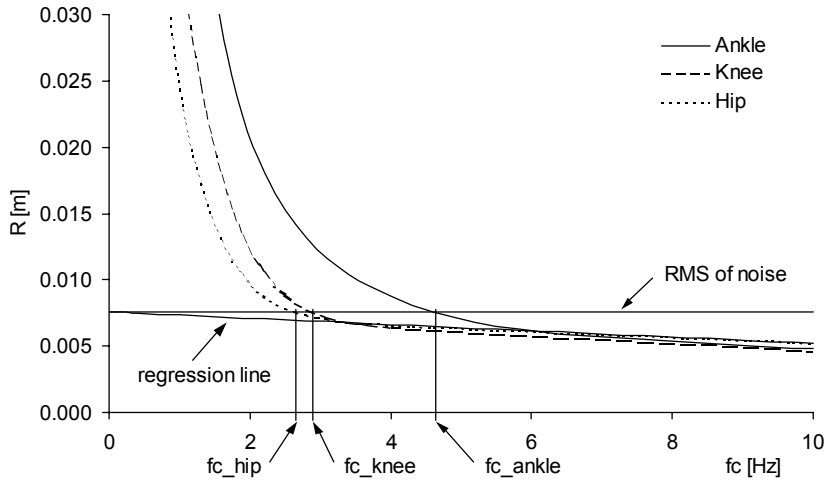

Figure 5.11: Residual analysis curves obtained for the *X* coordinate of points *3*, *4* and *5*, representing the ankle, knee and hip joints of the subject, respectively. The reconstructed Cartesian coordinates of these points are presented in Figure 5.4.

Although it is clear that the residual curve provides important information regarding the noise levels contained in the signal, it does not provide by itself, an estimation for the value of the cut-off frequencies. For that additional step to be accomplished, it is necessary to calculate, using a least-square approach, the regression line that best fits the linear part of the residual curve. This regression line represents the residual curve that would be obtained if only noise was present in the non-filtered signal. Therefore, its intersection with the vertical axis and the consequent calculation of the residual at this point, provides an estimation of the RMS of the noise, as illustrated in Figure 5.11.

However, since this method is implemented computationally, some care must be introduced during the automatic determination of the linear portion of the residual curve that will be used in the calculation of the regression line. As it can be observed in Figure 5.11, the beginning of this part of the residual curve differs from coordinate to coordinate. In order to assure the accuracy of the method, an iterative procedure is implemented in which the low frequency points of the residual curve are eliminated sequentially until a specified correlation, between the straight regression line and the linear part of the residual curve, is reached. As illustrated in Figure 5.12, different correlations produce different regression lines and therefore different RMS of the noise and cut-off frequencies. It is noticeable from the

observation of this figure that acceptable results can be expected for correlation coefficients higher than 90%. In this work, correlation coefficients between 97% and 99% are used.

The selection of the cut-off frequency is a compromise between the amount of noise allowed to pass through the filter and the amount of signal distortion. The amount of signal distortion is given by the vertical distance measured between the regression line and the residual curve, and the amount of noise passing through the filter is given by the vertical distance measured between the horizontal line of the RMS of the noise and the regression line. One possible compromise is obtained by choosing the cut-off frequency in which the amount of noise is equal to the amount of signal distortion. This cut-off frequency is found on the intersection of the horizontal line of the RMS of the noise with the residual curve. This process is graphically represented in Figure 5.11.

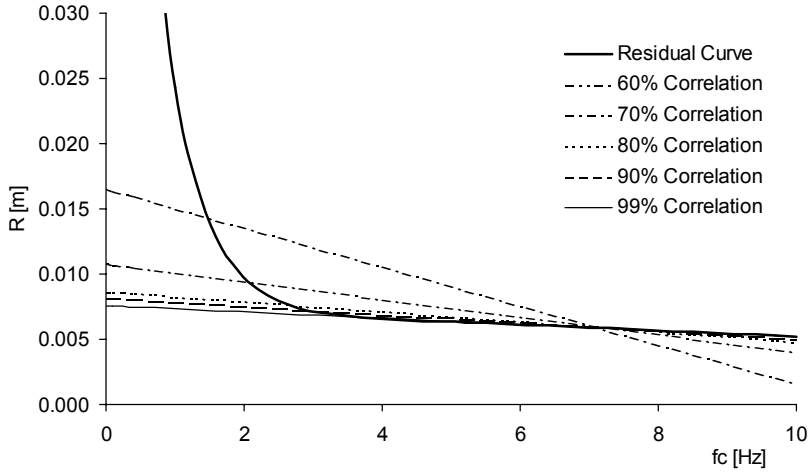

Figure 5.12: Influence of the correlation coefficient in the calculation of the regression line used to estimate the RMS of the noise and the cut-off frequency.

Using this type of analysis for the calculation of the cut-off frequency, each signal is filtered using a different cut-off frequency. It is expected that anatomical points with faster movement require higher cut-off frequencies than anatomical points with slower movement. In Figure 5.11, the cut-off frequencies, for the examples shown, range from 2.7 Hz to 4.3 Hz. The lower frequency is associated with the anatomical point of the hip and the higher frequency is associated with the anatomical point of the ankle. These cut-off frequencies are within the expected values for gait analysis (Winter, 1990).

5.2.3 Application to the Human Gait Example

The methodologies presented in this section are applied to the input data describing the normal cadence stride period, introduced in Section 5.1. Once the three-dimensional motion reconstruction process has been accomplished, using the Direct Linear Transformation method, the coordinates of the anatomical points are filtered using the Butterworth 2nd order low pass filter, with the cut-off frequencies estimated by residual analysis using a correlation coefficient of 0.99.

In Figure 5.13, a chart with the values calculated for the cut-off frequencies of each anatomical point is presented. Different frequency contents are found for different points. Points with faster movements, such as the feet (points *1-3*,*8-10*) and the hands (points *11-13*,*18-20*) have higher cut-off frequencies than points with slower movements such as the hips (points *5*,*6*), shoulders (points *15*,*16*) or the head (points *21-23*). Another important aspect is that the cut-off frequency obtained for the *X* coordinate of a point is in most cases higher than the cut-off frequency obtained for the *Y* and *Z* coordinates. The values of the cut-off frequencies range from 2 Hz to 5 Hz. These values are within the expected values for the type of movement under analysis.

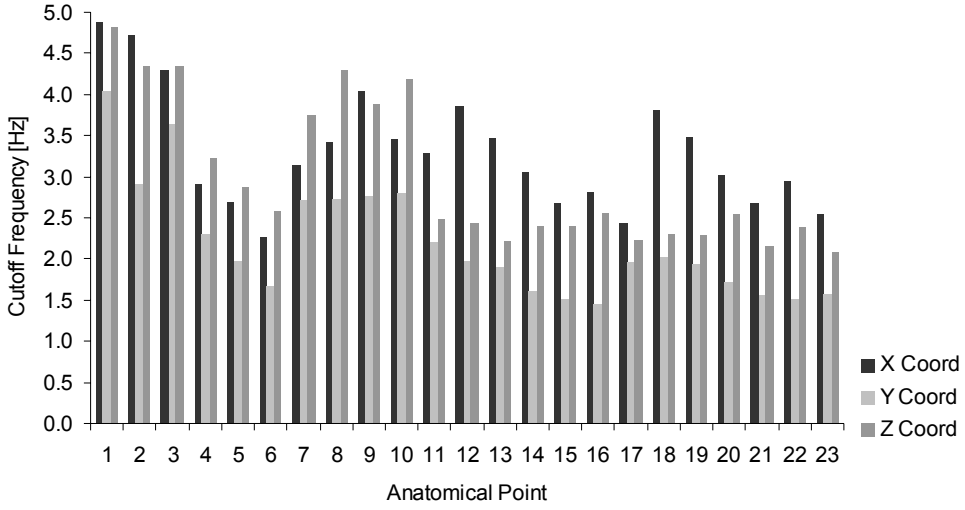

Figure 5.13: Cutoff frequencies obtained for each anatomical point of the biomechanical model. These frequencies are estimated using residual analysis. For the numbering of the anatomical points refer to Figure 5.2.

From the residual analysis the error committed during the digitization process can be estimated. The estimates of these errors are presented in Figure 5.14 and correspond to the values obtained for the y-intercept coefficients of the regression lines that best fit the linear part of the residual curves obtained for each anatomical point.

For each coordinate, all anatomical points present approximately the same level of error. An average RMS of error of 7.0 mm, 3.0 mm and 3.3 mm is found for the *X*, *Y* and *Z* coordinates, respectively. The estimation of the error in the *X* coordinate is higher than the error in the other two coordinates. This is expected considering that the motion under analysis occurs mainly in the sagittal plane.

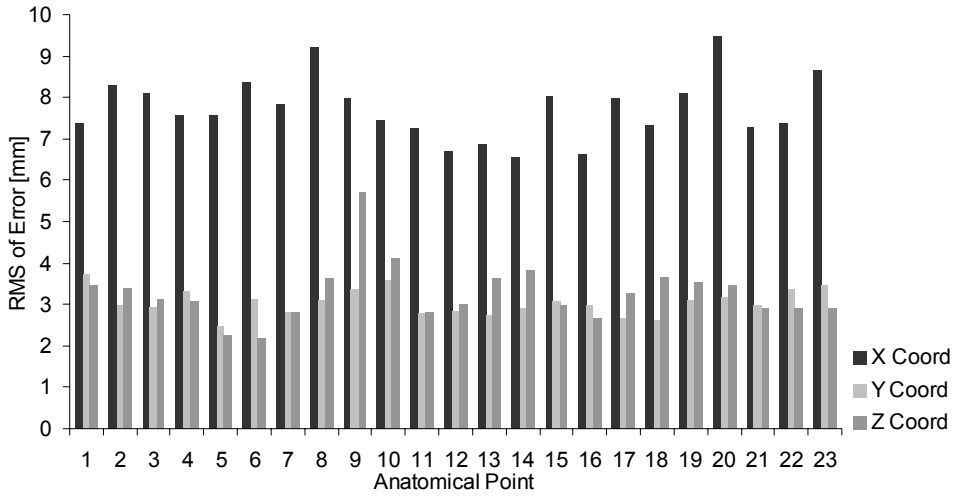

Figure 5.14: Estimation of the RMS of the error committed during the digitization process. This error estimation is performed using the residual analysis of the signals. For the numbering of the anatomical points refer to Figure 5.2.

An inverse dynamic analysis is performed using the previous filtered positions of the anatomical points, the filtered ground reaction forces and the anthropometric data are properly scaled to fit the dimensions of the subject under examination. The cut-off frequencies used to filter the external forces and the coordinates of their associated application points are also obtained by residual analysis. The reaction forces obtained in the right ankle, knee and hip joints as well as the net moments-of-force developed at these joints are presented in Figure 5.15 and Figure 5.16, respectively.

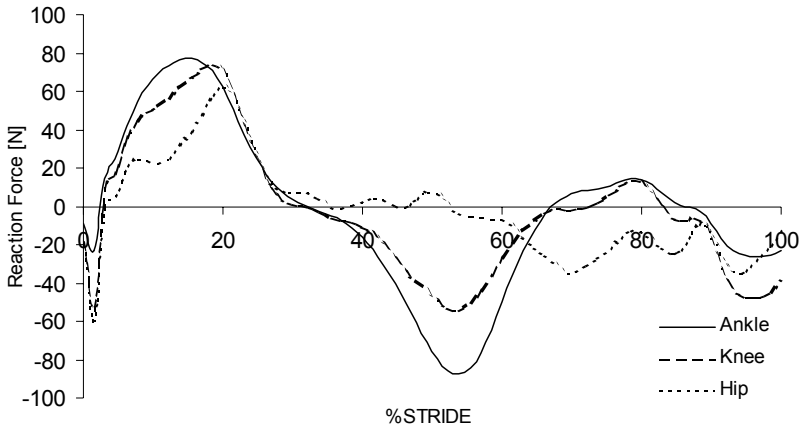

a)

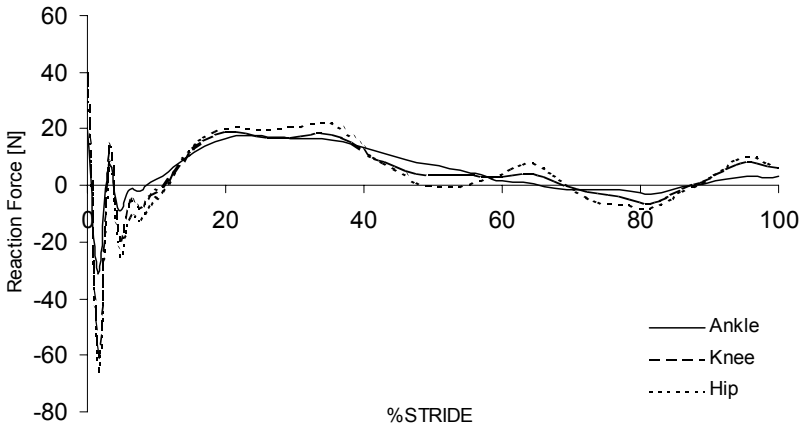

b)

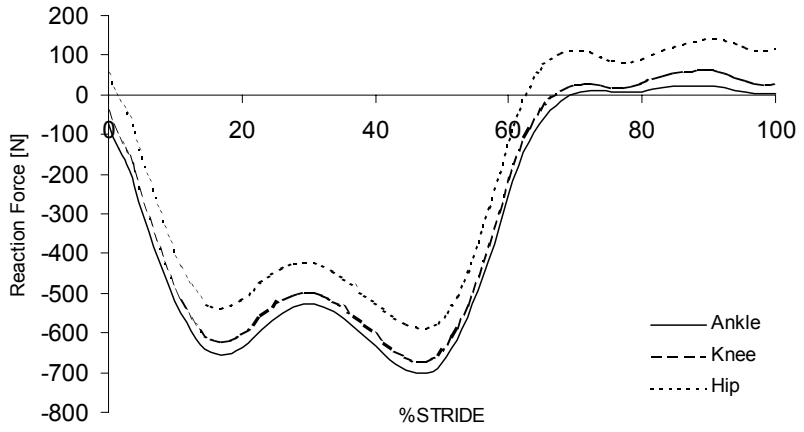

c)

Figure 5.15: Reaction forces, calculated during the inverse dynamic analysis, in the right ankle, knee and hip joints. a) *X* component; b) *Y* component; c) *Z* component.

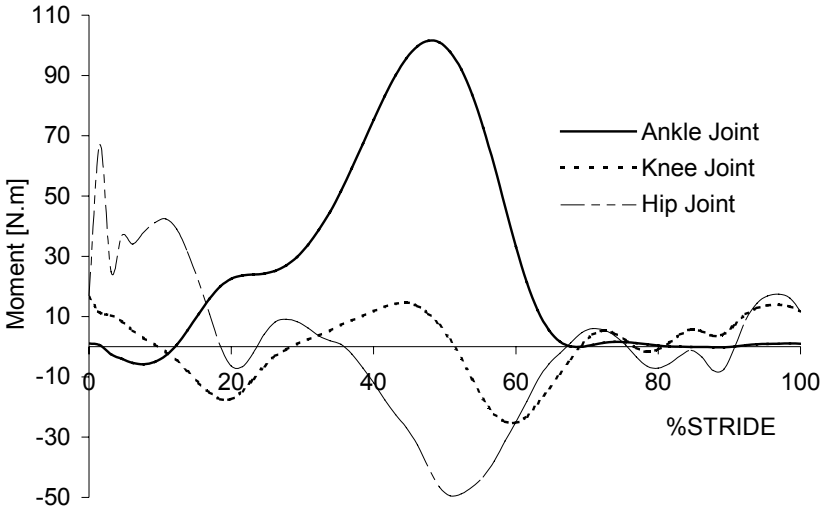

Figure 5.16: Net moments-of-force calculated, during the inverse dynamic analysis, in the right leg of the subject. The moments presented refer to the actuators associated to degrees-of-freedom 1, 4 and 7, to which are associated the flexion of the ankle, knee and hip joints, respectively.

It is clear from the observation of Figure 5.15 and Figure 5.16 that the high frequency components that were observed in the raw data, namely in the Cartesian coordinates of the digitized points, external forces, center-of-pressure curves and joint angles – presented respectively in Figure 5.4, Figure 5.5, Figure 5.6 and Figure 5.8 – are attenuated in the filtered data and, therefore, such behavior is also not detected in the analysis results. Moreover, the results demonstrate that the residual analysis performed to the raw data provide a valid set of cut-off frequencies, which are similar to the range of values proposed in the literature for this type of activity.

In order to evaluate the influence of the filtering procedure, several inverse dynamic analyses are performed with different cut-off frequencies. The results produced by these analyses, regarding the effects of different cut-off frequencies in the reaction forces and net moments-of-force at the ankle and knee joints are presented in Figure 5.17 and Figure 5.18 respectively. In particular, these two figures present the vertical component of the reaction force and the net moment-of-force in the sagittal plane for the referred joints. The results show that the coordinate filtering procedure plays a very important role in the quality of the results. The 2nd order Butterworth low-pass filter with the zero-phase lag reduced the noise

levels successfully. However, when no filtering is used the results show unwanted oscillations that compromise the quality of the results.

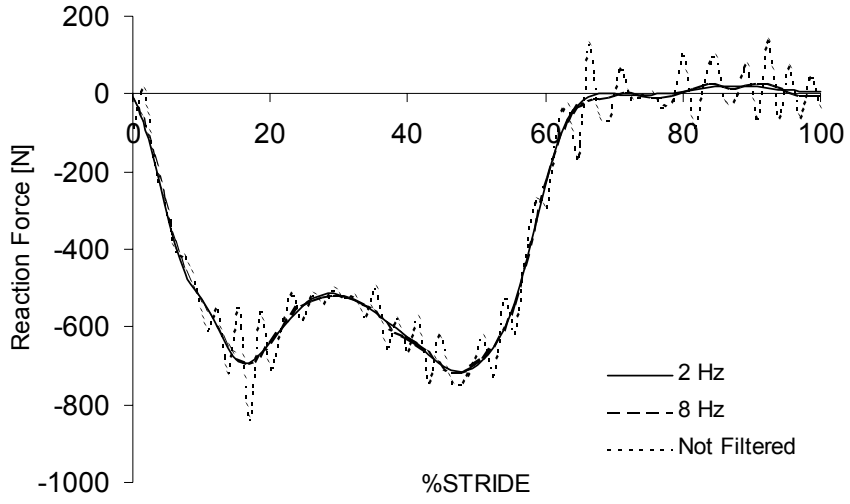

(a)

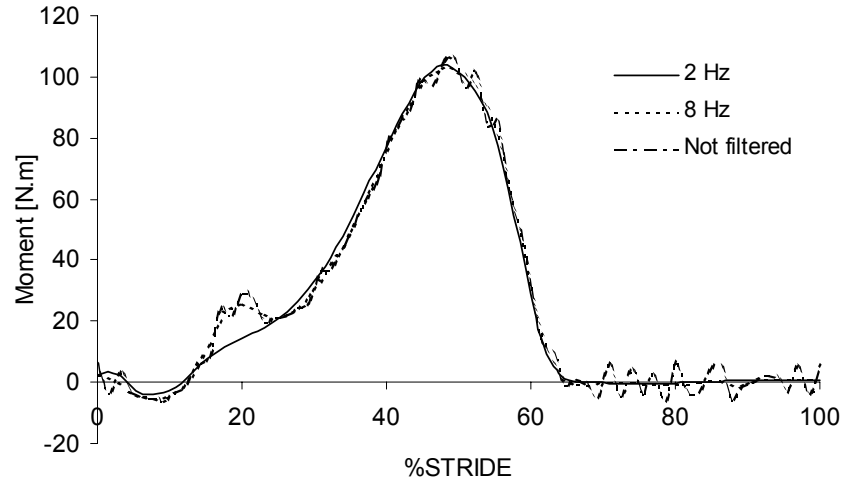

(b)

Figure 5.17:Results of the analysis in the ankle joint, using different cut-off frequencies. (a) Vertical component of the reaction force. (b) Moment-of-force in DOF 1.

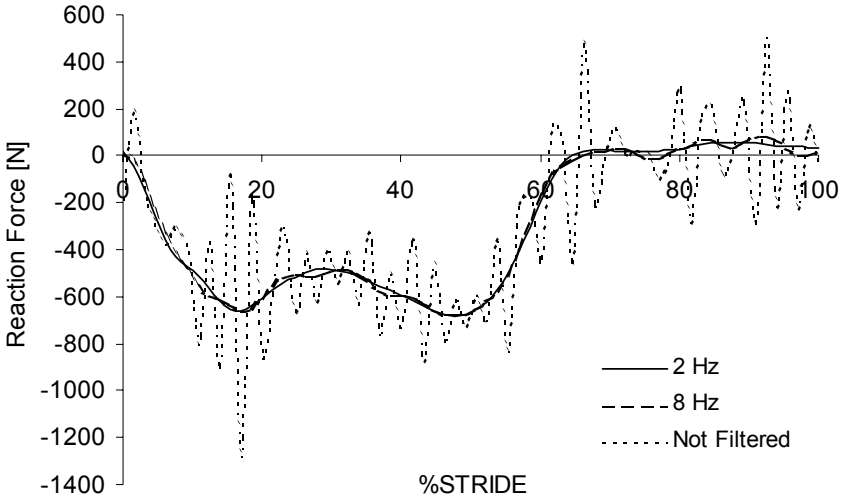

(a)

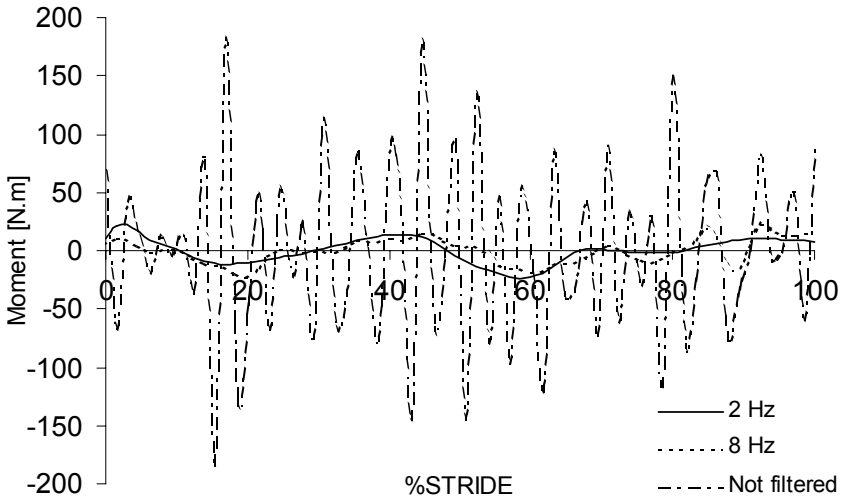

(b)

Figure 5.18:Results in the knee joint, using different cutoff frequencies: a) Vertical component of the reaction force; b) Net moment-of-force in DOF 4.

5.2.4 Discussion

In the present section, the methods used to obtain the raw position of the anatomical points and the subsequent filtering procedures that must be used to reduce the noise levels contained in that data, were presented within the framework of the biomechanical model selected and the multibody formulation used. The Direct Linear Transformation method allows for the

reconstruction of the Cartesian coordinates of the anatomical points, although a considerably amount of high frequency noise, inherent to the recording and reconstruction process is present in the raw coordinates that describe the motion of the biomechanical model. The use of a formulation with fully Cartesian coordinates has the advantage that the anatomical point positions correspond directly to the coordinates of the biomechanical model. The proposed filtering procedure based on the use of a Butterworth 2^{nd} order low pass filter with the zero-phase lag, proved to be an essential tool that has an important influence in the quality and accuracy of the produced results. The use of different cut-off frequencies in the filtering process of the raw data can lead to quite different results. The use of the residual analysis technique proved to be a very helpful numerical tool that can be used with success in the selection of the appropriate set of cut-off frequencies to filter the raw data. It was shown that for gait analyses with normal cadence stride periods, the use of cut-off frequencies ranging from 2 to 8 Hz provide suitable results.

5.3 Consistent Kinematic Data

In Section 5.2 a set of computational tools and numerical techniques essential for the improvement of the quality and accuracy of the results produced by an inverse dynamic analysis has been presented. However, either because the acquisition of the kinematic data is generally done independently of the biomechanical model effectively used or due to the filtering procedure, the processed kinematic data does not ensure that the kinematic constraints, associated to the biomechanical model, are fulfilled. The inverse dynamic analysis also requires that the system velocities and accelerations are known. A common process to obtain those involves the use a polynomial interpolation of the coordinates and the subsequent calculation of its time derivatives. This procedure does not ensure that the constraint velocity and acceleration equations are fulfilled, even if the position data is kinematically consistent. Consequently, spurious joints reaction forces and net moments-of-force, associated to these constraint violations, are generated in the solution of the inverse dynamic problem (Ambrósio *et al.*, 1999b; Silva and Ambrósio, 2002a).

To ensure the consistency of the kinematic data with the constraints of the biomechanical model it is proposed here that the kinematic positions are modified in order to fulfill the constraint equations. Furthermore, the velocity and acceleration of the system are obtained by using the constraint velocity and acceleration equations, given by Equations (2.8) and (2.11) respectively. The proposed methodology is applied to the analysis of the human gait with a normal cadence stride period, in order to obtain the consistent reaction forces and the net moments-of-force produced by the muscle apparatus.

5.3.1 Kinematically Consistent Positions

As illustrated in Figure 5.19, the process of acquiring the kinematic input data leads to errors in the evaluation of the distances between anatomical points. Therefore, the input data, collected using this process, is non-consistent with the kinematic structure of the biomechanical model, producing violations in the kinematic constraints of the mechanical system. These acquisition errors cannot be eliminated in general, and are due to the limited resolution of the video image, to operator digitizing errors, to skin movement or even due to the fact that anatomical joints are not perfect mechanical joints, as represented by the model.

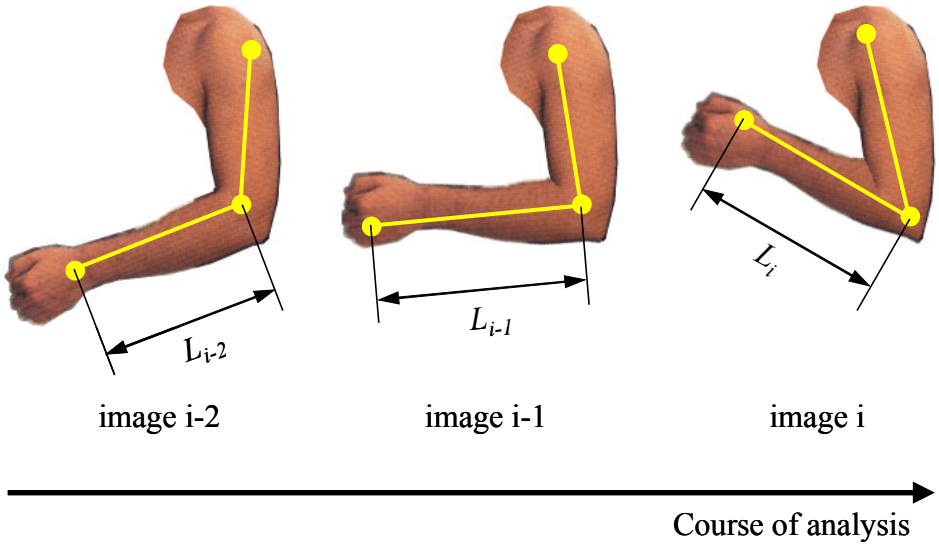

Figure 5.19: Example of inconsistent kinematic data. The distances, obtained during the digitization process, are not kept constant from image to image ($L_{i-2} \neq L_{i-1} \neq L_i$). This is due to errors that are inherent to the digitization process.

The first step towards the construction of kinematically consistent input data is to modify the Cartesian coordinates of the anatomical points in such a way that the kinematic constraints are fulfilled in general and, in particular, that the distances between anatomical points remain constant during the analysis. The procedure to calculate the new set of points is accomplished by performing a kinematic analysis of the system positions. First, the initially non-consistent positions are used to calculate average link lengths between the anatomical points. These average lengths are used to define the dimensions of the rigid bodies of the biomechanical model, so that the model has constant link lengths during the analysis. Alternatively, instead of using average link lengths, the effective anthropometric dimensions, obtained from direct measurements of the subject under analysis, can be used. Second, the biomechanical model is driven throughout the kinematic analysis, using the rotational driver constraint equations and the curves that express the evolution of the joint angles, denoted previously by $\phi(t)$. It is then possible, to evaluate the system position at any intermediate time step, even if it does not coincide with a frame acquired by the cameras. As a result, the kinematic analysis produces a new set of anatomical point positions, which are consistent with the kinematic structure of the biomechanical model.

In the numerical implementation of this procedure, due to the presence of redundant constraints, the Newton-Raphson iterative scheme is used in the sense of a least-square approach. This iterative scheme has a quadratic convergence in the neighborhood of the solution. Using the non-consistent positions as an initial guess to the Newton-Raphson procedure, a convergent solution is obtained after 3 or 4 iterations. The expression describing the iterative method is rewritten here as:

$$\left(\mathbf{\Phi}_{\mathbf{q}}^{\mathrm{T}}\mathbf{\Phi}_{\mathbf{q}}\right)_i\left(\mathbf{q}_{i+1}-\mathbf{q}_i\right)=-\left(\mathbf{\Phi}_{\mathbf{q}}^{\mathrm{T}}\right)_i\left(\mathbf{\Phi}\right)_i \tag{5.7}$$

where $\mathbf{q}$ is the vector of generalized coordinates and $\mathbf{\Phi}$ is the global constraint vector. The subscript i represents the iteration index.

Once the consistent positions of the system are calculated, the associated velocities and accelerations of the consistent points can be obtained using direct spline differentiation techniques or the method described hereafter.

5.3.2 Kinematically Consistent Velocities and Accelerations

A mechanical system is considered to be totally consistent if its velocities and accelerations are also consistent with the underlying kinematic structure. This means that the system velocities and accelerations must belong to the null-space of the Jacobian matrix. This is expressed by the velocity and acceleration equations, already introduced in Chapter 2 and rewritten here for convenience:

$$\mathbf{\Phi}_{\mathbf{q}}\dot{\mathbf{q}} = \boldsymbol{\nu} \tag{5.8}$$

$$\mathbf{\Phi}_{\mathbf{q}}\ddot{\mathbf{q}} = \boldsymbol{\gamma} \tag{5.9}$$

where $\dot{\mathbf{q}}$ and $\ddot{\mathbf{q}}$ are respectively the vectors of generalized velocities and accelerations of the system and $\boldsymbol{\nu}$ and $\boldsymbol{\gamma}$ the right-hand sides of the velocity and acceleration equations. Equations (5.8) and (5.9) represent a system of linear equations with the same leading matrix. The solution of Equations (5.8) and (5.9) is unique for a given position of the system and leads to the calculation of the generalized consistent velocities and accelerations.

5.3.3 Application to the Human Gait Example

The procedure described before is applied to the example introduced in Section 5.1. The input data, collected from cameras and force plates, is filtered in order to reduce the high frequency noise levels, using the filtering procedure described in Section 5.2, with properly chosen cut-off frequencies (Silva *et al.*, 2001).

In order to investigate the importance of the proposed procedure to the quality of the results, an inverse dynamic analysis is carried out with and without kinematically consistent input data, in the positions, velocities and accelerations of the anatomical points. The results are obtained for the complete set of kinematic joints of the inverse biomechanical model described before. However, only the results referring the right lower limb of the model are presented, together with reference results of similar gait analysis by Winter (Winter, 1990). These results are presented in Figure 5.20 to Figure 5.23 and illustrate the net moments-of-

force developed by the muscle apparatus in the Sagittal plane of the subject, respectively in the joints of the ankle, knee, hip and support.

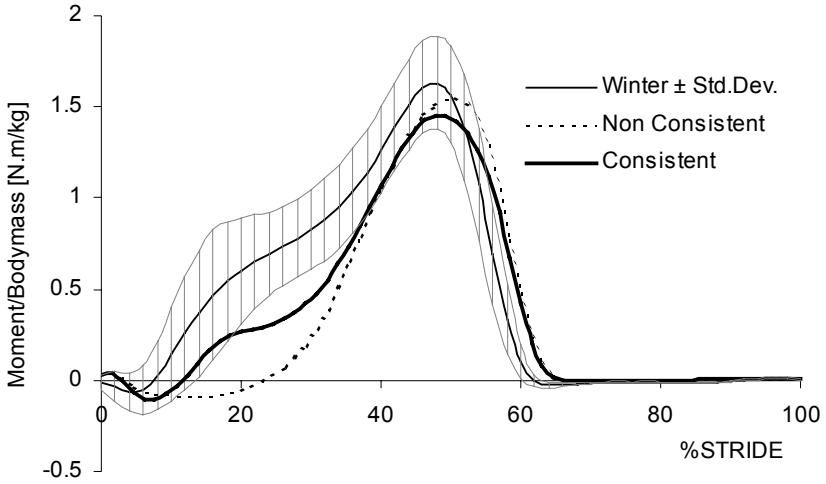

Figure 5.20: Net moment-of-force in the right ankle joint (sagittal plane), calculated using consistent and non-consistent kinematic data. The thin solid line and the dashed area correspond respectively to the average moment-of-force bounded by the standard deviation obtained by Winter (1990).

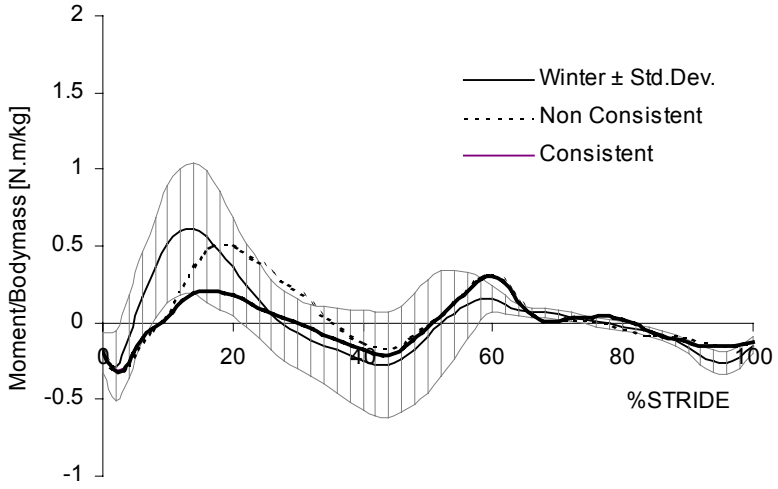

Figure 5.21: Net moment-of-force in the right knee joint (sagittal plane), calculated using consistent and non-consistent kinematic data. The thin solid line and the dashed area correspond respectively to the average moment-of-force bounded by the standard deviation obtained by Winter (1990).

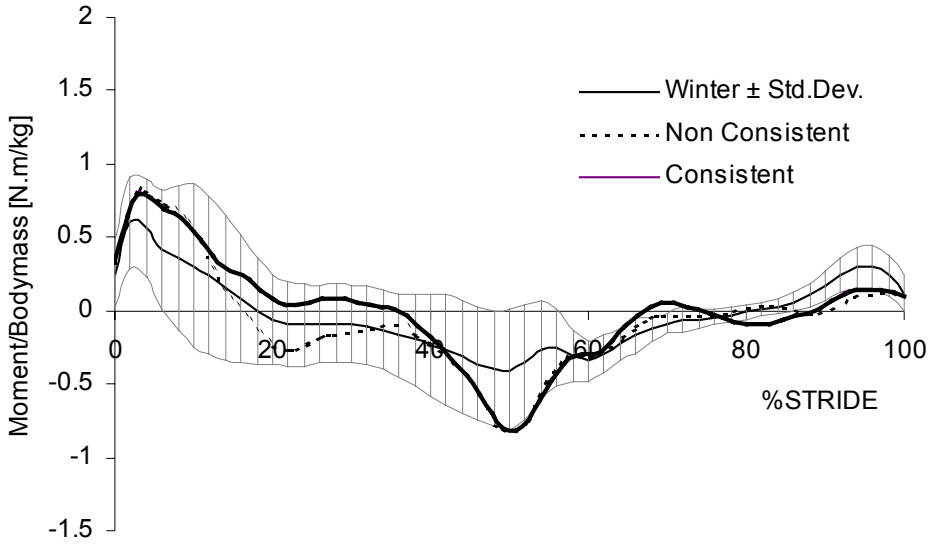

Figure 5.22: Net moment-of-force in the right hip joint (sagittal plane), calculated using consistent and non-consistent kinematic data. The thin solid line and the dashed area correspond respectively to the average moment-of-force bounded by the standard deviation obtained by Winter (1990).

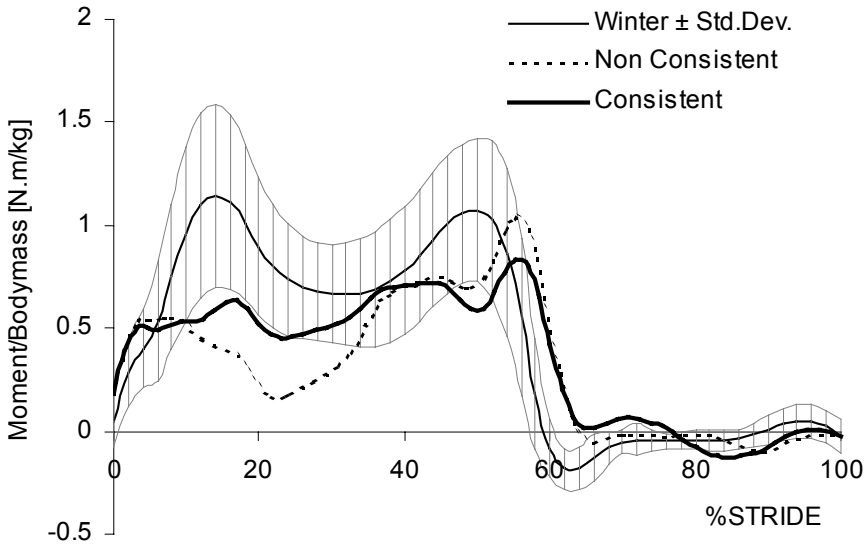

Figure 5.23: Net moment-of-force in the support (sagittal plane), calculated using consistent and non-consistent kinematic data. The thin solid line and the dashed area correspond respectively to the average moment-of-force bounded by the standard deviation obtained by Winter (1990).

Significant differences exist between the response of the system calculated using kinematically consistent and kinematically non-consistent data. The moments-of-force resulting from the inverse dynamic analysis using consistent kinematic data correlate better with the results of Winter (1990) than those obtained using non-consistent data. The improvements introduced by the described procedure are especially observed in the moment calculated for the ankle joint. The data provided by Winter is obtained using a two-dimensional model and a formulation based on joint coordinates, for which there are no constraint equations. Therefore, the reference moments-of-force are obtained from an inverse dynamic analysis in which the kinematic data is consistent by nature.

No differences are observed in the system response when comparing the results obtained with the kinematically consistent positions, velocities and accelerations with an input data set where only consistent positions are used. This result reveals that the process of direct spline differentiation of the consistent trajectory curves assures sufficient accuracy in the gait analysis for the type of motion acquired.

5.3.4 Discussion

The analysis of results reveals that the enforcement of the kinematic consistency of the position of the anatomical points improves the overall quality of the results. Therefore, after the reconstruction of the spatial motion of the anatomical points and consequent application of the filtering procedure, the kinematic data set should be made consistent, in order to fulfill the kinematic constraints imposed by the kinematic structure of the biomechanical model. Moreover, a procedure for the calculation of the kinematically consistent velocities and accelerations was also described in this Chapter. It was seen that the kinematically consistent velocities and accelerations of the anatomical points can be obtained using the time derivatives of the constraint equations rather than the standard procedure in which those are obtained using direct spline differentiation of the trajectory curves of the anatomical points. However, for the type of application cases presented, the net moments-of-force showed to be relatively insensible to the kinematic consistency of velocities and accelerations, provided that the positions of the anatomical points are consistent with the kinematic structure of the model.

5.4 Validation of Results Using a Classical Dynamics Approach

In the previous sections of this chapter, the computational procedures used in the treatment of the kinematic data, required for inverse dynamic analyses of biomechanical models, were reviewed in order to identify the principal sources of error in the input data, as well as to propose solution methods that, mitigating those errors, lead to visible improvements in the quality of the results. Following the same purpose, it is the objective of the present section to compare the quality of results produced by the proposed multibody methodology, using fully Cartesian coordinates, with the same type of results produced by an alternative procedure that uses directly the classical Newton-Euler equations.

The classical Newton-Euler approach is used since it takes advantage of the open-loop structure of general biomechanical systems, to solve the dynamic equilibrium equations of each anatomical segment sequentially, starting from the segments further away from the base body and moving inwards along the kinematic chain under analysis. Furthermore, due to its own nature, errors committed in the digitization of anatomical data of later segments do not influence the solution of the equilibrium equations of the anatomical segments solved first. The same is true for digitization errors committed in anthropometric segments belonging to other kinematic chains of the biomechanical model than the one where the solution is being calculated.

However, it should be noted that the classical Newton-Euler approach needs to be tailored to the kinematic requirements of each specific case, as well as it can only be applied to mechanical systems with open kinematic loops and for situations in which the task under analysis does not lead to loop closures. General multibody methodologies, in the other hand, can be applied to the simulation of general biomechanical models with open and closed loop topologies. However, considering that the solution for such type of approach is obtained for all anatomical segments at the same time, there is no assurance that errors in one kinematic chain do not propagate and interfere in the quality of the results of another chain. If both methodologies lead to similar results, it is demonstrated that such propagation of errors does not occurs in the multibody methodologies proposed here.

5.4.1 The Analytical Model

The analytical model used to calculate the reaction forces and moments at the joints of the subject, during the normal cadence stride period, is designated by classical Newton-Euler approach. This model uses the underlying kinematic structure presented in Figure 5.24. It consists in the three major anatomical segments of the right lower limb, i.e., foot, leg and thigh, interconnected by the ankle, knee and hip joints.

Figure 5.24: Kinematic structure of the analytical model. The results produced by this model are compared with the corresponding results produced by the multibody biomechanical model.

In order for the results to be comparable, it is necessary to construct equivalent biomechanical models, i.e., models with equivalent anthropometric, kinematic and kinetic input data. The anthropometric data that provides that equivalence is presented in Table 5.1 and it is obtained from the anthropometric data presented in Table 3.8 and from the anthropometric dimensions measured directly from the subject.

Table 5.1: Mass and inertial properties of rigid bodies used in the analytical model.

Body	Mass [kg]	Moments of Inertia		
		$I_{\xi\xi}$ [kg.m^2]	$I_{\eta\eta}$ [kg.m^2]	$I_{\zeta\zeta}$ [kg.m^2]
Foot	1.018	0.00155	0.00155	0.03095
Leg	1.562	0.00337	0.01187	0.00973
Thigh	4.241	0.00553	0.06147	0.03805
Total	70.250	–	–	–

Regarding the kinematic and dynamic input data, it is essential that both models use the same reconstructed and filtered positions of anatomical points as well as the same filtered ground reaction forces and respective application points.

The equations of motion, for an unconstrained rigid body in a three dimensional space, are written as (Meirovitch, 1970):

$$\begin{cases} \sum \mathbf{f} + m\mathbf{a}_G = m\mathbf{a} \\ \sum \mathbf{n} = \dot{\mathbf{h}}_G \end{cases} \tag{5.10}$$

where $\Sigma\mathbf{f}$ is the sum of all externally applied forces, m the mass of the rigid body, $\mathbf{a}$ the linear acceleration of its center-of-mass, $\mathbf{a}_G$ the gravitational field vector, $\Sigma\mathbf{n}$ the sum of the externally applied moments-of-force, and $\dot{\mathbf{h}}_G$ the first time derivative of the angular moment vector relative to the center-of-mass of the rigid body. For a rigid body in a three dimensional space, with the orientation of the local reference frame coincident with its principal axes of inertia, the $\dot{\mathbf{h}}_G$ vector is written as (Meirovitch, 1970):

$$\begin{cases} \dot{h}_\xi = I_\xi \dot{\omega}_\xi - (I_\eta - I_\zeta)\omega_\eta\omega_\zeta \\ \dot{h}_\eta = I_\eta \dot{\omega}_\eta - (I_\zeta - I_\xi)\omega_\zeta\omega_\xi \\ \dot{h}_\zeta = I_\zeta \dot{\omega}_\zeta - (I_\xi - I_\eta)\omega_\xi\omega_\eta \end{cases} \tag{5.11}$$

where I_ξ, I_η, I_ζ are the principal moments-of-inertia and ω_ξ, ω_η, ω_ζ and $\dot{\omega}_\xi, \dot{\omega}_\eta, \dot{\omega}_\zeta$ are the angular velocity and acceleration of the center-of-mass, respectively.

Free Body Diagram for the Foot

The equations of motion, expressed by Equation (5.10), are first applied to the foot segment. The free body diagram of this body is presented in Figure 5.25. The ground reaction force $\mathbf{f}_{\text{floor}}$ and its application point P are obtained by direct measurements in the force plate. Point A represents the joint center of the ankle joint its position is calculated from the digitized data. This data is also used to calculate the linear and angular acceleration vectors as well as the angular velocity vector for this rigid body, which are not represented in the diagram.

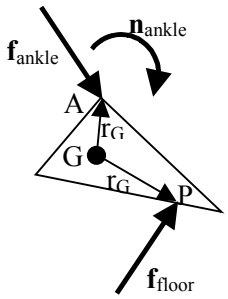

Figure 5.25: Free-body diagram of the rigid body describing the foot. The unknowns are the reaction force and the net moment-of-force at the joint center of the ankle joint, described by point *A*.

The only unknowns in this system are the reaction force at the ankle joint $\mathbf{f}_{ankle}$ and the net moment-of-force $\mathbf{n}_{ankle}$. These unknowns are obtained from the solution of the equations of motion (5.10) particularized for this rigid body and are written as follows:

$$\begin{cases} \mathbf{f}_{ankle} = m(\mathbf{a} - \mathbf{a}_G) - \mathbf{f}_{floor} \\ \mathbf{n}_{ankle} = \dot{\mathbf{h}}_G - \tilde{\mathbf{r}}_{GP}\mathbf{f}_{floor} - \tilde{\mathbf{r}}_{GA}\mathbf{f}_{ankle} \end{cases} \tag{5.12}$$

Free Body Diagram for the Leg

The free body diagram of the leg segment is represented in Figure 5.26. The reaction force and the moment at the ankle joint are now considered to be externally applied forces to this segment, i.e., it is assumed that Equation (5.12) has already been solved to obtain $\mathbf{f}_{ankle}$ and $\mathbf{n}_{ankle}$.

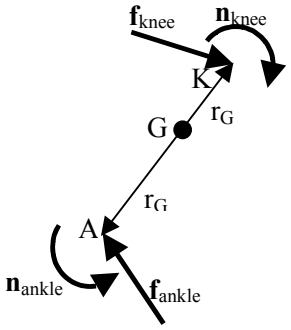

Figure 5.26: Free-body diagram of the rigid body describing the leg. The unknowns are the reaction force and the net moment-of-force at the joint center of the knee joint, described by point *K*.

The coordinates of point *K*, the angular velocities and the linear and angular acceleration vectors are calculated from the digitalized data.

Similar to the foot segment, the only unknowns are the reaction force $\mathbf{f}_{\text{knee}}$ and the net moment-of-force $\mathbf{n}_{\text{knee}}$, at the knee joint. These unknowns are calculated solving the equations of motion, expressed by Equation (5.10), particularized for this rigid body:

$$\begin{cases} \mathbf{f}_{knee} = m(\mathbf{a} - \mathbf{a}_G) + \mathbf{f}_{ankle} \\ \mathbf{n}_{knee} = \dot{\mathbf{h}}_G - \tilde{\mathbf{r}}_{GK}\mathbf{f}_{knee} + \tilde{\mathbf{r}}_{GA}\mathbf{f}_{ankle} + \mathbf{n}_{ankle} \end{cases} \tag{5.13}$$

Free Body Diagram for the Thigh

The procedure used to calculate the forces and moments on the thigh segment is quite similar to the one used in the leg segment. The free body diagram for this rigid body is depicted in Figure 5.27.

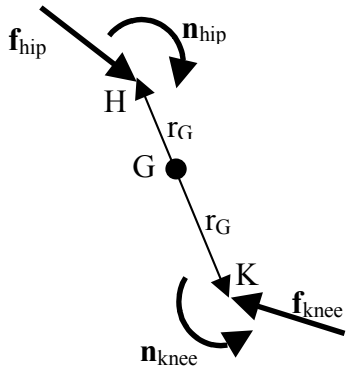

Figure 5.27: Free-body diagram of the rigid body describing the thigh. The unknowns are the reaction force and the net moment-of-force at the joint center of the hip joint, described by point *H*.

The reaction force and the net moment-of-force at the knee joint are now considered to be externally applied forces to this segment. Therefore, the unknowns are the reaction force $\mathbf{f}_{\text{hip}}$ and moment-of-force $\mathbf{n}_{\text{hip}}$ at the hip joint center, which are obtained from the solution of the equations of motion for this rigid body:

$$\begin{cases} \mathbf{f}_{hip} = m(\mathbf{a} - \mathbf{a}_G) + \mathbf{f}_{knee} \\ \mathbf{n}_{hip} = \dot{\mathbf{h}}_G - \tilde{\mathbf{r}}_{GH}\mathbf{f}_{hip} + \tilde{\mathbf{r}}_{GK}\mathbf{f}_{knee} + \mathbf{n}_{knee} \end{cases} \tag{5.14}$$

5.4.2 Application to the Human Gait Example

The analytical model presented before is applied to the inverse dynamic analysis of the normal cadence stride period that is being used throughout the chapter. The results concerning the moments-of-force occurring in the kinematic joints of the right ankle, knee and hip, are presented in Figure 5.28, Figure 5.29 and Figure 5.30, respectively.

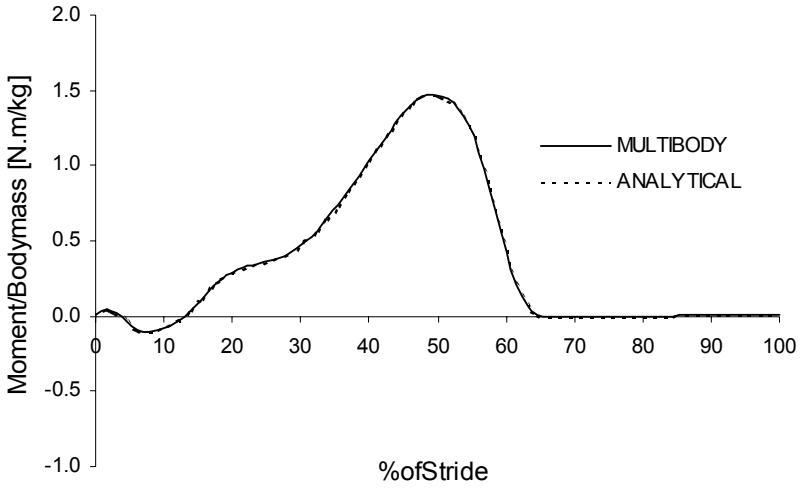

Figure 5.28: Comparison of results, produced for the moment of force at the Sagittal plane of the ankle joint, using two distinct methodologies: multibody analysis and classical Newton-Euler equations.

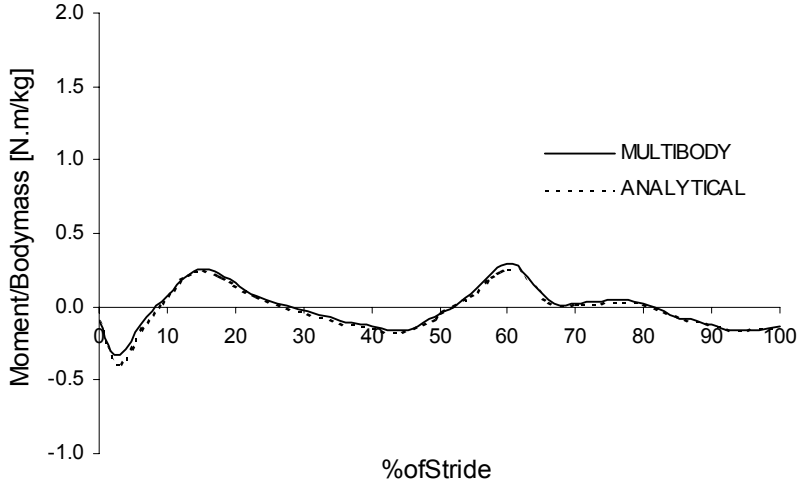

Figure 5.29: Comparison of results, produced for the moment of force at the Sagittal plane of the knee joint, using two distinct methodologies: multibody analysis and classical Newton-Euler equations.

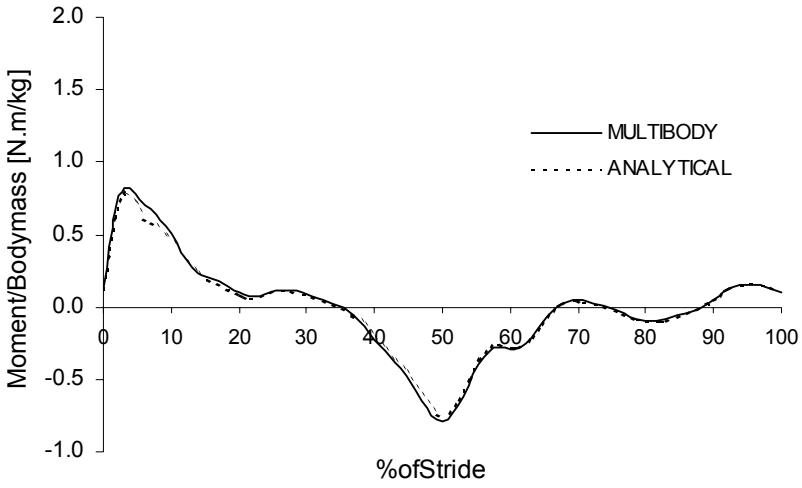

Figure 5.30: Comparison of results, produced for the moment of force at the Sagittal plane of the hip joint, using two distinct methodologies: multibody analysis and classical Newton-Euler equations.

From the analysis of the results, it can be concluded that very good correlation can be found between the two inverse dynamics analysis methods, i.e., for the same input data, the multibody methodology produces results similar to those obtained using the classical method.

5.4.3 Discussion

Two different inverse dynamic analysis procedures for the solution of the joint reaction forces and joint moments-of-force of the given biomechanical model have been compared. For the multibody methodology, the inverse dynamic problem is solved for the whole biomechanical model with the equations of motion being assembled in a systematic way and solved as a whole system. For the classical Newton-Euler procedure, the balance of forces and moments is performed sequentially and independently at each individual biomechanical segment. The comparison of the results obtained for both methods showed a very good correlation, which allows to conclude that the proposed multibody methodology is producing accurate results. Moreover, these preliminary results suggest that the general multibody formulation is able to effectively shield any error from spreading from a given kinematic chain to another. However, with respect to this issue, in the forthcoming section a more systematic approach is performed that allows for more sound conclusions to be drawn.

5.5 Sensitivity Analysis of Perturbed Input Data

The objective of this section is to evaluate the effects that perturbed input data have on the results produced by the inverse dynamic analysis, i.e., to investigate how sensitive the reaction forces and net-moments-of-force, calculated in the inverse dynamic analysis, are to the numerical inaccuracies generated during the kinematic and dynamic data reconstruction processes. For this purpose, the input data of the normal cadence stride period, which has been used throughout this chapter to demonstrate the application of several methodologies, is submitted to a sensitivity analysis in which several input parameters, identified with common sources of errors, are perturbed. To ensure that the numerical evaluation of the sensitivity of the gait results is properly done, different levels of perturbation are used to calculate the sensitivities.

5.5.1 Sensitivity Analysis

In order to evaluate the sensitivity of the multibody methodology to small perturbations introduced in the input data set, each parameter is independently perturbed and a new analysis is performed to evaluate the sensitivity of the results to that perturbation. The perturbed input data parameters are: head, right hand, lower torso, upper and lower leg masses, the Cartesian coordinates of the anatomical points at the top of the head and at the knee, the components of the ground reaction force for the right foot and the coordinates of the point of application of the ground reaction force in the right foot.

Two levels of perturbations are tested for each parameter to ensure the consistency of the results. The mass parameters are perturbed by 0.01kg and by 1.0kg, the length parameters are perturbed by 0.01m and by 0.1m, while the force parameters are perturbed by 1N and 9.8N. It should be noted at this point that errors of 1.0 kg in the anatomical segments masses or 0.1 m in the length parameters are not expected. Therefore, this level of perturbations must be understood as a form to ensure that the numerical evaluation of the sensitivities is reliable by being independent of the amount of perturbation actually used.

The sensitivities are expressed as the first derivative of a system response with respect to the perturbed parameter (Haftka and Gurdal, 1992). In this work, the moments-of-force in the joints of the biomechanical model are the system response, while the perturbed parameters are those described before. The first derivative is calculated using a finite-difference approximation (Haftka and Gurdal, 1992), written as:

$$\frac{\partial m}{\partial a} = \frac{m_P - m_{NP}}{a_P - a_{NP}} \tag{5.15}$$

where $\partial m/\partial a$ is the sensitivity of the moment m to the anatomical parameter a, m_P and m_{NP} are the perturbed and the non-perturbed response moments respectively and a_P and a_{NP} are the perturbed and the non-perturbed anatomical parameters respectively.

5.5.2 Sensitivity to a Perturbation in a Segment Mass

Perturbations of 0.01kg and 1.0kg are introduced in the body mass of the head (body 33), right hand (body 14) and lower torso (body 7). The sensitivities of the moments-of-force to these perturbations are calculated for every joint of the biomechanical model during the stride period. In Figure 5.7, the degree-of-freedom/joint numbers are presented for the whole biomechanical model. The curves of the non-zero sensitivities are plotted in Figure 5.31 and Figure 5.32. The labels on the charts represent the degree-of-freedom/joint number in which non-zero sensitivity occurs.

The results show that all the non-zero sensitivities are associated with kinematic joints located along the bold line of the biomechanical model shown next to each figure. The net-moments of force in all the other biomechanical joints are not sensitive to the perturbations introduced in the body mass of the selected anatomical segments.

The results show that with the exception of the lower torso, a perturbation introduced in a rigid body mass only affects the net moments-of-force directly associated with the kinematic branch to which the perturbed body belongs. This suggests that net moments-of-force occurring at kinematic joints belonging to other kinematic chains are shielded from perturbations committed in a particular branch of the kinematic structure. Therefore, a

variation in the head or hand mass does not affect the moments calculated at the ankle, knee or hip, because these joints belong to a different kinematic branch. Furthermore, the results also show that perturbations in the mass of the lower torso do not affect the net moments of force at any other biomechanical joint.

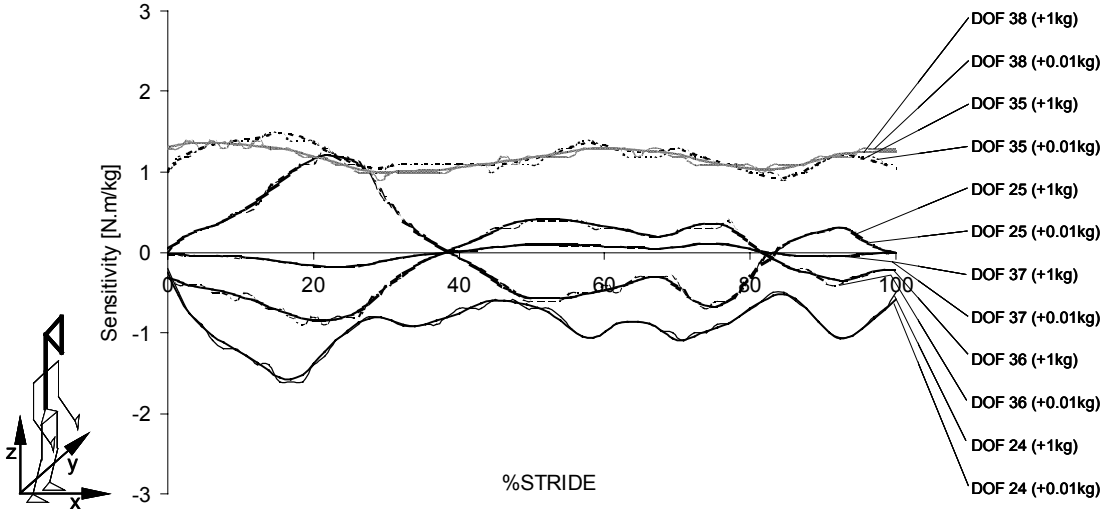

Figure 5.31:Sensitivity to a 0.01 kg and 1 kg perturbation of the head mass.

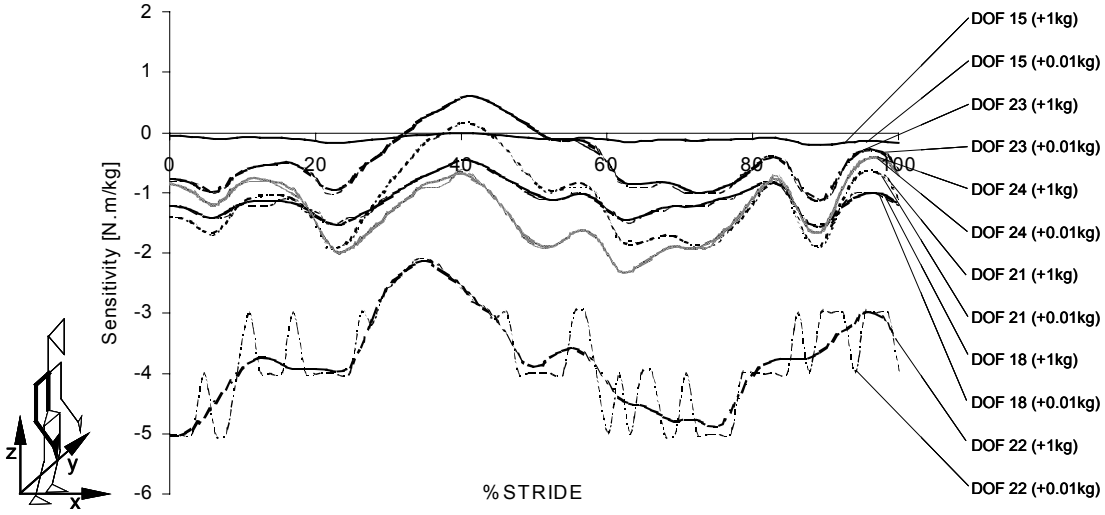

Figure 5.32:Sensitivity to a 0.01 kg and 1 kg perturbation of the right hand mass.

The sensitivities to 0.01 kg and 1 kg perturbations are very similar, showing that the finite differences are good approximations of the first derivative of the system response. Maximum

absolute values of approximately 2 Nm/kg and 5 Nm/kg are found for the sensitivity of the moments to changes in the head and hand mass respectively. This means that if an error of a 1 kg is made in the body mass of a rigid body a difference of less than 10 Nm is expected in the response of the system in terms of the moments-of-force in the joints. This indicates that the results, produced by the multibody methodology, are not very sensitive to small errors made in the determination of the mass of the anatomical segments.

5.5.3 Sensitivity to a Perturbation in the Coordinates of an Anatomical Point

Perturbations of 1 cm and 1 dm are introduced in the reconstructed coordinates of the anatomical point 23, located in the top of the head. The sensitivities of the net moments-of-force in all anatomical joints are calculated. The non-zero sensitivities are presented in Figure 5.33, Figure 5.34 and Figure 5.35.

The analysis of the results shows that a perturbation in the coordinates of a digitized point only affects the moments of the degrees-of-freedom directly associated with the kinematic branch to which the perturbed point belongs. Once again, the results show that the developed methodology does not propagate digitization errors outside the kinematic chain where they occur.

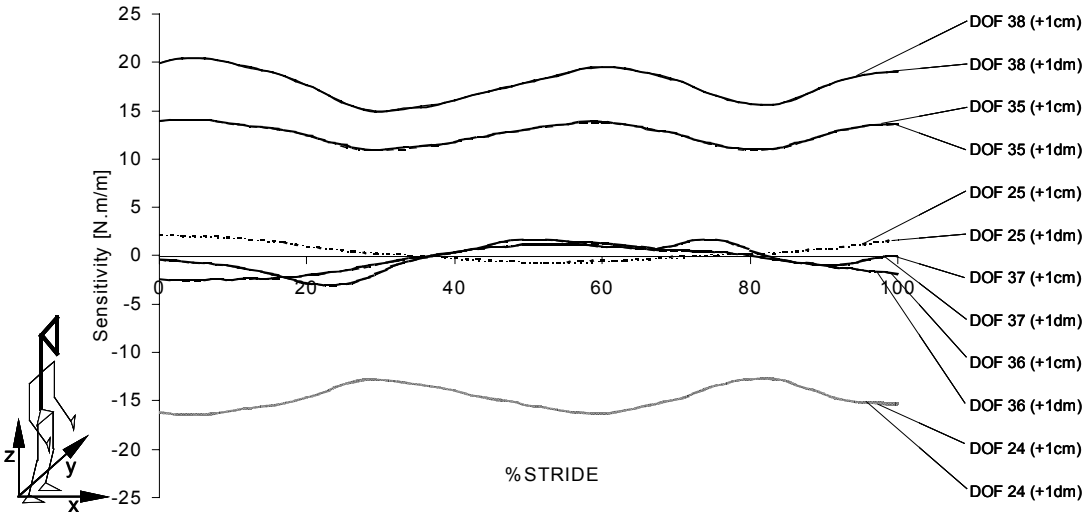

Figure 5.33:Sensitivity to 1 cm and 1 dm perturbation of the X coordinate of point 23.

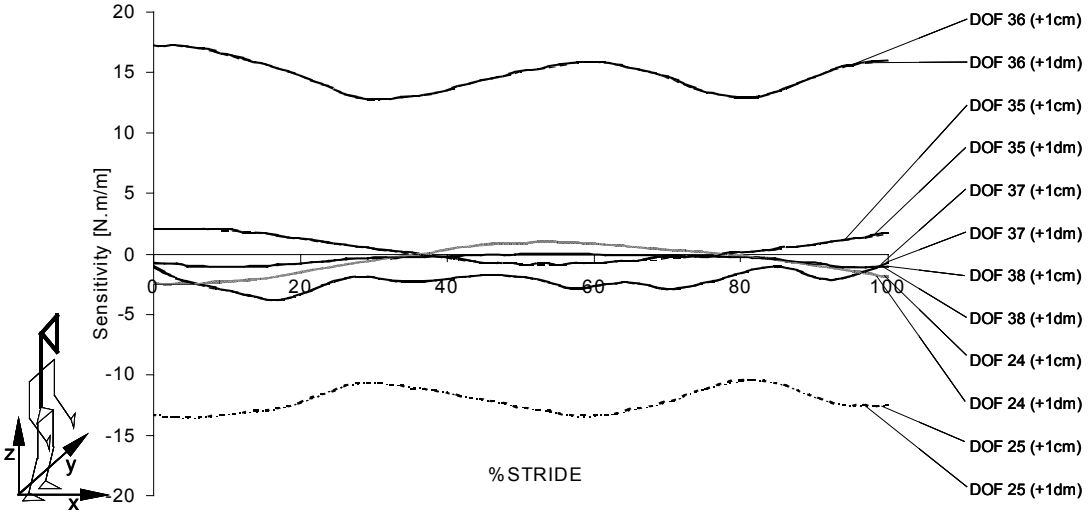

Figure 5.34:Sensitivity to 1 cm and 1 dm perturbation of the Y coordinate of point 23.

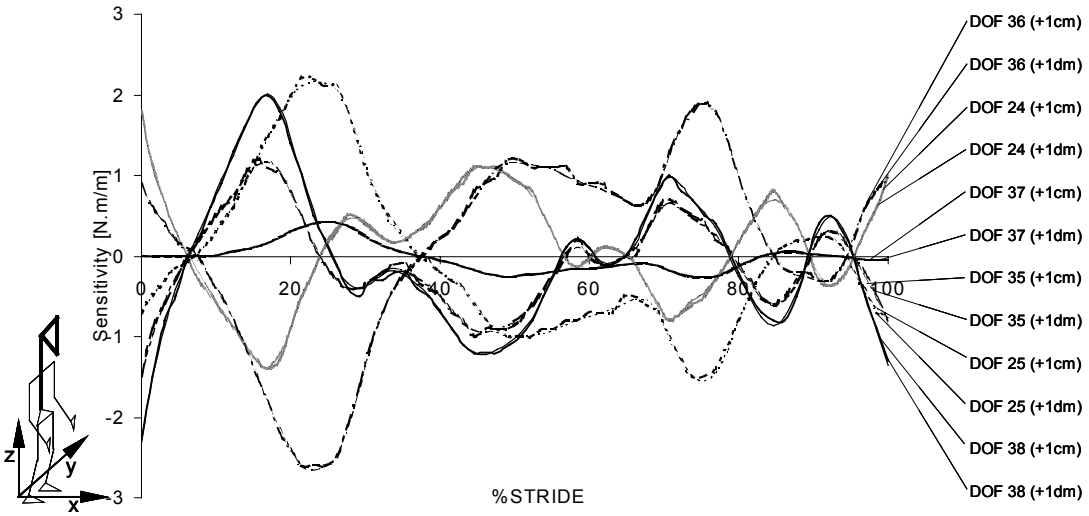

Figure 5.35:Sensitivity to 1 cm and 1 dm perturbation of the Z coordinate of point 23.

The sensitivity curves for 1 cm and 1 dm perturbations are similar indicating that the finite differences produce good results. Maximum absolute values of approximately 22 Nm/m, 18 Nm/m and 3 Nm/m are obtained for the sensitivities when perturbing the X, Y and Z point coordinates respectively. This result is directly associated with the typical errors made in the digitization process and shows that the results produced by the multibody methodology are not very sensitive to small errors committed during this process. For the case study presented,

a digitization error of 1 cm produces error that is less then 0.3 Nm in the response of the system.

5.5.4 Sensitivity to a Perturbation on the Components of an External Force

Perturbations of 1 N and 9.8 N are introduced in the components of the ground reaction force applied in the right foot. The sensitivities of the moments-of-force to this perturbation are calculated and presented in Figure 5.36, Figure 5.37 and Figure 5.38. A perturbation in the components of an externally applied force only affects the moments in the joints that are directly associated with the kinematic branch to which the perturbed force is applied. Maximum absolute values of approximately 0.8 Nm/N, 0.8 Nm/N and 0.7 Nm/N are obtained respectively when perturbing the X, Y and Z components of the external force.

These results reveal a measurable sensitivity to errors committed in the measurement of an external applied force since a small variation of 1 N, which can easily be committed by a force measuring device, can produce variations close to 1 Nm in the net-moments of force for the hip joint. According to Figure 5.29, the hip moment is within the range of 56 to -50 Nm. Therefore, for 10% of the stride the moment error due to a variation of 1 N of the ground reaction force is about 2% while for 20-30% of the stride such error is larger than 10%.

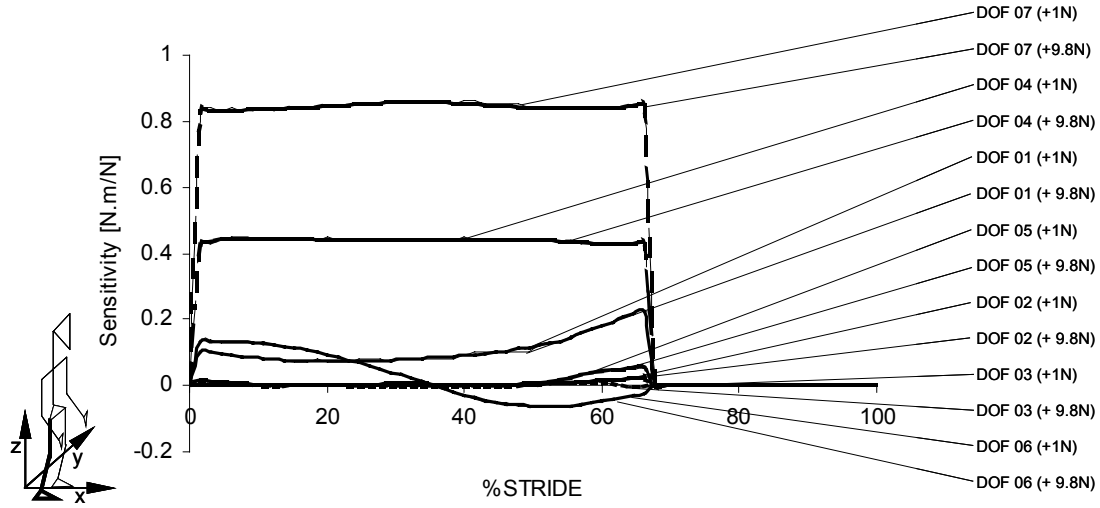

Figure 5.36: Sensitivity to 1 N and 9.8 N perturbation of the X component of the ground reaction force.

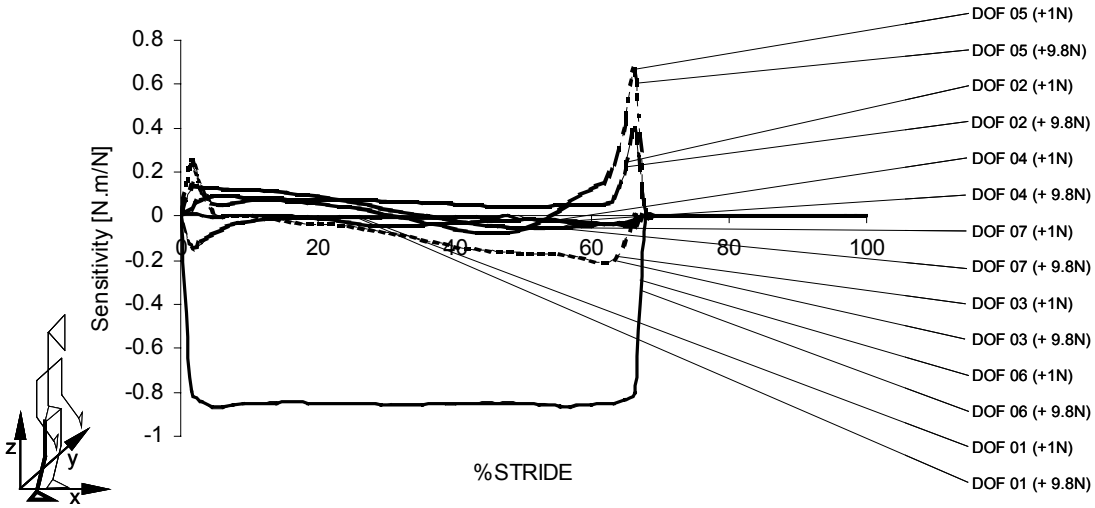

Figure 5.37: Sensitivity to 1 N and 9.8 N perturbation of the Y component of the ground reaction force.

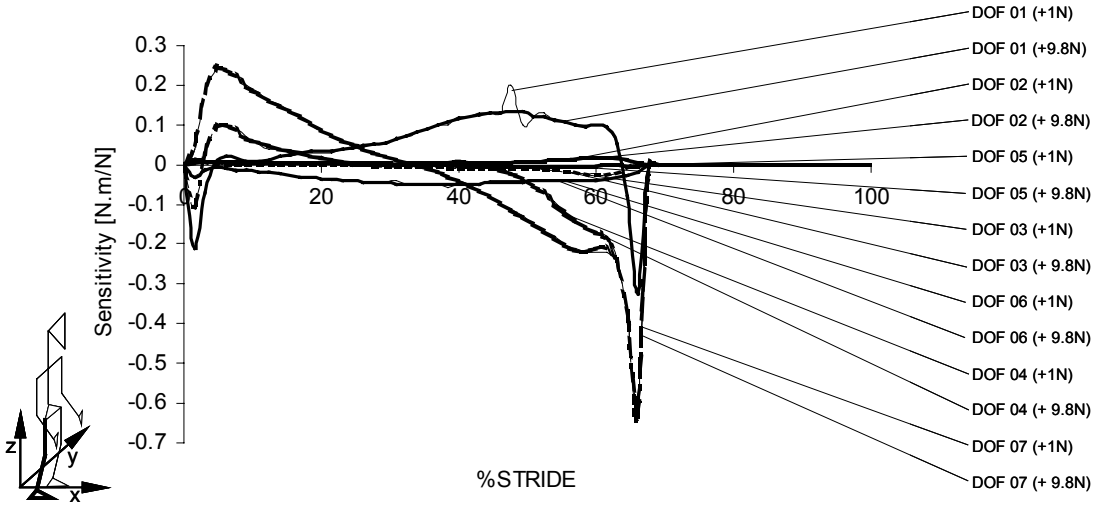

Figure 5.38: Sensitivity to 1 N and 9.8 N perturbation of the Z coordinate of the ground reaction forces.

5.5.5 Sensitivity to a Perturbation of the Application Point of an External Force

Perturbations of 1 cm and 1 m are introduced in the application point coordinates of the ground reaction force applied on the right foot. The sensitivities of the moments-of-force in the joints of the biomechanical model are calculated and presented in Figure 5.39, Figure 5.40

and Figure 5.41. Again, it must be emphasized the use of a perturbation of 1 m is intended only to ensure the consistency of the sensitivities. This level of uncertainties in the location of the point of application of the external forces it is not physically possible.

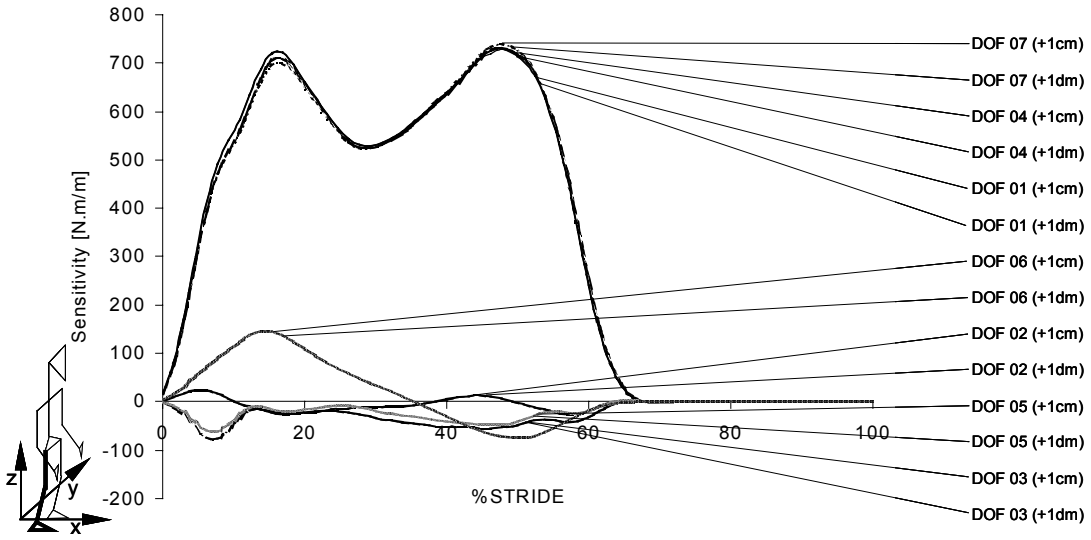

Figure 5.39: Sensitivity to 1 cm and 1 dm perturbation of the X coordinate of the application point.

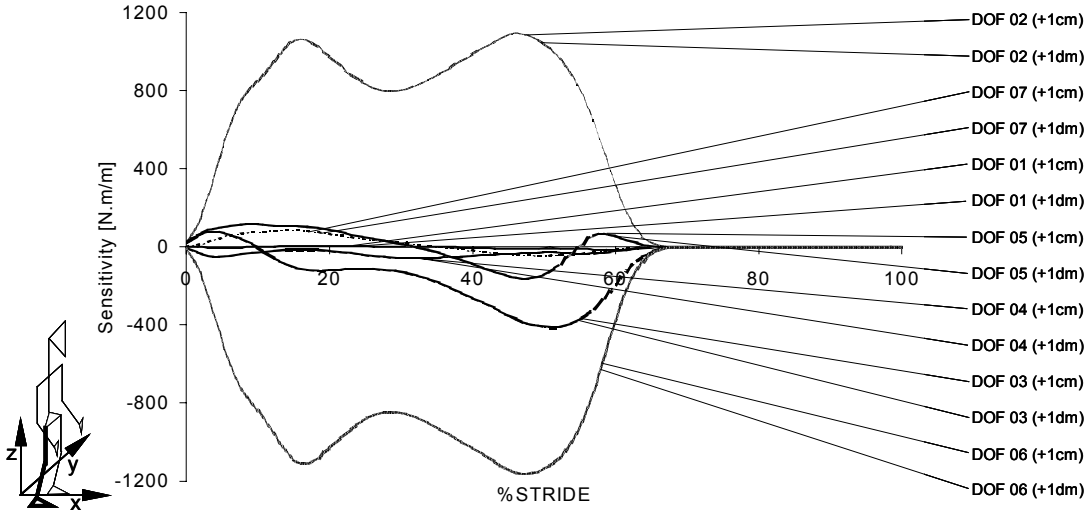

Figure 5.40: Sensitivity to 1 cm and 1 dm perturbation of the Y coordinate of the application point.

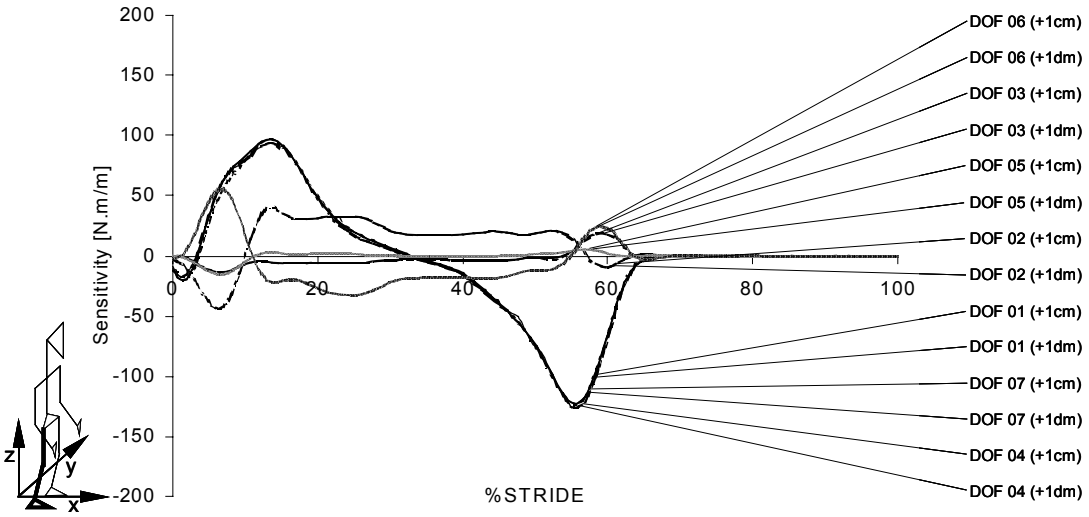

Figure 5.41: Sensitivity to 1 cm and 1 dm perturbation of the Z coordinate of the application point.

The results show that a perturbation in the application point coordinates of an external applied force only affects the moments in the degrees-of-freedom directly associated with the kinematic branch to which the perturbed contact point belongs. Maximum absolute values of approximately 750 Nm/m, 1100 Nm/m and 140 Nm/m are found when perturbing respectively the X, Y and Z coordinates of this point.

It is observed that the ankle, knee and hip joint moments-of-force in the sagittal plane, represented by the degrees-of-freedom 01, 04 and 07 respectively, are extremely sensitive to errors in the calculation of the coordinates of the application point of an externally applied force, especially for its X coordinate. The ankle and hip joint moments-of-force in the frontal plane, represented by degrees-of-freedom 02 and 06 respectively, are also sensitive to the precision of the calculation of the Y coordinate of the force application point. Due to the model used for the knee joint, i.e. a revolute joint, it is expected that the joint reaction moment in the knee joint presents a sensitivity similar to those of the ankle and hip net moments-of-force.

In order to present a quantitative measure for the influence of the errors made in the location of the external forces application points, the variation of 1 mm in the X coordinate of the contact point can produce an error of 0.5-0.8 Nm for the ankle and hip net moments-of-

force in the sagittal plane, throughout most of the stride period. Considering the ankle joint, that exhibits a maximum moment of 100 Nm for a 50%ile male, this error is less than 1% for the maximum moment. However, up to 20% of the stride period the net moment-of-force is within 0 and 17 Nm. Here, the moment error due to a 1 mm change of the force application point is higher than 6%. The relation between the errors in the net moments associated to the knee and hip joints and the precision in the acquisition of the location of the point of application of the external forces is similar to that of the hip moment for the first 20% of the stride period. Considering that, in this type of analysis, the calculation of the application point position is very error prone, it is expected that the results can be greatly affected by the precision with which this parameter is estimated.

5.5.6 Sensitivity to a Perturbation of the Coordinates of the Knee Joint

Perturbations of 1 cm and 1 mm are introduced in the reconstructed position of the knee anatomical point. The sensitivities of the moments-of-force in the joints of the biomechanical model are calculated and presented in Figure 5.42, Figure 5.43 and Figure 5.44. The numerical sensitivities are evaluated with 1 cm and 1 mm perturbations because the use of larger perturbations in the knee joint location would lead to unacceptable positions for the legs that would not be compatible with the motion of human subject.

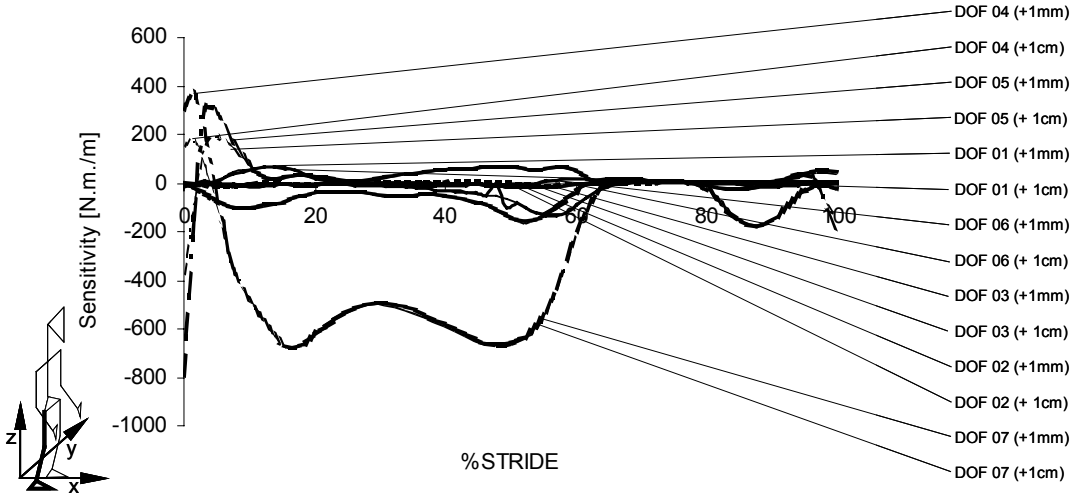

Figure 5.42: Sensitivity to 1 cm and 1 mm perturbation of the X coordinate of the knee anatomical point.

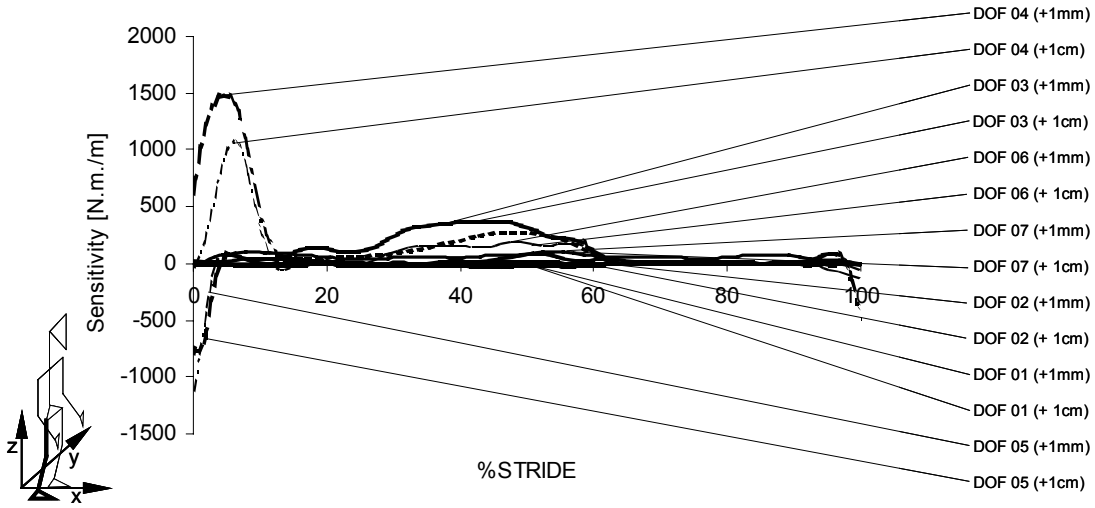

Figure 5.43: Sensitivity to 1 cm and 1 mm perturbation of the Y coordinate of the knee anatomical point.

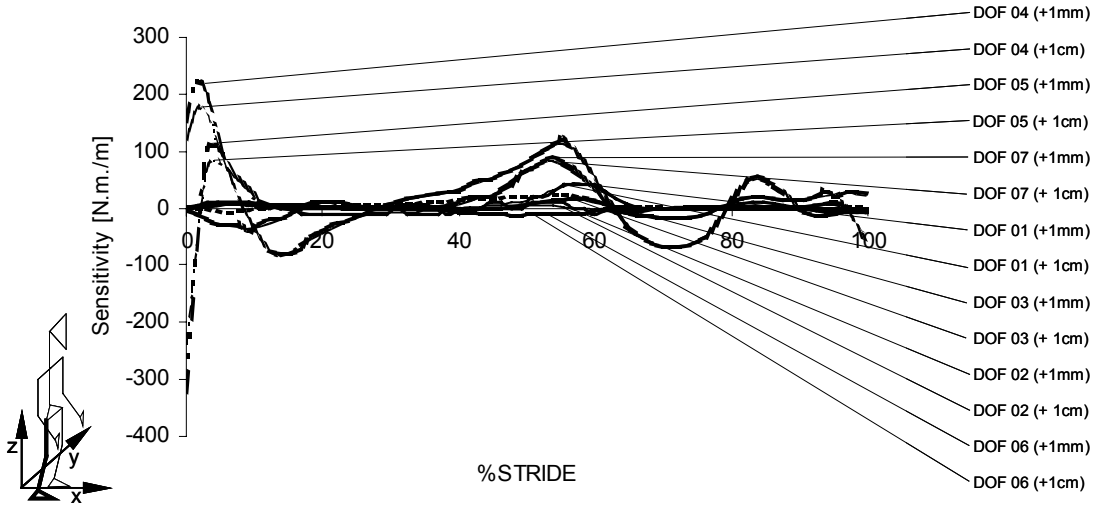

Figure 5.44: Sensitivity to 1 cm and 1 mm perturbation of the Z coordinate of the knee anatomical point.

Maximum sensitivities of 400 Nm/m, 1500 Nm/m and 200 Nm/m are obtained for the knee joint moment-of-force for perturbations of the X, Y and Z coordinates of the knee anatomical point respectively. The sensitivities observed for the knee anatomical point are similar to those obtained for the location of the point of application of the external forces. Therefore, the discussion carried there is still valid for these sensitivities.

5.5.7 Sensitivity to a Perturbation of the masses of the leg anatomical segments

Perturbations of 0.01kg and 1.0kg are introduced in the body mass of the upper leg and lower leg. The sensitivities that are not null are plotted in Figure 5.45 and Figure 5.46, respectively.

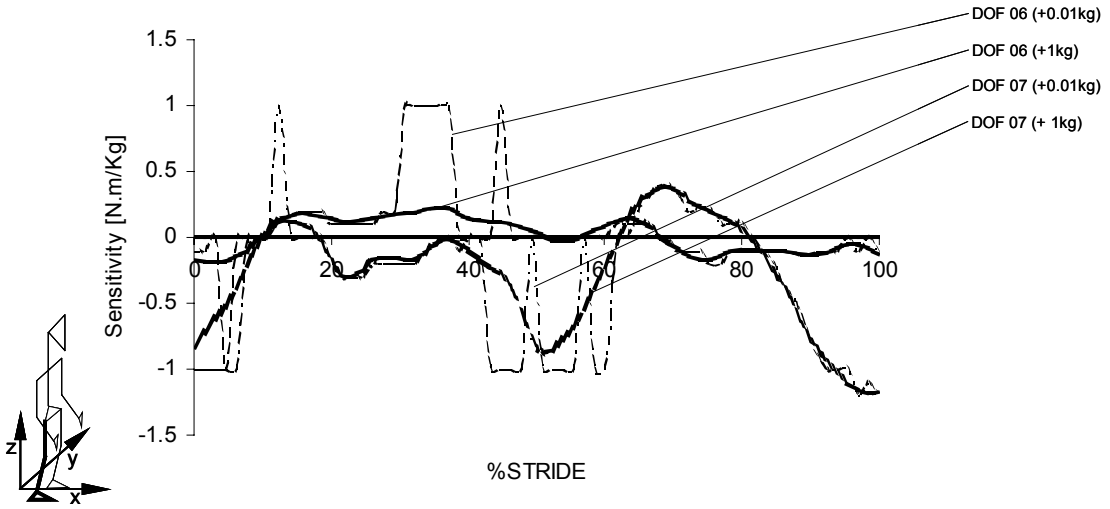

Figure 5.45:Sensitivity to 0.01 kg and 1 kg perturbation of the upper leg mass.

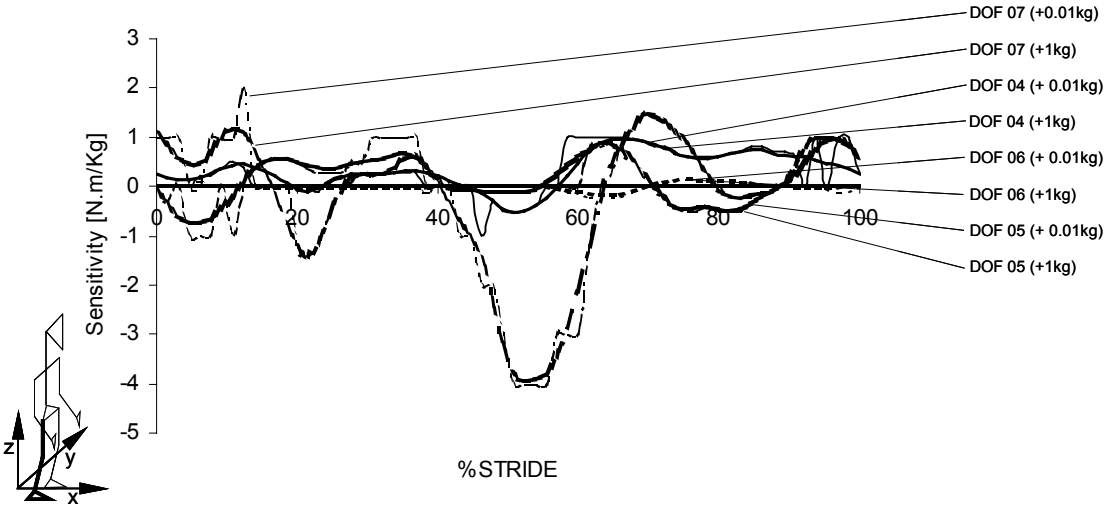

Figure 5.46:Sensitivity to 0.01 kg and 1 kg perturbation of the lower leg mass.

It is observed that the net moments-of-force present a low sensitivity to uncertainties in the evaluation of the legs anatomical segment masses. The hip moment-of-force, in the sagittal plane, has a maximum sensitivity of 4 Nm/kg with respect to the lower leg mass. Based on

Figure 5.29, the hip moment for a 70 kg male is 50 Nm, for 50% of the stride period. Therefore, an error of 0.1 kg in the lower leg mass corresponds to a variation of 0.4 Nm in that moment, which is an error smaller than 1%. This result is indicative of the differences to be expected in gait analysis due to the use of different tables for the anthropometric data. The sensitivities presented in Figure 5.45 and Figure 5.46 show that the gait results, in terms of the joint moments-of-force, are not very sensitive to these different anthropometric tables.

5.5.8 Discussion

In the present section, a sensitivity analysis was carried out to study the importance of the input data accuracy on the quality of the results produced by the inverse dynamic analysis, for a normal cadence stride period. The sensitivity calculation of the system response due to perturbations introduced in the input data reveals that only the net-moments of force in the joints belonging to the same kinematic chain of the perturbed parameter are affected. This shows that the methods used in the inverse dynamic analysis shield the results in a particular biomechanical chain from perturbations occurring in other kinematic branches of the biomechanical model. It is not expected that the lack of precision in the reconstruction of the head spatial motion or in the definition of the inertia properties of an arm, will affect the evaluation of the forces and moments at the knee joints, for example.

It was shown that the inverse dynamic analysis results are very sensitive to errors made in the acquisition process of the externally applied forces and their application points. Moreover, the quality of the gait analysis is also dependent on the precision of the spatial reconstruction of the anatomical point positions of the anatomical segments of the kinematic chains to which external forces are applied. It was observed that when there are no external forces, for instance during the aerial trajectory of a leg, the sensitivity of the net moments-of-force to imprecision in the anatomical points' positions becomes meaningless. It was demonstrated that the biomechanical model response is comparatively much less sensitive to errors in the estimation of the mass of the anatomical segments, even those that belong to kinematic chains that have external forces applied. This indicates that the sensitivity of the gait analysis results to different tables of anthropometric data is relatively low.

In conclusion, major improvements in the quality of gait analysis results can be obtained by: improving the evaluation of the points of application of external forces over the anatomical segments, i.e. the ground reaction forces; increasing the precision of the spatial reconstruction process of the anatomical points associated to the anatomical segments included in the kinematic chains where external forces are applied; improving the force acquisition process, including the synchronization between kinetic and kinematic data. The improvement of the precision with which other anatomical parameters are obtained, such as the spatial position of joint anatomical points in kinematic chains in which no external forces are applied, or of anthropometric parameters such as the anatomical segments masses, play a relatively smaller role in the improvement of the quality of the gait results.

5.6 Conclusions

In this chapter, the most common sources of uncertainties that affect the input data of an inverse dynamic analysis were identified and several numerical techniques were suggested that contribute significantly to reduce this type of problems, at the same time they increase the accuracy and quality of the outcome of the analysis. The proposed numerical techniques include: the DLT technique that is used to reconstruct the three-dimensional motion of the biomechanical system from two dimensional information; the Butterworth 2^{nd} order low pass filtering technique that plays an essential role in the quality of the results, reducing the high frequency noise levels and smoothing the trajectory curves of the anatomical points; and the kinematic consistency technique that is used to ensure that the kinematic data is coherent with the kinematics of the biomechanical model at any instant of the analysis.

Finally, a thorough analysis of the sensitivity of the results to perturbed input data is performed. In this analysis, several input parameters, which are usually associated with the most common sources of input errors, were perturbed in an independent way and the respective sensitivity of the results to these perturbed data were estimated. It was shown that the best way to improve the quality of the inverse dynamics analysis results is improving the quality of the kinematic data acquisition, especially in kinematic chains where external forces are applied.

Chapter 6

Inverse Dynamic Analysis of Indeterminate Biomechanical Systems

In the previous chapter, it has been demonstrated how multibody methodologies can be applied to the inverse dynamics analysis of determinate biomechanical systems, providing a way to calculate, without using invasive force measuring devices, the internal forces developed by a subject during the execution of a specified task. It was seen that when the aim of the analysis is to calculate exclusively reaction forces and net moments-of-force in a particular joint or set of joints, only joint actuators need to be introduced and the solution of the inverse dynamics problem is unique. However, when the evaluation of the muscle forces is necessary, the muscle apparatus under analysis needs to be modeled and that requires the introduction of several additional muscle actuators in the biomechanical model. The introduction of these additional actuators in the model, generates an indeterminate mechanical system with a redundant nature, in which there are more unknowns to calculate than available equations of motion.

From the physiological point of view, this indeterminacy is denoted by the fact that different muscle activation patterns can generate the same posture or movement of the human

body, being the selection and activation of the most appropriate set of muscles to carry out the specified task performed by the central nervous system, according to several physiological criteria. From the mathematical point of view, indeterminate biomechanical problems can be resolved through the use of proper optimization tools. These tools consider that muscle forces are generated according to the minimization of some performance criteria – also designated by cost functions – that represent the decisions taken by the central nervous system when executing the prescribed task. The optimal solution, calculated by the optimizer, not only minimizes the prescribed performance criteria but it also satisfies the equations of motion of the biomechanical system, i.e., the optimal solution must reproduce the observed motion, generating intersegmental resultant moments that are equal to the ones calculated as solution of the determinate inverse dynamics problem.

In the present chapter, the major issues involving the construction and solution of indeterminate biomechanical problems and the subsequent calculation of the redundant muscle forces are addressed. For that purpose, a brief review of the muscle anatomy and physiology is performed. Afterwards, the 'redundant problem in biomechanics' is identified and the concept of muscle actuator is introduced in the framework of the proposed multibody formulation. To each muscle actuator is associated a muscle model that simulates the muscle activation-contraction dynamics (Hatze, 1984; Kaplan, 2000; Zajac, 1989). In the present work, a Hill type muscle model is applied, being the force produced by the muscle contractile element calculated as a function of the muscle activation, maximum isometric peak force, muscle length and muscle rate of shortening. Using this constitutive law, the equations of motion of the biomechanical system and the performance criteria used in de optimization procedure become expressed in terms of muscle activations instead of muscle forces. This fact brings some advantages to the optimization procedure since the design variables, associated with the muscles, are now bounded between 0 and 1.

Regarding the optimization process, several optimization tools are presented. The optimization problem is stated in the framework of multibody dynamics, with the objective of its subsequent application to the solution of indeterminate biomechanical models with redundant muscle action. Several different performance criteria are presented and their

application to the calculation of the muscle forces developed in the locomotor apparatus of a subject during a normal cadence stride period is analyzed.

6.1 The 'Redundant Problem in Biomechanics'

In complex biomechanical systems such as the human body, almost every joint is crossed by several muscles or muscle groups. This means that different muscle activation patterns can generate forces that produce the same net moments-of-force at the joints and, therefore, a same posture or movement. It is the central nervous system that selects and activates the set of muscles that best fulfill specific physiological criteria, depending on the task being performed and/or the objectives to be achieved.

Historically termed 'the redundant problem in biomechanics' (Yamaguchi *et al.*, 1995), this redundancy results, from a mathematical point of view, from the fact that the number of load-transmitting elements at a joint usually exceeds the number of available equilibrium equations and consequently a unique solution for the analytical determination of those forces cannot be obtained (Collins, 1995). Optimization techniques are applied to resolve the indeterminate problem and to choose, from an infinite set of solutions, the optimal solution that minimizes one or more cost functions. The cost functions are mathematical expressions that simulate physiological principles used by the central nervous system to select the muscles to recruit for a given activity. Those physiological principles or criteria are, for instance, the minimization of muscle forces, muscle stresses, reaction forces, energy or even combinations of these.

6.2 Skeletal Muscle Anatomy and Physiology

In this section a brief introduction to the skeletal muscle anatomy and physiology is presented with the purpose of providing background to support the introduction of the muscle's mathematical model. It should be noted that here only the basic concepts regarding the shape, structure and function of the muscle are addressed. Muscle anatomy and muscle physiology involve many other important issues that are not discussed in this section although they can be found in detail in other references (Lieber, 1992; Schneck, 1992; Winters and Woo, 1990).

6.2.1 Basic Concepts of Skeletal Muscle Anatomy

Skeletal muscles are organs made of excitable tissue, whose contractible and elastic properties are responsible for the production of movement. Skeletal muscles are attached to the skeletal bones by tendons, which are highly flexible cord-like structures made of a fibrous tissue called collagen. The collagen fibers are packed side-to-side along the direction of the muscular action, providing the tendon with a high resistance to traction loads.

Skeletal muscles have a very complex, but at the same time, organized structure. As illustrated in Figure 6.1, the skeletal muscle can be viewed as a set of structural units of decreasing size, which are packed inside one another in a well-defined hierarchy (Nigg and Herzog, 1995). The outer cover of the muscle is called epimysium and is made of dense connective tissue. Underneath the epimysium cover are the blood vessels (not illustrated) and the many fascicles. A fascicle consists on a set of muscle fibers – or muscle cells – packed side-by-side. Each fascicle is covered and connected to the next one by a fibrous tissue, made of collagen (a protein substance), called perimysium.

The muscle fibers are the essence of the muscle, i.e., it is at their level that the actual contraction occurs. Muscle fibers are thin and elongated individual cells that are held together by a connective tissue, similar to the perimysium but more fluid and gelatinous, called endomysium. Each muscle fiber is surrounded by a thin and delicate cell membrane called sarcolemma that, among other things, is responsible to maintain an electrical membrane potential. Inside each muscle fiber there are many contractile filaments, called myofibrils, arranged in parallel and running its entire length. It may exist thousands of these filaments in a single muscle cell, representing approximately 80% of its volume.

The myofibrils filaments are composed of smaller contractile units called sarcomeres, which are arranged in series (Lieber, 1992). Sarcomeres are the functional unit of the muscle contraction, which means that the total distance of the myofibrillar shortening, due to this series arrangement, is equal to the sum of the individual shortening distance of each sarcomere (Lieber, 1992). As represented in Figure 6.1, the sarcomere has a typical striated pattern that gave rise to another possible term for skeletal muscle which is striated muscle.

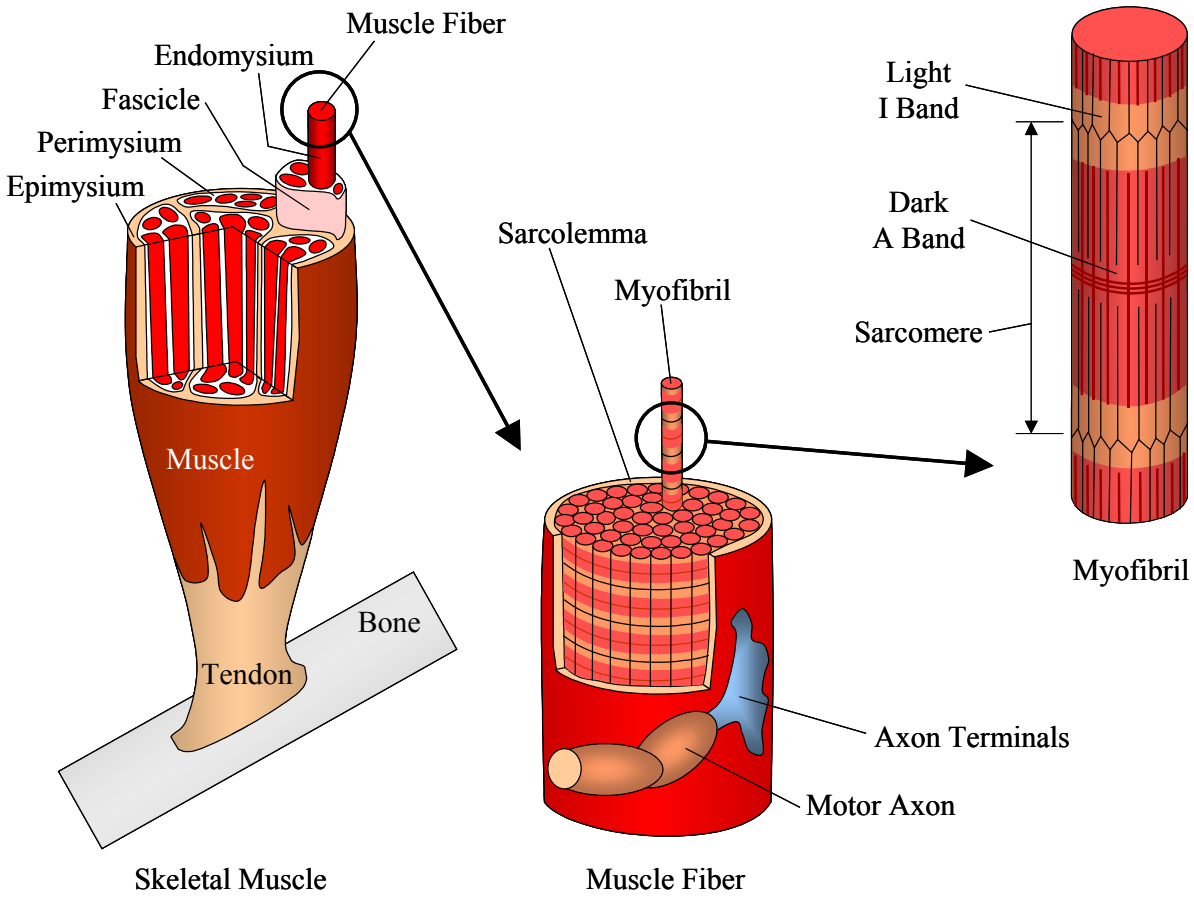

Figure 6.1: Skeletal muscle structure. Skeletal muscles have a very complex, yet, well organized anatomical structure. The skeletal muscle consists in a set of fascicles that are bundle together by connective tissue (epimysium). Inside each fascicle are the muscle fibers or muscle cells, where actual contraction occurs. Muscle fibers are packed together in each fascicle by another connective tissue (perimysium). Inside each muscle fiber there are hundreds to thousands of myofibril filaments packed in parallel by another connective tissue (endomysium). Each myofibril filament consists in a string of smaller contractile units called sarcomeres, arranged in series. Sarcomeres, with their striated appearance, are the fundamental unit of muscle contraction.

The anatomy of the sarcomere is made of two distinct types of protein filaments, as it is schematically represented in Figure 6.2. These are the thick myosin filaments and the thin actin filaments. In the thick myosin filaments several globular heads can be identified. These myosin heads are also designated by cross bridges because during the contraction period they establish the connection between the thick myosin filament and the thin actin filament.

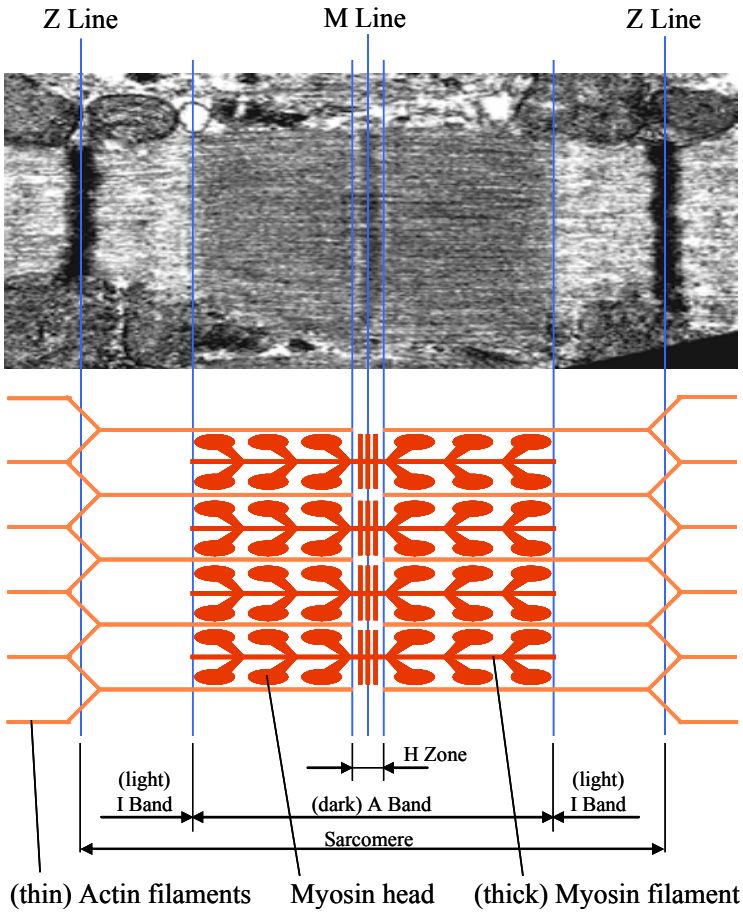

Figure 6.2: The sarcomere or the fundamental unit of muscle contraction. In the top of this figure an image of a real sarcomere obtained in a light microscope. Below the real image, the sliding-filament representation of the sarcomere is presented. Using the proposed parallel representation of both the real and the schematic sarcomere, it is clear the identification of the most relevant regions of the fundamental unit of the skeletal muscle.

Several important regions can be identified in a sarcomere: the Z line (from the German 'zwitter' that means 'between') – or the Z disc – is a protein sheet to which are attached or anchored the thin actin filaments of one sarcomere and the thin actin filaments of the next adjacent sarcomere. The distance between two Z lines provides the sarcomere length. To the dark region of the sarcomere, containing the myosin filaments is given the name of A-band (from the word 'anisotropic'). To the light region of the sarcomere, containing only thin actin filaments and divided in the middle by the Z-line, is given the name of I-band (from the word 'isotropic'). The H-zone (from the German 'helle' that means 'light') is defined as the region

of the sarcomere where there is no actin-myosin overlapping, while to the dark area, in the middle of the A-band is called the M-line. The M line contains the protein strands that hold together the several myosin filaments (Lieber, 1992; Nigg and Herzog, 1995).

During contraction, thick myosin and thin actin filaments are believed to remain at a constant length (Nigg and Herzog, 1995). Thus, the remarkable ability of muscles to shorten their length is associated to relative motion between the myofilaments, i.e., during contraction, the thin actin filaments slide over the thick actin filaments, causing the shortening of the I-band and H-zone, while the length of the A-band remains constant.

6.2.2 Basic Concepts of Skeletal Muscle Physiology

In the previous section, the fundamental aspects regarding the shape and structure of the skeletal muscle were presented. It was seen that muscle shortening is directly related with the shortening of the sarcomere and with the sliding of the thin actin filaments over the thick myosin filaments. However, the excitation process and the mechanism inherent to muscle contraction were not described. In the present section the basic physiological concepts regarding the activation and contraction sequence of the skeletal muscle are presented.

The contraction of skeletal muscles is voluntary, i.e., is controlled by the central nervous system through electrochemical stimuli (Nigg and Herzog, 1995). To the process that starts with the neural activation signal and ends with the contraction of the muscle is given the name of excitation-contraction coupling (Lieber, 1992). The central nervous system emanates a neural signal – or action potential – that is propagated through a particular type of cells, called motor neurons, until it reaches the specified muscle fibers to contract. As illustrated in Figure 6.3, the neural signal arrives to the muscle fibers through the motor axon of a motor neuron, which in turn is divided in smaller branches, the axon terminals, each one going to a specific muscle fiber. To this set of muscle fibers that are enervated by the same motor neuron is given the name of motor unit. The number of muscle fibers in a motor unit may differ considerably from several tens, corresponding to small motor units such as the ones of the muscles that produces the fine movements of the face and fingers, to several hundreds, corresponding to large motor units such as the ones associated to the muscles of the

locomotor apparatus. When a single neural signal arrives to a motor neuron, all the fibers belonging to the motor unit to which the stimulated motor neuron is attached, will experience a contraction-relaxation sequence usually designated by muscle twitch (Lieber, 1992; Nigg and Herzog, 1995; Winter, 1990).

To the connection between an axon terminal and a muscle fiber is usually given the name of neuromuscular junction. A neuromuscular junction is schematically represented in Figure 6.3. When a neural signal arrives to an axon terminal small quantities of acetylcholine (Ach) – a neurotransmitter that causes muscle fiber excitation – are released into the small gap existing between the axon terminal and the muscle fiber. The acetylcholine disseminates across the synaptic cleft until it binds with specialized receptors located in the muscle fiber membrane, the sarcolemma. This results in a depolarization of this membrane in its entire length originating the release of calcium ions (Ca^{++}) that will remove the inhibitory mechanism of actin-myosin cross-bridge formation, existing in the relaxed state, giving raise to sarcomere contraction (Nigg and Herzog, 1995).

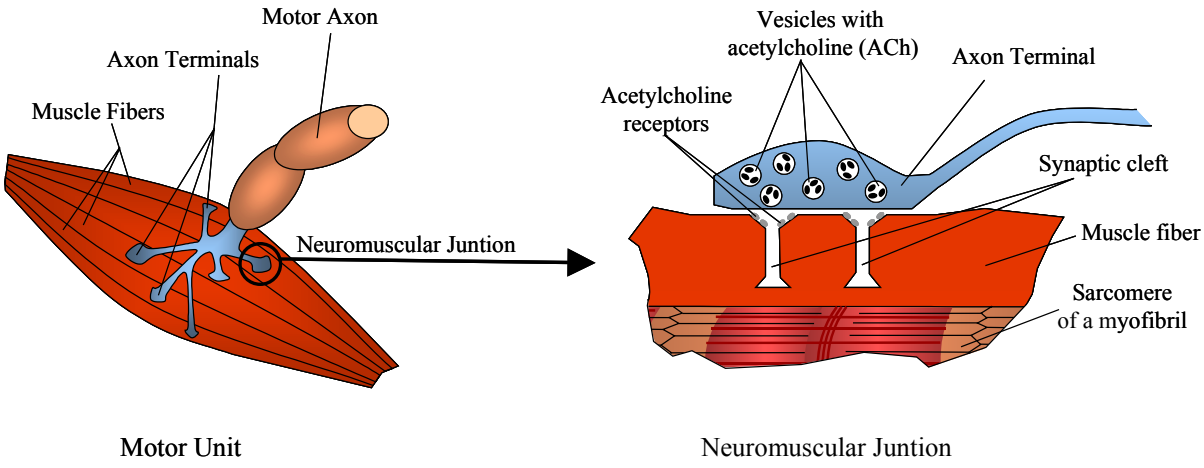

Figure 6.3: The motor unit and the neuromuscular junction. A motor unit is a set of muscle fibers that are enervated by the same motor neuron. To the connection between an axon terminal and a muscle fiber is given the designation of neuromuscular junction.

Sarcomere contraction is a physical process that occurs in four steps, as schematically represented in Figure 6.4. In the first step, the binding of the adenosine triphosphate enzyme

(ATP) – a molecule that stores energy in the form of chemical bounds – with the myosin head causes the release of the later from the actin filament initiating the contraction cycle. In the second step, the myosin head breaks down the chemical bounds of the ATP molecule into adenosine diphosphate molecules (ADP), inorganic phosphate molecules (P) and mechanical energy that causes the tilt of the myosin head to its excited state. In the third step, the P molecule is released from the myosin head exposing the binding site for the myosin head in the actin filament. The binding of the myosin head with the actin filament occurs, establishing a cross-bridge that will remain active until the end of the cycle. The forth and last step, the ADP molecule is released from the myosin head causing the myosin head to return to its initial state but this time tightly bound to the thin filament, generating the so-called 'power stroke', or in other words, the sliding of the actin filament over the myosin filament. The binding of a new ATP molecule to the myosin head causes the interruption of the cross-bridge and initiating a new contraction cycle. These contraction cycles continue until the muscle fiber stops being stimulated.

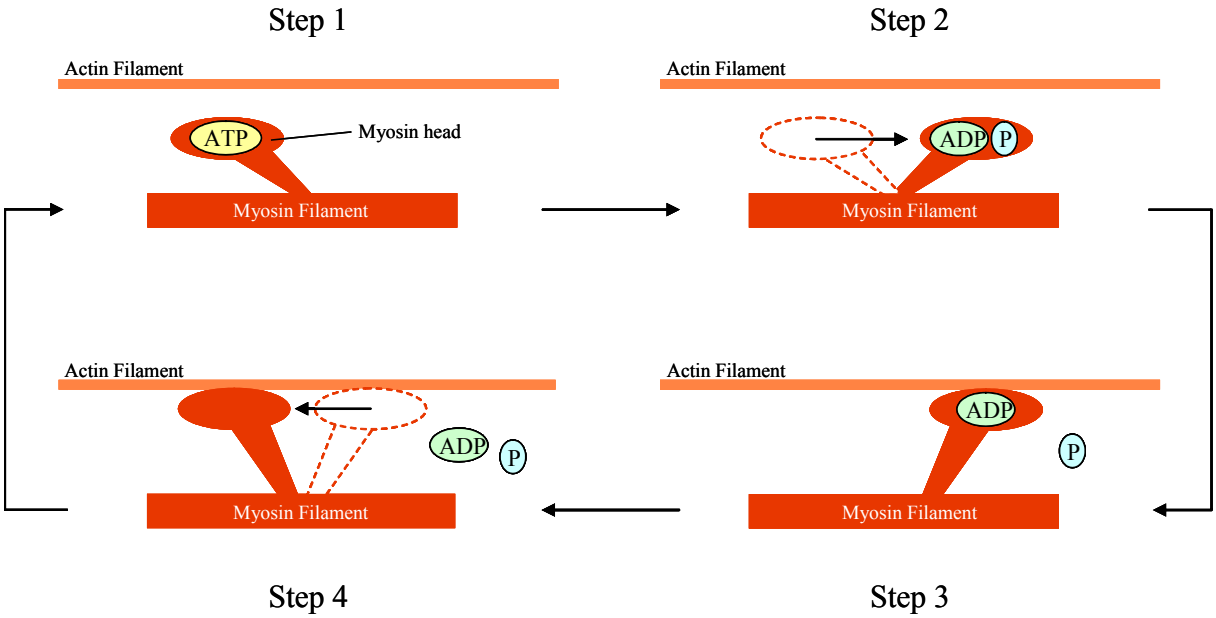

Figure 6.4: The ATP-myosin head cycle or cross-bridge cycle. Sarcomere contraction is a physical process that occurs in four steps.

The regulation of the muscle force is accomplished using two distinct physiological processes. Either the increment in the muscle force is obtained as a consequence of an increment in the stimulation frequency to which the neural signals arrive to the muscle fibers, or as the result of the recruitment of additional motor units, of larger size, following the so-called size principle (Winter, 1990).

Regarding the first regulation process, it should be stated that the increase of the stimulation frequencies reduces the time gap between two consecutive muscle twitches. Since a muscle twitch is not an instantaneous process – it has a finite duration that results from the time that takes activation, contraction and relaxation to occur – when this time interval becomes smaller than the twitch duration, a twitch superposition occurs producing an add-up effect that results in an increment of the muscular contraction force, as represented in Figure 6.5. Due to its time dependency, this process of muscle force regulation is usually referred as temporal summation (Lieber, 1992).

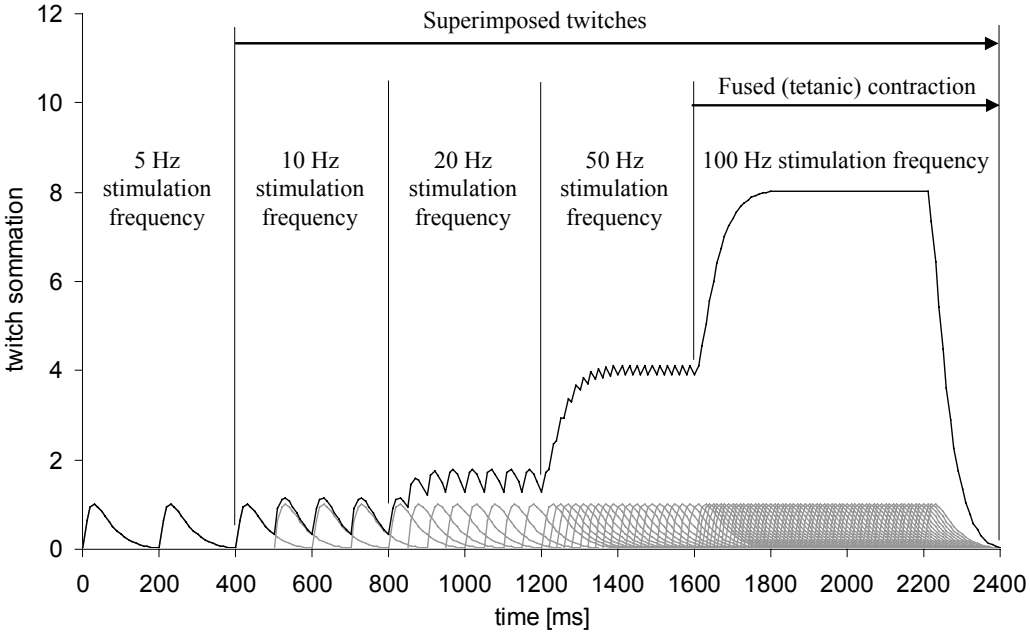

Figure 6.5: Temporal summation. One of the possible ways to regulate muscular force is by superimposing several sequential muscle twitches. An increase in the stimulation frequency reduces the time interval between consecutive muscle twitches, consequently increasing the contraction force. In the present example, the muscle twitches are approximated using the general expression of a second-order critically damped impulse (Winter, 1990).

However, this force increment only occurs for stimulation frequencies below a certain level. Once this level is reached, the muscle contracts tetanically (fused contraction) and further increments of the stimulation frequency will no longer produce force increments.

Additionally, it should be referred that the generation of muscular contraction forces also depends, on a macroscopic scale, on the muscle length and on the muscle rate of length change, the so-called force-length and force-velocity relationships. These two important aspects will be addressed later in this chapter, along with the presentation of the mathematical muscle model.

6.3 Muscle Actuators in Multibody Systems

Skeletal muscles are introduced in the equations of motion of the multibody system as point-to-point kinematic driver actuators, hereafter called muscle actuators. Depending on the complexity of the path of each skeletal muscle, muscle actuators can be defined using two or more points. In Figure 6.6, two skeletal muscles of the lower extremity muscle apparatus are schematically represented to illustrate the two types of muscle actuator definition: the *semimembranosus* and the *tensor fasciae latae*. The *semimembranosus*, due to its almost straight-line path, is represented with only two points that are used to describe the location of its origin and insertion points in the bony structures. The *tensor fasciae latae*, due to its more complex path, besides the location of the origin and insertion points in the skeletal structures, requires the use of two additional via points for an accurate geometric definition.

Muscle actuators are represented three-dimensionally. The Cartesian coordinates of the points used in the definition of the muscles, more precisely the origin, insertion and the via points, are provided with respect to the local reference frame of the rigid body to which they are attached. The use of via points allow for a definition of the muscle geometry that is much closer to the actual muscle. In the present work there can be up to five via points in the definition of a single muscle actuator. Via points are used to simulate the muscle wrap around joints and bones and also to simulate the interaction between two contacting muscles. Throughout the inverse analysis, via points cannot change their position with respect to the rigid body to which they are attached.

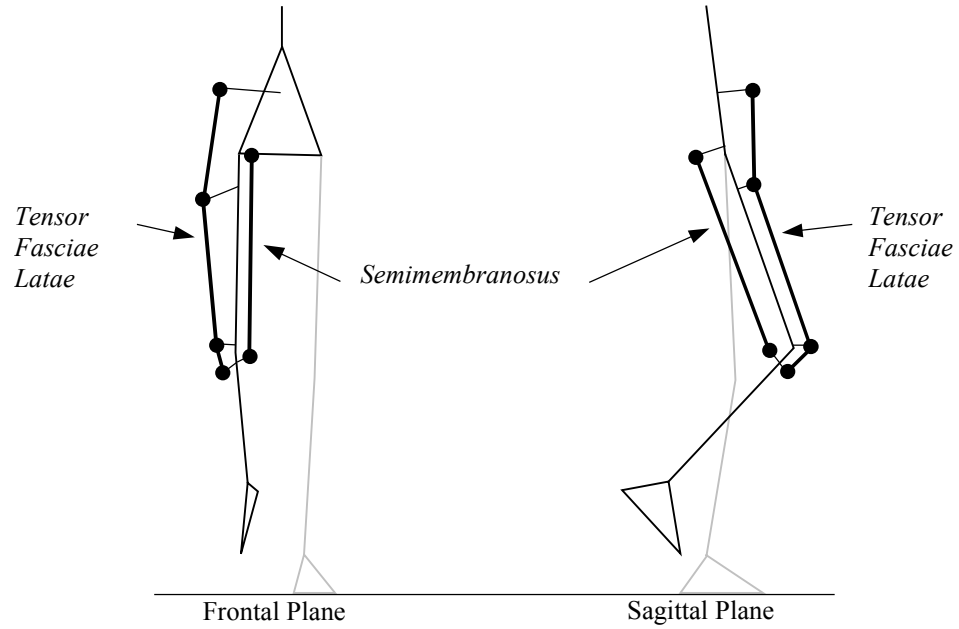

Figure 6.6: Muscle actuators defined with two or more points. The *semimembranosus*, a hip extensor and a flexor of the knee, due to its almost straight-line path, is represented using a two-point muscle actuator, while the *tensor fasciae latae*, a stabilizer of the hip and knee joints, due to a more complex path that wraps around two joints and contacts with several other muscles, is represented with a four-points muscle actuator, in which two of them are via points.

To each muscle actuator is associated a constraint equation that describes the way that the muscle path changes during the analysis period. These constraint equations are analytical expressions that constrain the distance between two generic points, of different rigid bodies, to change according to a specified length change history previously calculated. Considering the simplest case of a two-point muscle actuator, with an origin located in point n of rigid body i, and an insertion located in point m of rigid body j, as depicted in Figure 6.7, the mathematical expression used to define the constraint is written as:

$$\mathbf{\Phi}^{(MA,1)}(\mathbf{q},t) = \left(\mathbf{r}_m - \mathbf{r}_n\right)^T \left(\mathbf{r}_m - \mathbf{r}_n\right) - L_{nm}^2(t) = 0 \tag{6.1}$$

where $\mathbf{r}_m$ and $\mathbf{r}_n$ are respectively the global position vectors of the origin and insertion points and $L_{nm}(t)$ is the muscle total length, calculated for each time step of the analysis. It should be noted that n and m are two generic points of rigid bodies i and j, used only to define the muscle actuator and, therefore, do not belong to the vector of generalized coordinates of the

system, i.e., they do not belong to the set of points and unit vectors used in the construction of the rigid bodies to which they are attach. This means that Equation (6.1), as is, cannot be added to the global vector of constraints, described by Equation (2.2), because the quantities involved are not expressed in terms of the generalized set of coordinates. Therefore, a coordinate transformation needs to be applied in order to explicitly express this equation in terms of the natural coordinates used in the construction of rigid bodies *i* and *j*.

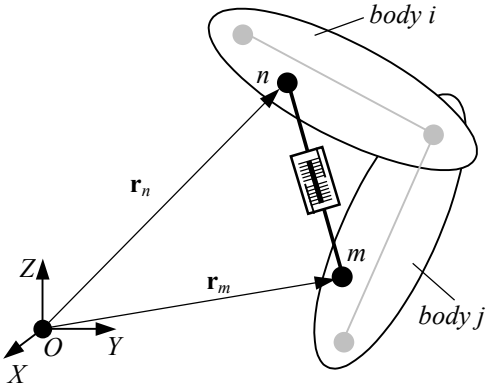

Figure 6.7: Muscle actuator defined between points *n* and *m* of rigid bodies *i* and *j*. Points *n* and *m* do not belong to the set of generalized coordinates describing the biomechanical system.

The required coordinate transformation is obtained expressing points *n* and *m* as function of the vectors $\mathbf{q}_i$ and $\mathbf{q}_j$ containing the generalized coordinates used in the definition of rigid bodies *i* and *j*. Hence, the coordinates of points *n* and *m* are rewritten as follows:

$$\begin{aligned} \mathbf{r}_n &= \mathbf{C}_i^n \mathbf{V}_i \mathbf{q}_i \\ \mathbf{r}_m &= \mathbf{C}_j^m \mathbf{V}_j \mathbf{q}_j \end{aligned} \tag{6.2}$$

where $\mathbf{C}_i^n$ and $\mathbf{C}_j^m$ are the constant transformation matrices introduced in Equation (2.42), relating the Cartesian coordinates of a generic point with the generalized coordinates of the basic rigid body, and $\mathbf{V}_i$ and $\mathbf{V}_j$ are the transformation matrices, introduced in Section 2.4.6, relating the generalized coordinates of the basic rigid body with the generalize coordinates of other types of rigid bodies, such as the ones used to describe the biomechanical model. More details on this issue can be found on Section 3.2.2.

Substituting Equation (6.2) in the muscle actuator constraint, given by Equation (6.1), the definitive form of the muscle actuator constraint equation is obtained:

$$\mathbf{\Phi}^{(MA,1)}(\mathbf{q},t) = \left(\mathbf{C}_j^m \mathbf{V}_j \mathbf{q}_j - \mathbf{C}_i^n \mathbf{V}_i \mathbf{q}_i\right)^T \left(\mathbf{C}_j^m \mathbf{V}_j \mathbf{q}_j - \mathbf{C}_i^n \mathbf{V}_i \mathbf{q}_i\right) - L_{nm}^2(t) = 0 \tag{6.3}$$

where all the quantities involved are expressed in terms of the generalized coordinates of rigid bodies *i* and *j*. As it can be observed, Equation (6.3) presents a quadratic dependency with the generalized coordinates, meaning that the contributions of this constraint for the Jacobian matrix of the constraints are linear.

In order to obtain the velocity equations associated to this constraint, it is necessary to differentiate Equation (6.3) with respect to time. After some algebraic manipulation, the following result is obtained:

$$\begin{aligned} \dot{\mathbf{\Phi}}^{(MA,1)}(\mathbf{q},t) \quad &= \frac{\partial \Phi^{(MA,1)}}{\partial \mathbf{q}_j}\dot{\mathbf{q}}_j + \frac{\partial \Phi^{(MA,1)}}{\partial \mathbf{q}_i}\dot{\mathbf{q}}_i + \nu^{(MA,1)}(t) \\ &= 2\left[\left(\mathbf{C}_j^m \mathbf{V}_j \mathbf{q}_j - \mathbf{C}_i^n \mathbf{V}_i \mathbf{q}_i\right)^T \mathbf{C}_j^m \left(\mathbf{V}_j + \bar{\mathbf{V}}_j\right)\right]\dot{\mathbf{q}}_j \\ &-2\left[\left(\mathbf{C}_j^m \mathbf{V}_j \mathbf{q}_j - \mathbf{C}_i^n \mathbf{V}_i \mathbf{q}_i\right)^T \mathbf{C}_i^n \left(\mathbf{V}_i + \bar{\mathbf{V}}_i\right)\right]\dot{\mathbf{q}}_i \\ &-2L_{nm}(t)\dot{L}_{nm}(t) \end{aligned} \tag{6.4}$$

where $\bar{\mathbf{V}}$ is an additional transformation matrix for rigid bodies with non-constant $\mathbf{V}$ matrices, i.e., $\bar{\mathbf{V}}$ is a transformation matrix similar to matrix $\mathbf{V}_{2\text{p1v}}$, given in Equation (2.68), in which the identity matrix $\mathbf{I}_3$ is replaced by the null matrix $\mathbf{0}_3$. The scalar $\dot{L}_{nm}$ is the rate of length change, obtained using cubic spline differentiation of the muscle length history curve, $L(t)$, with respect to time. For all other types of rigid bodies with constant $\mathbf{V}$ matrices, the matrix $\bar{\mathbf{V}}$ is a null matrix. From Equation (6.4), the contributions of the muscle actuator constraint to the Jacobian matrix, respectively the terms $\partial\mathbf{\Phi}^{(MA,1)}/\partial\mathbf{q}_i$ and $\partial\mathbf{\Phi}^{(MA,1)}/\partial\mathbf{q}_j$, are identified, as well as the right-hand side of the velocity equation given by $\nu^{(MA,1)}(t)$.

In order to obtain the right-hand side of the acceleration equation, Equation (6.3) is differentiated twice with respect to time. After some algebraic manipulation, the following result is obtained:

$$\begin{aligned}\boldsymbol{\gamma}^{(MA,1)}(\mathbf{q},t) \quad &= -2\left(\mathbf{C}_j^m\mathbf{V}_j\mathbf{q}_j - \mathbf{C}_i^n\mathbf{V}_i\mathbf{q}_i\right)^T\left[\mathbf{C}_j^m\left(\dot{\mathbf{V}}_j+\dot{\overline{\mathbf{V}}}_j\right)\dot{\mathbf{q}}_j - \mathbf{C}_i^n\left(\dot{\mathbf{V}}_i+\dot{\overline{\mathbf{V}}}_i\right)\dot{\mathbf{q}}_i\right] \\ &-2\left[\mathbf{C}_j^m\left(\mathbf{V}_j+\overline{\mathbf{V}}_j\right)\dot{\mathbf{q}}_j - \mathbf{C}_i^n\left(\mathbf{V}_i+\overline{\mathbf{V}}_i\right)\dot{\mathbf{q}}_i\right]^T\left[\mathbf{C}_j^m\left(\mathbf{V}_j+\overline{\mathbf{V}}_j\right)\dot{\mathbf{q}}_j - \mathbf{C}_i^n\left(\mathbf{V}_i+\overline{\mathbf{V}}_i\right)\dot{\mathbf{q}}_i\right] \\ &-2\left[L_{nm}(t)\ddot{L}_{nm}(t)+\dot{L}_{nm}^2(t)\right]\end{aligned} \tag{6.5}$$

where $\dot{\mathbf{V}}$ and $\dot{\overline{\mathbf{V}}}$ are the first time derivatives of the transformation matrices $\mathbf{V}$ and $\overline{\mathbf{V}}$ for rigid bodies with non-constant $\mathbf{V}$ matrices. For all other types of rigid bodies, these are null matrices. The term $\ddot{L}_{nm}(t)$ is the second time derivative of the muscle length curve, which is obtained using cubic spline differentiation.

A Lagrange multiplier is associated to each muscle actuator. The physical meaning of this multiplier, when associated to this type of actuators, is of a force per unit of length. In order to obtain muscle forces or muscle activations, these multipliers must be multiplied by proper scalar factors. These scalar factors depend on the type of muscle model used to estimate the muscle force. Their expressions are introduced later in this Chapter.

Regarding the contribution of muscle actuators defined with more than two points in the equations of motion of the system, these are introduced in the Jacobian matrix of the constraints as a sum of several two-point muscle actuators. This procedure is explained using the muscle *tensor fasciae latae*, presented in Figure 6.6.

According to the proposed procedure, the muscle *tensor fasciae latae* is described using three two-point muscle actuators, labeled respectively m_1, m_2 and m_3, as represented in Figure 6.8. The insertion point of muscle m_1 is coincident with the origin of muscle m_2 and the insertion point of muscle m_2 is coincident with the origin of muscle m_3. To the muscle actuators m_1, m_2 and m_3 are associated respectively the Lagrange multipliers λ_{m1}, λ_{m2} and λ_{m3}.

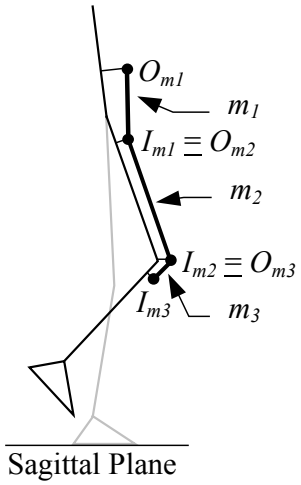

Figure 6.8: Muscle actuators with complex path. Muscle actuators with complex paths are described as a collection of simpler two-point muscle actuators.

With the information presented before, the term $\mathbf{\Phi}_{\mathbf{q}}^{T}\boldsymbol{\lambda}$ of the equation of motion of the system, is partially assembled for muscle actuators m_1, m_2 and m_3, and presented as:

$$\begin{array}{c} \\ \mathbf{q}_3 \\ \mathbf{q}_4 \\ \mathbf{q}_5 \\ \mathbf{q}_6 \\ \mathbf{q}_7 \end{array} \begin{array}{c} \begin{array}{ccc} m_1 & m_2 & m_3 \end{array} \\ \begin{bmatrix} \partial\mathbf{\Phi}^{m1}/\partial\mathbf{q}_3 & \mathbf{0} & \mathbf{0} \\ \partial\mathbf{\Phi}^{m1}/\partial\mathbf{q}_4 & \partial\mathbf{\Phi}^{m2}/\partial\mathbf{q}_4 & \mathbf{0} \\ \mathbf{0} & \partial\mathbf{\Phi}^{m2}/\partial\mathbf{q}_5 & \partial\mathbf{\Phi}^{m3}/\partial\mathbf{q}_5 \\ \mathbf{0} & \mathbf{0} & \mathbf{0} \\ \mathbf{0} & \mathbf{0} & \partial\mathbf{\Phi}^{m7}/\partial\mathbf{q}_5 \end{bmatrix} \end{array} \begin{Bmatrix} \lambda_{m1} \\ \lambda_{m2} \\ \lambda_{m3} \end{Bmatrix} \tag{6.6}$$

where $\mathbf{q}_3$ to $\mathbf{q}_7$ indicate the rows of the Jacobian matrix and represent the set of generalized coordinates defining the rigid bodies *3* to *7* of the kinematic structure of the inverse biomechanical model presented in Section 3.2.2, which are interconnected by the referred muscle. The terms $\partial\mathbf{\Phi}^{mi}/\partial\mathbf{q}_j$ are the partial derivatives of muscle actuator equation m_i, in order to the natural coordinate $\mathbf{q}_j$.

Assuming that any muscle must present, from its origin to its insertion, a constant force per unit of length, then for muscles defined with more than two points, the Lagrange multipliers associated with each one of the segments used in the muscle description must also present equal values. Hence, considering again the example of the muscle *tensor fasciae latae*, the Lagrange multipliers for the partial muscle actuators m_1 to m_3, are related as:

$$\lambda_{m1} = \lambda_{m2} = \lambda_{m3} = \lambda_{TFL} \tag{6.7}$$

Substituting this result in Equation (6.6), it is observed that the contributions of each muscle actuator m_1, m_2 and m_3 for the Jacobian matrix add up to form a single actuator contribution that express the kinematics of the muscle with a more complex path. This result is written as:

$$m_1 + m_2 + m_3$$

$$\begin{matrix} \mathbf{q}_3 \\ \mathbf{q}_4 \\ \mathbf{q}_5 \\ \mathbf{q}_6 \\ \mathbf{q}_7 \end{matrix} \begin{bmatrix} \partial\mathbf{\Phi}^{m1}/\partial\mathbf{q}_3 + \mathbf{0} + \mathbf{0} \\ \partial\mathbf{\Phi}^{m1}/\partial\mathbf{q}_4 + \partial\mathbf{\Phi}^{m2}/\partial\mathbf{q}_4 + \mathbf{0} \\ \mathbf{0} + \partial\mathbf{\Phi}^{m2}/\partial\mathbf{q}_5 + \partial\mathbf{\Phi}^{m3}/\partial\mathbf{q}_5 \\ \mathbf{0} + \mathbf{0} + \mathbf{0} \\ \mathbf{0} + \mathbf{0} + \partial\mathbf{\Phi}^{m3}/\partial\mathbf{q}_5 \end{bmatrix} \{\lambda_{TFL}\} \tag{6.8}$$

The result obtained for Lagrange multiplier λ_{TFL} represents a constant muscle force per unit of length from the origin to the insertion point of the muscle defined with more than two points.

The contributions of muscle actuators are introduced in the Jacobian matrix of the constraints together with the contributions of the rest of the kinematic constraints defining the kinematics of the biomechanical model and the kinematic joints. This means that an integrated solution is obtained for the inverse dynamics problem in terms of muscle and reaction forces, i.e., muscle forces are accounted for during the calculation of the reaction forces at the joints of the biomechanical model and vice-versa.

The joint rotational actuators, introduced in Chapter 5, must be removed from all the joints crossed by muscle actuators. However, in the remaining joints, where muscle actuators are not used, the joint rotational actuators are maintained. In this way, the biomechanical model is created with different kinds of driver actuators. This result shows that different types of drivers can be used at the same time and that muscle actuators need only to be introduced in the anatomical segments of the biomechanical model that are the target of the analysis, i.e., in those where the calculation of the redundant muscle forces is necessary.

6.4 Dynamics of Muscle Tissue

In Section 6.2, the anatomy and physiology of skeletal muscles were briefly introduced. This overview was made at a microscopic level with emphasis given to the analysis of the so-called excitation-contraction coupling, i.e., the physiological process that starts with the neural activation signal and ends with the contraction of the muscle (Lieber, 1992). However, in order to be used in the inverse dynamic analysis of the whole human body, it is essential to have a macroscopic description of the dynamics of the muscle tissue and of the corresponding mathematical models that allow its representation.

At a macroscopic level, the dynamics of muscle tissue can be divided into activation dynamics and muscle contraction dynamics (Zajac, 1989), as schematically indicated in Figure 6.9.

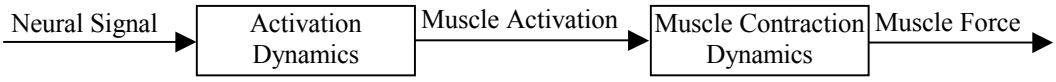

Figure 6.9: Schematic representation of the dynamics of muscle tissue. Activation dynamics corresponds to the transformation of the neural signal into activation of the contractile muscle apparatus, while muscle contraction dynamics corresponds to the transformation of muscle activation in muscle force.

Activation dynamics generates a muscle tissue state that transforms the neural excitation produced by the central nervous system, into activation of the contractile apparatus. Although not implemented in this work, the activation dynamics describes the time lag between neural signal and the corresponding muscle activation (Kaplan, 2000) and it is usually represented by first order differential equations (Hatze, 1984; Kaplan, 2000; Yamaguchi, 2001; Zajac, 1989).

The muscle contraction dynamics corresponds to the transformation of muscle activation in muscle force, as represented in Figure 6.9. To simulate this process, mathematical models of the muscle and soft tissues are used to relate the muscular force produced by a muscle with the resulting movement produced in the musculoskeletal system (Yamaguchi, 2001). The mathematical models can be either passive or active as represented in Figure 6.10. Passive models such as the Maxwell, the Voight and the Kelvin models are able to simulate accurately the behavior of soft tissues under both compressive and tensile loads (Yamaguchi, 2001). However, these models are not able to simulate active muscle action since they do not have a contractile element. This important issue was resolved by Hill in 1938, with the introduction of a new muscle model, in which the active muscle behavior is properly described using a contractile element.

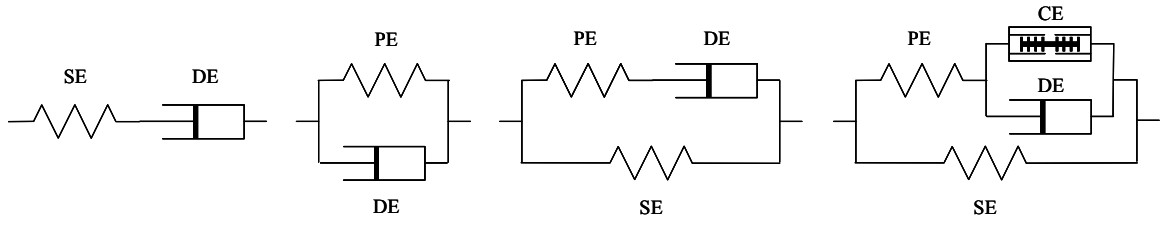

Figure 6.10: Different types of mathematical muscle models (not including tendon). (a) Maxwell muscle model (passive model). (b) Voight muscle model (passive model). (c) Kelvin muscle model (passive model). (d) Hill muscle model (active model). (SE – Series elastic Element; DE – Damping Element; PE – Parallel elastic Element; CE – Contractile Element).

The Hill's muscle model or variations of it are commonly used by many researchers to simulate active and passive muscle action. The Hill muscle model is an active muscle model that has its roots in the Kelvin's passive muscle model, to which it is added the contractile element (CE) represented in Figure 6.10(d). This element simulates at a macroscopic level, the active muscular action produced by the functional units of muscle contraction – the sarcomeres – and in particular the ATP-myosin cross-bridge cycle described previously in Section 6.2.2. Additionally, since this model is an evolution of the Kelvin's model, it also simulates accurately the passive soft tissue behavior of the muscle. For that purpose, it has a

parallel damping element (DE) that simulates the viscous force produced by intracellular and intercellular fluid within the muscle, a parallel element (PE) that simulates the non-linear passive elastic properties of the muscle and a series elastic element (SE) that simulates the elasticity of the actin-myosin cross bridges (Yamaguchi, 2001).

In this work, a Hill-type muscle model is implemented to simulate the muscle contraction dynamics. The model, depicted in Figure 6.11, is composed of an active Hill contractive element (CE), in which are included the damping properties of the damping element, and a passive element (PE). Both elements contribute to the total muscle force $F^m(t)$. In the present work, the series elastic element (SE) usually associated with cross-bridge stiffness is not included in the model since it can be neglected, with little inaccuracy, in coordination studies not involving short-tendon actuators (Zajac, 1989).

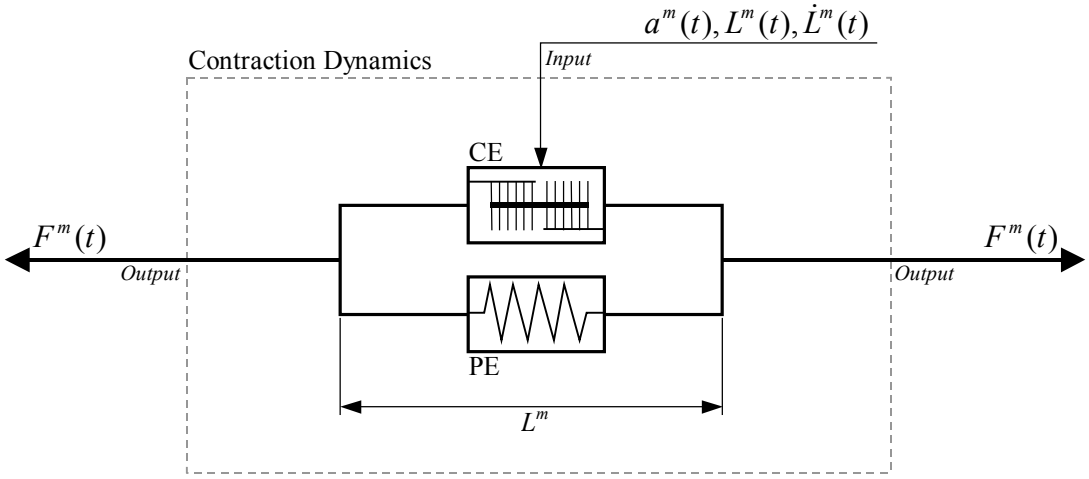

Figure 6.11: Hill-type muscle model used to simulate muscle contraction dynamics. The physical characteristics of the damping element are included in the contractile element (CE) and the action of the series elastic element (SE) is neglected.

In a Hill-type muscle model, the contractile properties of the muscle tissue are controlled by its current length $L^m(t)$, rate of length change $\dot{L}^m(t)$ and activation $a^m(t)$ in such a way that the force produced by the active Hill contractile element, for muscle *m*, is written as:

$$F_{CE}^m(a^m(t), L^m(t), \dot{L}^m(t)) = \frac{F_L^m(L^m(t))F_{\dot{L}}^m(\dot{L}^m(t))}{F_0^m} a^m(t) \tag{6.9}$$

where F_0^m is the maximum isometric force and $F_L^m(L^m(t))$ and $F_{\dot{L}}^m(\dot{L}^m(t))$ are two functions that represent the muscle force-length and force-velocity relationship, respectively (Kaplan, 2000; Zajac, 1989). These well known relationships state that the maximum contraction force that a skeletal muscle is able to produce is dependent of its actual length and on its rate of length change, also designated by shortening velocity.

Considering only the force produced by the contractile element, it can be stated that a muscle in an isometric contraction (i.e. producing force at a constant length) is only able to generate contraction force for muscle lengths that are roughly between half and one and a half times its resting length (Kaplan, 2000). In addition, it is also observed that during a concentric contraction (i.e., producing force while shortening) the force generated by the contractile element is smaller than the force it produces during an isometric contraction; while in the case of an eccentric contraction (i.e., producing force while lengthening) the opposite occurs and muscle forces greater than the muscle's maximum isometric force are observed.

Based on approximations to experimental data reported by other authors, Kaplan (2000) proposed analytical expressions for the force-length and force-velocity relationships. These analytical expressions are respectively:

$$F_L^m(L^m(t)) = F_0^m e^{-\left[\left[-\frac{9}{4}\left(\frac{L^m(t)}{L_0^m}-\frac{19}{20}\right)\right]^4-\frac{1}{4}\left[-\frac{9}{4}\left(\frac{L^m(t)}{L_0^m}-\frac{19}{20}\right)\right]^2\right]} \tag{6.10}$$

and

$$F_{\dot{L}}^m(\dot{L}^m(t)) = \begin{cases} 0 & -\dot{L}_0^m > \dot{L}^m(t) \\ -\dfrac{F_0^m}{\arctan(5)}\arctan\left(-5\dfrac{\dot{L}^m(t)}{\dot{L}_0^m}\right)+F_0^m & 0.2\dot{L}_0^m \geq \dot{L}^m(t) \geq -\dot{L}_0^m \\ \dfrac{\pi F_0^m}{4\arctan(5)}+F_0^m & \dot{L}^m(t) > 0.2\dot{L}_0^m \end{cases} \tag{6.11}$$

where L_0^m is the muscle resting length and $\dot{L}_0^m$ is the maximum contractile velocity above which the muscle cannot produce force (Zajac, 1989).

Using the expressions presented in Equations (6.10) and (6.11), the force-length and force-velocity curves are constructed and their behavior depicted in Figure 6.12. These curves represent, respectively, general isometric contractions performed with different muscle lengths and general concentric-eccentric contractions, in which the force value is measured when the muscle length is equal to its resting length.

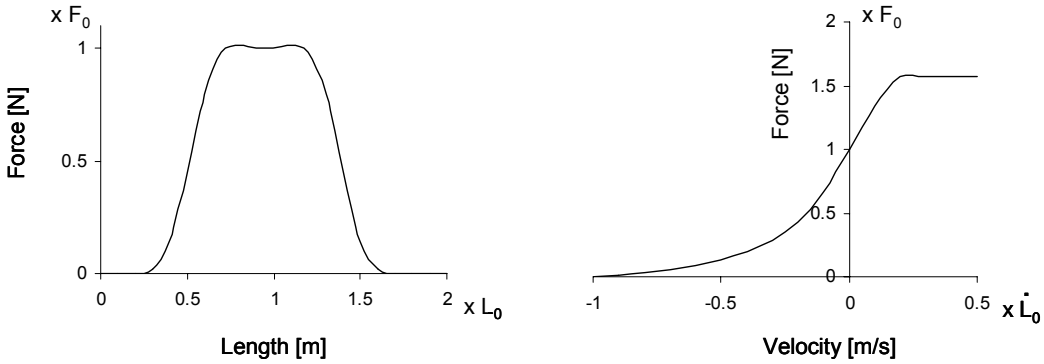

(a) (b)

Figure 6.12: Force-Length and Force-Velocity relationships obtained using Equations (6.10) and (6.11) and considering that the muscle is fully activated (i.e., *a(t) = 1*). (a) Force-length relationship representing a general isometric contraction performed with different muscle lengths. (b) Force-velocity relationship representing a general concentric-eccentric contraction in which the force value is measured when the muscle length is equal to its resting length.

The force produced by the passive element is independent of the muscle activation and it is only produced when the muscle is stretched beyond its resting length L_0^m. Such as in the previous situations, also the force produced by the passive element is approximated to experimental data using the following analytical expression (Kaplan, 2000):

$$F_{PE}^m(L^m(t)) = \begin{cases} 0 & L_0^m > L^m(t) \\ 8\dfrac{F_0^m}{L_0^{m^3}}\left(L^m - L_0^m\right)^3 & 1.63L_0^m \geq L^m(t) \geq L_0^m \\ 2F_0^m & L^m(t) > 1.63L_0^m \end{cases} \tag{6.12}$$

Equation (6.12) shows that the force produced by the passive element is only a function of the muscle length, being its value perfectly determined during the total time of the analysis. Therefore, since its value is not an unknown, the force produced by the passive element is treated like an external force, applied directly to the rigid bodies interconnected by the muscle. Using Equation (6.12), the force produced by the passive element is constructed and its behavior depicted in Figure 6.13. This curve represents the passive muscle force obtained for general isometric contractions performed with different muscle lengths.

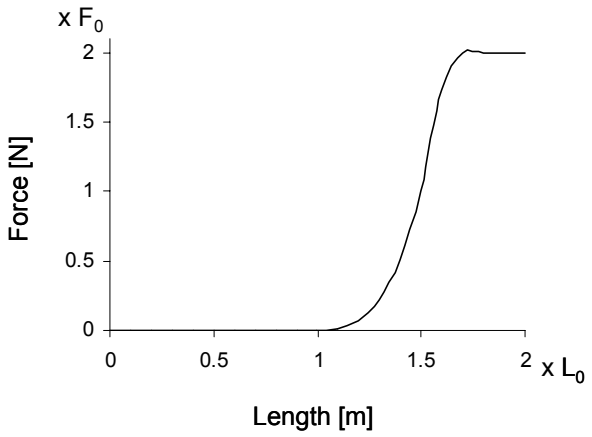

Figure 6.13: Force produced by the passive element. This curve is constructed using the analytical expression presented in Equation (6.12). The force produced by the passive element only depends of the muscle length, being independent of the shortening speed and muscle activation.

Equations (6.10) to (6.12) are used together to construct the four carpet plots presented in Figure 6.14. In this figure, the force produced by the contractile element, the passive element and the total muscle force are graphically represented, for different muscle activations, as function of the muscle length and muscle rate of length change. The thicker black lines represent the force-curves depicted in Figure 6.12 and Figure 6.13. It is clear from the observation of Figure 6.14 that the force produced by the contractile element is dependent of the muscle length, muscle rate of length change and activation, whereas the force produced by the passive element only depends on the muscle length, being independent of the activation and muscle rate of length change.

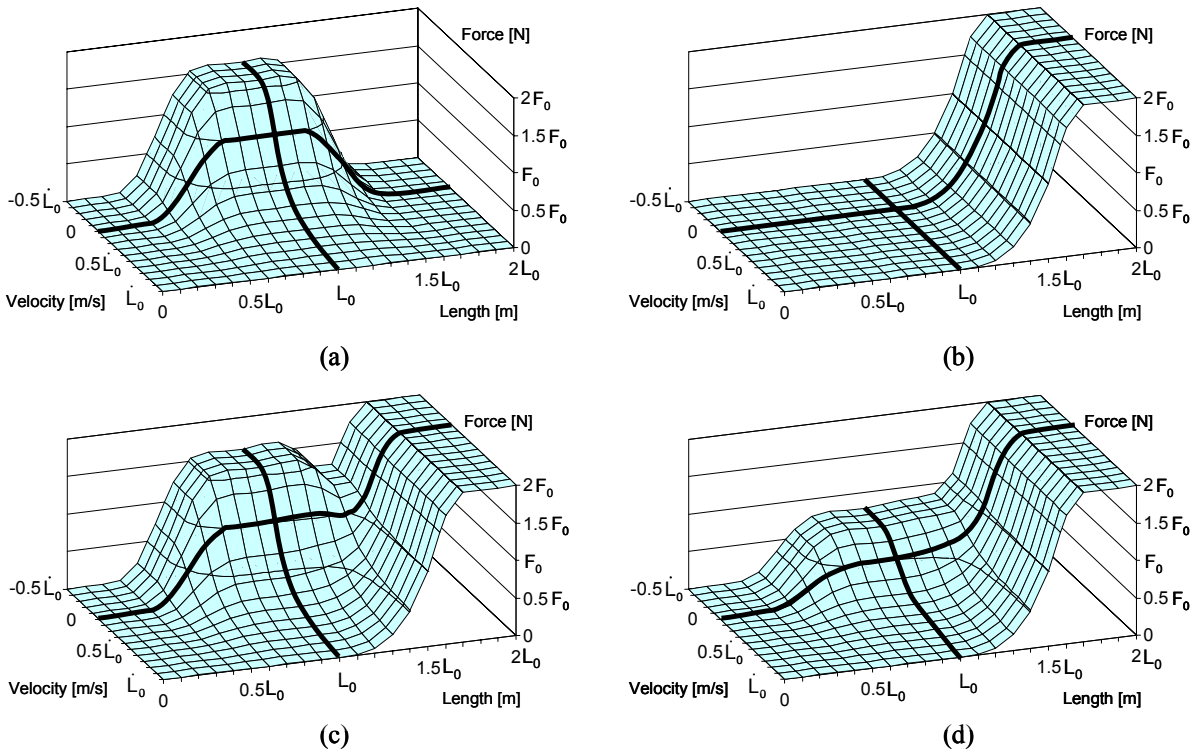

Figure 6.14: Carpet plots of the force-length and force-velocity relationships for the (a) contractile element; (b) passive element; (c) total muscle force and (d) total muscle force with 50% muscle activation.

Since the forces produced by the contractile element are the only unknowns, then in order to calculate these forces, a muscle actuator equation is associated to each muscle, as described in Section 6.3. This association is accomplished by multiplying the contribution of each muscle actuator for the Jacobian matrix by a proper scalar factor, so that the Lagrange multiplier associated to each actuator represents muscle force or muscle activation, depending on the objective of the analysis. These factors are respectively:

$$\begin{aligned} \mathcal{C}_{\lambda}^{m} &= \frac{1}{2L^{m}} \\ \mathcal{C}_{\lambda}^{m} &= \frac{F_{L}^{m} F_{\dot{L}}^{m}}{2F_{0}^{m} L^{m}} \end{aligned} \tag{6.13}$$

It should be noted that if the Lagrange multiplier represents muscle activation, the associated muscle force can be subsequently calculated using Equation (6.9).

6.5 Lower Extremity Muscle Apparatus

The expressions obtained in Sections 6.3 and 6.4, describing the muscle actuator and the muscle model, are general expressions that can be applied to any muscle apparatus of the human body. However, considering the importance that these methodologies have in the study and analysis of human gait, an accurate description of the lower extremity muscle apparatus needs to be provided. A muscle data base, in which the most relevant characteristics of the principal muscles of the lower extremity muscle apparatus are described, is presented hereafter. This database was initially compiled by Delp (1990), modified by Carhart (2000) and later reproduced in the work of Yamagushi (2001). It contains the required information for the accurate introduction of the muscle actuators in the inverse biomechanical model as well as to set up the Hill-type muscle model for each one of its 43 muscles.

In Table 6.1, the information contained in the muscle database is presented, along with complementary information describing the location of the origin and insertion of each one of the muscles as well as their action and graphical representation. The physiological information, provided in Table 6.1, for each muscle is: the maximum isometric force (F_0), the penation angle (α), the resting length (L_0), the tendon length (L_T), the number of points describing the muscle (in a minimum of two), the local reference frame number to which the local coordinates of the points are referred and the Cartesian coordinates of the origin, via and insertion points (in this order) that are used to describe the path of each muscle. These coordinates are provided with respect to four local reference frames, hereafter referred as Pelvic, Femoral, Tibial and Foot reference frames (Yamaguchi, 2001). These reference frames have the same orientation as the global reference frame when the inverse biomechanical model is in its reference seated position. The reference frames are rigidly attached to bodies 1, 3, 5 and 7 of the inverse biomechanical model and have their origin coincident with the mid lower torso (at the midpoint of line joining the anterior superior iliac spines); the right hip (at the centroid of the femoral head); the right knee (at the midpoint of

line joining the medial and lateral femoral condyles); and the right ankle (at the midpoint of line joining the apeces of the medial and lateral malleoli), respectively.

Additionally, it should be mentioned that the coordinates of the muscle origin, via and insertion points are scaled to best fit the anthropometric dimensions of the biomechanical model and consequently the dimensions of the subject under analysis. For that purpose, some of the anthropometric dimensions provided by Yamaguchi (2001) are used to calculate these scaling factors. These dimensions are the thigh length (0.4312 m), the shank length (0.4432 m) and the lateral distance between femoral heads (0.1650 m), respectively.

Table 6.1: Lower Extremity Muscle Apparatus. The information describing the muscle attachment points, maximum isometric force, penation angle, resting length and tendon length was initially compiled by Delp (1990), modified by Carhart (2000) and later reproduced in the work of Yamaguchi (2001). The graphical representation of each muscle as well as the remaining anatomical and physiological information was obtained from the site The Lower Extremity Muscle Atlas and it is reproduced in this work under the permission of the authors.

Name: *Gluteus Medius*

Origin: Dorsal ilium inferior to iliac crest.

Insertion: Lateral and superior surfaces of greater trochanter.

Action: Major abductor of thigh; anterior fibers help to rotate hip medially; posterior fibers help to rotate hip laterally.

	F_0 [N]	α [deg]	L_0 [m]	L_T [m]	N Pts.	Ref. *i*	ξ_i [m]	η_i [m]	ζ_i [m]
Anterior	546	8	0.0535	0.078	2	1	-0.0403	-0.1195	0.03
						2	-0.0235	-0.0599	-0.0126
Middle	382	0	0.0845	0.053	2	1	-0.0845	-0.0757	0.044
						2	-0.0279	-0.0569	-0.0063
Posterior	435	19	0.0646	0.053	2	1	-0.1208	-0.064	0.0104
						2	-0.0334	-0.056	-0.0051

Table 6.1: Lower Extremity Muscle Apparatus. (Continue)

Name: *Gluteus Minimus*

Origin: Dorsal ilium between inferior and anterior gluteal lines; also from edge of greater sciatic notch.

Insertion: Anterior surface of greater trochanter.

Action: Abducts and medially rotates the hip joint.

	F_0 [N]	α [deg]	L_0 [m]	L_T [m]	N Pts.	Ref. *i*	ξ_i [m]	η_i [m]	ζ_i [m]
Anterior	180	10	0.068	0.016	2	1	-0.0461	-0.1043	-0.0079
						2	-0.0078	-0.0605	-0.0112
Middle	190	0	0.056	0.026	2	1	-0.0625	-0.0979	-0.0064
						2	-0.0104	-0.0605	-0.0112
Posterior	215	21	0.038	0.051	2	1	-0.0824	-0.0846	-0.0062
						2	-0.0146	-0.0594	-0.009

Name: *Gluteus Maximus*

Origin: Posterior aspect of dorsal ilium posterior to posterior gluteal line, posterior superior iliac crest, posterior inferior aspect of sacrum and coccyx, and sacrotuberous ligament.

Insertion: Primarily in fascia latae at the iliotibial band; also into the gluteal tuberosity on posterior femoral surface.

Action: Major extensor of hip joint; helps to laterally rotate hip; superior fibers help to abduct hip; inferior fibers help to tighten iliotibial band.

	F_0 [N]	α [deg]	L_0 [m]	L_T [m]	N Pts.	Ref. *i*	ξ_i [m]	η_i [m]	ζ_i [m]
Anterior	382	5	0.142	0.125	4	1	-0.1181	-0.0692	0.0605
						1	-0.1276	-0.0875	0.0012
						2	-0.0494	-0.0423	-0.0268
						2	-0.0299	-0.0508	-0.0611
Middle	546	0	0.147	0.127	4	1	-0.1333	-0.0556	0.0174
						1	-0.136	-0.0903	-0.0514
						2	-0.046	-0.0316	-0.0572
						2	-0.0169	-0.0453	-0.1097
Posterior	368	5	0.144	0.145	4	1	-0.1537	-0.0057	-0.031
						1	-0.1511	-0.0396	-0.1039
						2	-0.0323	-0.0146	-0.1126
						2	-0.0065	-0.0444	-0.1534

Table 6.1: Lower Extremity Muscle Apparatus. (Continue)

Name: *Adductor Longus*

Origin: Anterior surface of body of pubis, just lateral to pubic symphysis.

Insertion: Middle third of linea aspera, between the more medial adductor magnus and brevis insertions and the more lateral origin of the vastus medialis.

Action: Adducts and flexes the thigh, and helps to laterally rotate the hip joint.

F_0 [N]	α [deg]	L_0 [m]	L_T [m]	N Pts.	Ref. *i*	ξ_i [m]	η_i [m]	ζ_i [m]
418	6	0.138	0.11	2	1	-0.0312	-0.0167	-0.0826
					2	0.0054	-0.0253	-0.2281

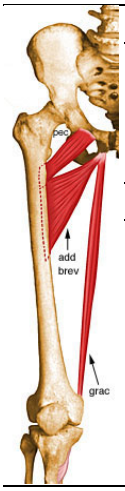

Name: *Adductor Brevis*

Origin: Anterior surface of inferior pubic ramus, inferior to origin of adductor longus.

Insertion: Pectineal line and superior part of medial lip of linea aspera.

Action: Adducts and flexes the thigh, and helps to laterally rotate the thigh.

F_0 [N]	α [deg]	L_0 [m]	L_T [m]	N Pts.	Ref. *i*	ξ_i [m]	η_i [m]	ζ_i [m]
286	0	0.133	0.02	2	1	-0.058	-0.0162	-0.0904
					2	0.001	-0.0318	-0.1292

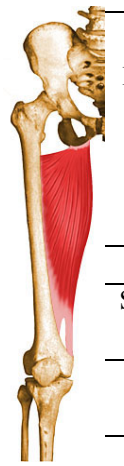

Name: *Adductor Magnus*

Origin: Inferior pubic ramus, ischial ramus, and inferolateral area of ischial tuberosity.

Insertion: Gluteal tuberosity of femur, medial lip of linea aspera, medial supracondylar ridge, and adductor tubercle.

Action: Powerful thigh adductor; superior horizontal fibers also help flex the thigh, while vertical fibers help extend the thigh.

	F_0 [N]	α [deg]	L_0 [m]	L_T [m]	N Pts.	Ref. *i*	ξ_i [m]	η_i [m]	ζ_i [m]
Superior	346	5	0.087	0.06	2	1	-0.0723	-0.0252	-0.116
						2	-0.0049	-0.0366	-0.1309
Middle	312	3	0.121	0.13	2	1	-0.0821	-0.0304	-0.1178
						2	0.0058	-0.0245	-0.2469
Inferior	444	5	0.131	0.26	2	1	-0.0762	-0.0273	-0.1167
						2	0.0076	0.0287	-0.4147

Table 6.1: Lower Extremity Muscle Apparatus. (Continue)

Name: *Tensor Fasciae Latae*

Origin: Anterior superior iliac spine, outer lip of anterior iliac crest and fascia latae.

Insertion: Iliotibial band.

Action: Helps stabilize and steady the hip and knee joints by putting tension on the iliotibial band of fascia.

F_0 [N]	α [deg]	L_0 [m]	L_T [m]	N Pts.	Ref. *i*	ξ_i [m]	η_i [m]	ζ_i [m]
155	3	0.095	0.425	4	1	-0.0307	-0.1226	0.0211
					2	0.0318	-0.0645	-0.1075
					2	0.0058	-0.0386	-0.4376
					3	0.0062	-0.0306	-0.0502

Name: *Pectineus*

Origin: Pecten pubis and pectineal surface of the pubis.

Insertion: Pectineal line of femur.

Action: Adducts the thigh and flexes the hip joint.

F_0 [N]	α [deg]	L_0 [m]	L_T [m]	N Pts.	Ref. *i*	ξ_i [m]	η_i [m]	ζ_i [m]
177	0	0.133	0.001	2	1	-0.0426	-0.0446	-0.0759
					2	-0.0132	-0.0273	-0.0888

Name: *Iliacus* and *Psoas*

Origin: *Psoas*: From anterior surfaces and lower borders of transverse processes of L1 - L5 and bodies and discs of T12 - L5.

Iliacus: From upper 2/3 of iliac fossa of ilium, internal lip of iliac crest, lateral aspect of sacrum, ventral sacroiliac ligament, and lower portion of iliolumbar ligament.

Insertion: Lesser trochanter.

Action: Flex the torso and thigh with respect to each other.

	F_0 [N]	α [deg]	L_0 [m]	L_T [m]	N Pts.	Ref. *i*	ξ_i [m]	η_i [m]	ζ_i [m]
Iliacus	429	7	0.1	0.09	5	1	-0.0666	-0.0844	0.0361
						1	-0.0215	-0.0841	-0.0543
						1	-0.0291	-0.0845	-0.08
						2	0.0018	-0.0062	-0.0587
						2	-0.0208	-0.0139	-0.0671
Psoas	371	8	0.104	0.13	5	1	-0.0639	-0.0286	0.0876
						1	-0.0235	-0.075	-0.0563
						1	-0.0289	-0.0838	-0.0795
						2	0.0017	-0.0041	-0.0548
						2	-0.0203	-0.0112	-0.0645

Table 6.1: Lower Extremity Muscle Apparatus. (Continue)

Name: *Quadratus Femoris*, *Gemellus (Inferior - Superior)* and *Piriformis*

Origin: *Quadratus Femoris*: Lateral margin of obturator ring above ischial tuberosity.
Gemellus: (Inf.) Posterior portions of ischial tuberosity and lateral obturator ring; (Sup.) Ischial spine.
Piriformis: Anterior surface of lateral process of sacrum and gluteal surface of ilium at the margin of the greater sciatic notch.

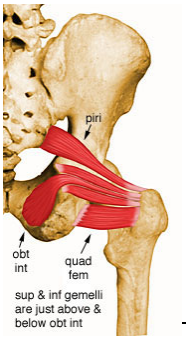

Insertion: *Quadratus Femoris*: Quadrate tubercle and adjacent bone of intertrochanteric crest of proximal posterior femur.
Gemellus: Medial surface of greater trochanter of femur.
Piriformis: Superior border of greater trochanter.

Action: *Quadratus Femoris*: Rotates the hip laterally; also helps adduct the hip.
Gemellus: Rotates the thigh laterally; also helps abduct the flexed thigh.
Piriformis: Lateral rotator of the hip joint; also helps abduct the hip if it is flexed.

	F_0 [N]	α [deg]	L_0 [m]	L_T [m]	N Pts.	Ref. *i*	ξ_i [m]	η_i [m]	ζ_i [m]
Quad Fem	254	0	0.054	0.024	2	1	-0.1129	-0.0514	-0.1137
						2	-0.0412	-0.0395	-0.0388
Gemellus	109	0	0.024	0.039	2	1	-0.1119	-0.0705	0.081
						2	-0.0153	-0.0479	-0.0036
Piriformis	296	10	0.026	0.115	3	1	-0.1379	-0.0232	0.0003
						1	-0.1179	-0.0649	-0.0273
						2	-0.016	-0.0472	-0.0039

Name: *Semitendinosus*

Origin: From common tendon with long head of biceps femoris from superior medial quadrant of the posterior portion of the ischial tuberosity.

Insertion: Superior aspect of medial portion of tibial shaft.

Action: Extends the thigh and flexes the knee, and also rotates the tibia medially, especially when the knee is flexed.

F_0 [N]	α [deg]	L_0 [m]	L_T [m]	N Pts.	Ref. *i*	ξ_i [m]	η_i [m]	ζ_i [m]
328	5	0.201	0.262	4	1	-0.1222	-0.0596	-0.1031
					3	-0.0324	0.015	-0.0562
					3	-0.0116	0.0253	-0.0769
					3	0.0028	0.0199	-0.0985

Table 6.1: Lower Extremity Muscle Apparatus. (Continue)

Name: *Semimembranosus*

Origin: Superior lateral quadrant of the ischial tuberosity.

Insertion: Posterior surface of the medial tibial condyle.

Action: Extends the thigh, flexes the knee, and also rotates the tibia medially, especially when the knee is flexed.

F_0 [N]	α [deg]	L_0 [m]	L_T [m]	N Pts.	Ref. *i*	ξ_i [m]	η_i [m]	ζ_i [m]
1030	15	0.08	0.359	2	1	-0.1178	-0.0687	-0.1003
					3	-0.025	0.02	-0.0553

Name: *Biceps Femoris (Long Head)*

Origin: From common tendon with semitendinosus from superior medial quadrant of the posterior portion of the ischial tuberosity.

Insertion: Primarily on fibular head; also on lateral collateral ligament and lateral tibial condyle.

Action: Flexes the knee, and also rotates the tibia laterally; long head also extends the hip joint.

F_0 [N]	α [deg]	L_0 [m]	L_T [m]	N Pts.	Ref. *i*	ξ_i [m]	η_i [m]	ζ_i [m]
717	0	0.109	0.341	2	1	-0.1229	-0.0658	-0.0989
					3	-0.0083	-0.0436	-0.0751

Name: *Biceps Femoris (Short Head)*

Origin: From lateral lip of linea aspera, lateral supracondylar ridge of femur, and lateral intermuscular septum of thigh.

Insertion: Primarily on fibular head; also on lateral collateral ligament and lateral tibial condyle.

Action: Flexes the knee, and also rotates the tibia laterally; long head also extends the hip joint.

F_0 [N]	α [deg]	L_0 [m]	L_T [m]	N Pts.	Ref. *i*	ξ_i [m]	η_i [m]	ζ_i [m]
402	23	0.173	0.1	2	2	0.0054	-0.0253	-0.2281
					3	-0.0104	-0.0419	-0.0747

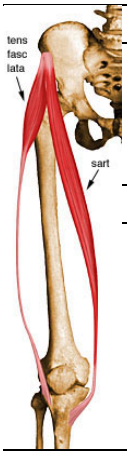

Name: *Sartorius*

Origin: Anterior superior iliac spine.

Insertion: Superior aspect of the medial surface of the tibial shaft near the tibial tuberosity.

Action: Flexes and laterally rotates the hip joint and flexes the knee.

F_0 [N]	α [deg]	L_0 [m]	L_T [m]	N Pts.	Ref. *i*	ξ_i [m]	η_i [m]	ζ_i [m]
104	0	0.579	0.04	5	1	-0.0151	-0.1227	-0.0013
					2	-0.0032	0.0455	-0.3855
					3	-0.0058	0.0411	-0.0432
					3	0.0062	0.0395	-0.0607
					3	0.025	0.026	-0.0866

Table 6.1: Lower Extremity Muscle Apparatus. (Continue)

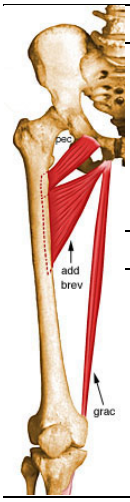

Name: *Gracilis*

Origin: Inferior margin of pubic symphysis, inferior ramus of pubis, and adjacent ramus of ischium.

Insertion: Medial surface of tibial shaft, just posterior to sartorius.

Action: Flexes the knee, adducts the thigh, and helps to medially rotate the tibia on the femur.

F_0 [N]	α [deg]	L_0 [m]	L_T [m]	N Pts.	Ref. *i*	ξ_i [m]	η_i [m]	ζ_i [m]
108	3	0.352	0.14	3	1	-0.0556	-0.0078	-0.1026
					3	-0.0159	0.0369	-0.049
					3	0.0062	0.0235	-0.0862

Name: *Rectus Femoris*

Origin: (Straight head) From anterior inferior iliac spine; (Reflected head) From groove just above acetabulum.

Insertion: Base of patella to form the more central portion of the quadriceps femoris tendon.

Action: Extends the knee and flexes the hip.

F_0 [N]	α [deg]	L_0 [m]	L_T [m]	N Pts.	Ref. *i*	ξ_i [m]	η_i [m]	ζ_i [m]
779	5	0.084	0.346	5	1	-0.0291	-0.0956	-0.0307
					2	0.0392	-0.0028	-0.434
					3	0.0609	-0.0035	0.0224
					3	0.0506	-0.0026	-0.0211
					3	0.0403	0	-0.0847

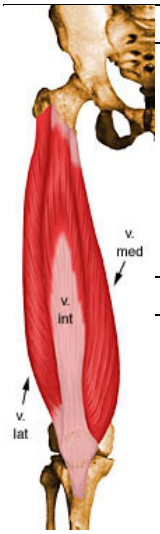

Name: *Vastus Medialis*

Origin: Inferior portion of intertrochanteric line, spiral line, medial lip of linea aspera, superior part of medial supracondylar ridge of femur, and medial intermuscular septum.

Insertion: Medial base and border of patella; also forms the medial patellar retinaculum and medial side of quadriceps femoris tendon.

Action: Extends the knee.

F_0 [N]	α [deg]	L_0 [m]	L_T [m]	N Pts.	Ref. *i*	ξ_i [m]	η_i [m]	ζ_i [m]
1294	5	0.089	0.126	6	2	0.0151	-0.0203	-0.2268
					2	0.0385	-0.001	-0.2992
					2	0.0441	0.0129	-0.4382
					3	0.0549	0.015	0.0232
					3	0.0506	-0.0026	-0.0211
					3	0.0403	0	-0.0847

Table 6.1: Lower Extremity Muscle Apparatus. (Continue)

Name: *Vastus Intermedius*

Origin: Superior 2/3 of anterior and lateral surfaces of femur; also from lateral intermuscular septum of thigh.

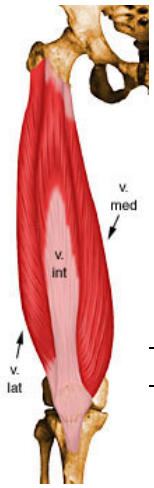

Insertion: Lateral border of patella; also forms the deep portion of the quadriceps tendon.

Action: Extends the knee.

F_0 [N]	α [deg]	L_0 [m]	L_T [m]	N Pts.	Ref. *i*	ξ_i [m]	η_i [m]	ζ_i [m]
1365	3	0.087	0.136	6	2	0.0313	-0.0335	-0.2079
					2	0.0362	-0.0308	-0.2252
					2	0.0382	-0.0073	-0.4339
					3	0.0544	-0.0019	0.0268
					3	0.0506	-0.0026	-0.0211
					3	0.0403	0	-0.0847

Name: *Vastus Lateralis*

Origin: Superior portion of intertrochanteric line, anterior and inferior borders of greater trochanter, superior portion of lateral lip of linea aspera, and lateral portion of gluteal tuberosity of femur.

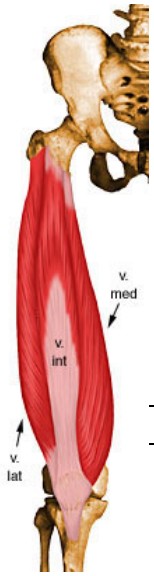

Insertion: Lateral base and border of patella; also forms the lateral patellar retinaculum and lateral side of quadriceps femoris tendon.

Action: Extends the knee.

F_0 [N]	α [deg]	L_0 [m]	L_T [m]	N Pts.	Ref. *i*	ξ_i [m]	η_i [m]	ζ_i [m]
1871	5	0.084	0.157	6	2	0.0052	-0.0377	-0.2004
					2	0.0291	-0.0442	-0.28
					2	0.0414	-0.0238	-0.4366
					3	0.0591	-0.017	0.0209
					3	0.0506	-0.0026	-0.0211
					3	0.0403	0	-0.0847

Table 6.1: Lower Extremity Muscle Apparatus. (Continue)

Name: *Gastrocnemius (Medial and Lateral heads)*

Origin: (Medial head) From posterior nonarticular surface of medial femoral condyle; (Lateral head) From lateral surface of femoral lateral condyle.

Insertion: The two heads unite into a broad aponeurosis which eventually unites with the deep tendon of the soleus to form the Achilles tendon, inserting on the middle 1/3 of the posterior calcaneal surface.

Action: Powerful plantar flexor of ankle.

	F_0 [N]	α [deg]	L_0 [m]	L_T [m]	N Pts.	Ref. *i*	ξ_i [m]	η_i [m]	ζ_i [m]
Medial	1113	17	0.045	0.408	3	2	-0.0137	0.0254	-0.4246
						2	-0.0273	0.0281	-0.441
						3	-0.0224	0.0304	-0.0502
Lateral	488	8	0.064	0.385	4	2	-0.0167	-0.0294	-0.4264
						2	-0.0303	-0.029	-0.4447
						3	-0.0249	-0.0242	-0.0496
						4	-0.0439	-0.0026	-0.0108

Name: *Soleus*

Origin: Posterior aspect of fibular head, upper 1/4 - 1/3 of posterior surface of fibula, middle 1/3 of medial border of tibial shaft, and from posterior surface of a tendinous arch spanning the two sites of bone origin.

Insertion: Eventually unites with the gastrocnemius aponeurosis to form the Achilles tendon, inserting on the middle 1/3 of the posterior calcaneal surface.

Action: Powerful plantar flexor of ankle.

F_0 [N]	α [deg]	L_0 [m]	L_T [m]	N Pts.	Ref. *i*	ξ_i [m]	η_i [m]	ζ_i [m]
2839	25	0.03	0.268	2	3	-0.0025	-0.0073	-0.158
					4	-0.0439	-0.0026	-0.0108

Table 6.1: Lower Extremity Muscle Apparatus. (Continue)

Name: *Tibialis Posterior*

Origin: Posterior aspect of interosseous membrane, superior 2/3 of medial posterior surface of fibula, superior aspect of posterior surface of tibia, and from intermuscular septum between muscles of posterior compartment and deep transverse septum.

Insertion: Splits into two slips after passing inferior to plantar calcaneonavicular ligament; superficial slip inserts on the tuberosity of the navicular bone and sometimes medial cuneiform; deeper slip divides again into slips inserting on plantar sufraces of metatarsals 2 - 4 and second cuneiform.

Action: Principal invertor of foot; also adducts foot, plantar flexes ankle, and helps to supinate the foot.

F_0 [N]	α [deg]	L_0 [m]	L_T [m]	N Pts.	Ref. *i*	ξ_i [m]	η_i [m]	ζ_i [m]
1270	12	0.031	0.31	4	3	-0.0097	-0.002	-0.139
					3	-0.0148	0.0236	-0.4177
					4	-0.007	0.0205	-0.0084
					4	0.0281	0.02	-0.0257

Name: *Tibialis Anterior*

Origin: Lateral condyle of tibia, proximal 1/2 - 2/3 or lateral surface of tibial shaft, interosseous membrane, and the deep surface of the fascia cruris.

Insertion: Medial and plantar surfaces of 1st cuneiform and on base of first metatarsal.

Action: Dorsiflexor of ankle and invertor of foot.

F_0 [N]	α [deg]	L_0 [m]	L_T [m]	N Pts.	Ref. *i*	ξ_i [m]	η_i [m]	ζ_i [m]
603	5	0.098	0.223	3	3	0.0185	-0.0119	-0.1674
					3	0.0339	0.0182	-0.4073
					4	0.0671	0.0224	-0.0239

Name: *Flexor Digitorum Longus*

Origin: Posterior surface of tibia distal to popliteal line.

Insertion: Splits into four slips after passing through medial intermuscular septum of plantar surface of foot; these slips then insert on plantar surface of bases of 2nd - 5th distal phalanges.

Action: Flexes toes 2 - 5; also helps in plantar flexion of ankle.

F_0 [N]	α [deg]	L_0 [m]	L_T [m]	N Pts.	Ref. *i*	ξ_i [m]	η_i [m]	ζ_i [m]
310	7	0.034	0.4	5	3	-0.0086	0.0019	-0.2109
					3	-0.0159	0.0202	-0.4177
					4	-0.0051	0.0199	-0.0104
					4	0.0218	0.0182	-0.024
					4	0.1157	-0.0193	-0.0495

Table 6.1: Lower Extremity Muscle Apparatus. (Continue)

Name: *Flexor Hallucis Longus*

Origin: Inferior 2/3 of posterior surface of fibula, lower part of interosseous membrane.

Insertion: Plantar surface of base of distal phalanx of great toe.

Action: Flexes great toe, helps to supinate ankle, and is a very weak plantar flexor of ankle.

F_0 [N]	α [deg]	L_0 [m]	L_T [m]	N Pts.	Ref. *i*	ξ_i [m]	η_i [m]	ζ_i [m]
322	10	0.043	0.38	5	3	-0.0081	-0.0252	-0.2406
					3	-0.0192	0.0179	-0.4205
					4	-0.0113	0.016	-0.0141
					4	0.0544	0.0175	-0.0348
					4	0.1224	0.0188	-0.0468

Name: *Extensor Digitorum Longus*

Origin: Lateral condyle of fibula, upper 2/3 - 3/4 of medial fibular shaft surface, upper part of interosseous membrane, fascia cruris, and anterior intermuscular septum.

Insertion: Splits into 4 tendon slips after inferior extensor retinaculum, each of which insert on dorsum of middle and distal phalanges as part of extensor expansion complex.

Action: Extend toes 2 - 5 and dorsiflexes ankle.

F_0 [N]	α [deg]	L_0 [m]	L_T [m]	N Pts.	Ref. *i*	ξ_i [m]	η_i [m]	ζ_i [m]
341	8	0.102	0.345	4	3	0.0033	-0.0284	-0.1424
					3	0.0298	-0.0074	-0.413
					4	0.0429	-0.0077	-0.0032
					4	0.1116	-0.0207	-0.036

Name: *Extensor Hallucis Longus*

Origin: Anterior surface of the fibula and the adjacent interosseous membrane.

Insertion: Base and dorsal center of distal phalanx of great toe.

Action: Extends great toe and dorsiflexes ankle.

F_0 [N]	α [deg]	L_0 [m]	L_T [m]	N Pts.	Ref. *i*	ξ_i [m]	η_i [m]	ζ_i [m]
108	6	0.111	0.305	5	3	0.0012	-0.0235	-0.1821
					3	0.0336	0.0088	-0.4108
					4	0.0477	0.0131	-0.0031
					4	0.0796	0.0176	-0.011
					4	0.1232	0.0199	-0.0277

Table 6.1: Lower Extremity Muscle Apparatus. (Continue)

Name: *Peroneus Brevis*

Origin: Inferior 2/3 of lateral fibular surface; also anterior and posterior intermuscular septa of leg.

Insertion: Lateral surface of styloid process of 5th metatarsal base.

Action: Everts foot and plantar flexes ankle.

F_0 [N]	α [deg]	L_0 [m]	L_T [m]	N Pts.	Ref. *i*	ξ_i [m]	η_i [m]	ζ_i [m]
348	5	0.05	0.161	5	3	-0.0072	-0.0335	-0.2727
					3	-0.0204	-0.0292	-0.4313
					3	-0.0148	-0.0298	-0.4427
					4	-0.0017	-0.0309	-0.0147
					4	0.0187	-0.0417	-0.0196

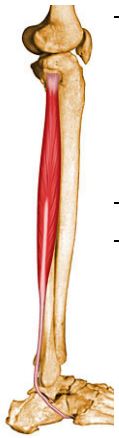

Name: *Peroneus Longus*

Origin: Head of fibula, upper 1/2 - 2/3 of lateral fibular shaft surface; also anterior and posterior intermuscular septa of leg.

Insertion: Plantar posterolateral aspect of medial cuneiform and lateral side of 1st metatarsal base.

Action: Everts foot and plantar flexes ankle; also helps to support the transverse arch of the foot.

F_0 [N]	α [deg]	L_0 [m]	L_T [m]	N Pts.	Ref. *i*	ξ_i [m]	η_i [m]	ζ_i [m]
754	10	0.049	0.345	7	3	0.0005	-0.0373	-0.1616
					3	-0.0213	-0.0295	-0.4334
					3	-0.0167	-0.0298	-0.4452
					4	-0.0049	-0.0297	-0.0187
					4	0.0191	-0.0359	-0.031
					4	0.036	-0.0195	-0.0346
					4	0.0707	0.0104	-0.0331

Name: *Peroneus Tertius*

Origin: Arises with the extensor digitorum longus from the medial fibular shaft surface and the anterior intermuscular septum (between the extensor digitorum longus and the tibialis anterior).

Insertion: Dorsal surface of the base of the fifth metatarsal.

Action: Works with the extensor digitorum longus to dorsiflex, evert and abduct the foot.

F_0 [N]	α [deg]	L_0 [m]	L_T [m]	N Pts.	Ref. *i*	ξ_i [m]	η_i [m]	ζ_i [m]
90	13	0.079	0.1	3	3	0.001	-0.0238	-0.289
					3	0.0236	-0.0164	-0.4194
					4	0.0365	-0.0374	-0.019

The muscle apparatus described in Table 6.1 is assembled to the inverse biomechanical model described in Chapter 3. The stick figure of this biomechanical model, in which is included the complete muscle apparatus for the right lower leg, is presented in Figure 6.15.

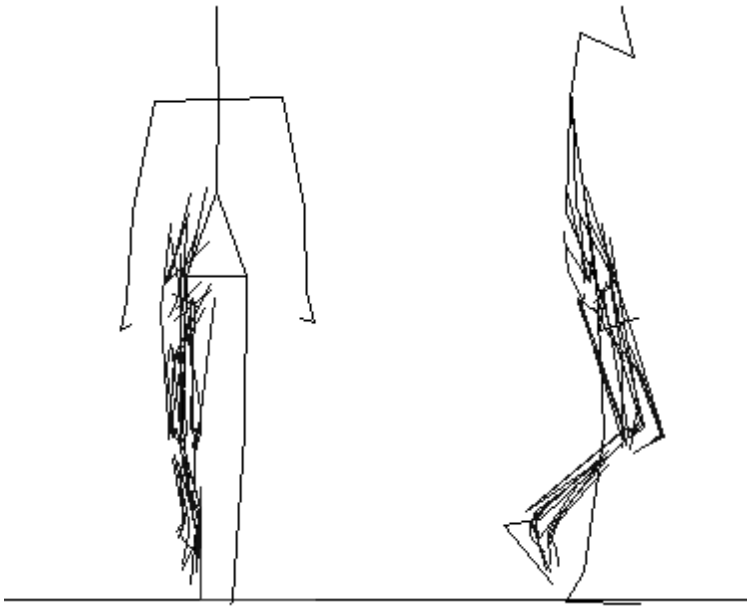

Figure 6.15:Stick figure of the inverse biomechanical model in which the complete lower extremity muscle apparatus is represented for the right leg.

6.6 Static Optimization

The inverse dynamics problem with muscle actuators instead of joint actuators is indeterminate because there are more unknowns to calculate than available equations of motion for the biomechanical system. Indeterminate systems present an infinite set of possible solutions, from which only one is the effectively adopted by the central nervous system of the subject when executing the task. The major difficulty, in this type of problems, is the identification of such solution. There are at least three possible approaches to this type of problems and for each one of these approaches there are several possible methods of implementation. Two possible approaches that can be used to obtain a solution of the indeterminate problem consist either in the reduction of the number of unknowns until a number equal to the number of available equations is obtained or, alternatively the increase of

the number available equations until a number equal to the number of unknowns is obtained. Although relatively simple in concept these two approaches present several drawbacks, in which the most relevant are: in the first approach, the reduction method, the loss of information regarding the unknowns that were grouped or removed; and in the second approach, the difficulty to obtained and evaluate the additional equations (Tsirakos *et al.*, 1997).

The third possible approach is the use of optimization methods. The aim of optimization techniques is to find, from all the possible solutions, the one that minimizes a prescribed objective or cost function, subjected to a certain number of restrictions or constraints. This approach is the one used in this work to calculate the redundant muscle forces in the muscle apparatus of the lower extremity and is briefly described in the forthcoming sections. For more detailed descriptions of the optimization methodologies, the interested reader is referred to more specialized literature (Arora, 1989; Haftka and Gurdal, 1992; Tavares and Correia, 1986; Vanderplaats, 1984).

6.6.1 General Optimization Problem

Mathematically, a general optimization problem can be formulated as (Arora, 1989; Haftka and Gurdal, 1992):

$$\begin{aligned} &\text{Given:} && \mathbf{x} = \{x_i\} \quad \wedge \quad i = 1,...,n_{cv} \\ &\text{Minimize:} && \mathcal{F}_0(\mathbf{x}) \\ &\text{Subject to:} && \begin{cases} f_j(\mathbf{x}) = 0 & j = 1,...,n_{ec} \\ f_j(\mathbf{x}) \geq 0 & j = (n_{ec}+1),...,n_{ic} \\ x_i^{lower} \leq x_i \leq x_i^{upper} & \end{cases} \end{aligned} \tag{6.14}$$

where $\mathbf{x}$ is the vector containing the control variables, $\mathcal{F}_0(\mathbf{x})$ is the objective or cost function to be minimized and $f_j(\mathbf{x})$ are the constraint equations that the control variables need to fulfill. There are a total number of n_{cv} control variables x_i, being each one of them

respectively bounded between x_i^{lower} and x_i^{upper}, the so-called side constraints. There is a total number of n_{tc} constraint equations $f_j(\mathbf{x})$, from which n_{ec} are of equality type. In an optimization problem, the total number of constraint equations is necessarily smaller than the number of control variables (i.e., $n_{tc} < n_{cv}$), meaning that $f_j(\mathbf{x})$ represents an indeterminate system of equations (Tavares and Correia, 1986). The optimal solution corresponds to the vector of control variables $\mathbf{x}^*$ that minimizes the cost-function $\mathcal{F}_0(\mathbf{x})$ and at the same time fulfils the restrictions imposed by the constraint equations $f_j(\mathbf{x})$.

If the objective function and the constraint functions depend linearly on the control variables, then the optimization problem is said to be linear and it is commonly represented by letters LP (meaning Linear Programming). Conversely, if the objective function presents a non-linear dependency on the control variables, then, independently of the type of dependency observed in the constraint equations, the optimization problem is said to be non-linear, and it is commonly represented by the letters NLP (meaning Non-Linear Programming). Additionally, optimization problems can be divided in two distinguished groups: constrained optimization problems, when there is a set of equations that the control variables must fulfill and unconstrained optimization problems, when the only objective is to minimize the cost function.

Historically, due to restrictions regarding the available computer power, many authors have been confined to the use of LP optimization techniques in the solution of the redundant problem in biomechanics (Tsirakos *et al.*, 1997). However, due to several mathematical limitations – in which the most relevant has to do with the fact that any optimal solution to a LP problem must lie at the intersection of two or more constraint equations and therefore cannot be located in the interior of the feasible design space (Haftka and Gurdal, 1992) – LP algorithms are considered to be inadequate in the estimation of the force sharing problem, not predicting the co-activation of agonist (synergistic) and antagonist muscles (Tsirakos *et al.*, 1997). For this reason, in this work the 'redundant problem in biomechanics' is addressed and formulated as a constrained NLP problem.

6.6.2 Cost-Functions and Optimization Constraints

The minimization of cost functions simulates the physiological criteria adopted by the central nervous system when deciding which muscles to recruit and with what level of activation, to produce the adequate motion or posture for the task being undertaken. Several cost functions have been used by researchers in the study of the redundant problem in biomechanics (Collins, 1995; Crowninshield and Brand, 1981; Yamaguchi *et al.*, 1995). The selection of the most appropriate criterion to use in the optimization process resides upon several important aspects such as the type of motion under analysis, the objectives to achieve or the presence of any type of pathology. For instance, if the subject under analysis suffers from severe pain in the knee joint – due to pathologies in the articular layers of the patellar and femoral surfaces of this joint – then its central nervous system is, most probably, adopting an activation of the muscle apparatus that contributes to the minimization of the pain in the referred joint. Therefore, a possible criterion could be the minimization of the reaction forces at the defected knee joint, which definitely would contribute to a minimization of the knee pain. In a normal gait example, the central nervous system is probably more interested in maximizing the comfort, i.e., the muscle endurance, and therefore, minimizing the muscle fatigue. In this example two possible criteria could be the minimization of the total muscle stress or the minimization of the total muscle force, which is generally accepted to be closely related with the minimization of the muscular fatigue (Crowninshield and Brand, 1981; Yamaguchi *et al.*, 1995).

The two previous examples show that each human task is thoroughly controlled by the central nervous system using a particular criterion or a set of criteria. This is one of the reasons justifying the existence in the literature of so many different cost functions and also the reason to believe that many more are yet to be identified. A cost function should be able to reflect the inherent physical activity or pathology as well as it should be able to include relevant physiological characteristics and functional properties such as the maximum isometric force or electromyographic activity, respectively (Tsirakos *et al.*, 1997). From the computational point of view, a cost function should also be numerically stable and provide

small evaluation times. Some of most commonly used, non-linear, cost functions are presented hereafter:

i) Sum of the Square of the Individual Muscle Forces:

$$\mathcal{F}_0 = \sum_{m=1}^{n_{ma}} \left(F_{CE}^m \right)^2 \tag{6.15}$$

This cost function was initially presented by Pedotti et al. (Tsirakos *et al.*, 1997), for applications to the human locomotion, and its minimization is considered to fulfill the objective of energy minimization. However, this cost-function does not include any physiological or functional capabilities (Tsirakos *et al.*, 1997).

ii) Sum of the Cube of the Individual Average Muscle Stresses:

$$\mathcal{F}_0 = \sum_{m=1}^{n_{ma}} \left(\sigma_{CE}^m \right)^3 \tag{6.16}$$

This cost function, introduced by Crowninshield and Brand (1981), is based on a quantitative force-endurance relationship and on experimental results. It includes physiological information, namely the value of the physiological cross sectional area of each muscle. According to the authors, this cost-function is able to predict co-activation of muscle groups in a more physiologically realistic manner (Tsirakos *et al.*, 1997).

iii) Sum of the Square of the Individual Normalized Muscle Forces:

$$\mathcal{F}_0 = \sum_{m=1}^{n_{ma}} \left(\frac{F_{CE}^m}{F_0^m} \right)^2 \tag{6.17}$$

This cost function, also proposed by Pedotti et al. (Tsirakos *et al.*, 1997), is similar to the function provided in Equation (6.15) but includes some physiological information, namely the maximum isometric force that each muscle is able to produce.

iv) Sum of the Square of the Individual Muscle Forces Normalized by the Maximum Instantaneous Muscle Moment:

$$\mathcal{F}_0 = \sum_{m=1}^{n_{ma}} \left(\frac{F_{CE}^m}{M^m} \right)^2 \tag{6.18}$$

This cost function, proposed by Herzog (Tsirakos *et al.*, 1997), has the important particularity of including physiological and functional information. The calculation of the maximum instantaneous moment that the muscle is capable to generate not only requires the use of the maximum isometric force for that muscle but also its instantaneous moment arm that is closely related to the observed kinematics and therefore with the function of that specific muscle.

v) "Soft saturation" Cost Function:

$$\mathcal{F}_0 = \sum_{m=1}^{n_{ma}} \sqrt{1 - \left(\frac{F_{CE}^m}{F_0^m} \right)^2} \tag{6.19}$$

This cost function was proposed by Siemiensky (Tsirakos *et al.*, 1997). According to the author, the minimization of this cost function, which includes physiological information regarding the maximum isometric force of each muscle, produces a more realistic synergistic function of the muscle in particular in what the activation and co-activation of muscles is concerned.

Alternatively to the functions proposed in Equations (6.15) through (6.19), cost functions can also be the sum of the instantaneous muscle power or the sum of the square of the total reaction forces at the joints. For a comprehensive discussion on this subject the references (Collins, 1995; Tsirakos *et al.*, 1997) are of major interest.

In the present work the principle of minimization of the sum of the square of the muscle forces (Collins, 1995) and the principle of minimization of the sum of the cube of the individual muscle stresses (Crowninshield and Brand, 1981) are used in applications

involving human locomotion. Substituting Equation (6.9) in Equations (6.15) and (6.16), the following mathematical expressions for the referred cost functions are obtained:

$$\mathcal{F}_0 = \sum_{m=1}^{n_{ma}} \left(F_{CE}^m \right)^2 = \sum_{m=1}^{n_{ma}} \left(\frac{F_L^m F_{\dot{L}}^m}{F_0^m} a^m \right)^2 \tag{6.20}$$

$$\mathcal{F}_0 = \sum_{m=1}^{n_{ma}} \left(\sigma_{CE}^m \right)^3 = \sum_{m=1}^{n_{ma}} \left(\bar{\sigma} \frac{F_L^m F_{\dot{L}}^m}{F_0^{m\,2}} a^m \right)^3 \tag{6.21}$$

where n_{ma} are the number of muscle actuators and $\bar{\sigma}$ is the specific muscle strength with a constant value of 31.39 N/cm^2 (Yamaguchi, 2001). Note that only control variables associated with muscle actuators are used to evaluate the cost functions, although the complete set of variables also include the Lagrange multipliers associated with the rest of the kinematic constraints. Using these cost functions, the control variables associated with muscle actuators represent muscle activations and for that reason are bounded by side constraints to assume values between 0 and 1. No bounds are specified for the remaining variables.

In inverse dynamic analysis, the constraint equations that control variables must fulfill are the equations of motion of the biomechanical system. This means that in these problems, all the constraint equations are of equality type and in a number equal to the number of equations of motion, i.e., equal to the number of generalized coordinates defining the system. A vector containing all optimization constraints is defined as follows:

$$\mathbf{f} = \begin{Bmatrix} f_1 \\ \vdots \\ f_{n_{tc}} \end{Bmatrix} = \mathbf{\Phi}_\mathbf{q} \boldsymbol{\lambda} + \left(\mathbf{M}\ddot{\mathbf{q}} - \mathbf{g} \right) = \mathbf{0} \tag{6.22}$$

Equation (6.22) represents a set of linear equations on the control variables, represented by the vector of Lagrange multipliers. Hence, the gradients of these equations can be obtained

analytically, i.e., the gradient of vector **f** with respect to the control variables, is given by the Jacobian matrix of the constraints that is already calculated. This is written as:

$$\nabla_{\lambda}\mathbf{f} = \frac{\partial \mathbf{f}}{\partial \boldsymbol{\lambda}} = \boldsymbol{\Phi}_{\mathbf{q}} \tag{6.23}$$

This important result reveals that there is no need of calculating the sensitivities by finite differences or any other numerical method, because these quantities are already known, in analytical form, needing only to be introduced in the optimization process, without any additional calculation.

6.6.3 Methods for Solving Non Linear Optimization Problems

There are many numerical methods to estimate an optimal solution of a Nonlinear Optimization Programming (NLP) problem. One possible method, designated by Sequential Linear Programming (SLP), consists in approximating the NLP problem by a sequence of several LP problems that are subsequently solved iteratively. The simplicity of implementation of this method can be viewed as its main advantage, being the lack of robustness its major drawback (Arora, 1989). To overcome the drawbacks of the SLP approach, the modern and powerful Sequential Quadratic Programming (SQP) methods are being used with increasing success. The SQP is an iterative method that approximates the NLP problem as a sequence of Quadratic Programming (QP) subproblems, i.e., optimization subproblems with quadratic cost function and linear constraints, being the search direction for the SQP method, calculated using the Constrained Steepest Descendent (CSD) algorithm (Arora, 1989).

There are other optimization methods that can be applied to solve the NLP problem, namely the Method of Feasible Directions (MFD) or the Gradient Projection method (GP), just to mention two of them. The first of these methods is one of the classical approaches that can be applied to NLP problems, however, since it uses linear approximations, it is difficult to maintain the feasibility with respect to equality constraints (Arora, 1989). The second method uses a similar approach to the NLP problem but instead of calculating a feasible direction

using a solution of a LP problem (which in many cases is very time consuming), it uses an explicit expression that is obtained projecting the search direction into the subspace tangent to the active constraints (Arora, 1989; Haftka and Gurdal, 1992). This method provides search directions that are very simple to calculate, although less accurate than the ones produced by the MFD.

Many of the previous methods are not able to distinguish between local and global minima. Given an initial approximation, the method converges to the nearest optimal solution, which in many cases might not be the only one and, therefore, might not correspond to the global minimum. A procedure that is often used, when an optimization problem is thought to have several local minimums, is to start the optimization process with several different initial approximations. However, for optimization problems with many variables, not only the convergence to a global minimum is not fully guaranteed but also it becomes computationally more expensive. To overcome this problem, several modifications were introduced in many classical optimization methods, bringing them closer to achieve global convergence. At the same time, entirely new methods were developed using different approaches. Examples of that are the following globally convergent methods: the Method of Moving Asymptotes (MMA) (Svanberg, 1987, 1999), Genetic Algorithms (GA) (Raikova and Aladjov, 2002; Tavares and Correia, 1986) and the Feasible Directions Interior Point Technique (FDIPT) (Herskovits, 1998).

In the present work, three optimization packages are applied to the optimization of the redundant muscle forces: the DOT 5.0 - Design Optimization Tools (Vanderplaats, 1999), the routine DNCONG from IMSL Library (Numerics, 1995) and the MMA – Method of Moving Asymptotes (Svanberg, 1987, 1999). The first package is a well-known optimization program, widely used in the structural design community, which offers three optimization methods to solve the constrained NLP problem, namely the Modified MFD, the SLP and the SQP. The second package is a routine available in the IMSL-Mathematical and Statistical Library. This routine is based on a FORTRAN code by Schittkowski (1986), in which a SQP method is used to solve a NLP problem (Numerics, 1995). The method formulates and solves, iteratively, successive QP subproblems, which are obtained using a quadratic

approximation of the Lagrangian and a linearization of the constraints. The third package is a FORTRAN code that uses the globally convergent method of moving asymptotes with inner and outer iterations to solve a NLP problem (Svanberg, 1987).

Analytical gradients of the cost function and optimization constraint equations are supplied to the three optimization routines. If desired, the packages DOT 5.0 and DNCONG also allow for the numerical calculation of these quantities using finite differences.

6.7 Application Case to a Normal Gait Stride Period

The methodologies presented in this Chapter are applied to the normal cadence stride period presented in Chapter 5. As described before, the subject under analysis is a 25-year-old male with a height of 1.70 m and a total body mass of 70.250 kg. The subject is wearing running shoes. The trial starts at the time step just before right heel contact with the floor, and continues until the subsequent occurrence of the same foot. During the stride period, the subject has to walk over three force plates that measure the ground reaction forces for both feet. A total number of 66 frames are recorded with a sampling frequency of 60 Hz. The trial has a total duration of 1.083s that corresponds to a walking cadence of approximately 111 steps per minute.

The muscle forces developed in the right leg during the stride period are calculated using the cost-functions given by Equations (6.20) and (6.21), with the optimization constraints given by the equations of motion of the biomechanical system. The control variables representing the muscle activations have side constraints bounding their values between 0 and 1. Muscle actuators are introduced in the biomechanical model in order to describe the muscular apparatus presented in Table 6.1. Conversely, the joint actuators, used in Chapter 5 to guide the joints that are now crossed by the muscle apparatus, are now removed.

The three optimization methods of the DOT 5.0 package were experimented in this work. The results produced using the SLP method are considered to be the best ones obtained with this package. The DNCONG routine produced similar results to the DOT 5.0 package but with a much higher computational efficiency. The MMA code, possibly because of the

considerably high number of equality constrains of the present biomechanical application case, did not produce any result, suggesting that further and deeper research must be performed to identify the actual applicability of this global optimization method to the solution of the 'redundant problem in biomechanics'. Regarding the results produced by the two different cost functions, given in Equations (6.20) and (6.21), no significant differences were found. This result is in agreement with similar results and conclusions reported in the literature (Li, 1999; Raikova, 1999).

In Figure 6.16, the results obtained with the DOT 5.0 package and with the DNCONG routine from the IMSL mathematical library are presented, for comparison, using of the criterion of the minimization of the Sum of the Cube of the Individual Average Muscle Stresses as cost function. The results reported in Figure 6.16 refer to the muscles *Gluteus Minimus* (an abductor of the hip) and *Soleus* (a powerful plantar flexor of the ankle). In general terms, the muscle forces present a similar behavior, although different force levels can be identified. In terms of CPU time, the optimization package DNCONG took 45 seconds to optimize the 66 time steps, while the DOT package took approximately 2 hours to produce similar results.

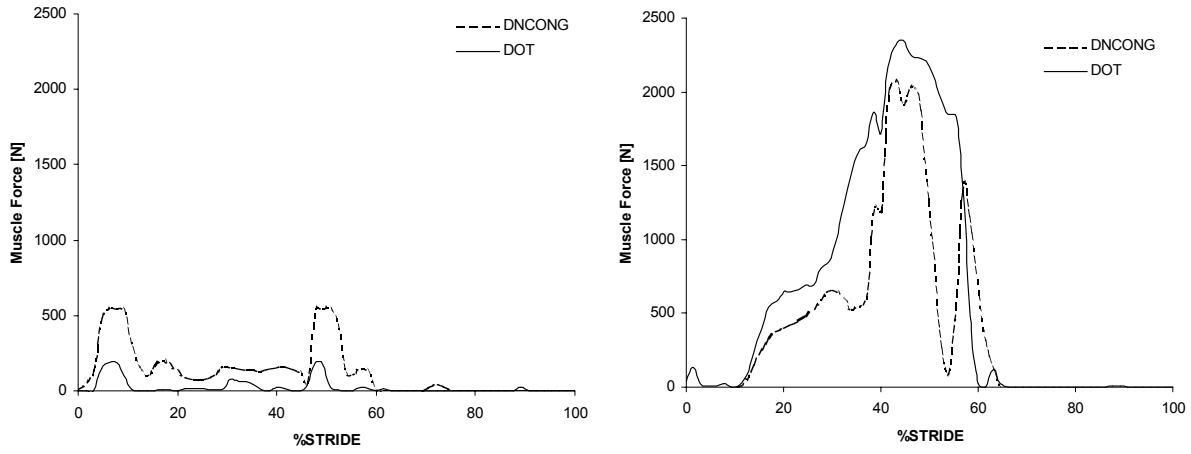

Figure 6.16: Redundant muscle forces obtained in two of the muscles of the lower extremity muscle apparatus: (a) *Gluteus Minimus*. (b) *Soleus*.

It should be noted that, in both packages, the net moments-of-force produced by the calculated muscle forces of the muscles crossing a specified joint is equal to the net moments-of-force calculated using joint actuators in the determinate inverse dynamics problem, as presented in Figures 5.28 to 5.30. This means that the results presented in Figure 6.16 are two possible solutions obtained by different optimization packages and that both solutions fulfill the equations of motion of the system.

In Figure 6.17, the activation patterns obtained for the complete set of muscles, used to describe the locomotor apparatus of the right leg, are presented. The comparison of the results obtained for the activations of the referred muscles, during the normal cadence stride period, with those obtained by other authors, and in particular with those provided by Crowninshield and Brand (1981), reveals a good agreement, i.e., it is observed that the activation patterns, shown in Figure 6.17, are similar to EMG activation patterns reported in the referred work for many of the muscles.

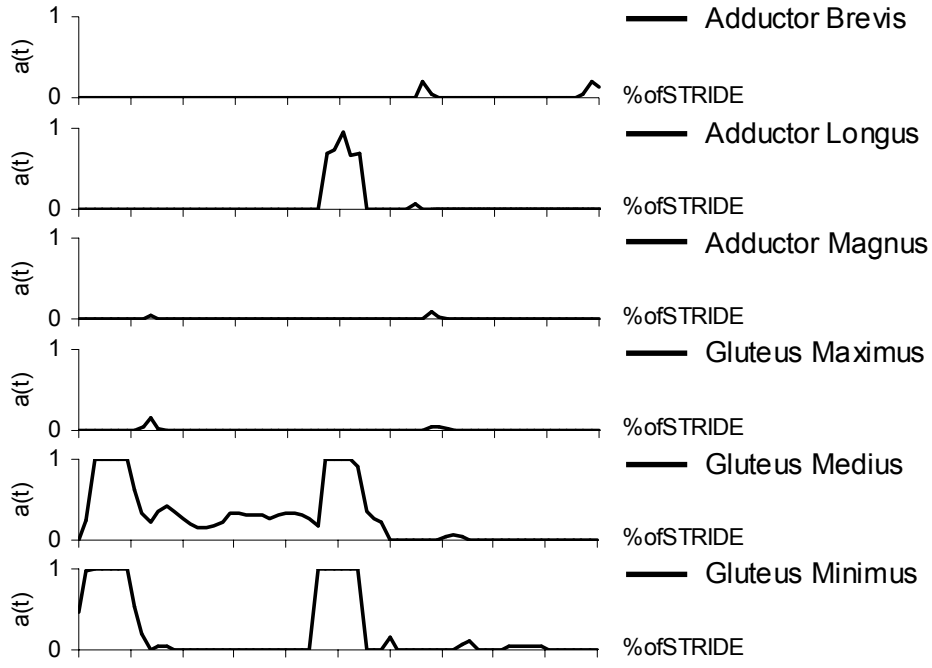

Figure 6.17: (cont.)

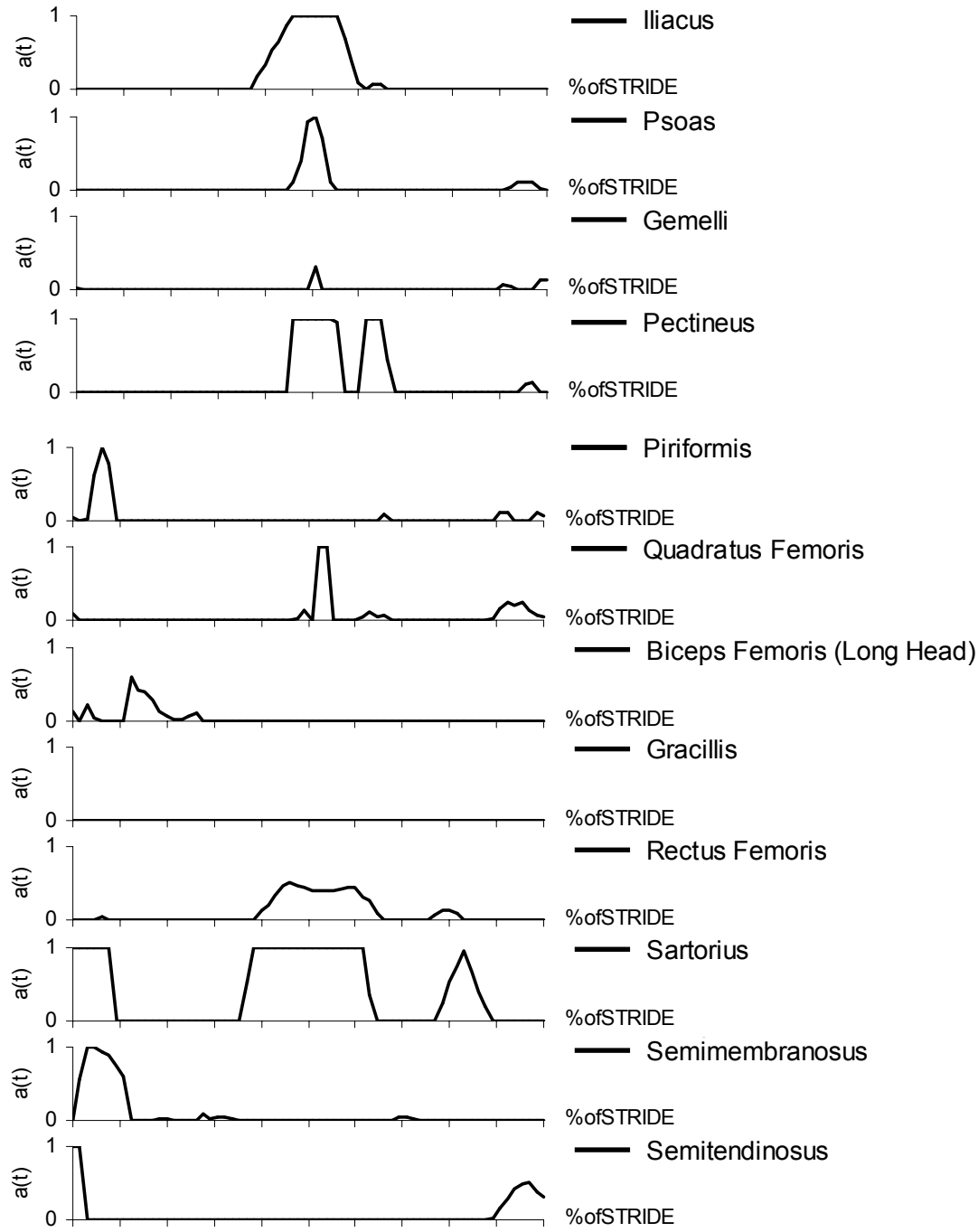

Figure 6.17: (cont.)

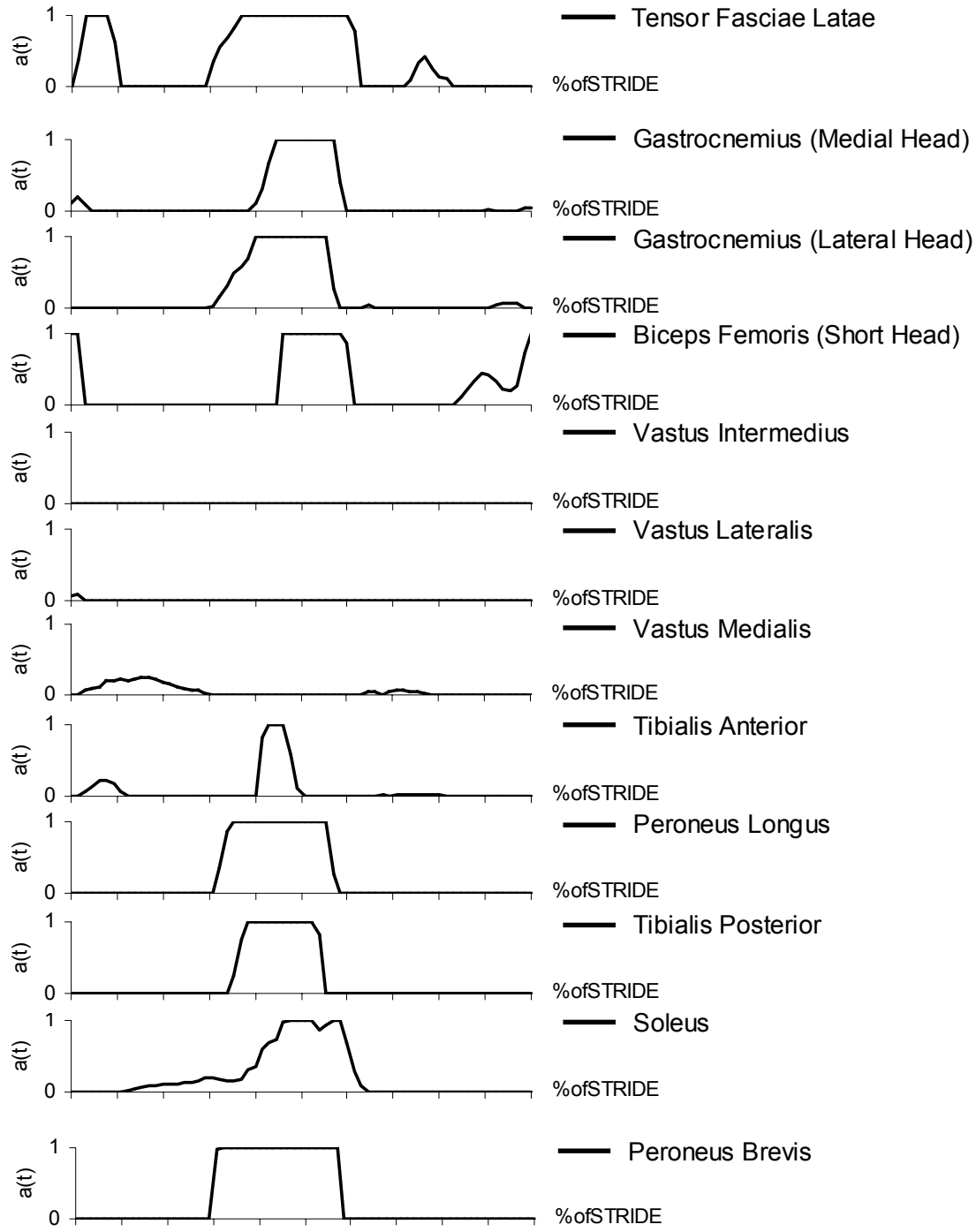

Figure 6.17: (cont.)

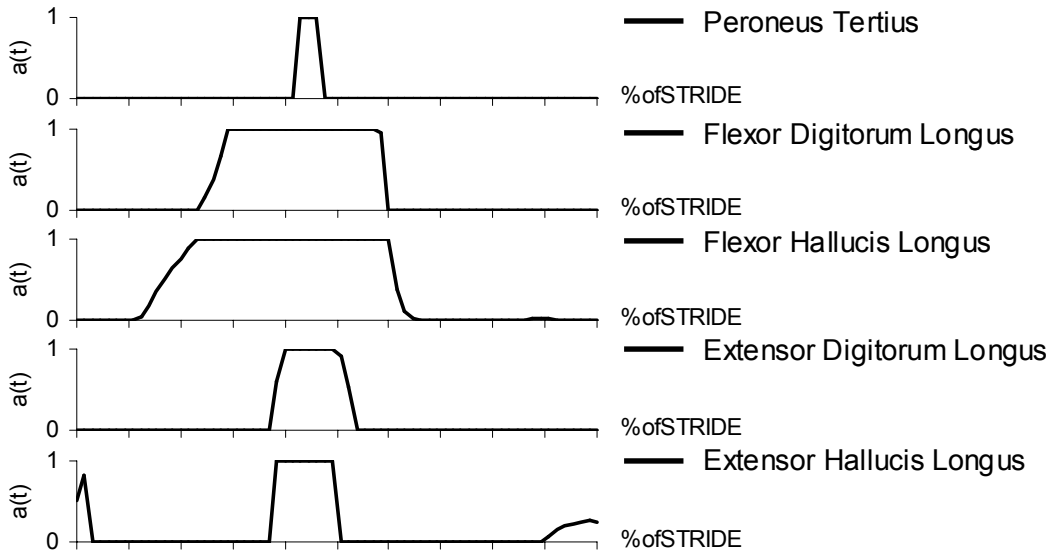

Figure 6.17: Activation patterns for the muscles of the locomotor apparatus (right leg).

As it was already described in this Chapter, the activation patterns for the muscles of the locomotor apparatus, represented in Figure 6.17, cannot be directly translated in to muscle forces, as these are also related with the muscle length and muscle contraction velocity by the force-length and force-velocity relationships, given in Equations (6.10) and (6.11). Hence, the forces of the complete muscle apparatus are displayed in Figure 6.18. Also in this case, the muscle forces obtained for many of the muscles described in Figure 6.18 are similar to the muscle forces reported by Crowninshield and Brand (1981). It is believed that most of the differences observed when comparing the results, are mainly due to the use of different optimization procedures and to the fact that the number of muscles used in the referred work are in a smaller number than the muscles used in the present biomechanical model. Additionally, the fact that the muscles in this work are represented, when necessary, with a complex path, conversely to the solution adopted in the referred work, in which the muscles are considered to be straight lines, may also have contributed to the reported differences.

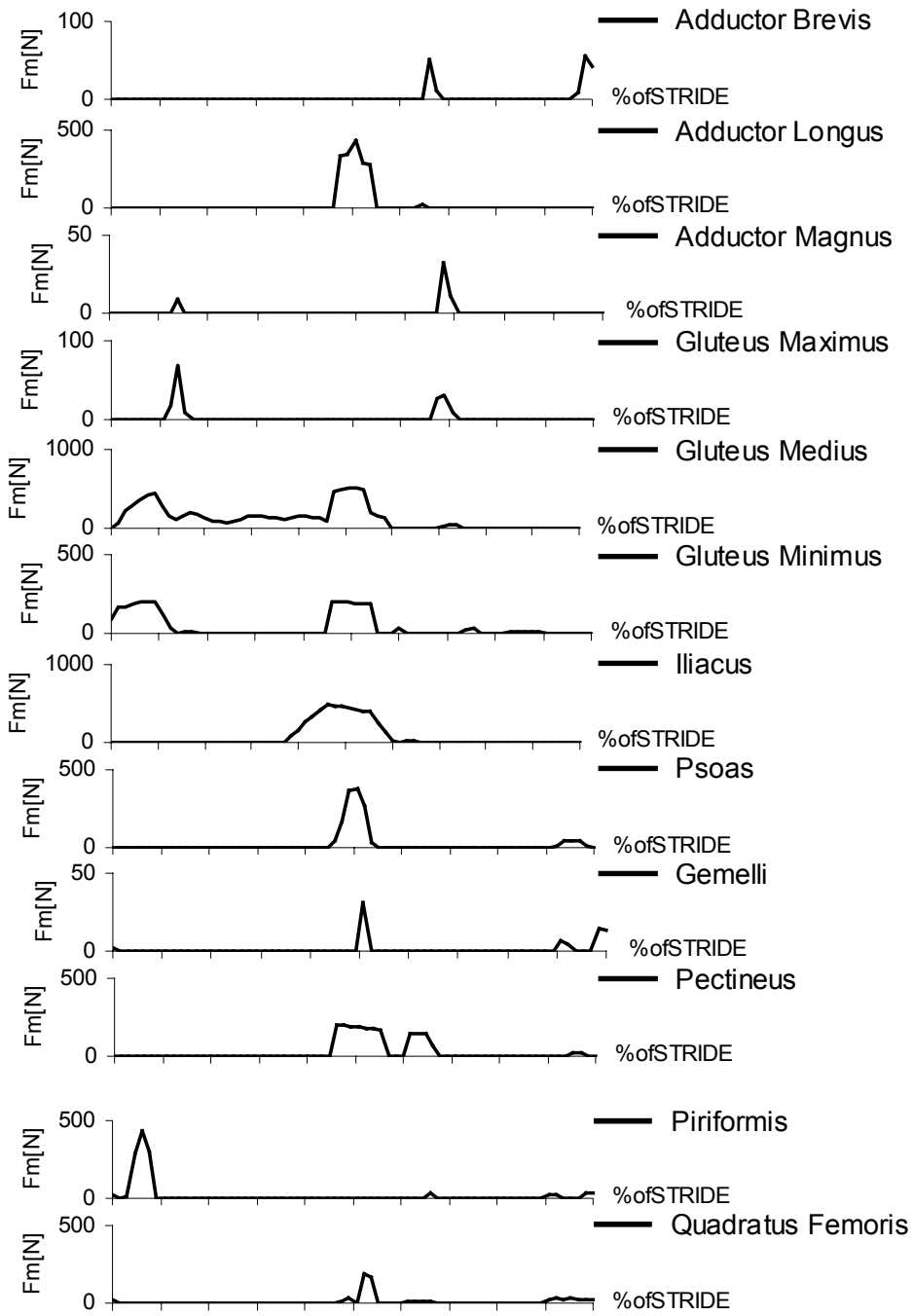

Figure 6.18: (cont.)

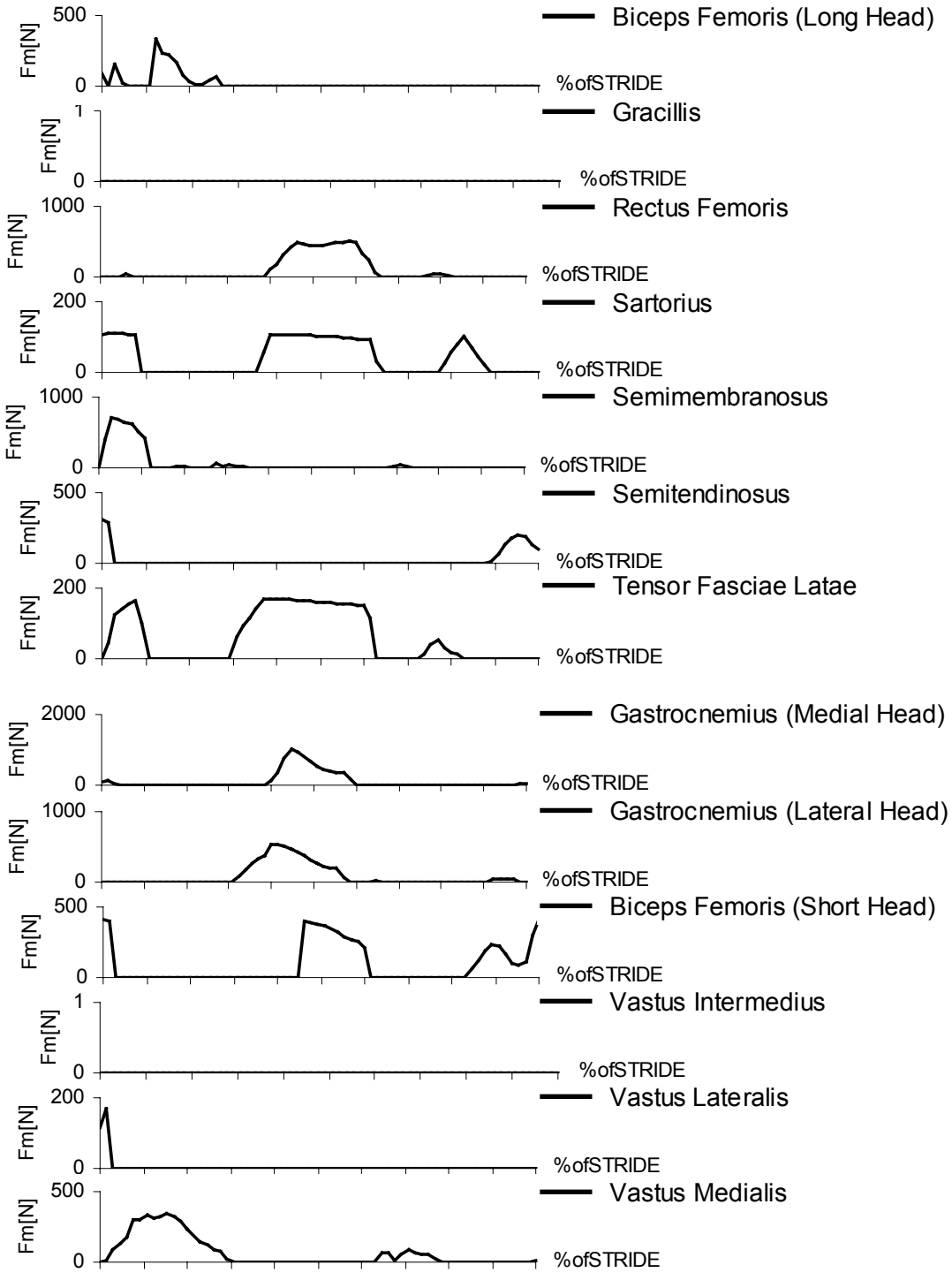

Figure 6.18: (cont.)

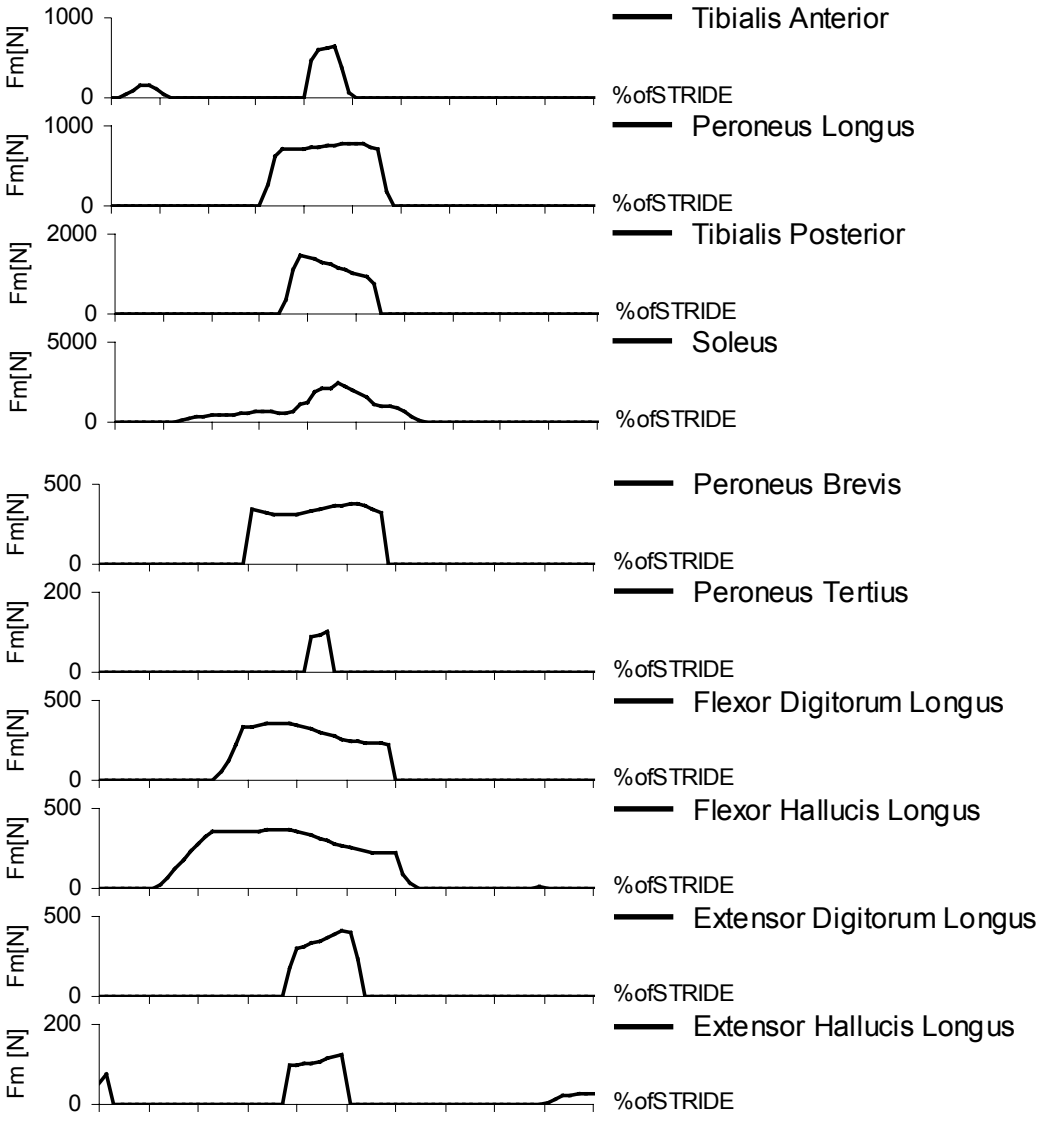

Figure 6.18:Muscle forces for the muscles of the locomotor apparatus (right leg).

6.8 Discussion on the Prediction of Muscle Forces by Different Approaches

In this section, the results obtained for the redundant muscle forces of the lower extremity muscle apparatus during the normal cadence gait cycle are discussed with reference to results obtained by other investigators. The analysis of the existing literature shows that the data

provided by many authors is not sufficient to perform a quantitative comparison between their results and the ones obtained in this work. In some cases only the temporal patterns of registered muscle activity are provided (Collins, 1995). In other cases, the muscle forces are presented but only in qualitative terms (Yamaguchi *et al.*, 1995), or in terms of their activation patterns (Anderson and Pandy, 2001a). However, in works where qualitative and quantitative information is provided, it is observed that the comparison of the results still may be difficult and misleading. To demonstrate this, the results obtained for the individual muscle forces are compared, whenever possible, with similar results provided in the works of Patriarco *et al.* (1981) and Crowninshield *et al.* (1981). The outcome of such comparison is presented in Figure 6.19 for the following muscles: Iliacus, Soleus, Adductor Brevis and Biceps Femoris (SH).

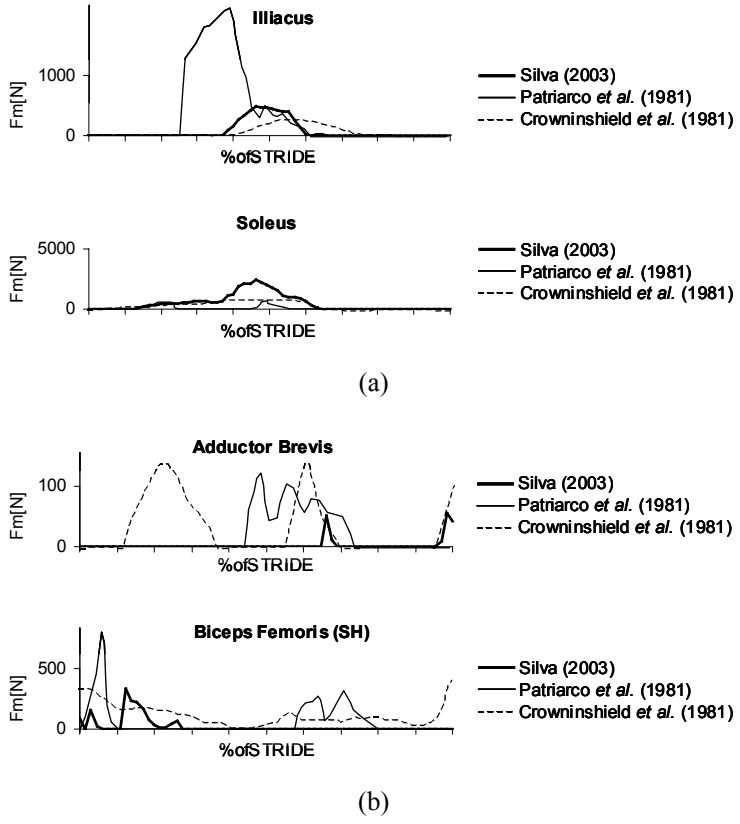

Figure 6.19: Comparison of results of individual muscle forces obtained by different authors during a normal gait stride period. (a) A minimum correlation is observed between the results of the different works. (b) No correlation is observed between the results of the different works.

The analysis of the muscle forces presented in Figure 6.19 shows that there are several muscles where a minimum correlation can be obtained between the compared works (see Figure 6.19(a)), but there are also some muscles where no correlation is found at all, even between the results presented by the referred authors (see Figure 6.19(b)).

The type of problems and difficulties in validating results against published data was already diagnosed in the literature. In its work, Patriarco *et al.* (1981) refers that comparisons between different approaches and results of different investigators are difficult. Pedersen *et al.* (1987), also refers that the solutions of the redundant muscle problem, predicted by different investigators, differ considerably for a variety of reasons, in which are included the use of different mathematical approaches, biomechanical models, input data, anthropometric models, acquisition devices, human subjects, muscle models, optimization techniques or objective functions.

A way of overcoming these difficulties is to compare the results for the redundant muscle forces, considering the physiological function of each muscle group and their action on the observed motion. With such purpose and for simplicity reasons, the muscles are grouped considering their most important function. Eight different muscle groups are assembled: the hip adductors, composed by the *adductor brevis*, *adductor longus*, *adductor magnus*, *pectineus* and *quadratus femoris*; the hip abductors, composed by the *gluteus minimus*, *gluteus medius*, *gemelli* and *piriformis*; the ilipsoas, composed by the *iliacus* and *psoas*; the *quadriceps femoris*, composed by the *vastus medialis*, *vastus intermedius*, *vastus lateralis* and *rectus femoris*; the hamstrings, composed by the *semitendinosus*, *semimembranosus*, *biceps femoris*, *sartorius* and *gracilis*; the *triceps surae*, composed by the *soleus* and the two heads of the *gastrocnemius*; the ankle plantar flexors (without the *triceps surae* group), composed by the *tibialis posterior*, *peroneus brevis*, *peroneus longus*, *flexor digitorum longus* and *flexor hallucis longus*; and the ankle dorsiflexors, composed by the *tibialis anterior*, *peroneus tertius*, *extensor digitorum longus* and *extensor hallucis longus*. The force developed by each one of these muscle groups as a function of the percentage of stride is represented in Figure 6.20.

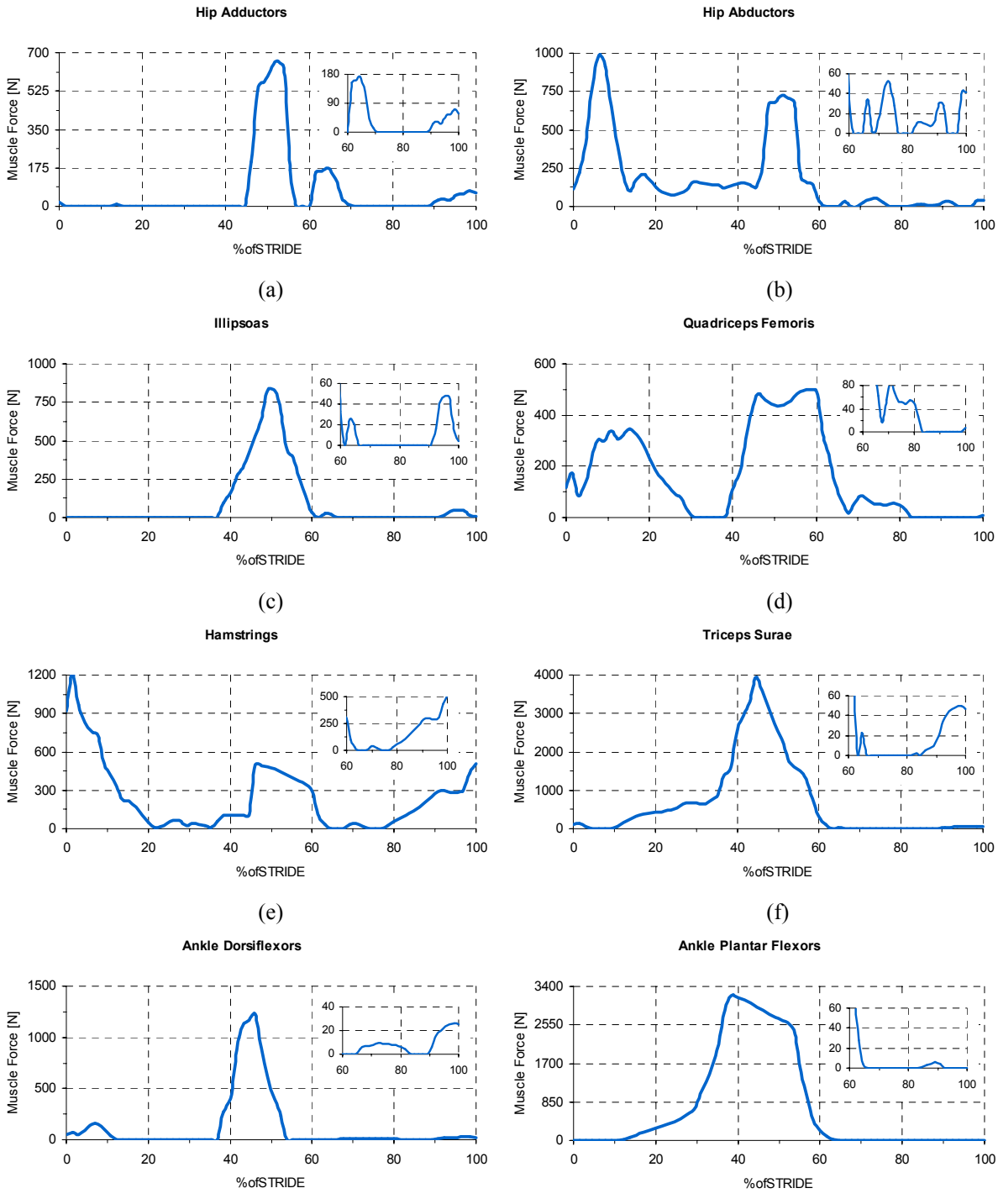

Figure 6.20: Muscle forces arrange by functional muscle groups. (a) Hip adductors; (b) Hip abductors; (c) Ilipsoas; (d) Quadriceps femoris; (e) Hamstrings; (f) Triceps surae; (g) Ankle dorsiflexors; (h) Ankle plantar flexors.

In the remaining paragraphs of the current section, the physiological analysis of the forces produced by the selected muscle groups is carried out. The results obtained are discussed and compared with an analogous description available in the literature (Palastanga *et al.*, 2002). Six important events occurring during the stride period are highlighted, considering their relevance for the physiological analysis that follows. These events are: the initial (right) heel-strike (HS) at 0% of stride, the opposite (left) toe-off (OTO) that occurs roughly after 15% of stride, the moment when the left foot passes a point immediately below the right hip joint (LFRH) at approximately 30% of stride, the opposite (left) heel-strike (OHS) that occurs at 50% of stride, the moment when the right foot passes a point immediately below the left hip joint (RFLH) approximately at 80% of stride, and the consecutive right HS at 100% of the stride period.

The results presented in Figure 6.20 allow to distinguish two major and distinct phases during the stride period. The *stance phase* that starts after right heel-strike (HS), at 0% of stride, and ends with right toe-off (TO), shortly after 60% of stride. The *swing phase* that starts after right TO and ends with the succeeding right HS at 100% of stride. The stance phase is characterized by high levels of muscle activation and consequently by high levels of muscle forces, which develop to support the body weight and to thrust the body forward. Conversely the swing phase is characterized by small levels of muscle activity and consequently by considerably small muscle forces. In this latter phase, the central nervous system takes advantage of the pendulum-like motion of the leg, using the momentum of the body to reduce muscular activity.

From the analysis of the graphics, it is observed that after initial HS, there is a contraction of the ankle dorsiflexors represented in Figure 6.20(b), which is carried out in particular by the *tibialis anterior* and *extensor hallucis longus*. This initial activity of the ankle dorsiflexors is aimed to support the arches of the foot, promoting its controlled landing on the supporting surface while ensuring the stability to the ankle joint. The initial activity of the *tibialis anterior* is also reported in the literature as being aimed to promote a slight inversion of the foot, which allows for the initial contact of the heel with the supporting surface to occur on its lateral side (Palastanga *et al.*, 2002).

After HS and before OTO there is muscular contraction of the hamstrings, as observed in Figure 6.20(e), which is carried out in particular by the *semimembranosus* and *biceps femoris* (long head). This contraction, together with the help provided by the momentum of the body, is responsible for the extension of the hip joint (Palastanga *et al.*, 2002). In the literature an activity of the *gluteus maximus* is also reported in this stage of the stride for fast cadence walking (Palastanga *et al.*, 2002). In the present results, considering the normal cadence of the gait period, such activity was not detected.

During almost all the stance phase, activation of the hip abductors is detected, as reported in Figure 6.20(b), with special emphasis on the *gluteus medius* and the *gluteus minimus*. This activity, which is stronger in the instants after HS and before TO, has the objective of maintain the pelvis in a more or less leveled position, allowing the opposite foot to be raised from the ground (Palastanga *et al.*, 2002).

Also during the stance phase and before LFRH, a co-activation of the antagonistic muscles *quadriceps femoris* and hamstrings is observed, as represented in Figure 6.20(d) and Figure 6.20(e). This muscular activity promotes the stabilization in the knee joint during the transference of the full body weight to the supporting surface as well as it produces a small flexion wave in the knee joint, as referred in the literature (Palastanga *et al.*, 2002).

During the stance phase, after OTO and until LFRH an activity of the ankle plantar flexors and in particular of the *soleus* is detected, as observed in Figure 6.20(h) and Figure 6.20(f). The objective of such activity is to control the pivoting of the right lower leg around the ankle joint and, in this way, to control the advance of the body, stabilizing at the same time the ankle joint (Palastanga *et al.*, 2002).

Right after LFRH a strong contraction of the ankle plantar flexors is detected. This powerful contraction, carried out in particular by the *triceps surae* group, as represented in Figure 6.20(f), is responsible to push the body forwards (Palastanga *et al.*, 2002). Moreover, near TO, a contraction of the *quadriceps femoris* group is also detected, as seen in Figure 6.20(d). This contraction is aimed to promote an extension of the knee joint almost until its limit and to keep it almost fully extended while the powerful thrust from the foot is

being transmitted to the hip, pelvis and trunk, which, due to their forward inclination are pushed forwards and upwards (Palastanga *et al.*, 2002).

After TO and almost during all swing phase, a small activity of the ankle dorsiflexors is detected, as observed in Figure 6.20(g). This activity is promoted to maintain the foot in a more or less level position in respect to the lower leg. The reported activity slightly increases near the end of the stride in order to achieve a small dorsiflexion of the foot, preparing it to the next HS.

During all swing phase a general flexion of the hip joint is observed. This flexion is strongly aided by the momentum of the body and also by the hip adductors, specially the *pectineus*, and by the *iliacus*, between 60% and 70% of the stride, by the *rectus femoris* between 70% and 80% of the stride, by *sartorius* between 80% and 90% of the stride and finally by the *psoas* between 90% and 100% of stride, as reported in Figure 6.20(a) and by Palastanga *et al.* (2002).

Still during the swing phase, in order to promote a lateral rotation of the hip, an activity of the hip abductors is also detected between 70% and 100% of the stride (Palastanga *et al.*, 2002). This activity is observed in Figure 6.20(b) and results first from the activation of the *gluteus medius*, after by the activation of the *gluteus minimus* and *piriformis* and in the latter stage by the activation of the *piriformis* and *gemelli*.

As seen in Figure 6.20(d), some muscular activity is also detected in the *quadriceps femoris* group during the swing phase, shortly after TO and until RFLH. The aim of this activity is to promote an extension of the knee joint and, at the same time, to increase the angular velocity around the knee joint of the lower leg and foot.

At the end of the swing phase, after RFLH and until next HS, an increased activity of the hamstrings is registered as represented in Figure 6.20(e). This activity is used to decelerate the lower leg and foot, reducing their angular velocity, until an almost stop near a position corresponding to the almost full extension of the knee, immediately before HS.

In summation, from a quantitative point of view, the comparison of results with those reported by other investigators, is difficult and eventually misleading. If there are cases of individual muscle forces for which a minimum correlation can be found between all works,

there are other muscles for which no correlation can be obtained at all, even when comparing the results among the other referred investigators. However, when the results obtained in this work, for the solution of the force-sharing problem and prediction of the individual muscle forces, are grouped in terms of their action and after that they are analyzed from a physiological point of view and compared with a similar procedure obtained from the literature, a strong agreement is observed in all the phases of the stride period and for every muscle group considered in the study.

6.9 Conclusions

In this chapter, a methodology was presented that allows for the calculation of the redundant muscle forces developed in a specific muscle apparatus of a subject describing a prescribed motion. The subject of the analysis was simulated using the inverse biomechanical model presented in Chapter 3. The model is driven through the prescribed motion using kinematic driver actuators of two types: joint driver actuators and muscle driver actuators. To each driver actuator is associated a Lagrange multiplier that, depending on the actuator type, represents, for the case of a joint actuator, the net moment-of-force produced by all the muscles crossing the specified joint, or, in the case of the muscle actuator, the muscle force associated with a specified muscle or muscle complex. Depending on the objectives of the analysis, the two types of actuators can be used independently or in a coexisting way.

Optimization techniques were proposed to solve the 'redundant problem in biomechanics' with analytical cost-functions representing the action of the Central Nervous System. These techniques present a powerful tool that allows for the selection, from the infinite set of possible solutions, the one that minimizes the associated cost-function.

Although not used in this work, it is believed that optimization techniques based in Genetic Algorithms (GA) may reduce the computational costs associated with the calculation of a solution for the redundant problem in biomechanics. It is well known that the global convergence feature of these algorithms is partially due to the increased number of possible designs that is initially considered, meaning that an increased number of function evaluations is expected for problems with populations of considerable size. Therefore, an increasing

performance is expected in optimization problems with cost functions with small evaluation periods, such as the ones proposed in this work. In fact, the cost functions arising in this type of biomechanical applications have smaller evaluation periods when comparing, for instance with structural design analyses, in which several Finite Element Analysis must be carry out for the evaluation of a single cost function.

Finally it should be mentioned that in this work only single criterion optimization problems were considered. However, it is well known that in many of our daily life activities the physiological response that is obtained is the result of the optimization (minimization or maximization) of several physiological criteria by the Central Nervous System. Therefore, there is a high potential in the use of multiple criteria optimization procedures to solve the indeterminate biomechanical problem (Stadler, 1984).

Chapter 7

Conclusions and Future Developments

7.1 Conclusions

In this work, an integrated multibody methodology for the dynamic analysis of complex, three-dimensional, human motions was developed and demonstrated. In the framework of the proposed methodology, two types of problems have been analyzed: forward dynamics problems in which the principal aim is to calculate the dynamic response of the human body when submitted to external forces; and, inverse dynamics problems, in which the principal objective is to calculate the muscle-skeletal forces developed by the muscles and at the anatomical joints of the human body while performing a prescribed movement. The procedures presented lay their foundations in the use of reliable and accurate mathematical models of the human body, having the remarkable advantage of being able to obtain, without using intrusive techniques, qualitative and quantitative results regarding the human body structure and motion.

Comprehensive mathematical models of the human body were thoroughly described in this work using a general-purpose multibody formulation in which the position and orientation of the anatomical segments of the human body are represented using fully Cartesian coordinates.

This formulation, which allows for kinematic and dynamic analyses of three-dimensional mechanical systems to be performed, was chosen among other types of coordinates due to the advantages it presents in the description of biomechanical systems. It was observed that since rigid bodies are modeled as a collection of points and unit vectors, it becomes very convenient, in biomechanical applications, to use the location of important anatomical landmarks, such as joints and extremities, directly in the construction of the rigid bodies describing the anatomical segments of the biomechanical model. Other important features of the proposed multibody formulation, that are not specific to biomechanical modeling, are: the inexistence of angular variables, which simplifies the mathematical formalism inherent to the formulation, at the same time it increases its efficiency from the computational point of view; the possibility of sharing points and vectors between rigid bodies, which reduces the total number of generalized coordinates and kinematic constraint equations, at the same time it defines simple kinematic joints in a natural way; and the quadratic or linear nature of the kinematic constraint equations, which contribute to the construction of a Jacobian matrix with linear or constant dependency on the generalized coordinates.

The multibody formulation used in the definition of the biomechanical models follows the methodologies described by Jalón and Bayo (1994). An alternative perspective for the use of these coordinates, suggested by Silva and Ambrósio (2003a), introduces simplifications in the definition of rigid bodies, mass matrices, kinematic joint constraints and kinematic drivers. This new perspective shortens the gap existing between formulations using fully Cartesian coordinates and formulations using standard Cartesian coordinates in terms of the definition of the inputs for the models, at the same time it preserves all major advantages as well as the essence inherent to its original formulation. In order to reduce the kinematic constraint violation and handle redundant constraint equations, the Augmented Lagrange Formulation was included in the multibody formulation. This formulation consists is an iterative procedure for the stabilization the equations of motion that does not fail near a singular position or in the present of redundant kinematic constraints.

A general-purpose gross-motion simulator was developed in a FORTRAN computer code, using the described multibody formulation with fully Cartesian coordinates. This numeric

tool was the supporting computational framework for all the kinematic and dynamic analyses performed in this work.

A comprehensive anthropometric model, described with sixteen three-dimensional anatomical segments, was used to characterize the principal physical characteristics and anthropometric dimensions of the human body. The information regarding these properties is contained in a database and it refers to the fifty percentile human male. Besides the most important anthropometric data, the referred database also includes the information regarding the joint motion-limiting moments, used to prevent the models from achieving unfeasible postures or movements. The database can be expanded any time the anthropometric data of a particular individual is obtained. Therefore, it can accommodate other anthropometric models with different percentiles and/or different physiological characteristics that are introduced to reflect their gender, age, disabilities or pathologies. Alternatively, it was seen that the anthropometric dimensions of the subject under analysis could be explicitly provided to the gross-motion simulation tool, being the database information, regarding the anthropometric model, used to scale complementary anthropometric data for the subject such as center-of-mass locations and moments of inertia of the anatomical segments.

It was seen that, in order to allow the application of the proposed methodology to the two different types of dynamic analyses, two distinct biomechanical models, with different kinematic structures and topology, were required: the *forward biomechanical model*, with twenty-nine degree-of-freedom and a straightforward structure made of twelve rigid bodies, interconnected by revolute and spherical joints; and, the *inverse biomechanical model*, with forty-four degrees-of-freedom and a more detailed kinematic structure made of thirty-three rigid bodies, interconnected by revolute and composite joints. The kinematic structure of the former biomechanical model was proposed considering the type of the applications foreseen in impact biomechanics, in which the computational time required to integrate the equations of motion of the system can be substantially reduced using biomechanical models with simple kinematic structures. Regarding the kinematic structure of the latter model, it was observed that the proposed structure is the result of a more detailed description of the wrist and ankle joints and of the replacement of every spherical joint by an equivalent composite joint made

of a revolute and a universal joints and an additional rigid body. This replacement is necessary due to the fact that, since the motion used in this type of analyses is obtained from direct measurements of the human movement, then only mechanical joints with fixed axis of rotation, such as the case of the proposed composite joint, can be used in the representation of the model's anatomical joints.

In both biomechanical models, the relative motion between anatomical segments was described using a set of nominal or geometrical ideal joints. This type of joint description was adopted since it is considered to be the most suitable and efficient solution for the type of analyses foreseen, i.e., analyses involving gross-motion activities in which specific details of the joint motion are not an issue. Restrictions on the relative range of motion between different biomechanical segments were introduced using joint motion-limiting moments. These moments are applied between adjacent anatomical segments, anytime their relative position is detected to be outside the cone of feasible motion of the anatomical joint connecting them. This procedure is particularly important in forward dynamic analyses, since it prevents unfeasible human postures or movements to occur, and less relevant in inverse dynamic analyses since it was considered that during the execution of a normal activity, the anatomical joints never reach, or exceed, their natural limits. Finally, it should be mentioned that, in both models, Lagrange multipliers were associated to each nominal joint, which allow the calculation of the respective joint reaction forces, during the course of the analysis.

The proposed methodologies and biomechanical models were applied to the forward dynamic simulation of five selected case tests, which were considered to reflect a wide range of situations and scenarios. These test cases included a sportive activity, a complex vehicle rollover scenario and an accident reconstruction of a pedestrian run-over. The proposed test cases showed that the biomechanical models presented are suitable for use in many different application fields in which human activity is involved. A continuous contact/impact force model was used to describe the contact between anatomical segments and between anatomical segments and the surrounding environment. The combined use of the joint motion-limiting moments and the referred contact/impact force model results in numerically stable biomechanical models, suitable to be used in a wide variety of scenarios, where contact of the

human body plays an important role. However, more investigation is required to identify the relative range of motion between adjacent anatomical segments. Also, a better characterization of the mechanical properties and geometry of contacting surfaces is required. It was also observed that, using the proposed methodologies an effective coupling between the biomechanical models and other complex mechanical systems, such as an automotive vehicle or a bus, is successfully achieved. The methodologies proposed showed to be flexible and numerically efficient to simulate the coupled motion of the vehicle and occupant under severe impact conditions. The results obtained, predict a realistic motion for the occupant and vehicle as well as force and acceleration levels comparable to those reported in the literature. Regarding the results obtained for the accident reconstruction case, a good correlation was observed with the witnesses' testimonials of the actual accident. Moreover, it is expected that the inclusion of reflexive muscle activation in the actual biomechanical model, will contribute to a decisive improvement of the human response to impact. The rollover case-tests have also demonstrated that realistic initial positions, based on experimental data, can be incorporated in the simulation using the Direct Linear Transformation technique, usually applied in inverse dynamic analyses, to reconstruct the three-dimensional motion of the human body from a set of digitized anatomical points. However, special care should be put in the reconstruction process, in order to obtain initial positions and velocities consistent with the kinematic constraints of the system. Though the vehicle model used in the rollover simulation is fully validated, the results obtained for the kinematics of the biomechanical models lack validation, as they do not correspond to any situation experimentally analyzed in great detail. Nevertheless, provided that the vehicle model can include airbags and/or intelligent restraint systems, the models proposed and the techniques associated to them are valuable tools to evaluate the performance of such systems in face of out-of-position occupants. Moreover, due to the ease and flexibility in the reconstruction of the initial conditions of out-of-position occupants, the methodologies proposed are also suitable to evaluate the sensitivity of several smart systems, whose behavior and function is designed to change according with the occupants' positions.

In the sequel of the proposed case-tests, several important mathematical models were introduced, which were fundamental for an accurate description of the interaction between the biomechanical model and the surrounding environment. These models consist on a contact/impact force model, a rigid seat model and a seat belt model. These models, not only provide a way to calculate the contact forces generated due to the interaction between the biomechanical model and the exterior, but also contribute for the stability of the integration procedure since they introduce damping and consequent energy dissipation, which eliminates the spurious high frequencies from the system's response. The test cases proposed were also used to introduce some injury levels required to quantify the potential risk of permanent injuries to occur in different anatomical segments of the biomechanical model. It was emphasized the importance that the evaluation of this type of indicators have in the early phases of design, when the shape of an impact surface or a specific material characteristic are still being investigated.

The application of the biomechanical models to the inverse dynamic analysis of the human motion was a major objective of the work now presented. It was shown that the set of input data required to this type of analysis is obtained experimentally by videotaping the human motion and by acquiring the external forces, applied over the human body, using force plates. The computational techniques, used in the treatment of the input data required for inverse dynamic analyses of biomechanical systems, were reviewed to identify sources of error in the results and propose solutions. Several techniques were suggested that reduce the problems associated to such uncertainties, while, at the same time they increase the accuracy and quality of the outcome of the analysis. The proposed numerical techniques were the Direct Linear Transformation technique, which is used to reconstruct the three-dimensional motion of the biomechanical system from two dimensional information obtained from at least two video cameras; the Butterworth 2^{nd} order low pass filter, which was the filtering technique that proved to play an essential role in the quality of the results, reducing the high frequency noise levels and smoothing the trajectory curves of the anatomical points; and the kinematic consistency technique, which was used to make the kinematic data coherent with the kinematics of the biomechanical model at any instant of the analysis.

These methods were presented within the framework of the biomechanical model selected and the multibody formulation used. It was seen that the use of fully Cartesian coordinates in the description of the model brings an additional advantage, since the reconstructed positions of the anatomical points correspond directly with the coordinates of the points defining the model. It was shown that the coordinate filtering procedure plays a very important role in the quality of the results and that different cutoff frequencies may lead to completely different results. Moreover, it was concluded that for normal cadence gait analyses, the use of cutoff frequencies ranging from 2 Hz to 8 Hz provide good results.

The kinematic consistency of the input data is also an important issue for the quality of the results of the inverse dynamic analysis. It was shown that the consistency of the kinematic data led to results with better quality. In particular, the positions of the anatomical points must be consistent with the biomechanical model's constraint equations, or otherwise, spurious reaction forces are obtained. However, for the calculation of the consistent velocities and accelerations, no significant differences were found between the two proposed procedures, being the direct spline differentiation more attractive because of its simplicity and efficiency. To conclude, it was seen that the results obtained present a good correlation when compared with results of other authors, confirming that the techniques described can be applied to the inverse dynamic analysis of the human body motion with success. The kinematic consistency of the biomechanical model together with an appropriate filtering technique is, therefore, of major importance in order to achieve results with good quality.

In order to validate the proposed inverse dynamic analysis procedure, an alternative methodology based in classical dynamics techniques was applied to the gait input data. The results produced by the two independent methods were compared for the solution of the joint reaction forces and joint moments-of-force of the biomechanical model considered. It was concluded that for the multibody methodology, the inverse dynamic problem was solved for the whole biomechanical model with the equations of motion being assembled in a systematic way and solved as a whole system; while in the classical dynamics technique, the balance of forces and moments was performed sequentially and independently at each individual anatomical segment. The comparison of the results obtained by both methods showed a very

good correlation, leaving the idea that the proposed multibody methodology appears as a compromise solution to calculate the reaction forces and the net moments-of-force at the joints of the biomechanical model. Computationally, the multibody methodology is not expensive and it can be efficiently used in more complex biomechanical models or in applications where the loop closure of the kinematic chain is required.

A sensitivity analysis was carried out to study the importance of the accuracy of the input data on the quality of the results produced by the inverse dynamic analysis of a human stride period. The sensitivity calculation of the system response due to perturbations introduced in the input data showed that only the net-moments of force in the joints belonging to the same kinematic chain of the perturbed parameter were affected. This shows that the methods used in the inverse dynamic analysis shielded the results in a particular biomechanical chain from perturbations occurring in other kinematic branches of the biomechanical model. It was not expected that the lack of precision in the reconstruction of the head spatial motion or in the definition of the inertia properties of an arm, would, for example, affect the evaluation of the forces and moments at the knee joints.

In order to simulate the imprecision of the input data, each parameter was independently perturbed and a new analysis was performed to evaluate the sensitivity of the results to that perturbation. It was shown that the inverse dynamic analysis results were very sensitive to errors made in the acquisition of the externally applied forces and their application points. Moreover, the quality of the gait analysis was also dependent on the precision of the spatial reconstruction of the anatomical point positions of the anatomical segments of the kinematic chains to which external forces were applied. It was observed that when there were no external forces, for instance during the aerial trajectory of a leg, the sensitivity of the net moments-of-force to imprecision in the anatomical points' positions became meaningless. The most common errors resulted from uncertainties in the segment body mass and inertia, errors in the reconstruction of the spatial coordinates of the digitized points and inaccuracies in the acquisition of the externally applied forces and respective application points. The model's response was comparatively much less sensitive to errors in the estimation of the mass of the anatomical segments and even those kinematic chains that had external forces

applied to them. This indicates that the sensitivity of the gait analysis results to different tables of anthropometric data is relatively low.

In conclusion, major improvements in the quality of gait analysis results can be obtained by: improving the evaluation of the points of application of ground reaction forces; increasing the precision of spatial reconstruction of the anatomical points associated to the anatomical segments in the kinematic chains where external forces are applied; improving force acquisition, and including the synchronization between kinetic and kinematic data. The improvement of the precision with which other anatomical parameters are obtained, such as the spatial position of joint anatomical points in kinematic chains in which no external forces are applied, or of anthropometric parameters such as the anatomical segments masses, play a relatively less important role in the improvement of the quality of the gait results.

The inverse dynamics analysis procedure was also extended to the calculation of the redundant muscle forces developed, in a particular muscle apparatus, of a subject performing a prescribed activity. It was seen that the inclusion of additional muscle driver actuators lead to an indeterminate system of equations of motion. Optimization techniques were proposed to solve the "redundant problem in biomechanics" with analytical cost-functions simulating the action of the Central Nervous System. These techniques present a powerful tool that allows for the selection, from the infinite set of possible solutions, the one that minimizes a specified cost-function used to simulate the decisions made by the Central Nervous System of the subject during the analysis period.

From the analysis of the results obtained for the redundant muscle activation patterns and associated redundant muscle forces, it was concluded that the comparison of the results obtained for the activations of the referred muscles, with those obtained by other authors, and in particular with those provided by Crowninshield and Brand (1981), reveals a good agreement, i.e., it is observed that the activation patterns are similar to EMG activation patterns reported in the referred work for many of the muscles. With respect to the redundant muscle forces, it was also concluded that these are similar to the muscle forces reported by Crowninshield and Brand (1981). It is believed that some of the differences that were observed are mainly due to the use of different optimization procedures as well as to the fact

that the number of muscles used in the referred work are in a smaller number than the muscles used in the present biomechanical model. Moreover, the fact that the muscles in this work are represented, when necessary, with a complex path, conversely to the solution adopted in the referred work, in which the muscles are considered to be straight lines, may also have contributed to the reported differences.

Finally, in the present work, only single criterion optimization problems were considered. However, it is well known that in many of our living day activities the dynamic response that is obtained is the result of the optimization (minimization or maximization) of several physiological criteria by the Central Nervous System. Therefore, it can be advantageous to improve the quality of the results of certain types of applications, if multicriteria optimization routines were introduced in future simulations of indeterminate biomechanical problems.

7.2 Future Developments

Biomechanics is a complex interdisciplinary research field that only in recent decades has experienced its major developments. Therefore, when referring to future developments in this type of methodologies and formulations, there are essentially three major directions to follow: to produce research in new or barely touched areas related with biomechanics; to produce research in existing areas with the objective of improving the performance and accuracy of the existing methods and techniques; and to stimulate the interactivity between the different disciplines that contribute to biomechanics, in order to develop more realistic models of biomechanical systems. Considering these three major guidelines, the following paragraphs are identified as subjects for future developments.

In order to increment the computational efficiency of the proposed multibody formulation, a different approach can be used to construct the bodies, mass matrices, kinematic joints and joint/muscle actuators. This alternative approach produces sparse leading matrices that suggest the use of sparse algorithms to solve the equations of motion of the system. The increment of the computational efficiency of the multibody formulation, combined with the increasing computer power will definitely stimulate the construction of more detailed biomechanical models, able to produce more reliable results in a wider range of applications.

Due to the format of the anthropometric database, it is possible to include in it a very large number of biomechanical models that describe particular individuals. Therefore, it also would be important to include other types of anthropometric models with different percentiles, different genders and ages. For certain types of simulations, such as the ones involving car crash accidents, it would be important to have anthropometric models describing the anthropometrics of children, pregnant women and crash test dummies. All these different anthropometric models would have different mass distributions, center-of-mass locations and joint limiting angles.

It would also be an important development if the anthropometric characteristics of the Portuguese population could be reflected in these anthropometric models. Such a development would require the creation of an expert team, of people with different backgrounds – including human motivity, medicine and engineering experts – that would conduct a survey to a specific sample of people, statistically obtained to reflect the total Portuguese population.

Regarding the biomechanical models, future developments can also be expected. The kinematic structure of the biomechanical models can be modified in order to improve the models' response in certain types of simulations. In simulations that involve specific details of the joint motion, it would be important to incorporate a detailed joint description, in which the relevant aspects of the geometry and physiology of the most important joints are considered.

The inclusion of a more detailed description of the human spine – cervical, thoracic and lumbar – would lead to important improvements. This could be achieved using a rigid multibody approach, in which each vertebrae or set of vertebras is modeled as a rigid body interconnected by specific kinematic joints or, alternatively, by specific sets of non-linear spring-dampers. The use of a flexible multibody approach, in which a group of vertebras is modeled as a flexible body, would be an alternative modeling technique. However, this second approach would also require the implementation of flexible bodies in the gross-simulation tool. This detailed description of the human spine can be of great importance in the simulation of car crash accidents, since it increases the accuracy and reliability of the

injury criteria calculated for the spine, at the same time it allows for the estimation of the inter-vertebrae forces.

Additionally, it would also be important to provide biomechanical models with versatility that would allow the easy removal of a limb or part of it. This characteristic would be very important in simulations involving the inverse dynamic analyses of clinical cases with disabilities such as amputations or malformations.

Regarding ergonomic aspects, such as the interaction between the biomechanical models and the surrounding environment, it would be an important development to improve the contact/impact force models in order to include the possibility to provide complex descriptions of the contact surfaces. This development not only involves the introduction of other methods for the geometric description of surfaces but also the improvement of the contact detection procedures. Moreover, it would be important to introduce other types of contacting interfaces such as airbags, flexible seats and general deformable structures.

Regarding the input data acquisition for inverse dynamic analyses, it would be important to put together, in one single integrated tool, the three-dimensional motion reconstruction technique and the kinematic consistent position, velocity and acceleration correction procedure. This integrated tool could use optimization techniques to calculate the optimal solution (for the subject's kinematics) that minimize the distance between digitized positions, fulfilling at the same time the kinematic constraints inherent to the biomechanical model. Additionally, the filtering technique could also be integrated in this enhanced motion reconstruction tool, in such a way that the reconstructed motion not only minimizes the referred objective function but it also maximizes the smoothness of the trajectory curves, fulfilling the kinematic constraints of the biomechanical model.

Another important development that could be introduced at the level of the acquisition of input data for the inverse dynamic analysis is the optimization of the point of application of the external forces or ground reaction forces in the case of gait analyses. It was observed in this work that the calculation of the moments of force at the joints of the biomechanical model is very sensitive to small changes in the point of application of these external forces. Moreover, it was also observed that associated with the motion of the base body there are six

residual forces and moments, whose non-zero values are associated with inconsistencies generated between kinematic input data and dynamic input data. Therefore, a future development could be the calculation of the optimal center-of-pressure curve at the feet that would minimize the residual forces and moments observed in the base body.

Regarding the calculation of the redundant muscle forces, there are other issues that can also be improved. Starting from the cost functions used in the optimization procedure, it would be an important development the construction of new cost functions in which the physiological and functional components would be increased. Also regarding the cost functions, it would be important to develop specific cost functions that simulate the criteria used by the central-nervous system of individuals with pathologies at the neurological level. These cost functions, especially tailored to simulate cases with pathologies, would also require that complementary developments would be made to the muscle model used.

Another future development that should be considered is to use qualitative EMG information in the optimization procedure of redundant muscle force prediction. At a first stage the EMG information could probably be used for comparison of results, but in a later stage, it could be included in the optimization procedure as activation constraints, i.e., for muscles or muscle groups whose EMG information is available, their activation patterns should follow a pattern similar with the ones acquired during EMG recording. This development would be especially important in simulations involving subjects with pathologies and disabilities.

Another future development, regarding the calculation of the redundant muscle forces, would be to simulate the activation dynamics of muscles. At its actual stage, muscles are considered to have instantaneous activation characteristics, which is not what happens in reality. If activation dynamics were to be considered, the activation contraction patterns of each muscle would need to be corrected, in a post processing phase, in order to account the activation and relaxation delay of each muscle.

At the muscle model level, an important future development would be the introduction of tendons and the calculation of the tendon force during the execution of a prescribed task.

Testing other types of optimization routines is also regarded as a future development. In particular, the application of optimization techniques based in Genetic Algorithms can improve the optimization process significantly, reducing the total time of the analysis. It is well known that the global convergence feature of these algorithms is partially due to the increased number of possible designs that is initially considered, meaning that an increased number of function evaluations is expected for problems with populations of considerable size. Therefore, an increasing performance is expected in optimization problems with cost functions with small evaluation periods, such as the ones proposed here. Another development, considering the application of different types of optimization techniques, would be the use of multicriteria optimization for the solution of the redundant muscle forces, since it is considered that in many important human tasks the central nervous system makes its decisions by the optimization of more than one physiological criterion. Therefore, better performances are to be expected in the simulation of the behavior of the central nervous system if a multicriteria approach is used.

Finally, regarding the calculation of the redundant muscle forces, it would be an important development to consolidate the results produced with the inverse dynamic analysis approach with similar results produced using a forward dynamic analyses approach. In the later case, a dynamic optimization technique would be required, using a bilevel approach, i.e., optimizing not only the muscle forces necessary to produce the desired task but also the optimal motion or posture to perform the task. In parallel to the calculation of the muscle forces, several developments can be introduced to the muscle database, in terms of the description of muscle path, muscle shape and of the contact between muscles. Also important would be to extend the existing muscle database to other important muscle apparatus such as the upper limbs, the head-neck and the spine.

At a general level there are also several developments that can be implemented. At the present stage it is considered to be fundamental to extend the application of the methodology to different areas such as sport activities, ergonomics, bioengineering and physical rehabilitation. This step forward would definitely increase the level of expertise, as well as it would probably reveal other types of problems to research and solve.

References

Abdel-Rahman, E. and Hefzy, M., "A Two-Dimensional Dynamic Anatomical Model of the Human Knee Joint", *Journal of Biomechanical Engineering*, **115**, 357-365, 1993.

Addel-Aziz, Y. and Karara, H.,"Direct linear transformation from comparator coordinates into object space coordinates in close-range photogrammetry", *Symposium on Close-range Photogrammetry*, Falls Church, Virginia, 1-18, 1971.

Adolfsson, J., Dankowicz, H. and Nordmark, A., "3D Passive Walkers: Finding Periodic Gaits in the Presence of Discontinuities", *Nonlinear Dynamics*, **24**, 205-229, 2001.

Ait-Haddou, R., Binding, P. and Herzog, W., "Theoretical Considerations on Cocontraction of Sets of Agonistic and Antagonistic Muscles", *Journal of Biomechanics*, **33**, 1105-1111, 2000.

Aleshinsky, S. and Zatsiorsky, V., "Human Locomotion in Space Analysed Biomechanically Through a Multi-Link Chain Model", *Journal of Biomechanics*, **11**, 101-108, 1978.

Allard, P., Stokes, I. and Blanchi, J.-P., *Three-Dimensional Analysis of Human Movement*, Human Kinetics, Champaign, IL, 1995.

Alvarez, G., Gutierrez, A., Serrano, N., Urban, P. and Jalón, J.,"Computer Data Acquisition, Analysis and Visualization of Elite Athletes Motion", *Fourth International Symposium on Computer Simulation in Biomechanics (satelite event of the XIVth ISB Congress)*, Montlignon-Paris, 1993a.

Alvarez, G., Serrano, N., Gutierrez, A., Urban, P. and Avello, A.,"Computer Animation of Human Body Motion in Sport, Using Real Captured Data and a "Consistent" Mechanical Model", *IInd International Symposium on Three-Dimensional Analysis of Human Movement*, Parc du Futuroscope, Poitiers, France, 1993b.

Ambrósio, J., Pereira, M. and Silva, F., *Crashworthiness of Transportation Systems: Structural Impact and Occupant Protection*, Kluwer Academic Press, Dordrecht ; Boston, 1997.

Ambrósio, J., Silva, M. and Abrantes, J.,"Inverse Dynamic Analysis of Human Gait Using Consistent Data", *IV International Symposium on Computer Methods in Biomechanics and Biomedical Engineering*, Lisbon, Portugal, 275-282, 1999a.

Ambrósio, J., Silva, M. and Gonçalves, J., "Development of Energy Absorbing Devices Using a Kinetostatic Multibody Dynamics Methodology", *International Journal of Crashworthiness*, **1**(2), 127-143, 1996.

Ambrósio, J., Silva, M. and Lopes, G.,"Reconstrução do Movimento Humano e Dinâmica Inversa Utilizando Ferramentas Numéricas Baseadas em Sistemas Multicorpo", *IV Congreso de Métodos Numéricos en Ingeniería*, Sevilha, Spain, 1999b.

Amirouche, F., Ider, S. and Trimble, J., "Analytical Method for the Analysis and Simulation of Human Locomotion", *Journal of Biomechanical Engineering*, **112**, 379-386, 1990.

Anderson, F. and Pandy, M., "Dynamic Optimization of Human Walking", *Journal of Biomechanical Engineering*, **123**, 381-390, 2001a.

Anderson, F. and Pandy, M., "Static and Dynamic Optimization Solutions for Gait are Practically Equivalent", *Journal of Biomechanics*, **34**, 153-161, 2001b.

Andriacchi, T. and Hurwitz, D., "Gait Biomechanics and the Evolution of Total Joint Replacement", *Gait and Posture*, **5**, 256-264, 1997.

Arabyan, A. and Wu, F., "An Improved Formulation for Constrained Mechanical Systems", *Multibody System Dynamics*, **2**(1), 49-69, 1998.

Arora, J., *Introduction to Optimum Design*, McGraw-Hill Book Company, New York, NY, 1989.

Ascher, U., Chin, H., Petzold, L. and Reich, S., "Stabilization of Constrained Mechanical Systems with Daes and Invariant-Manifolds", *Mechanics of Structures and Machines*, **23**(2), 135-157, 1995.

Avello, A. and Bayo, E., "A Singularity-free Penalty Formulation for the Dynamics of Constrained Multibody Systems", *Mechanical Design and Synthesis*, **46**, 643-649, 1992.

Ball, K. and Pierrynowski, R., "Classification of Errors in Locating a Body", *Journal of Biomechanics*, **29**(9), 1213-1217, 1996.

Bandak, F., Eppinger, R. and Ommaya, A., *Traumatic Brain Injury, Bioscience and Mechanics*, Mary Ann Liebert, Inc, New York, NY, 1996.

Bartz, J., "A three-dimensional computer simulation of a motor vehicle crash victim", Calspan Report VJ-2978-V11971.

Baruh, H., "Another Look at the Describing Equations of Dynamics", *Journal of the Chinese Society of Mechanical Engineers*, **21**(1), 15-24, 2000.

Baumgarte, J., "Stabilization of Constraints and Integrals of Motion", *Computer Methods in Applied Mechanics and Engineering*, **1**, 1-16, 1972.

Bayo, E., Jimenez, J., Serna, M. and Bastero, J., "Penalty Based Hamiltonian Equations for the Dynamic Analysis of Constrained Mechanical Systems", *Mechanisms and Machine Theory*, **29**(5), 725-737, 1994.

Bedewi, P. and Bedewi, N., "Modeling of Occupant Biomechanics with Emphasis on Analysis of Lower Extremity Injuries", *International Journal of Crashworthiness*, **1**(1), 50-72, 1996.

Blajer, W. and Czaplicki, A., "Modeling and Inverse Simulation of Somersaults on the Trampoline", *Journal of Biomechanics*, **34**, 1619-1629, 2001.

Bogert, A., Read, L. and Nigg, B., "A Method for Inverse Dynamic Analysis Using Accelerometry", *Journal of Biomechanics*, **29**(7), 949-954, 1996.

Borghese, N., Cerveri, P. and Ferrigno, G., "Statistical Comparison of DLT Versus ILSSC in the Calibration of a Photogrammetric Stereo-System", *Journal of Biomechanics*, **30**(4), 409-413, 1997.

Bosio, A. and Bowman, B., "Analysis of head and neck dynamic response of the US adult military population: Articulated total body (ATB) model." Wright-Paterson Air Force Base, UMTRL-86-14, Ohio, 1986.

Brelin-Fornari, J., Arabyan, A. and Deng, Y.-C.,"Use of Active Muscles in a Model of the Human Head and Neck", *42th Stapp Car Crash Conference*, 1998.

Carhart, M.R., "Biomechanical Analysis of Compensatory Steping: Implications for paraplegics Standing Via FNS", Ph.D. Dissertation, Arizona State University, Arizona, 2000.

Celigüeta, J.T.,"Multibody Simulation of Human Body Motion in Sports", *XIV International Symposium on Biomechanics in Sports*, Madeira, Portugal, 81-94, 1996.

Chau, T., "A Review of Analytical Techniques for Gait Data. Part 2: Neural Network and Wavelet Methods", *Gait and Posture*, **13**, 102-120, 2001.

Cole, G., Nigg, B., Ronsky, J. and Yeadon, "Application of the Joint Coordinate System to Three-Dimensional Joint Attitude and Movement Representation: A Standardization Proposal", *Journal of Biomechanical Engineering*, **115**, 344-349, 1993.

Collins, J.J., "The redundant nature of locomotor optimization laws", *Journal of Biomechanics*, **28**(3), 251-267, 1995.

Crowninshield, R.D. and Brand, R.A., "Physiologically Based Criterion of Muscle Force Prediction in Locomotion", *Journal of Biomechanics*, **14**(11), 793-801, 1981.

Day, T. and Garvey, J., "Applications and Limitations of 3-Dimensional Vehicle Rollover Simulation", *SAE*, **Paper 2000-01-0852**, 1-14, 2000.

Delp, S., Loan, P., Hoy, M., Zajac, F., Topp, E. and Rosen, J., "An Interactive Graphics-Based Model of the Lower Extremity to Stydy Orthopaedic Surgical Procedures", *IEEE Transactions on Biomedical Engineering*, **37**(8), 757-767, 1990.

Dinis, P., Martins, J. and Pires, E.,"Finite Element Simulation of the Forarm Flexion", *Fourth International Symposium on Computer Methods in Biomechanics and Biomedical Engineering*, Lisbon, 295-300, 1999.

Dostal, W. and Andrews, J., "A Three-Dimensional Biomechanical Model of the Hip Musculature", *Journal of Biomechanics*, **14**(11), 803-812, 1981.

Duda, G., Brand, D., Freitag, S., Lierse, W. and Schneider, E., "Variability of Femoral Muscle Attachements", *Journal of Biomechanics*, **29**(9), 1185-1190, 1996.

Dynamics, M., "ADAMS User Manual", Mechanical Dynamics, Ann Arbor, Michigan, 1998.

Eberhard, P., Spagele, T. and Gollhofer, A., "Investigations for the Dynamicsl Analysis of Human Motion", *Multibody System Dynamics*, **3**(1), 1-20, 1999.

Eng, J., Winter, D. and Patla, A., "Strategies for Recovery from a Trip in Early and Late Swing During Human Walking", *Experimental Brain Research*, **102**, 339-349, 1994.

Engel, G., Martins, J., Mateus, C. and Pires, E.,"Técnicas de Optimização na Análise de Movimento e das Forças Musculares no Membro Superior", *V Encontro Nacional de Mecânica Computacional*, Guimarães-Portugal, 1181-1191, 1997.

Flashner, H., Beuter, A. and Arabyan, A., "Modeling of Control and Learning in a Stepping Motion", *Biological Cybernetics*, **55**, 387-396, 1987.

Flashner, H., Beuter, A. and Arabyan, A., "Fitting Mathematical Functions to Joint Kinematics During Stepping: Implications for Motor Control", *Biological Cybernetics*, **58**, 91-99, 1988.

Fujie, H., Livesay, G.A., Woo, S.L.-Y., Kashiwaguchi, S. and Blomstrom, G., "The Use of a Universal Force-Moment Sensor to Determine In-Situ Forces in Ligaments: A New Methodology", *Journal of Biomechanical Engineering*, **117**(1), 1-7, 1995.

Gear, C.,"Numerical solution of differential-algebric equations", *IEE Transaction on Circuit Theory*, 89-95, 1981.

Gerritsen, K., Bogert, A. and Nigg, B., "Direct Dynamics Simulation of the Impact Phase in Heel-Toe Running", *Journal of Biomechanics*, **28**(6), 661-668, 1995.

Giakas, G. and Baltzopoulos, V., "A Comparison of Automatic Filtering Techniques Applied to Biomechanical Walking Data", *Journal of Biomechanics*, **30**(8), 847-850, 1997a.

Giakas, G. and Baltzopoulos, V., "Optimal Digital FIltering Requires a Different Cut-Off Frequency Strategy for the Determination of the Higher Derivatives", *Journal of Biomechanics*, **30**(8), 851-855, 1997b.

Gilchrist, L. and Winter, D., "A Two-Part, Viscoelastic Foot Model for Use in Gait Simulations", *Journal of Biomechanics*, **29**(6), 795-798, 1996.

Gim, G., "Vehicle Dynamic Simulation with a Comprehensive Model for Pneumatic Tyres", PhD. Thesis, University of Arizona, Arizona, AR, 1988.

Glitsch, U. and Baumann, W., "The Three-Dimensional Determination of Internal Loads in the Lower Extremity", *Journal of Biomechanics*, **30**(11,12), 1123-1131, 1997.

Glos, D., Butler, D., Grood, E. and Levy, M., "In Vitro Evaluation of an Implantable Force Transducer (IFT) ina Patellar Tendon Model", *Journal of Biomechanical Engineering*, **115**, 335-343, 1993.

Goldberg, D., *Genetic Algorithms in Search, Optimization and Machine Learning*, Addison-Wesley, New York, 1989.

Greenwood, D., *Principles of Dynamics*, Prentice-Hall, Inc., Englewood Cliffs, NJ, 1965.

Gruber, S. and Schiehlen, W.,"Biped Walking Machines: A Challenge to Dynamics and Mechatronics", *Fifth WOrld Congress on Computational Mechanics*, Vienna, Austria, 2002.

Haftka, R. and Gurdal, Z., *Elements of Structural Optimization*, Kluwer Academic Publishers, Dordrecht, 1992.

Halquist, J., "Theoretical Manual for DYNA-3D", Lawrence Livermore Laboratory1982.

Hanavan, E., "A Mathematical Model of the Human Body", *AMRL-TR-64-102*, Aerospace Medical Research Laboratories, Washington, 1964.

Hatze, H., "The Use of Optimally Regularized Fourier Series for Estimating Higher-Order Derivatives of Noisy Biomechanical Data", *Journal of Biomechanics*, **14**, 13-18, 1980.

Hatze, H., "A Comprehensive Model for Human Motion Simulation and Its Application to the Take-Off Phase of the Long Jump", *Journal of Biomechanics*, **14**(3), 135-142, 1981.

Hatze, H., "Quantitative analysis, synthesis and optimization of human motion", *Human Movement Science*, **3**, 5-25, 1984.

Haug, E., *Computer Aided Kinematics and Dynamics of Mechanical Systems*, Allyn and Bacon, Boston, 1989.

Haug, E., "Biomechanical Models in Vehicle Accident Simulation", Crashworthiness of Transportation Systems: Structural Impact and Occupant Protection, J. Ambrósio, M. Pereira and F. Silva, eds., Kluwer Academic Publishers, Dordrecht, 1996.

Haug, E., Clinckemaillie, J. and Aberlenc, F.,"Contact-Impact Problems for Crash", *Post Symposium Short Course of the Second International Symposium of Plasticity*, Nagoya, Japan, 1989.

Haug, E. and Ulrich, D.,"The PAM-CRASH Code as an Efficient Tool for Crashworthiness Simulation and Design", *Second European Car/Trucks Simulation Symposium*, Munich, Germany, 1988.

Herskovits, J., "A Feasible Directions Interior Point Technique for Nonlinear Optimization", *Journal of Optimization Theory and Applications*, **99**(1), 121-146, 1998.

Hertz, H.,"Gesammelte Werke 1", Leipzig, Germany., 1895.

Holland, J., *Adaptation in Natural and Artificial Systems: An Introductory Analysis with Applications to Biology, Control and Artifitial Intelligence*, MIT Press, Cambridge, MA, 1992.

Horak, F., "Clinical Assessment of Balance Disorders", *Gait and Posture*, **6**, 76-84, 1997.

Horst, M., Thunnissen, J., Happee, R., Haaster, R. and Wismans, J.,"The Influence of the Muscle Activity on Head-Neck Response During Impact", *41th Stapp Car Crash Conference*, Orlando-USA, 487-507, 1997.

Huang, S.-C., "Modeling Human Body Motion With Application in Crash Victim Simulation", *Journal of Applied Biomechanics*, **11**, 322-336, 1995.

Huston, R., *Multibody Dynamics*, Butterworth-Heinemann, Stonehan, MA, 1990.

Hutchinson, J., Kaiser, M. and Lankarani, H., "The Head Injury Criterion (HIC) Functional", *Journal of Applied Mathematics and Computation*, **Vol. 96**(1), 1-16, 1998.

Jalón, J. and Bayo, E., *Kinematic and dynamic simulation of multibody systems : the real-time challenge*, Springer-Verlag, New York ; Hong Kong, 1994.

Jensen, R. and Davy, D., "An Investigation of Muscle Lines of Action About the Hip: A Centroid Line Approach Vs The Straight Line Approach", *Journal of Biomechanics*, **8**, 103-110, 1975.

Kan, C.-D., Marzougui, D., Bahouth, G. and Bedewi, N., "Crashworthiness Evaluation Using Integrated Vehicle and Occupant Finite Element Models", *International Journal of Crashworthiness*, **6**(3), 387-398, 2001.

Kapandji, I., *The Physiology of the Joints. Volume 3: The Trunk and Vertebral Column*, L. Honore, translator, Churchill Livingstone, London, UK, 1973.

Kapandji, I., *The Physiology of the Joints. Volume 1: The Upper Extremity*, Churchill Livingstone, London, UK, 1974a.

Kapandji, I., *The Physiology of the Joints. Volume 2: The Lower Extremity*, Churchill Livingstone, London, UK, 1974b.

Kaplan, M., "Efficient Optimal Control of Large-Scale Biomechanical Systems", Ph.D. Dissertation, Stanford University, Stanford, 2000.

Kaplan, M., Silva, M. and Ambrósio, J., "Inherent Inconsistencies of Inverse Dynamics Analyses", *Journal of Biomechanics*, (Submitted), 2001.

King, A., "Occupant Kinematics and Impact Biomechanics", Crashworthiness of Transportation Systems: Structural Impact and Occupant Protection, J. Ambrósio, M. Pereira and F. Silva, eds., Kluwer Academic Publishers, Dordrecht, 3-23, 1996.

Kingma, I., Looze, M., Toussaint, H., Klijnsma, H. and Bruijnen, T., "Validation of a Full Body 3-D Dynamic Linked Segment Model", *Human Movement Science*, **15**(6), 833-860, 1996.

Klisch, T.,"Contact Mechanics in Multibody Systems", *Computational Methods in Mechanics*, Varna, Bulgaria, 179-188, 1997.

Komistek, R., Stiehl, J., Dennis, D., Paxson, R. and Soutas-Little, R., "Mathematical Model of the Lower Extremity Joint Reaction Forces Using Kane's Method of Dynamics", *Journal of Biomechanics*, **31**, 185-189, 1998.

Kroemer, K., Snook, S., Meadows, S. and Deutsch, S., *Ergonomic Models of Anthropometry, Human Biomechanics, and Operator-Equipment Interfaces: Proceedings of a Workshop*, Committee on Human Factors

National Research Council, Washington, 1988.

Kwon, Y.-H. and Fiaud, V.,"Experimental Issues in Data Acquisition in Sport Biomechanics: Camera Calibration", *XXth International Symposium on Biomechanics in Sports*, Caceres, Spain, 3-15, 2002.

Laananen, D., "Computer Simulation of an Aircraft Seat and Occupant in a Crash Environment - Program SOM-LA/SOM-TA User Manual", *DOT/FAA/CT-90/4*, US Department of Transportation, Federal Aviation Administration1991.

Laananen, D., Bolukbasi, A. and Coltman, J., "Computer Simulation of an Aircraft Seat and Occupant in a Crash Environment - Volume 1: Technical report", *DOT/FAA/CT-82/33-I*, US Department of Transportation, Federal Aviation Administration1983.

Lankarani, H.,"Occupant Dynamic Responses for Evaluation of Complience Characteristics of Aircraft Bulkheads", *Advances in Design Automation*, Scottsdale, AZ, 391-397, 1992.

Lankarani, H., Ma, D. and Menon, R., "Impact Dynamics of Multibody Mechanical Systems and Application to Crash Responses of Aircraft Occupant/Structure", Computational Dynamics in Multibody Systems, M. Pereira and J. Ambrósio, eds., Kluwer Academic Publishers, Dordrecht-Netherlands, 239-265, 1995.

Lankarani, H. and Nikravesh, P., "Canonical impulse-momentum equations for the impact analysis of multibody systems", *ASME Journal of Mechanical Design*, **114**, 180-186, 1992.

Lanshammar, H., "On Practical Evaluation of Differentiation Techniques for Human Gait Analysis", *Journal of Biomechanics*, **15**(2), 99-105, 1982.

Leal, R., Costa, L., Oliveira, P. and Figueiredo, I.,"Algoritmos Genéticos na Optimização de Laminados", *VI Congresso Nacional de Mecânica Aplicada e Computacional*, Aveiro, 343-366, 2000.

Leardini, A., O'Connor, J., Catani, F. and Giannini, S., "A Geometric Model of the Human Ankle Joint", *Journal of Biomechanics*, **32**, 585-591, 1999.

Ledesma, R. and Bayo, E., "A Lagrangian Approach to the Non-Casual Inverse Dynamics of Flexible Multibody Systems: The Three-Dimensional Case", *International Journal for Numerical Methods in Engineering*, **37**, 3343-3361, 1994.

Lee, J.-N. and Nikravesh, P., "Steady-State Analysis of Multibody Systems With Reference to Vehicle Dynamics", *Nonlinear Dynamics*, **5**, 181-192, 1994.

Leva, P., "Joint Center Longitudinal Positions Computed From a Selected Subset of Chandler's Data", *Journal of Biomechanics*, **29**(9), 1231-1233, 1996.

Li, G.,"Prediction of Antagonistic Muscle Forces Using Inverse Dynamic Optimization During Flexion/Extention of the Knee", *1999 Bioengineering Conference*, Big Sky, Montana, Canada, 1999.

Lieber, R., *Skeletal Muscle Structure and Function: Implications to Rehabilitation and Sports Medicine*, Wiliams and Wilkins, Baltimore, Maryland, 1992.

Lo, J., Huang, G. and Metaxas, D., "Human Motion Planning Based on Recursive Dynamics and Optimal Control Techniques", *Multibody System Dynamics*, **8**(4), 433-458, 2002.

Lu, T.-W., Taylor, S., O'Connor, J. and Walker, P., "Influence of Muscle Activity on the Forces in the Femur: An In Vivo Study", *Journal of Biomechanics*, **30**(11/12), 1101-1106, 1997.

Mackay, M., "A Riview of the Biomechanics of Impacts in Road Accidents", Crashworthiness of Transportation Systems: Structural Impact and Occupant Protection, J. Ambrósio, M. Pereira and F. Silva, eds., Kluwer Academic Publishers, Dordrecht, 115-138, 1996.

Madeira, J., Rodrigues, H. and Pina, H., "Genetic Methods in Multi-objective Optimization of Structures with an Equality Constraint on Volume", Evolutionary Multi-Criterion Optimization : Second International Conference, C. Fonseca, ed., Springer, New York, 767-781, 2003.

Marsden, J. and West, M., "Descrete Mechanics and Variational Integrators", Cambridge University Press, Acta Numerica, 357-514, 2001.

Maurel, W. and Thalmann, D.,"A Computer Model of the Human Shoulder Including Scapulo-Thoracic Constraints and Joint Sinus Cones", *Fourth International Symposium on Computer Methods in Biomechanics and Biomedical Engineering*, Lisbon, 313-318, 1999.

Medved, V., *Measurement of Human Locomotion*, CRC Press LLC, New York, NY, 2001.

Meirovitch, L., *Methods of analytical dynamics*, McGraw-Hill, New York,, 1970.

Merletti, R., Knaflitz, M. and DeLuca, C., "Electrically Evoked Myoelectric Signals", *Critical Reviews in Biomedical Engineering*, **11**(4), 293-340, 1992.

Miller, K. and Chinzei, K., "Constitutive Modelling of Brain Tissue: Experiment and Theory", *Journal of Biomechanics*, **30**(11/12), 1115-1121, 1997.

Mommersteeg, T., Huiskes, R., Blankevoort, L., Kooloos, J. and Kauer, J., "An Inverse Dynamics Modeling Approach to Determine the Restraining Function of Human Knee Ligament Bundles", *Journal of Biomechanics*, **30**(2), 139-146, 1997.

Morecki, A., Ekiel, J. and Fidelus, K., *Cybernetic Systems of Limb Movements in Man, Animals and Robots*, Ellis Horwood Limited, New York, 1984.

Morecki, A., Jaworek, K., Olszewski, J., Koozekanani, S., McGhee, R., Rahmani, S. and Johnson, E.,"Reduced Order Dynamic Models for Computer Analysis of Human Gait", *Fourth Symposium on Theory and Practice of Robots and Manipulators*, Zaborow, Poland, 368-381, 1981.

Morrison, J., "The Mechanics of Muscle Function in Locomotion", *Journal of Biomechanics*, **3**, 431-451, 1969.

Mow, V. and Hayes, W., *Basic Orthopaedic Biomechanics*, Lippincott-Raven Publishers, New York, NY, 1997.

Nigg, B. and Herzog, W., *Biomechanics of the musculo-skeletal system*, J. Wiley, Chichester ; New York, 1995.

Nikravesh, P., *Computer-aided analysis of mechanical systems*, Prentice-Hall, Englewood Cliffs, N.J., 1988.

Nikravesh, P.,"Construction of the Equations of Motion for Multibody Dynamics Using Point and Joint Coordinates", *Computer-aided analysis of rigid and flexible mechanical systems*, Tróia, Portugal, xvi, 619, 1994.

Nikravesh, P., Ambrósio, J. and Pereira, M., "Rollover Simulation and Crashworthiness Analysis of Trucks", *Journal of Forensic Engineering*, **2**(3), 387-401, 1990.

Numerics, V., "IMSL FORTRAN Numerical Libraries - Version 5.0", Microsoft Corp., 1995.

Olney, S. and Winter, D., "Predictions of Knee and Ankle Moments of Force in Walking From EMG and Kinematic Data", *Journal of Biomechanics*, **18**(1), 9-20, 1985.

Ounpuu, S., Davis, R. and DeLuca, P., "Joint Kinetics: Methods, Interpretation and Treatment Decision-Making in Children with Cerebral Palsy and Myelomeningocele", *Gait and Posture*, **4**, 62-78, 1995.

Palastanga, N., Field, D. and Soames, R., *Anatomy and Human Movement - Structure and Function*, Elsevier, 2002.

Panero, J. and Zelnik, M., *Human Dimension and Interior Space: A Source Book of Design Reference Standards*, S. Castán, translator, Watson-Guptill Publications, New York, 1987.

Parenteau, C., Gopal, M. and Viano, D., "Near and Far-Side Adult Front Passenger Kinematics in a Vehicle Rollover", *SAE*, **Paper 2001-01-0176**, 1-8, 2001.

Patriarco, A., Mann, R., Simon, S. and Mansour, J., "An Evaluation of the Approaches of Optimization Models in the Prediction of Muscle Forces During Gait", *Journal of Biomechanics*, **14**(8), 513-525, 1981.

Pedersen, D., Brand, R., Cheng, C. and Arora, J., "Direct Comparison of Muscle Force Predictions Using Linear and Nonlinear Programming", *ASME Journal of Biomechanical Engineering*, **109**, 192-199, 1987.

Pereira, M. and Ambrósio, J., *Computer-aided analysis of rigid and flexible mechanical systems*, Kluwer Academic Press, Dordrecht ; Boston, 1994.

Pereira, M. and Ambrósio, J., *Computational Dynamics in Multibody Systems*, Kluwer Academic Publishers, Dordrecht, The Netherlands, 1995.

Petzold, L., Yen, J. and Raha, S., "A Time Integration Algorithm for Flexible Mechanism Dynamics: The DAE Alpha-Method", *Computer Methods in Applied Mechanics and Engineering*, **158**, 341-355, 1998.

Prasad, P., "An Overview of the Major Occupant Simulation Models", Mathematical Simulation of Occupant and Vehicle Kinematics, SAE Publication, 146, 1984.

Prilutsky, B., Herzog, W. and Allinger, T., "Forces of Individual Cat Ankle Extensor Muscles During Locomotion Predicted Using Static Optimization", *Journal of Biomechanics*, **30**(10), 1025-1033, 1997.

Prince, F., Corriveau, H., Hebert, R. and Winter, D., "Gait in the Elderly", *Gait and Posture*, **5**, 128-135, 1997.

Raasch, C., Zajac, F., Ma, B. and Levine, S., "Muscle Coordination of Maximum-Speed Pedeling", *Journal of Biomechanics*, **30**(6), 595-602, 1997.

Raikova, R., "About Weight Factors in the Non-Linear Objective Functions Used for Solving Indeterminate Problems in Biomechanics", *Journal of Biomechanics*, **32**, 689-694, 1999.

Raikova, R. and Aladjov, H., "Hierarchical Genetic Algorithm Versus Static Optimization - Investigation of Elbow Flexion and Extention Movements", *Journal of Biomechanics*, **35**(8), 1123-1135, 2002.

Rasmussen, J. and Damsgaard, M.,"Optimization of Biomechanical Multibody Systems", *Second World Congress of Structural and Multidisciplinary Optimization*, Zakopane, Poland, 1997.

Rasmussen, J., Damsgaard, M., Christensen, S. and Surma, E., "Design Optimization with Respect to Ergonomic Properties", *Structural and Multidisciplinary Optimization*, **24**(2), 89-97, 2002a.

Rasmussen, J., Vondrak, V., Damsgaard, M., de Zee, M., Christensen, S. and Dostal, Z.,"The AnyBody project - Computer Analysis of the Human Body", *International Congress of Biomechanics - Biomechanics of Man 2002*, Cejkovice, Czech Republic, 2002b.

Reich, J., Swoboda, S., Steiner, R. and Daunicht, W.J.,"BIOMEX 2 - An Environment for Complex Biomechanical Simulations", *VIIth International Symposium on Computer Simulation in Biomechanics*, Calgary, Canada, 1999.

Renfroe, D., Partain, J. and Lafferty, J., "Modeling of Vehicle Rollover and Evaluation of Occupant Injury Potential Using MADYMO", *SAE*, **Paper 980021**, 1998.

Riener, R., Quintern, J. and Schmidt, G., "Biomechanical Model of the Human Knee Evaluated by Neuromuscular Stimulation", *Journal of Biomechanics*, **29**(9), 1157-1167, 1996.

Roberson, R. and Schwertassek, R., *Dynamics of Multibody Systems*, Springer-Verlag, New York, NY, 1988.

Rouvière, H., *Anatomie humaine, descriptive et topographique - Tome 1*, Masson et cie, Paris,, 1924.

Rouvière, H., *Anatomie humaine, descriptive et topographique - Tome 2*, Masson, Paris,, 1943.

Rouvière, H., *Anatomie humaine, descriptive et topographique - Tome 3*, Masson, Paris,, 1954.

S.A.E., "Human Tolerance to Impact Conditions as Related to Motor Vehicle Design", *SAE J885 APR80*, Body Engineering and Automotive Safety Committees, Society of Automotive Engineers, Warrendale, PA, 1980.

Sadeghi, H., Allard, P., Prince, F. and Labelle, H., "Symmetry and Limb Dominance in Able-Bodied Gait: A Review", *Gait and Posture*, **12**, 34-45, 2000.

Saha, N., Mahadevan, S., Midoun, D. and Yang, J.,"Finite Element Structure-Dummy System Model for Side Impact Simulation", *Crashworthiness and Occupant Protection in Transportation Systems*, 1991.

Sathasivam, S. and Walker, P., "A Computer Model with Surface Friction for the Prediction of Total Knee Kinematics", *Journal of Biomechanics*, **30**(2), 177-184, 1997.

Schaffner, G., Newman, D. and Robinson, S.,"Inverse Dynamic Simulation and Computer Animation of Extra Vehicular Activity (EVA)", *35th Aerospace Sciences Meeting and Exhibit*, Reno, NV, 1997.

Schiehlen, W., *Multibody Systems Handbook*, Springer-Verlag, Berlin, Germany, 1990.

Schiehlen, W., *Advanced Multibody System Dynamics - Simulation and Software Tools*, Kluwer Academic Publishers, Dordrecht, The Netherlands, 1993.

Schneck, D., *Mechanics of Muscle: Second Edition*, New York University Press, New York, NY, 1992.

Seireg, A. and Arvikar, R., "A Mathematical Model for Evaluation of Forces in Lower Extremities of the Musculo-Skeletal System", *Journal of Biomechanics*, **6**, 313-326, 1973.

Seireg, A. and Arvikar, R., "The Prediction of Muscular Load Sharing and Joint Forces in the Lower Extremities During Walking", *Journal of Biomechanics*, **8**, 89-102, 1975.

Seireg, A. and Arvikar, R., *Biomechanical Analysis of the Muscoloskeletal Structure for Medicine and Sports*, Hemisphere Publishing Corporation, New York, NY, 1989.

Shabana, A., *Computational Dynamics*, Wiley, New York, 1994.

Shelburne, K. and Pandy, M., "A Musculoskeletal Model of the Knee for Evaluating Ligament Forces During Isometric Contractions", *Journal of Biomechanics*, **30**(2), 163-176, 1997.

Silva, M., "Modelo biomecânico para a dinâmica computacional do movimento humano articulado", *IDMEC/CPM/96/003,1996*, IDMEC - Instituto Superior Tecnico, Lisbon, 1996.

Silva, M. and Ambrósio, J., "Pedestrian Impact and Run Over Using a Multibody Simulation Tool", *International Journal of Crashworthiness*, **4**(3), 261-271, 1999.

Silva, M. and Ambrósio, J., "Kinematic Data Consistency in the Inverse Dynamic Analysis of Biomechanical Systems", *Multibody System Dynamics*, **8**(2), 219-239, 2002a.

Silva, M. and Ambrósio, J.,"A Multibody Based Methodology for the Solution of the Redundant Nature of the Muscle Forces Using Static Optimization", *V Congreso de Métodos Numéricos en Ingeniería*, Madrid, Spain, 2002b.

Silva, M. and Ambrósio, J.,"Out-of-Position Vehicle Occupants Models in a Multibody Integrated Simulation Environment", *The 2002 IRCOBI Conference on the Biomechanics of Impact*, Munich, Germany, 2002c.

Silva, M. and Ambrósio, J., "Solutions of Redundant Muscle Forces in Human Locomotion with Multibody Dynamics and Optimization Tools", *Journal of Mechanics Based Design of Structures and Machines*, **31**(3), 381-411, 2002d.

Silva, M. and Ambrósio, J.,"Nova Perspectiva Sobre a Modelação de Sistemas de Corpos Múltiplos Utilizando Coordenadas Naturais", *VII Congresso de Mecânica Aplicada e Computacional*, Évora, Portugal, 2003a.

Silva, M. and Ambrósio, J., "Sensitivity of the Results Produced by the Inverse Dynamic Analysis of a Human Stride to Perturbed Input Data", *Gait and Posture*, Article in Press, 2003b.

Silva, M., Ambrósio, J., Abrantes, J. and Veloso, A., "Gait Analysis Using Multibody Simulation Tools and Inverse Dynamic Procedures", *Journal of Computer Methods in Biomechanics and Biomedical Engineering*, (Submitted), 2001.

Silva, M., Ambrósio, J. and Pereira, M., "A Multibody Approach to the Vehicle and Occupant Integrated Simulation", *International Journal of Crashworthiness*, **2**(1), 73-90, 1997.

Singerman, R., Berilla, J. and Davy, D., "Direct In Vitro Determination of the Patellofemoral Contact Force for Normal Knees", *Journal of Biomechanical Engineering*, **117**, 9-14, 1995.

Stadler, W., "Multicriteria Optimization in Mechanics (A Survey)", *Applied Mechanics Reviews*, **37**(3), 277-286, 1984.

Steele, B. and Lankarani, H., "A brief examination and comparision between the federal motor vehicle safety standards and the federal aviation regulations", National Institute for Aviation Research, NIAR Report 91-25, Wichita State University, 1991.

Svanberg, K., "The Method of Moving Asymptotes - A New Method for Structural Optimization", *International Journal for Numerical Methods in Engineering*, **24**, 359-373, 1987.

Svanberg, K.,"The MMA for Modeling and Solving Optimization Problems", *Third World Congress of Structural and Multidisciplinary Optimization*, Buffalo, New-York, 1999.

T.N.O., "MADYMO - User's Manual 3D", TNO Road-Vehicles Research Institute, 1997.

Tavares, L. and Correia, F., *Optimização Linear e Não Linear. Conceitos, Métodos e Algoritmos*, Fundação Calouste Gulbenkian, Lisbon, 1986.

TNO, "MADYMO - User's Manual 3D", TNO Road-Vehicles Research Institute, 1997.

Tsirakos, D., Baltzopoulos, V. and Bartlett, R., "Inverse Optimization: Functional and Physiological Considerations Related to the Force-Sharing Problem", *Critical Reviews in Biomedical Engineering*, **25**(4&5), 371-407, 1997.

Tumer, S. and Engin, A., "Three-Body Segment Dynamic Model of the Human Knee", *Journal of Biomechanical Engineering*, **115**, 351-356, 1993.

Vanderplaats, G., *Numerical Optimization Techniques for Engineering Design*, McGraw-Hill Book Company, New York, NY, 1984.

Vanderplaats, G., "DOT - Design Optimization Tools - USERS MANUAL - Version 5.0." 1999.

Vaughan, C., Davis, B. and O'Connor, J., *Dynamics of Human Gait*, Human Kinetics Publishers, Champaign, IL, 1992.

Viano, D. and King, A., "Injury Mechanisms and Biofidelity of Dummies", Crashworthiness of Transportation Systems: Structural Impact and Occupant Protection, J. Ambrósio, M. Pereira and F. Silva, eds., Kluwer Academic Publishers, Dordrecht, 25-51, 1996.

Wang, J.T.,"Recent Advances in Modeling of Pyrotechnic Inflators for Inflatable Restraint Systems", *Crashworthiness and Occupant Protection in Transportation Systems*, 89-93, 1989.

Wang, J.T. and Ngo, T., "Modeling of Passenger Side Airbags with Complex Shape", *SAE*, **Paper 900545**, 117-123, 1990.

West, M., Kane, C., Marsden, J. and Ortiz, M.,"Variational Integrators, The Newmark Scheme, and Dissipative Systems", *International Conference on Differencial Equations*, Berlin, 109-1011, 2000.

Winter, D., "Pathologic Gait Diagnosis With Computer-Averaged Electromyographic Profiles", *Archives of Physical Medicine and Rehabilitation*, **65**, 393-398, 1984.

Winter, D., *Biomechanics and motor control of human movement*, Wiley, New York, 1990.

Winter, D., *The biomechanics and motor control of human gait: Normal, elderly and pathological*, University of Waterloo Press, Waterloo, Canada., 1991.

Winter, D., "Human Balance and Posture Control During Standing and Walking", *Gait and Posture*, **3**, 193-214, 1995.

Winter, D. and Yack, H., "EMG Profiles During Normal Human Walking: Stride-to-Stride and Inter-Subject Variability", *Electroencephalography and Clinical Neurophysiology*, **67**, 402-411, 1987.

Winters, J. and Woo, S.L.-Y., *Multiple Muscle Systems: Biomechanics and Movement Organization*, Springer-Verlag, New York, NY, 1990.

Wismans, J., "A three-Dimensional Mathematical Model of the Human Knee Joint", PhD Thesys, Eindhoven University, Eindhoven, 1980.

Wismans, J., "Models in Injury Biomechanics for Improved Passive Vehicle Safety", Crashworthiness of Transportation Systems: Structural Impact and Occupant Protection, J. Ambrósio, M. Pereira and F. Silva, eds., Kluwer Academic Publishers, Dordrecht, 1996.

Wismans, J., Janssen, E., Beusenberg, M., Koppens, W. and Lupker, H., *Injury Biomechanics*, Eindhoven University of Technology, Eindhoven, The Netherlands, 1994.

Wismans, J., Maltha, J., Van Wijk, J. and Jansen, E.,"MADYMO - A crash victim simulation computer program for biomechanical research and optimization of design for impact injury prevention", *AGARD Meeting*, Koln, Germany, 1982.

Wynarsky, G. and Greenwald, A., "Mathematical Model of the Human Ankle Joint", *Journal of Biomechanics*, **16**(4), 241-251, 1983.

Yamaguchi, G.T., *Dynamic Modeling of Musculoskeletal Motion*, Kluwer Academic Publishers, Boston, Massachussetts., 2001.

Yamaguchi, G.T., Moran, D.W. and Si, J., "A computationally efficient method for solving the redundant problem in biomechanics", *Journal of Biomechanics*, **28**(8), 999-1005, 1995.

Yang, J., Winter, D. and Wells, R., "Postural Dynamics in the Standing Human", *Biological Cybernetics*, **62**, 309-320, 1990.

Zahalak, G. and Ma, S.-P., "Muscle Activation and Contraction: Constitutive Relations Based Directly on Cross-Bridge Kinetics", *Journal of Biomechanical Engineering*, **112**, 52-62, 1990.

Zajac, F.E., "Muscle and Tendon: Properties, Models, Scaling, and Application to Biomechanics and Motor Control", *Critical Reviews in Biomedical Engineering*, **17**(4), 359-411, 1989.

Zappa, B., Casolo, F. and Legnani, G.,"Analysis and Synthesis of 3D Motion for Multi-Body Systems with Regards to Sport Performances", *Ninth World Congress on the Theory of Machines and Mechanisms*, Milano, Italy, 1995.

Zatsiorsky, V., *Kinematics of Human Motion*, Human Kinetics, Champaign, IL, 1998.